Experimental and numerical study of air distribution and thermal environment control for chilled food manufacturing facilities

A thesis submitted for the degree of

Doctor of Philosophy (PhD)

by

Dimitris Parpas

(1127057)

Department of Mechanical, Aerospace and Civil Engineering

College of Engineering, Design and Physical Science

Brunel University London

Abstract

Thermal environment control of chilled food manufacturing facilities plays a critical role in maintaining the required food product temperature during processing to ensure food quality and maximise shelf life. The provision of cooling to maintain the required temperatures in the processing halls, which should be in the range between 4 $^{\circ}$C and 12°C also impacts on energy consumption and CO2 emissions.

Chilled food manufacturing facilities normally have high ceilings to provide flexibility in their use and accommodate different height equipment. In these facilities cooling is commonly provided by fan coil units installed at ceiling level that recirculate air in the space through the cooling coils with high velocities. Small amounts of fresh air can also be provided to the space through a separate fresh air system. The low temperatures and high velocity of air circulating in the space lead to uncomfortable environments for the workers and high energy consumption. Refrigeration systems in chilled food manufacturing facilities account for more than 60% of the energy consumption in the plant so identifying ways of improving the thermal environment in these facilities and reducing energy consumption can lead to increased productivity and profitability of chilled food operations.

This thesis makes a contribution to this challenge by investigating alternative air distribution approaches for both existing and new facilities. A primary consideration was to identify solutions that could be easily retrofitted to existing cooling systems in the space at low cost and minimum disruption to the production. The research involved the investigation of two chilled food manufacturing spaces with different cooling system arrangements to establish their performance characteristics and ability to provide the required conditions of temperature and velocities at low level in the space to minimise thermal discomfort. Learnings from these investigations were used to develop in the laboratory a test facility that could reproduce chilled food manufacturing environments at a smaller scale and enable the investigation of different cooling systems and air distribution arrangements. CFD models were also developed and validated against temperature and air velocity data from the chilled food spaces in the factories and the test facility. The models were then used to evaluate different chilled air distribution designs prior to them being manufactured and installed for evaluation in the test facility. The main objective was to achieve temperature stratification and low air velocities at low levels in the space.

Key findings and contribution to knowledge for science and technology of cold processing areas are the follow:

i)   The monitoring of the two case studies provided evidence of the air-temperature distribution issues in existing chilled food facilities such as high velocities, poor temperature distribution, cooling of the whole space and increased energy consumption.

ii)   Numerical and experimental results of this research provided guidelines of how air distribution solutions in existing chilled food facilities can be improved regarding their air temperature efficacy and energy efficiency. For example, supplying air from evaporator coils at medium level with circular or semi-circular fabric ducts as air distribution solutions, could achieve temperature stratification in the space with lower temperatures at low level covering the manufacturing area and higher temperatures towards the ceiling; In addition, medium level air supply with fabric duct was shown to provide in the region of 9% reduction in energy consumption compared to high level supply with the same duct; Furthermore, medium level air supply with a fabric duct provided 23% energy savings compared to air supply with an un-ducted fan-coil system which is the most common air distribution method in chilled food factories;

iii)   Numerical and experimental results derived guidelines of which air distribution systems should be avoided in new chilled food facilities. Tests and CFD modelling comparing air distribution with circular fabric duct and metal duct with linear diffusers showed that the circular fabric duct provided a better thermal environment in terms of temperature uniformity and low air velocities; Furthermore, comparing the air flow velocities obtained from the air distribution system via non-ducted coil and fabric ducts as air distribution solutions, it can be highlighted that the fabric duct provided much lower air flow velocities. This is beneficial to achieve some temperature stratification in the space and reduce the discomfort of the workers produced by high velocities as seen in the case of the non-ducted coil.

iv)   A simulation tool developed that couples refrigeration system and CFD modelling has been shown to be able to simulate the dynamics of air distribution and refrigeration system energy consumption in chilled food spaces. The tool can be used to optimise the design of air distribution systems from both thermal environment and energy consumption perspectives.

Acknowledgments

Contents

Table of figures

In Appendices

List of Tables

In Appendices

Abbreviation and glossary

AHU   Air handling units

HVAC   Heating, ventilation and air-conditioning

CFD   Computational fluid dynamics

ASHRAE   American society of heating refrigerating and air-conditioning engineers

CIBSE   Chartered Institution of Building Services Engineers

EES   Engineering equation solver

OC   Occupants

3D   Three dimensional

COP   Coefficient of performance

TRNSYS   Transient system simulation tool

UK   United Kingdom

DF1L   1-way lay-in displacement diffusers

DF1   Rectangular 1 way-displacement diffuser

CS-F   2-slot diffuser

L   Lights

Evap   Evaporator

Spot   Spot of measurement

BS   British standard

EN   European standards

ISO   International organization for standardization

EC   Commission Regulation

CO_2 Carbon dioxide

O_2 Oxygen

RSM   Reynolds stress model

RNG   Renormalisation-group

A/C   Air-conditioning

SST   Menter's Shear Stress Transport turbulence model

k-ε   K-epsilon turbulence model

RANS   Reynolds averaged Navier Stroke equations

k-ω   k–omega turbulence model

UDS	Upwind differencing scheme	
2-D	Two dimensional	
DE	Discrete element	
UDF	User defined functions	
PMV	Predicted mean vote	
CFA	Chilled food association	
DEFRA	Department for environment, food and rural affairs	
FISS	Food industry sustainability strategy	
GHG	Greenhouse gas emissions	

List of symbols

A	Area	(m2)
Bo	Boiling number	
Cp	Specific heat	(kJ/kg.k)
d	Thickness	(m)
D_ω	Cross-diffusion term	
D_ω		
E	Enchancement factor	
G	Refrigerant mass flux	
h	Enthalpy	(kJ/kg)
Jg	Dimensionless vapor velocity	
$\dot{m}$	Mass flow rate	(kw/hr)
P	Power consumption	(kW)
P	Pressure	(pa)
Pr	Prandtl number	
q	Heat flow per unit area	(W/m^2)
Q	Therma load capacity	(kW)
R	Thermal resistance	((m^2 K)/W)
Re	Reynolds number	
SP	Static pressure	(Pa)
S	Suppressuib factor	
S	Generalized source term corresponding to φ	
St	Stanton number	
T	Temperature	(°C)
U	Heat transfer coefficient	(W/(m^2 K))
W	Power consumption	(kW)

Xtt	Martinelli parameter	
Y	Dissipation of k and ω	
Z	Shah's correlating parameter	

α	Convective heat transfer coefficients	
Γ	Effective diffusivity	
γ	Diffusion coefficient corresponding to φ	
ε	Efectiveness	
η	Efficiency	
λ	Thermal conductivity	(W/(m K))
μ_t	Turbulent viscosity	
σ_κ	Turbulent prandtl numbers	
φ	General variable	
$\widetilde{G_k}$	Turbulence kinetic energy	J/kg

Subscript

evap	Evaporator
cond	Condenser
comp	Compressor
on	Compressor on Period
off	Compressor off Period
si	Inside surface
se	Outside surface
E air in	Air temperature entering evaporator
E air out	Evaporator discharging air temperature
Evap in	Refrigerant temperature entering evaporator
Evap out	Refrigerant temperature leaving evaporator
comp in	Refrigerant entering compressor
comp out	Refrigerant leaving compressor
c air in	Air temperature entering condenser
c air out	Condenser discharging air temperature
Cond in	Refrigerant temperature entering condenser
Cond out	Refrigerant temperature leaving condenser

Chapter 1.   Introduction

The chilled food industry has shown significant growth in the last three decades. Based on data from the Chilled Food Association (CFA) the chilled food industry in the UK grew from £550m in 1989 to £12,000m in 2017. In recent years, chilled food manufacturing in the UK has experienced annual increases of around 10 %. The industry also has high environmental impacts, and to reduce these, the CFA, has set ambitious goals. These are (CFA, 2012):

- Achieve a 30% reduction in CO_2 emissions by 2030 compared with 1990, and 40% by 2023.

- Make significant reductions in water use to help reduce stress on water supplies and contribute to meeting the Defra's Food Industry Sustainability Strategy (FISS). Absolute target is to reduce water use by 20% by 2020 compared to 2007.

- Support ethical sourcing practices incorporating sustainability principles.

The chilled food chain relies heavily on refrigeration for the maintenance of low temperatures during processing, transportation and retail of chilled food products. Refrigeration systems in the UK cold food chain are estimated to be responsible for 16,100 GWh energy use and 13.7 MtCO2e Greenhouse Gas Emissions. These represent approximately 28 % of final energy use and 7 % of GHG emissions of the whole food-chain (Defra 2012). In chilled food processing facilities, refrigeration can account for up to 60 % of the total energy consumption.

Chilled food products have short shelf lives and need to be processed in facilities at temperatures in the range between +4 to +12 ºC depending on the type of product (below 7°C for red meat, below 5°C for white meat and below 12 ºC for salad), processing time and the desired minimum shelf time. Current food processing takes place in large spaces with high ceilings. In these spaces cooling is normally provided by ceiling mounted fan coil units, drawing air from the space and discharging it at high velocity directly back to the space. For the system to be effective, large air circulation rates and air velocities are required which, combined with the low temperatures, cause high energy consumption and in most cases, discomfort for the workers in the space. Therefore, air distribution is an essential factor that needs to be carefully considered in order to create an environment capable of maintaining food quality and shelf live without excessive energy consumption and worker discomfort.

Mixing ventilation is the most commonly used air distribution method in chilled food processing environments by which air is mixed through the entire room volume. This results in fairly uniform environments in terms of temperature and contaminant concentration but leads to energy wastage as all of the air in the space is cooled to low temperature even though only the air at low level, just above the food processing lines needs to be maintained at low temperature for food safety and shelf life.

Localising the low temperature only to areas occupied processing activities will lead to significant energy savings. The challenge is to achieve these energy savings in existing chilled food factories within the techno-economic frameworks. In order to succeed this task the completely renewal of the existing chilling equipment may be prohibitive. As a result the air distribution solution should be capable to be adapted by the existing refrigeration equipment. Furthermore, the air distribution solution must be designed in a way that will comply with the hygienic standards of air distribution systems in food factories and ensure that the staff comfort would not be affected in a negative way.

1.1   Research project description

The scope of this research is to improve the efficiency of cold air distribution in chilled food processing areas. Improved temperature distribution should lead to the reduction of the overall energy consumption of the refrigeration plant. To date, there has been very little work reported in the literature on air distribution systems and energy consumption of chilled food processing areas.

This research focused on understanding, the air flow and temperature variation in existing chilled food facilities using measurements and CFD modelling. In addition, this research deals with experimental investigations of different air distribution methods. A modelling tool based on computational fluid dynamics was developed in order to simulate the air flow and the thermal environment of chilled food facilities. Once the CFD model was validated, it was then used to investigate the air flow and temperature distribution from different air distribution systems. Taking into account the modelling results the most promising air distribution approaches were selected to be constructed and assessed in the laboratory. The experimental study was used to identify the most appropriate approaches in terms of temperature stratification in the space and the energy consumption of the refrigeration system.

Finally, a transient simulation tool was developed in order to identify the energy impact of different air distribution systems. The transient simulation tool involved the coupling between the CFD air distribution model with a numerical model that simulated the refrigeration system, hence the consumed energy. This coupling tool was validated through experimental measurements. This coupling tool can be used in order to define and design an energy-efficient air distribution system.

1.2   Research objectives

The primary objective of this research is to improve the efficiency of cold air-temperature distribution in chilled food processing areas. Improved air distribution should lead to the reduction of the overall energy consumption of the refrigeration plant. The main objectives of this research are summarised as follows:

Objective 1:

Conduct a detailed literature review covering the background of this study. This literature includes the understanding of air distribution in cold rooms and food regulation regarding temperature control. CFD modelling procedures and their effectiveness in predicting air temperature and velocity profiles in cold rooms and large spaces. In addition, the review covers thermal comfort for chilled food factories.

Objective 2:

Monitor two existing chilled food facilities and analyse the results to understand the air temperature and velocity distribution in existing facilities and conventional cooling systems. Develop and validate a scaled test facility replicating at small scale, chilled food facilities and air distribution systems currently in operation in the UK.

Objective 3:

Develop and validate a 3-D CFD air distribution model capable of predicting the air temperatures and velocities in the space. Use the developed CFD model to investigate different approaches of air distribution methods.

Objective 4:

Implement the most promising air distribution methods in the scaled test facility in order to identify the most appropriate approaches in terms of temperature stratification in the space and the energy consumption of the refrigeration system.

Objective 5:

Develop and validate a refrigeration model on the EES platform. Integrate and validate the CFD/EES model. Apply the CFD/EES integrated model to a section of a chilled food facility in order to evaluate the energy efficiency of different air distribution systems.

1.3 Structure of thesis

This thesis consists of nine chapters. **Chapter 1** provides an introduction to the chilled food industry and its heavy reliance on refrigeration. Chapter 1 also provides a general description of the thesis, the research scope and objectives. **Chapter 2** provides an overview of information related to the background of the research. **Chapter 3** presents the monitoring of two existing chilled food production facilities using different air distribution systems. **Chapter 4** presents the development and testing of a scaled facility representing a section of an actual chilled food processing room.

Chapter 5 provides a description of the development of a 3-D CFD air distribution model capable of predicting the air temperatures and velocities over the space. In addition, the developed CFD model was validated through measurements taken in two existing chilled food facilities and from the developed scaled facility monitoring. **Chapter 6** presents the investigation and evaluation of different air distribution systems with the developed 3-D CFD modelling tool. The aim was to identify the most appropriate approach in terms of uniform temperatures and low velocities at horizontal level and temperature stratification from floor to ceiling. **Chapter 7** presents the experimental study of different air distribution systems applied to chilled food production facilities. The experimental study was used to identify the most appropriate approaches in terms of temperature stratification in the space and the energy consumption of the refrigeration system.

Chapter 8 presents the development of an EES model capable to predict the performance of the refrigeration system under different conditions. In addition, Chapter 8 presents the novel development of a coupling tool integrating the CFD air distribution model and the EES refrigeration model. The coupling can be used to design optimum air distribution systems in terms of air conditions in the space and energy consumption. **Chapter 9** details the conclusions of this research and identifies areas for further work.

1.4 Publications

The research has resulted in a number of outputs that have been published in the form of journal papers, conference proceedings and a book chapter. These are detailed below.

Journal Publications:

Parpas, D., Amaris, C. and Tassou, S.A. (2017) "Experimental investigation and modelling of thermal environment control of air distribution systems for chilled food manufacturing facilities", Applied Thermal Engineering 127C (2017) pp. 1326-1339

Parpas, D., Amaris, C. and Tassou, S.A. (2017) "Investigation into air distribution systems and thermal environment control in chilled food processing facilities", Journal of refrigeration (under revision)

Book Chapters:

Co-authored, 'Modelling cold food chain processing and display, environments' S.A. Tassou, B.L. Gowreesunker, D. Parpas, A. Raeisi. In Modelling of Food processing Operations, Woodhead Publishing, 2015, Pages 185–208, 2015. doi:10.1016/B978-1-78242-284-6.00007-6

Conference Publications:

Parpas, D, S.A. Tassou, B.L. Gowreesunker, A.H. Raeisi "Air Distribution and Temperature Control in Chilled Food Manufacturing Facilities" IIR 2014 / 23rd – 25th June, St Mary's University College, Twickenham, London

Parpas, D, C. Amaris, S.A. Tassou, B.L Gowreesunker "Investigation into air distribution systems and temperature control in chilled food manufacturing facilities" SusTEM 2015 Sustainable Thermal Energy Management Network, 3rd Sustainable Thermal Energy Management Int. Conf., Newcastle upon Tyne, UK, 7-8 July, (2015) 110-119.

Parpas, D, Carlos Amaris, Savvas A. Tassou "Experimental study and modelling of air distribution systems and temperature control in a scaled test facility for chilled food factories" SET 2015 / 14th International Conference on Sustainable Energy Technologies, Nottingham, UK, 25 – 27 August, (2015),Volume II, pp 85-95

Parpas, D, Carlos Amaris, Savvas A. Tassou "Coupled Air Flow and Refrigeration System Modelling for Chilled Food Manufacturing Facilities" EFFoST 2015 / 10th – 12th November, Athens

Parpas, D., Amaris, C., Sun, J., Tsamos, K.M. & Tassou, S.A. 2017, "Numerical study of air temperature distribution and refrigeration systems coupling for chilled food processing facilities", Energy Procedia, vol. 123, pp. 156-163.

Chapter 2.   Literature review

2.1 Introduction

Refrigeration systems consume a big portion of the overall chilled food factories energy consumption. The refrigeration systems are used to maintain the food freshness, quality and nutritional value by conditioning the air temperature and humidity during the follow stages: (Bryan Hackett 2005)

- Initial Cooling/ Quick Freezing
- Cooling during processing
- Storage in cold rooms

Depending on the type of chilled product being processed, the processing facilities are normally maintained at temperatures in the range between +4 and +12°C. During the production process, the food product passes through different equipment and any temperature and humidity heterogeneity can affect its quality (Laguerre, 2013). It is therefore very important to maintain constant temperature and humidity conditions in food processing areas and in particular around the processing equipment.

2.2 Food regulations regarding temperature control

EC Regulation 852/2004 contains general requirements regarding the temperature control for food products. In general, EC Regulation 852/2004 defines that any 'raw materials, ingredients, intermediate products and finished products likely to support the reproduction of pathogenic micro-organisms or the formation of toxins are not to be kept at temperatures that might result in a risk to health. The cold chain is not to be interrupted. However, limited periods outside temperature control are permitted, to accommodate the practicalities of handling during preparation, transport, storage, display and service of food, provided that it does not result in a risk to health'.

Regarding the limited periods that food products can be held outside temperature control the specific national requirements for England, Wales and Northern Ireland set out the permitted times and conditions and should be taken into account. Considering the cooling procedure, EC Regulation 852/2004 defines that any food product that is to be held or served at chilled temperature must be cooled as quickly as possible following the heat-processing stage, or final preparation stage if no heat process is applied, at a temperature that will prohibit any risk to the consumer health (EC Regulation 852/ Annex II, Chapter IX, 6 states).

The National Food Hygiene Regulations of 2006 requires that in England, Wales and Northern Ireland, food products which are likely to support the growth of pathogenic micro-organisms or the formation of toxins, must be held at or below 8°C, or, at or above 63°C. Some exemptions are allowed from the requirements mainly for practical considerations (for example processing or handling). In the cases that food products are not likely to support the growth of pathogenic micro-organisms or the formation of toxins and thus are not covered by the requirements, it may be advantageous that are maintained at or below 12°C to maintain freshness and quality and extend shelf-life.

2.3   Air temperature distribution in cold rooms

In the majority of chilled food processing facilities, air temperature is maintained at permitted levels by convection heat transfer systems. Therefore, air distribution is an essential parameter that needs to be carefully studied in order to create a proper environment capable of maintaining food quality.

The air distribution pattern can be obtained from experimental tests and from flow visualization studies. Airflow models have also been developed over the last 30 years in order to provide a better understanding of the air distribution in cold rooms. The most powerful tool that is used nowadays to study complex air flows and temperature distribution is CFD (computational fluids dynamics). CFD modelling can also be used to optimize the refrigeration system design and reduce the overall energy consumption of the thermal environment control system in chilled food manufacturing facilities.

2.4   Air temperature patterns in large spaces

The air distribution patterns in large spaces can be obtained from experimental tests including flow visualisation studies and from modelling approaches. Studies to date have focused on air distribution in large spaces in commercial buildings for ventilation and air conditioning applications to provide thermal comfort for the occupants and reduce energy consumption and on cold rooms where the priorities are to maximise the holding volume and provide uniform temperatures in the space.

Very little work has been reported in the literature on air distribution in chilled food factories where the objective is to maintain the temperature at low levels for food safety and quality at the expense of high energy consumption of the refrigeration plant.

Therefore, improvement of the efficiency of the cold air distribution in chilled food processing areas is important in reducing the energy consumption of the plant.

Airflow modelling techniques such as Computational Fluid Dynamics (CFD) have become popular in recent years as they provide a better understanding of air flow and temperature patterns in different situations in comparison with time-consuming and costly experimental tests. For instance, Rees et. al. (2013) studied experimentally the air flow mixing and overall temperature gradient in a room with displacement ventilation and chilled ceiling for office environments. Cheng et al. (2013) analysed the effect of different locations for the supply and return grilles on thermal comfort and energy savings. The authors showed that temperature stratification in the space can provide both energy savings and thermal comfort for the occupants. Fathollahzadeh et al. (2015) studied the effect of using two types of inlet diffusers (direct and swirl) with combined and separate return and exhaust air vents on the thermal comfort, indoor air quality and energy consumption in an indoor environment. Main results showed that the energy consumption of the system decreased by reducing the height of return air vent from ceiling to floor height.

Lin and Tsai (2014) studied the effect of supply diffuser position and supply air flow rate on the thermal environment of an indoor space. The authors reported that for a given diffuser, the temperature gradient in the space reduces as the supply air flow increases due to greater mixing between the space and supply air. Jurelionis et al. (2015) investigated the impact of the air supply method on the ventilation efficiency in a test chamber. In this investigation, the aerosol particle dispersion with different air distribution methods was analysed. For this method application aerosol particles are injected into the test chamber. The concentration of particles is measured in different sections of the room usually for 10 minutes after the injection using optical particle counters in order to evaluate the effectiveness of the ventilation systems. Results showed that the one-way mixing ventilation ceiling diffuser with low flow rate was more efficient compared with four-way mixing and high air exchange rate diffusers. Rhee et al. (2015) evaluated the performance of an active chilled beam system in terms of thermal environment uniformity in a full-scale test bed. The authors reported acceptable thermal uniformity with the active chilled beam system even at low air flow rates.

Moureh et al. (2005) analysed the velocity characteristics throughout a long ventilated enclosure considering different inlet flow arrangements. The authors employed the high and low Reynolds number form of the two-equation k–ε model and the Reynolds stress model (RSM). According to the results, the RSM was able to predict correctly the general behaviour of primary and secondary air flow recirculation. Subsequently, Moureh et al. (2009a,b) investigated the airflow patterns above and within an enclosure with vented boxes. The authors found that the RSM turbulence model represent reasonably well the air ventilation level values obtained by experimentation.

2.5 CFD modelling procedure and importance

Airflow modelling techniques such as Computational Fluid Dynamics (CFD) have become popular in recent years as they can provide a better understanding of the air flow and heat transfer processes in complex air flow and heat transfer problems. CFD can be used to simulate any problem that can be solved numerically (heat transfer, phase change of a material, mechanical movements, chemical reactions etc). The CFD model/simulation process can be divided into three stages (Smale, 2006):

- Pre-processing
- Solving
- Post-processing

Pre-processing is the stage where the user choses the domain to represent the problem under investigation. After the computational domain definition, the domain is subdivided into smaller elements in order to create the 'mesh' to be used for the simulations. The mesh creation and the size of the elements is determined by the desired accuracy of the results. Where high accuracy is needed the elements dimension should be decreased. The user should be aware that once the elements dimension is decreased the simulation time and the required memory will be increased (powerful computer is needed). Therefore the mesh creation should be carefully implemented to the actual requirements of the problem. The remaining steps of the pre-processing is to define the fluid properties and the boundary conditions. In order to create a realistic model, the user must have deep knowledge's concerning the problem physics and be aware of all the factors that can affect the results. The main factors that can affect the modelling results are improper mesh generation, wrongly defined boundary conditions, non-steady boundary conditions and post-processing user errors.

Solving is the procedure by which the partial differential equations that describe the problem are numerically solved. The user must choose between dynamic and steady state simulation. Dynamic simulation is used when the process variables change with time and the modelling needs to capture the variations. Dynamic simulations take longer time to be solved. In the case of chilled food factory manufacturing areas, dynamic simulation should be used to simulate the air flow and temperature patterns in the space as these change with the process and controls of the cooling systems. Conditions varying with time include the external weather conditions, the internal heat gains, occupancy density etc.

Post-processing is the process by which the user interprets and evaluates the simulation results. For this to be successful, a map must be created over the mesh domain to display and visualise the results.

As it was described before, the main heat transfer mechanism in cold rooms is convection. As a result, the air distribution pattern should be able to maintain the air at set point temperature by removing the heat from the internal and external heat gain sources. Solving Air Distribution models in CFD is complex and the user should be aware of all the factors that can influence the results.

2.6 CFD modelling for predicting air temperature distribution in cold rooms

A mathematical model in CFD can be applied to simulate flow and heat transfer processes in two or three dimensions. Three dimensional models are significantly more computationally intensive than two dimensional models and are normally used when there is no symmetry in the flow domain. The following paragraphs review literature on the use of CFD modelling of air flows in large indoor conditioned spaces. The accepted prediction errors percentage in CFD modelling depends from the type of application. In the case of chilled food factories, chilled food products enters the production rooms for a limited period of time. Before and after the production rooms chilled food products are usually kept in cold stores. Any small temperature fluctuations in the range of $\pm 2\,^{\circ}C$ are accepted. Therefore, for the case of chilled food production facilities, air temperature CFD prediction errors in the range of $\pm 2\,^{\circ}C$ is accepted.

A large number of CFD models have been developed and applied in recent years for the simulation of air flow and temperature distribution in cold rooms. Some are described here. Nahor et al. (2005) developed a transient 3-D CFD model using the k-ε turbulence model in order to predict velocity, temperature and moisture distribution in an existing empty and loaded cold store. The heat of respiration, heat and mass transfer coefficients, saturated partial vapour pressure and the latent heat of evaporation were calculated using the equations and correlations reported by Hoang et al. (2003). Regarding the velocity magnitudes, the results showed a 22 % average accuracy inside the empty cold store and 20% average accuracy inside the loaded cold store. Air and product temperatures were predicted with reasonable accuracy.

Xie et al. (2006) developed a simplified 2-D CFD model to predict the air flow and temperature patterns in a cold store and investigated factors that influence the uniformity of those patterns. They used constant-property Boussinesq fluid as a reference and assumed a 2-dimensional incompressible turbulent flow. They used the k-ε turbulence model in the simulations. Experimental tests showed that the approximations used in the model limited the quantitative accuracy of the results but nevertheless led to a simplified and practicable model that can be used to predict the air flow and temperature patterns in a cold store.

Smale et al. (2006) reviewed CFD modelling for the prediction of airflow in refrigerated food storage applications. They reported that the k-ε turbulence model was not accurate enough to be used in many refrigerated food storage applications because it could not predict well the Coanda effect over the wall jets and under adverse pressure gradients. Also, none from the k-ε , LRN k-ε, two layer k-ε, two scale k-ε and RNG k-ε models could predict the presence of secondary recirculation flow. In contrast the RSM (Reynolds Stress Model) was found to be able to predict the separation between the wall jets and the airflow patterns related to primary and secondary recirculations.

Chourasia and Goswami (2007a,b,c) developed a three dimensional model to predict the airflow, temperature distribution and moisture loss in a potato loaded cold room. They applied the RNG k-ε turbulence model with the finite volume solution technique. The potato bulk was considered as a porous medium. The model predictions were compared with experimental data. Average overall errors of 19.5%, 0.5°C and 0.61% were found for air velocity, product temperature and moisture loss from the potatoes respectively.

Chanteloup and Mirade (2009) developed a model to predict the local mean age of the air in a ventilated food storage space using CFD. Local mean age of air is a useful indicator of air change efficiency. The mean age of air is defined by the time that contaminated air has spent in a zone of a space which can be helpful to assess the quality of ventilation. They implemented 3 different modelling methods, two transient and one steady state. All predictions were compared with experimental data and the errors did not exceed 20%. The optimum method in terms of prediction accuracy and computational time was found to be the steady-state. This method was then used to identify the ventilation efficiency of the space. The Navier-Stokes equations with the k-ε turbulence model and first-order upwind differencing discretisation scheme were employed to predict the air temperature and relative humidity distribution patterns.

Delele et al. (2009) applied multi-scale CFD to predict air velocity, temperature and humidity distribution in a loaded cold room. The stacked products were considered as a porous medium and their loss coefficient was derived from the DE-CFD model combination. The authors tested four different two-equation eddy-viscosity turbulence models and compared the results against experimental measurements. The four different models with their individual prediction accuracy regarding the air velocity were the Standard k-ε model with 24.3 % error, Realizable k-ε model with 23.5 % error, RNG k-ε model with 22.4 % error and Standard k- ω /SST k-ω models with 18.2% error.

Ho et al. (2010), studied air velocity and temperature distribution for a refrigerated space with steady state airflow and heat transfer using a 3-D and a 2-D model for comparison purposes. They used the finite element method for the CFD modelling and considered the air inside the cold room as an incompressible fluid with constant properties. Furthermore, it was assumed that the fluid density variation affected only the temperature. From the comparison between the 3-D and 2-D model results, they concluded that the two models were in good agreement. As a result they concluded that 2-D modelling can be employed with good accuracy.

Ambaw et al. (2013) reviewed the application of CFD for the modelling of post-harvest refrigeration processes. They identified the most common solution method to be the finite volume method with the upwind differencing scheme (UDS). In addition, it was reported that the Reynolds Stress model (RSM) provides more accurate predictions compared to the conventional k-ε model, but the k-ε model is more commonly used due to its lower

computational requirements. For air velocity prediction, the SST- k-ω model produced the smallest error compared to the RSM and k-ε models.

Delele et al. (2013) developed a 3-D model in CFD in order to predict air-flow and heat transfer characteristics of a horticultural produce packaging system. In contrast to previous studies which considered the bulk of the product as a porous media due to the limitations in computational power and time, such as that of Tassou and Xiang (1998). Delele's study took into account the detailed geometry and properties of the packaging material. The air flow in the space was solved using the Reynolds averaged Navier Stokes equations (RANS). A tetra-hedral hybrid mesh was applied for the discretisation of the computational domain and enhanced wall functions were considered for the model. They applied a transient simulation with a time step of 180 s (50 iterations per time step) and the governing equations were discretised using a second order upwind scheme. The standard k-ε, RNG k-ε and standard k-ω two equation turbulence models were considered and the SST-k-ω was found to produce the most accurate predictions. Validation was performed against experimental values and the prediction error was calculated using the absolute relative deviation of predicted results from measured results. Comparison between predicted air pressure drop and produce temperature and measured values showed a good agreement with an average relative error of 13.80% and 16.27%, respectively.

Laguerre et al. (2015), in order to avoid the computational time of a CFD model, created a simplified model of a cold room using the knowledge obtained from experimental measurements of air velocity, air temperature and food product weight losses. The model was separated into zones and heat balance equations for each zone were developed. The simplified model was found to predict the product cooling rate and the final product temperature at different positions in the cold room quite well.

Ning et al (2016) used CFD to evaluate the effects of supplying air at different heights in the space on the ventilation performance of an air conditioning system. In this study, the SST turbulence model was used to predict the air velocity and temperature fields inside a room. Results suggested that supplying air at a lower level can be beneficial in terms of both saving energy and CO_2 removal from the breathing zone. Pasut et al (2014) simulated underfloor air distribution via fabric ducts and rigid ducts. The authors mainly focused on the analysis of the discharge air temperature and flows through the diffusers.

The k–e turbulence model was employed in the CFD model. The authors also conducted experiments in a full-scale underfloor plenum in order to validate the developed CFD models. Experimental and numerical results proved that by using fabric ducts to directly discharge supply air into the perimeter plenum "reverses" the typical temperature distribution, with colder air in the perimeter and warmer air in the interior zone.

2.7 Thermal comfort

Thermal comfort in an environment is mainly affected by the following parameters:

- Air dry-bulb temperature
- Radiant temperature
- Relative humidity
- Air velocity/ air movement
- Activity and clothing/metabolic rate

These parameters need to be considered in order to provide a satisfactory living and working environment. In addition individual personal characteristics such as age, sex level of fitness and the length of time an individual is exposed to cold or warm environments should be considered.

During the 1960s, international thermal comfort standards were developed based on a large number of experiments (BRITISH STANDARD, 2005). These thermal comfort standards create a narrow range of acceptable indoor environment conditions. In order to achieve these conditions in a building, high amounts of energy are needed. The adaptive thermal comfort approach shows that people can accept a wider range of environment conditions than the one predicted by the PMV method (BRITISH STANDARD, 2005). The adaptive thermal comfort approach is based on the theory that people adapt to their thermal environment. The adaptive behaviour of the occupants will allow a wider range of acceptable indoor conditions in cold or warm environments which can reduce energy consumption.

2.7.1 *Thermal comfort at chilled food factories*

Chilled food factories have a high demand on productivity and any potential delays to the production lines can cause large financial losses. Employers and operators are obligated by law to provide information, instruction, training and supervision to all the employees

that are working in cold storage facilities in order to perform their work in a safe manner and without any risk to their health (HSE, 2007).

The thermal conditions required in chilled food factories to satisfy food quality and safety requirements, 6-12 ℃, do not match the thermal comfort requirements of the workers in the factory which depending on the air velocities in the space, activity and clothing insulation level could range between 14 ℃ to 18 ℃.

Health and safety regulations specify that temperatures in an indoor workplace shall be reasonable and at least 16℃ (HSE, 1999). For lower temperatures measures are required to be taken which apart from clothing with suitable thermal insulation properties include reduction of air velocities and drafts.

The environmental conditions required in a chill food factory to satisfy food quality and safety can create health risks for the workers. A cold environment can be defined as the environment that may result in a greater thermal loss to the body than it can tolerate. In such situations cold stress symptoms can occur such as:

- Shivering and vasoconstriction
- Increased oxygen consumption and accelerated respiration
- Elevated blood pressure and increased cardiac output

Furthermore, cold environments can cause hypothermia to an occupant. Hypothermia is the phenomenon when a human body loses heat faster than it is produced. The potential risk of hypothermia and the impact of cold stress should be recognized by the employers who should ensure a safe environment for their employees. Measures to achieve this include (HSE 2007):

- Time limits for working at a cold environment (Body activity/duration of occupant exposure to the cold environment).
- Mandatory rest periods to be spend in easily accessible warm rooms
- Sufficient provision of protective clothing and footwear that are suitable for cold environments
- Employees task rotation within workplaces at higher operating temperatures
- Sufficient supervision/ appropriate training on cold hazards/ proper first aids facilities

- Eliminate physical activities that can cause sweating resulting in a decreased body temperature

- Medical examinations and health monitoring

2.8 Traditional air distribution systems

During the design stage of a cold facility the following guidelines should be taken into account in order to minimise/eliminate the risk of exposure to thermal stress:

- The positioning of the refrigeration equipment (air flow outlets/inlets)

- The air supply/return direction and velocity provided from the refrigeration equipment

- Design should be implemented for minimum draughts and air velocities.

The traditional and most used way of air distribution in occupied spaces is called mixing ventilation. Mixing ventilation systems supply conditioned air at high velocity through a supply diffuser (usually at ceiling level) and recycle the conditioned air through a return diffuser, Figure 2-1. As a result, the air is mixed through the entire room volume without allowing any temperature stratification to occur. These systems results a uniform temperature and contaminant concentration through the space volume.

This type of systems can work efficiently at spaces with a maximum height of 2.4 meters (Price Engineer's 2013). In a space with height greater than 2.4 meter the unoccupied volume at high levels will also be air conditioned and this will lead to energy wastage.
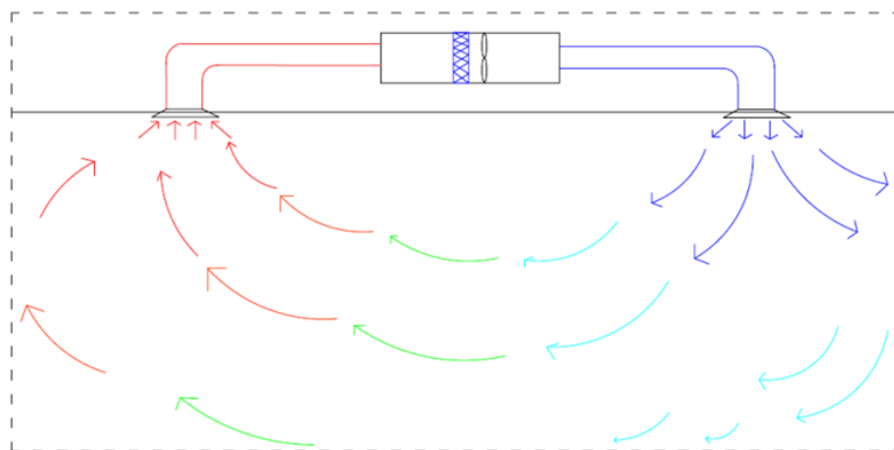
Figure 2-1. Mixing ventilation system

2.9 Displacement ventilation

Displacement ventilation is an air distribution system that produces a comfortable indoor environment by supplying low-velocity (0.1-0.2m/s) cool-air (2-6 ℃ below room temperature, at low level into an occupied space, Figure 2-2, (Halton 2013).
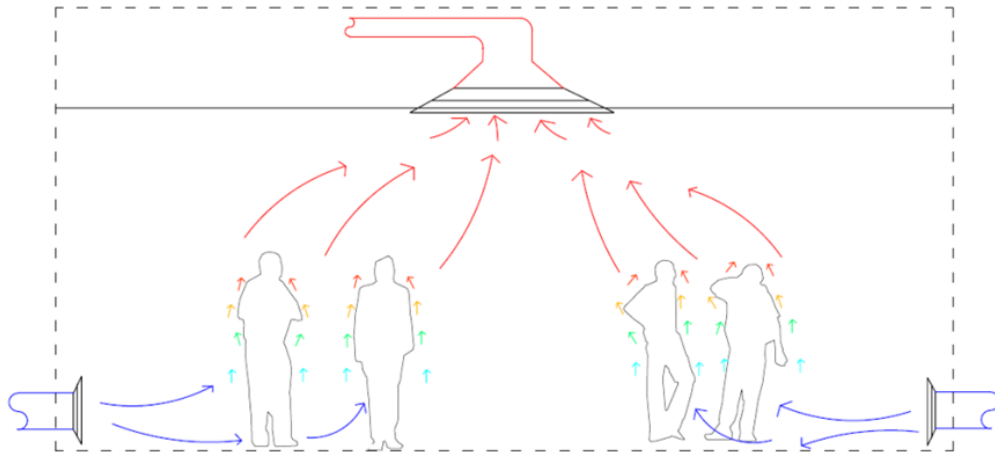
Figure 2-2. Displacement ventilation

In contrast with mixing ventilation, displacement ventilation systems supply conditioned air at low level and exploits the internal heat gains (people, lighting, equipment etc.) to generate buoyancy forces and create a thermal plume to drive the air to higher levels in the occupied space (cooling mode). This system creates temperature stratification through the different heights of the space. Temperature stratification in these systems is directly influenced by the follows factors (Price Engineer's 2007):

- Supply air volume rates and temperature
- Cooling load and set point temperature
- Internal heat gain types and locations
- Height of the ceiling and location of the diffusers

2.9.1 *Displacement ventilation design*

Despite the fact that displacement ventilation systems supply the air at higher temperatures, the critical factor that will determine any potential energy savings is the temperature difference between the supplied and the returned air. The displacement ventilation supply/return air temperature difference should be lower than that for mixing ventilation systems to achieve energy savings (Halton 2013, Skistad 2003, Price

Engineer's 2007). The design should be carefully implemented in a way that will prevent any potential draught along the floor that will lead to occupant's discomfort. The big challenge of a displacement ventilation design is to manage to supply large amounts of volumetric air flow rates through the diffusers without causing discomfort. In order to avoid drafts the supplied air must be supplied at low velocity and be uniform spread across the floor.

2.9.1.1 *Displacement ventilation advantages / disadvantages*

The main advantages of displacement ventilation systems are the following (Lau and Chen 2006, Halton 2013, Skistad 2003):

- A more comfortable environment in terms of air quality and thermal comfort (in commercial and industrial applications improved occupant comfort leads to an increased productive environment)
- Potential energy savings by supplying the air at lower velocity and higher temperatures (Refrigeration plant operates at higher efficiencies reducing the consumed energy and providing energy savings 15-20 % depending on the local climate and the type of the building).
- Potential use of free cooling (higher supply temperatures leads to longer periods of free cooling)
- Higher ventilation efficiency compared with mixing ventilation systems

The main disadvantages of the displacement Ventilation systems are the follow:

- Displacement ventilation needs larger diffusers
- Limitations in the maximum cooling capacity (119 W/m²) in order to ensure thermal comfort (Price Engineer's 2013)
- Higher supply air temperatures lead to lower dehumidification capacity.

2.9.1.2 *Typical applications of displacement ventilation*

Displacement Ventilation has been successfully used in a wide variety of different type of buildings. Some of these are:

- Schools/ Open plan offices
- Restaurants/ Theatres/ Casinos
- Industrial spaces/ Hospitals/ Supermarkets

2.9.1.3 Displacement ventilation Contaminant Distribution

Contaminant distribution influences significantly the indoor air quality. The indoor air quality is an important parameter that affects occupant comfort and compliance with hygiene standards. The contaminant distribution is directly influenced by the air distribution method. In displacement ventilation systems the air is moving with an upward direction from the low level diffusers to the extract diffusers at ceiling level. This upward motion of the air can drive the contaminants to the unoccupied high level of the space creating a better environment in terms of air quality (Figure 2-3), (Price Engineer's 2013).
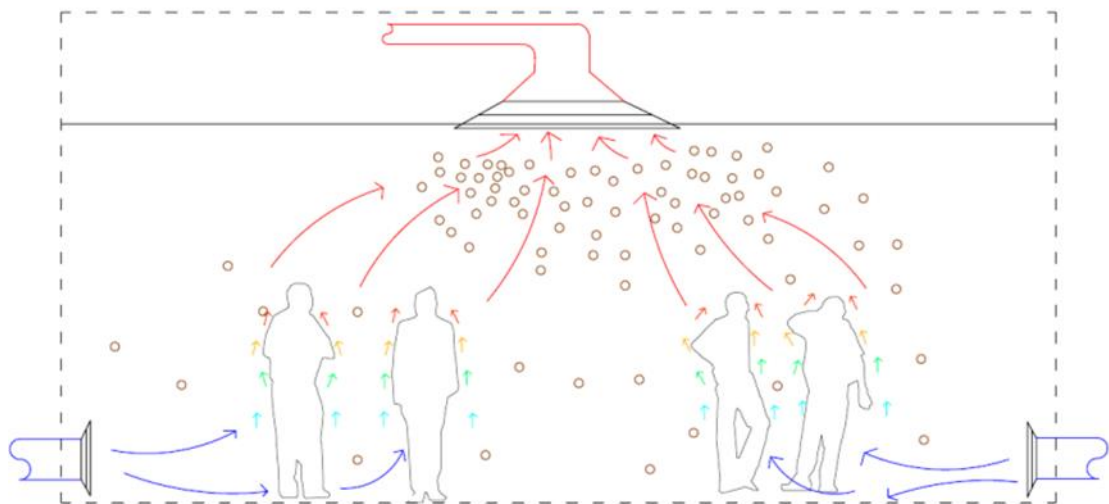
Figure 2-3. Displacement ventilation - Contaminant distribution

During the design stage of a displacement ventilation system the contaminant source and type should be studied. If the contaminants are heavier than the indoor ambient air, then they need to be extracted at low level. As a result, displacement ventilation may not be appropriate in these cases.

2.9.1.4 Favourable conditions for displacement ventilation appliance

In order to apply a displacement ventilation system the characteristics of the space must comply with the following: (Halton 2013, Skistad 2003, Price Engineer's 2007)

- High levels of specific air flow rate per m² (3-10l/s per m² theatres, conference rooms etc.)
- High air flow ventilation rates per person (more than 15-20 l/s per person)
- High levels of contaminant concentration and heat dissipation (smoking areas, industrial spaces etc.)

- Spaces with a ceiling height greater than 3 meters

- Moderate Cooling loads (25-80 W/m²)

- Contaminants are lighter than the indoor air

2.9.1.5 *Displacement ventilation at heating mode*

If the heating loads are low enough (20-40 W/m²), displacement ventilation systems can be also be used for space heating without any changes to the system. Nevertheless, the system will operate like a mixing ventilation system during the heating process. In this case the return air diffuser should not be placed directly above the supply diffuser in order to avoid short circuits of the hot air supply that will lead to the occupied space being bypassed by the heating system. If the heating loads are higher than the capabilities of the system, there are some alternative solutions that can be used. These solutions are:

- Diffusers with integrated heaters

- Displacement ventilation combined with hydronic systems

- (floor heating, radiant heating, convectors)

2.9.2 *Displacement ventilation thermal comfort*

The target of displacement ventilation is to achieve a high Energy Efficient Building, without causing a negative effect on indoor air quality and thermal comfort. Potential draughts along the floor that will lead to occupant discomfort should be prevented. Generally, in order to avoid discomfort the supply diffusers should be placed at least 0.6m away from an occupant and the supply air velocity about 0.1-0.20 m/s (Price Engineer's 2007). The stratification should be designed and controlled in a way to ensure that the temperature difference between head height and floor does not exceed 3.6º C for standing persons and 3.0º C for seated persons in order to avoid occupant discomfort (ASHRAE Standard 55:2010).

Displacement Ventilation compared with mixing ventilation systems, could provide an improved environment for workers in cold environments. They may also lead to higher supply air temperatures, lower air supply velocities and lower energy consumption. These characteristics will be investigated in this thesis.

2.10 Summary of Chapter 2

This chapter provided a literature review covering the background of this study. The literature provided understanding of air distribution in cold rooms and the application of CFD techniques for the modelling of air velocity and temperature distribution. It was identified that no previous study was reported on the investigation of air supply in chilled food processing facilities with the aim to establish temperature stratification in the space.

The following chapter presents an investigation of air distribution systems in two actual chilled food manufacturing facilities. Data of temperature and velocities at different locations were collected from the two facilities in order to establish the thermal environment of the spaces.

Chapter 3. Existing chilled food facilities monitoring

3.1 Introduction

The scope of this research aims to improve the efficiency of cold air-temperature distribution in chilled food processing areas. Improved air-temperature distribution should lead to the reduction of the overall energy consumption of the refrigeration plant. The first stage of this research focuses on understanding the air flow and the temperature variation in existing chilled food production facilities. Two existing chilled food production facilities (case study 1 and case study 2) using different air distribution systems were monitored. The monitoring of the facilities was implemented in order to understand the temperature and velocity distribution in the space and also to validate the CFD models.

Temperature control in these facilities is achieved by cooling-coils operating with 100 % of recirculated air and controlled by individual thermostats. Fresh air is supplied periodically in the space at room temperature without providing any contribution to the cooling process.

Temperature and relative humidity data were collected using HOBO U12-013 type data loggers (TEMPCON 2016) which were installed along the length at three different heights (knee level, head level and ceiling level) in the space. The data were logged every 5 minutes over a 14 days period. Air velocity, air dry-bulb temperature and relative humidity were also measured at the 3 different heights using a portable meter TSI TA465-P with a thermoanemometer articulated probe 966 (TSI AIRFLOW INSTRUMENTS Ltd 2016). Based on the type and the arrangement of the air distribution systems, for a better view and understanding of the airflow direction, measurements in two directions were applied (longwise and widthwise the facilities) for each measurement point. The logging interval of the instrument was set to 1 second and data were averaged over a period of 1 minute.

In order to measure at different heights, the TSI meter was attached at a telescopic pole. The portable measuring tool is indicated at Figure 3-1. The logging interval of the instrument was set to 1 second and data were averaged over a period of 1 minute. Table 3-1 presents the measurement uncertainties of the sensors used.

Table 3-1. Sensor and measurement uncertainties

Sensors	Range	Uncertainty
HOBO – Temperature Sensor (ºC)	0 to 50	± 0.35 ºC
HOBO – RH sensor (%)	10 to 90	± 2.5 %
Thermoanemometer – Temperature Sensor (ºC)	-10 to 60	± 0.30 °C
Thermoanemometer - Air flow meter (m.s^{-1})	0 to 50	± 3.0 %
Thermoanemometer - RH sensor (%)	5 to 95	± 3.0 %

Figure 3-1. Portable measuring tool

3.2   Case study 1: Air distribution via supply/return diffusers

The dimensions of case study 1 chilled food processing area under investigation are 17 m wide, 40 m deep and 4 m high. Case study 1 chilled food factory is located in UK in the area of Newark-on-Trent. Figure 3-2 shows the space geometry of case study 1. The HVAC system consists of 4 individually controlled Air Handling Units (AHU) installed in the roof void, supplying air to the space through 4 diffusers at each AHU. The location of the diffusers and the measurement points are shown in Figure 3-3, which is a plan view of the facility. In addition, the horizontal black lines in Figure 3-3 indicates the production

lines locations over the facility. The arrows indicate the diffusers fins which were adjusted by the occupants. The portable meter was used for the data collection. The data were logged at 3 different heights (ceiling, head and knee level) and two different directions for each measurement point.
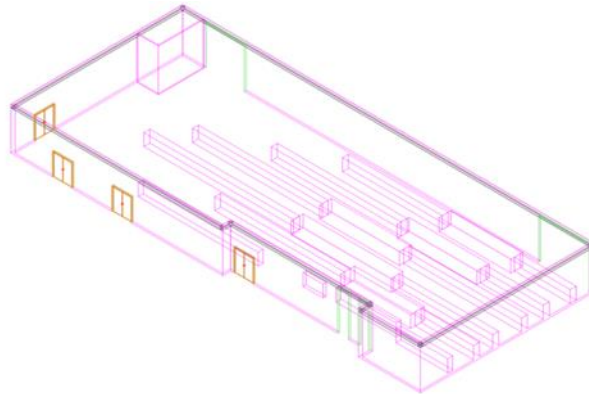
Figure 3-2. Case study 1 geometry
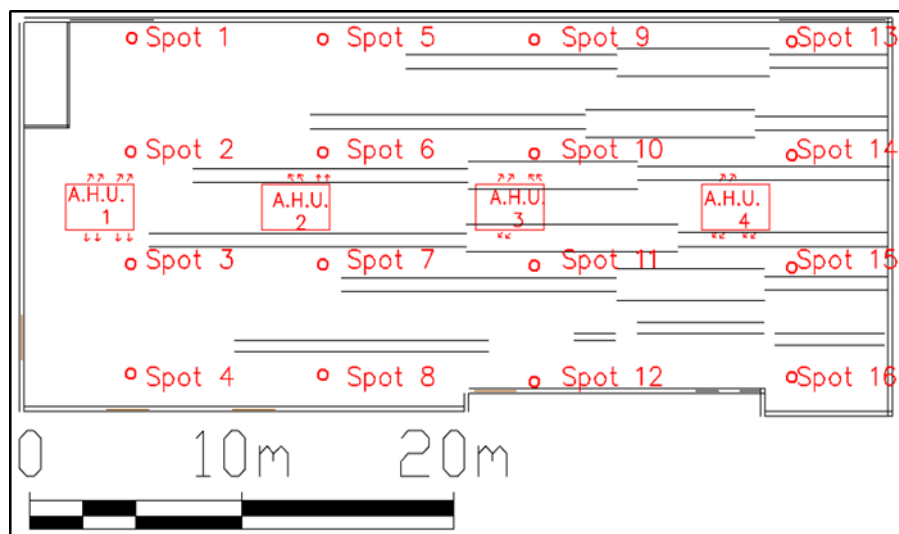
Figure 3-3. Case study 1: Measuring spots

The diffusers are combined supply/return diffusers (Figure 3-4) and supply air from two sides along the width of the space and air is returned through a return grille at the bottom face of the diffuser. The thermostats, which are located on the return duct, are set to 10 ºC, and the air handling units operate 24 hours per day. The supply from each air handling unit to the room space is approximately 1.4 m³s^{-1}. Figure 3-5 shows the labour density for case 1 production lines at the 21st October 2013. The maximum occupancy density of the space is 110 labourers which occurs from 06:00 - 08:00am and 09:30-10:30am (maximum occupancy density indicated with the light blue line). Each production lines has from 10-20 workers carrying out similarly light activity. During a working day, on average 80 labourers are located in the space.

Figure 3-4. Case study 1: Air distribution system via supply/return diffusers.
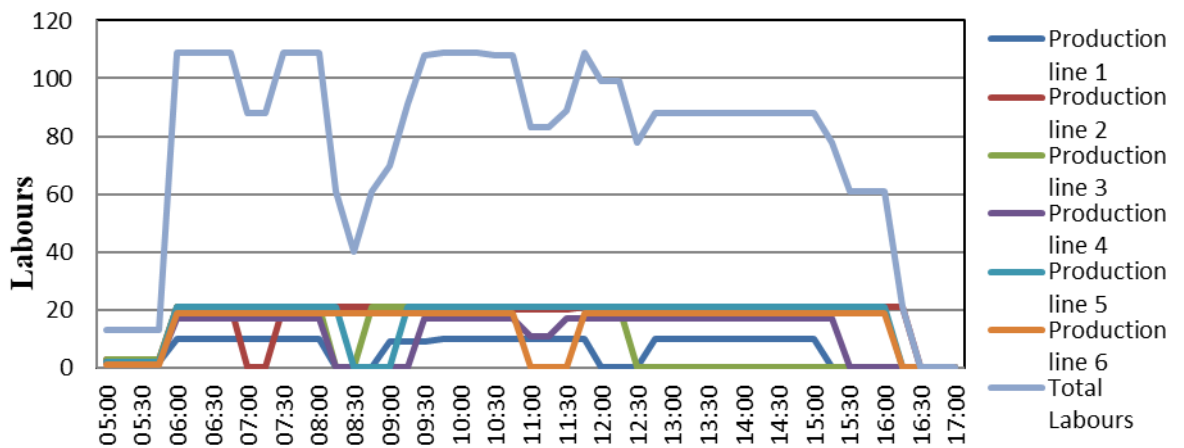
Figure 3-5. Case study 1: Labourers density

3.2.1 *Case study 1: Air temperature measurements*

This section presents an analysis of the thermal environment in terms of air temperature of case study 1. The temperature variations over the space of case study 1 facility can be observed in Figure 3-6. In this figure can be noted that the average air temperature in the space varied between 11.5 ℃ and 14.0 ℃. In addition, Figure 3-7 shows that the supplied temperature during refrigeration system operation is average at 7.0 ℃.

According to the measurements, it can be observed that the air distribution system via supply/return diffusers is effective to keep the required conditions of temperature around the production lines, and therefore to maintain the quality of the food during it's processing. However, it can be inferred that this air distribution configuration is not efficient in terms of rational energy use given the poor temperature stratification observed in the whole space of the facility if compared with an air distribution system capable of localizing the cold where it is needed.

In addition, according to the recorded data, the vertical temperature gradients around the space are insignificant. Also, temperatures measured at the different spots in horizontal direction showed similar values. This means that the air distribution configuration via supply/return diffusers cools down the whole space including a large unoccupied volume. In addition, measured data was found to vary up to ±0.5 ℃ in each spot of measurement. With respect to the relative humidity in the space, measured data varied between 55 and 60 %.
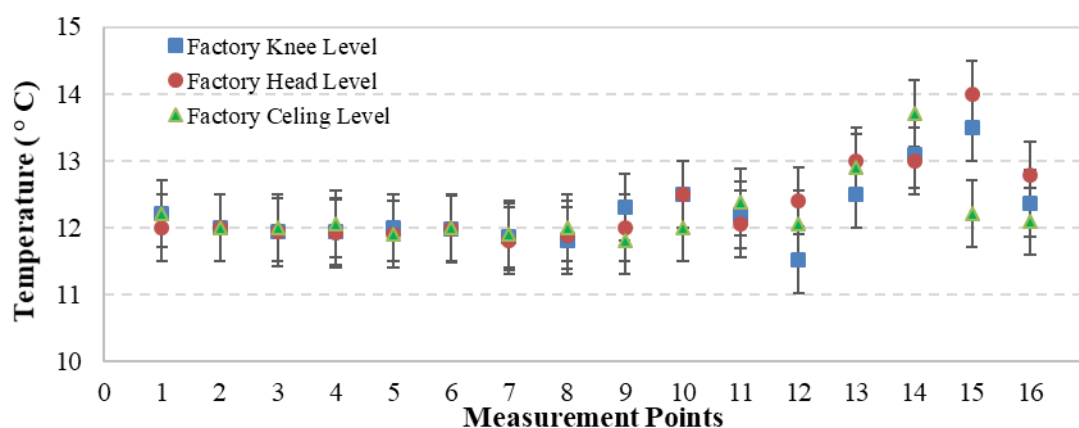
Figure 3-6. Case study1: Air temperature measurements
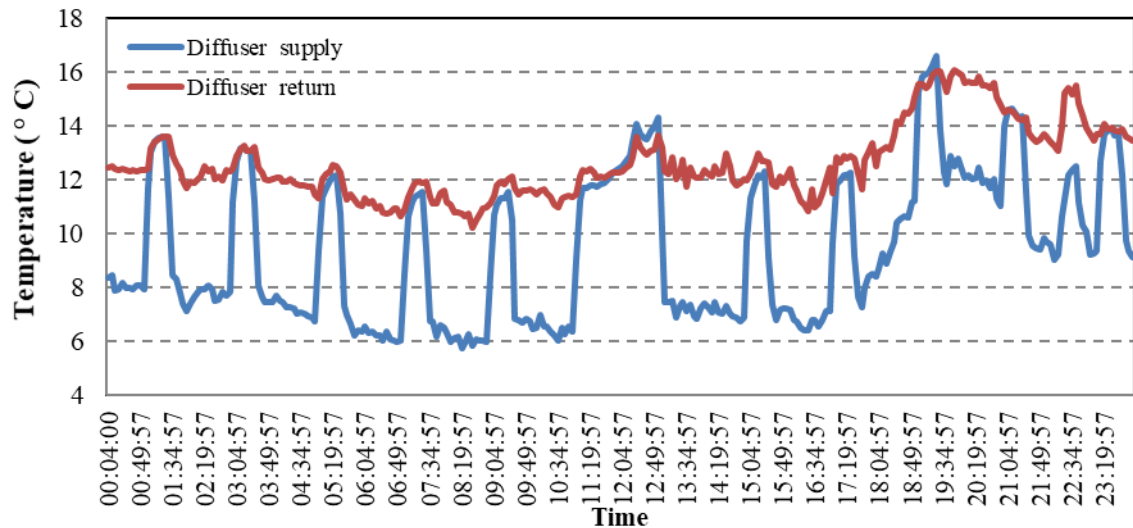
Figure 3-7. Case study 1: Diffuser supply temperatures

Figure 3-8, Figure 3-9 and Figure 3-10 shows the air temperature distribution for case study 1 at the 3 different heights that data were measured with the portable air flow meter. It can be easily observed that near the openings along production line 1, a temperature rise occurs due to the connections with the cleaning rooms that operate in higher temperatures. In contrast, the opening along production line 6 observed a slight temperature drop due to a draft that is created between the next rooms which are operating in similar temperatures. In addition, Figure 3-7 shows that after 18:00 p.m. a temperature rise in the supply/return air temperatures occurs due to the cleaning process that is carried out on that time. For the cleaning process, hot water under high pressure is used in order to clean all the production lines and equipment. Generally, the temperature varies between 11ºC - 14 ºC with average temperatures cross all the measuring points for knee, head and ceiling level where 12.2 ºC, 12.3 ºC and 12.1 respectively.
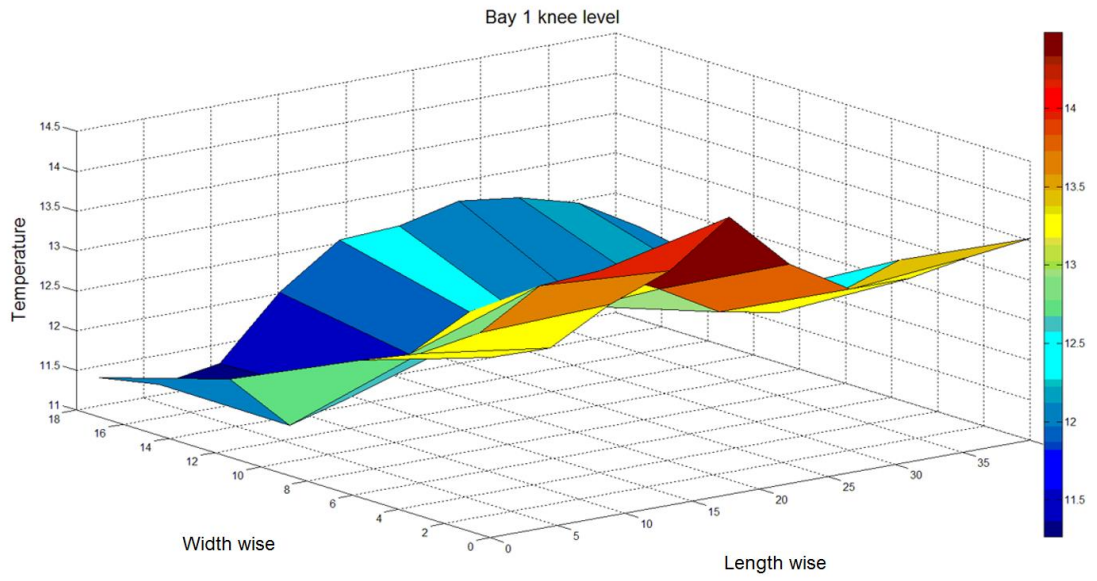
Figure 3-8. Case study 1: Temperature distribution at knee level
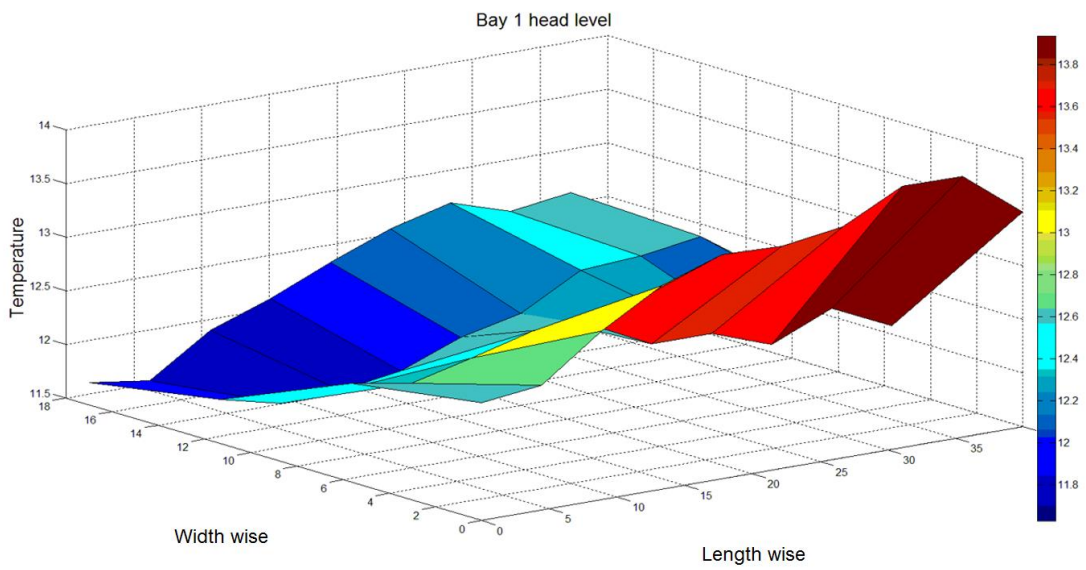
Figure 3-9. Case study1: Temperature distribution at head level
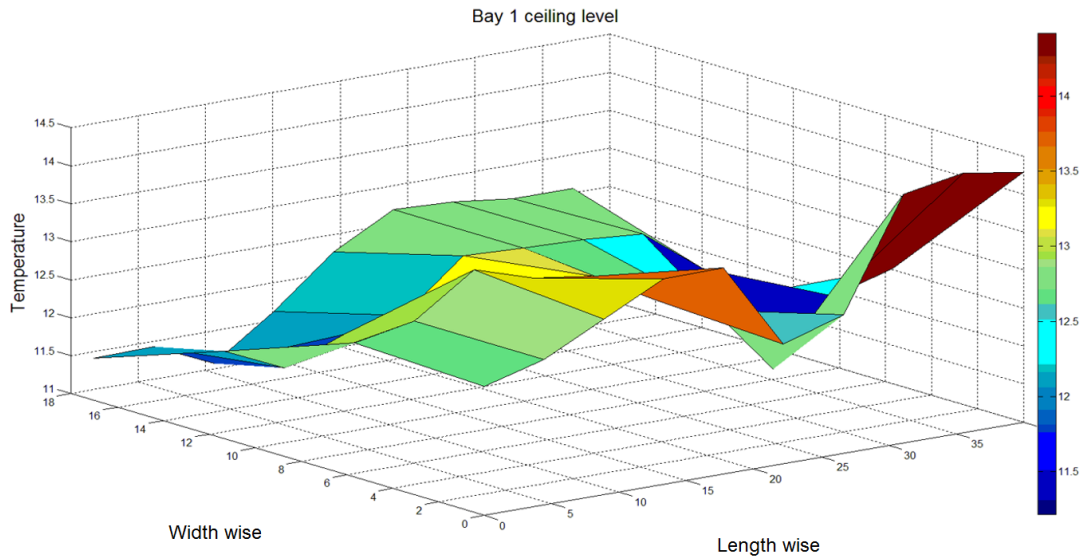
Figure 3-10. Case study 1: Temperature distribution at ceiling level

3.2.2 *Case study 1: Air velocity measurements*

This sub-section presents an analysis of the thermal environment in terms of air flow for case study 1. The velocity variations over the space of the case study 1 facility can be observed in Figure 3-11. In this figure can be noted that the average air velocities in the space varied between 0.1 and 1.4 m.s^{-1}. Air velocities in each spot of measurement were found to vary up to ±0.3 m.s^{-1}.
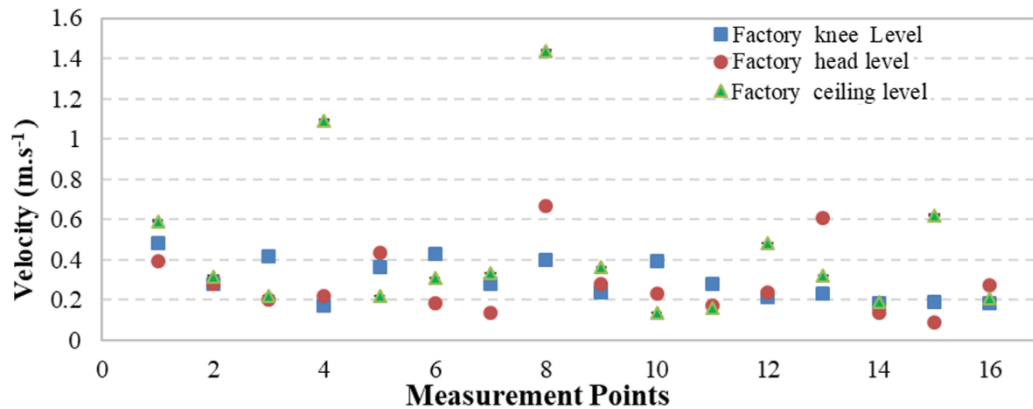
Figure 3-11. Case study 1: Air velocity measurements

According to the recorded data, the average velocities cross all the measuring points for knee, head and ceiling level where 0.3 m.s^{-1}, 0.3 m.s^{-1} and 0.46 m.s^{-1} respectively. Regarding the air velocities around the space, the highest values were obtained at the ceiling level and the lowest values at the head and knee level. In addition, in Figure 3-3 the red arrows indicate the on-site diffusers fins adjustment and the supply air discharge

direction. The occupants were adjusting the diffusers fins in order to satisfy their personal comfort preference. This onsite diffuser fins adjustment resulted to significant velocity variations in short distance. At head level, the velocity in some locations was as high as 0.6 m.s^{-1} which together with the low temperatures it can lead to excessive percentage dissatisfied discomfort up to 60 % or higher for the occupants according to the BS EN ISO 7730:2005.In addition, Figure 3-12, Figure 3-13 and Figure 3-14 show graphically the air velocity distribution along case study 1 space at the 3 different Heights that data were measured.
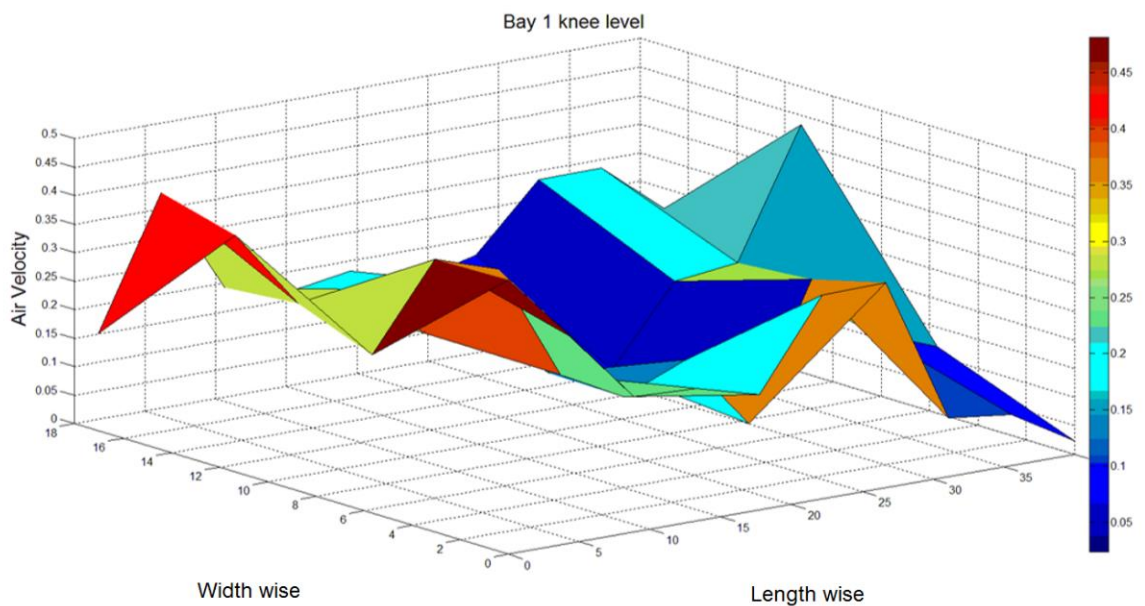
Figure 3-12. Case study 1: Knee level air velocity distribution
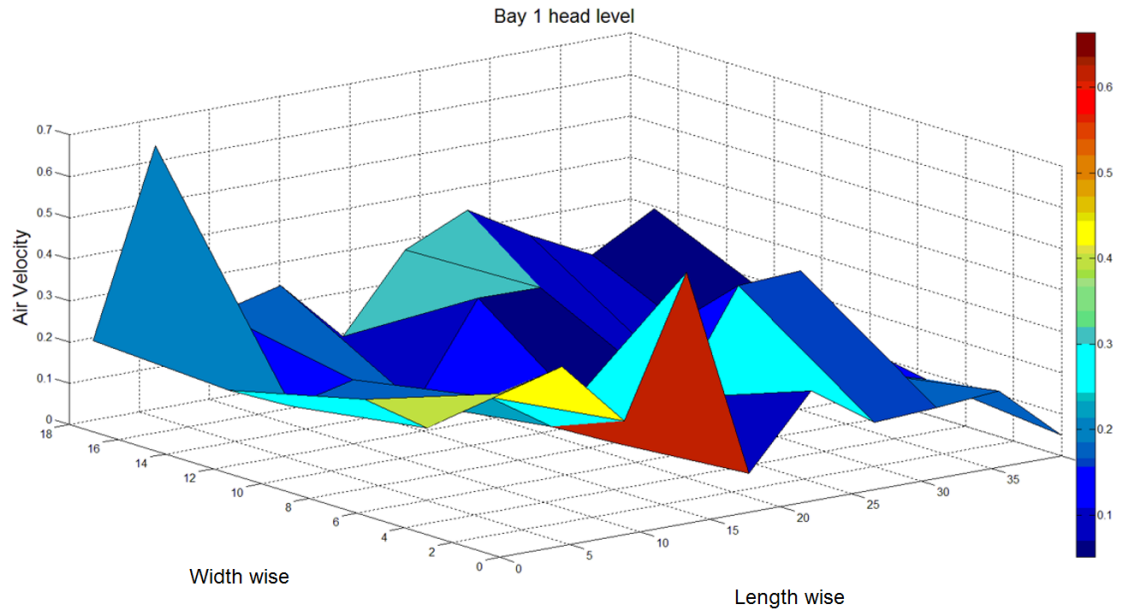
Figure 3-13. Case study 1: Head level air velocity distribution
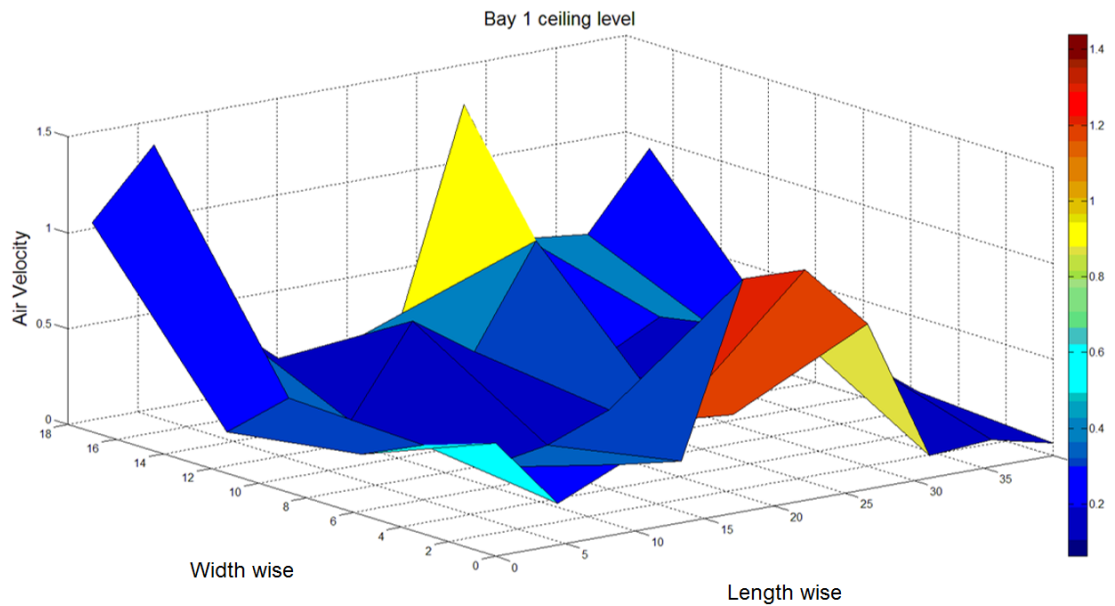
Figure 3-14. Case study 1: Ceiling level air velocity distribution

3.3 Case study 2: Air distribution via circular fabric ducts

The dimensions of case study 2 chilled food processing area under investigation are 21m wide, 24 m deep and 6.5 m high. Figure 3-15 shows the space geometry of case study 2. Case study 2 chilled food factory is located in UK in the area of Wisbech. The HVAC system consists of 5 evaporator coils distributing the air with fabric ducts with diameter

of 0.9 m located at 6.0 m height (Figure 3-16). Table 3-2 shows the air distribution system details. Each evaporator is distributing the air with a single fabric duct. The temperature in this facility is controlled by individual thermostats located at the back of each evaporator with 8 - 9°C set point temperature.

Table 3-2. Case study 2: Air distribution system details

Fabric duct/evaporator	1	2	3	4	5
No. of fans	1	1	1	1	1
Fan diameter (mm)	900	900	900	900	500
Fan power (kW)	2.5	2.5	2.5	2.5	0.45
Cooling coil capacity (kW)	27.5	27.5	27.5	27.5	6.3
Air flow rate (m3/s)	4.5	4.5	4.5	4.5	1.77
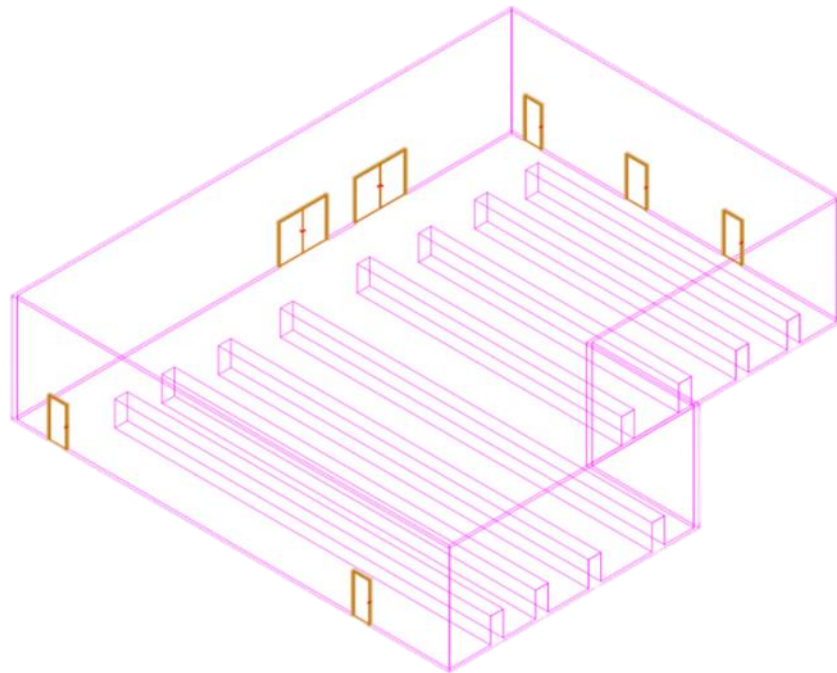
Figure 3-15. Case study 2: Geometry

Figure 3-16. Case study 2: Air distribution system via circular fabric ducts

The location of the evaporators is also shown in Figure 3-18. The air flow rate that is recirculated from each evaporator is approximately 4.5 m³.s^{-1}. The target in an air-sock is to achieve a constant static pressure inside the sock which will maintain it inflated and will give a uniform discharge air velocity across the whole surface (normally around 0.1 m.s^{-1}). The discharge air surface velocity is too low to give a momentum to the air to be thrown into the space. Due to the density difference between the supplied air and the room air, the supply air is displaced towards the floor immediately after passing through the sock surface. The maximum occupancy density of the space is 96 people and 60 on average. Red circles in Figure 3-18 show the points where the Hobos data loggers were located. The data loggers were installed at 3 different height levels for each measuring point.
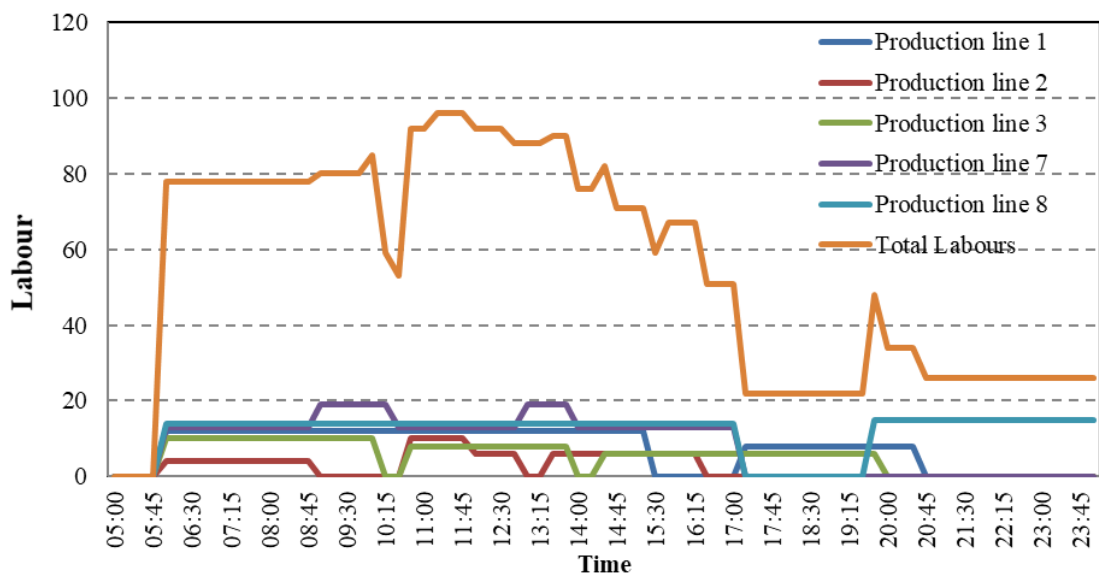
Figure 3-17. Case study 2: Labourers density
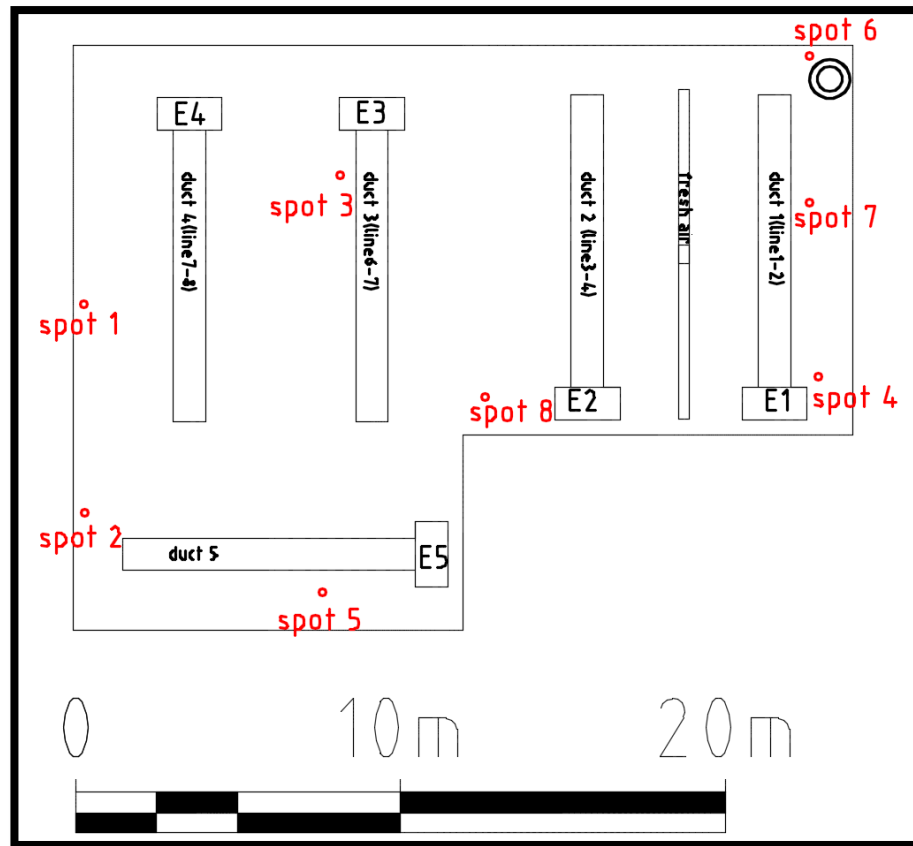
Figure 3-18. Case study 2: Measuring spots

3.3.1 <u>Case study 2: Air temperature measurements</u>

This section presents an analysis of the thermal environment in terms of air temperature of case study 2. Figure 3-19shows the temperature trends over the space for case study 2. In this case, the relative humidity in the space varied between 65 and 70 %. In contrast to case study 1, monitoring of the case study 2 facility showed some temperature stratification, with the lowest temperatures measured at knee level and highest at ceiling level. With a supply temperature from the air socks at 8 °C, the average temperature in the bulk of the space varied between 9.0 °C and 13.5 °C with a ±0.5 °C variation in each point of measurement. It was also observed that the temperature stratification between the three measuring heights followed an apparent steady distribution pattern.
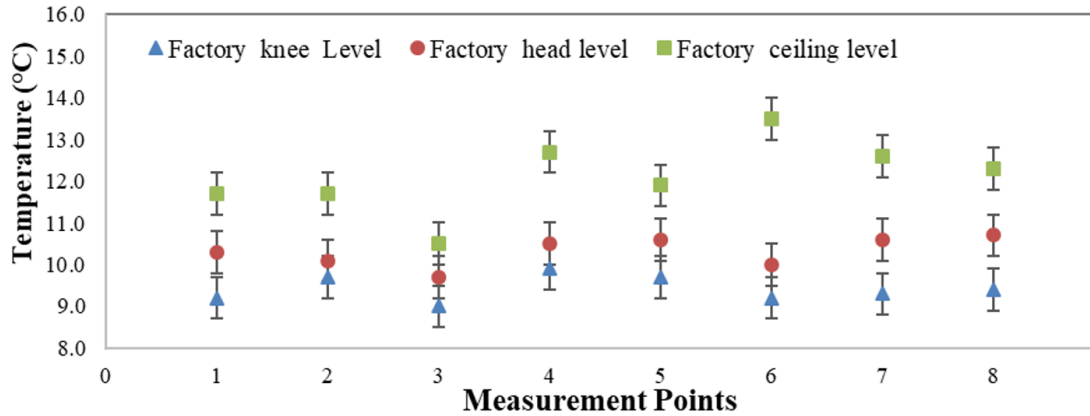
Figure 3-19. Case study2: Air temperature measurements
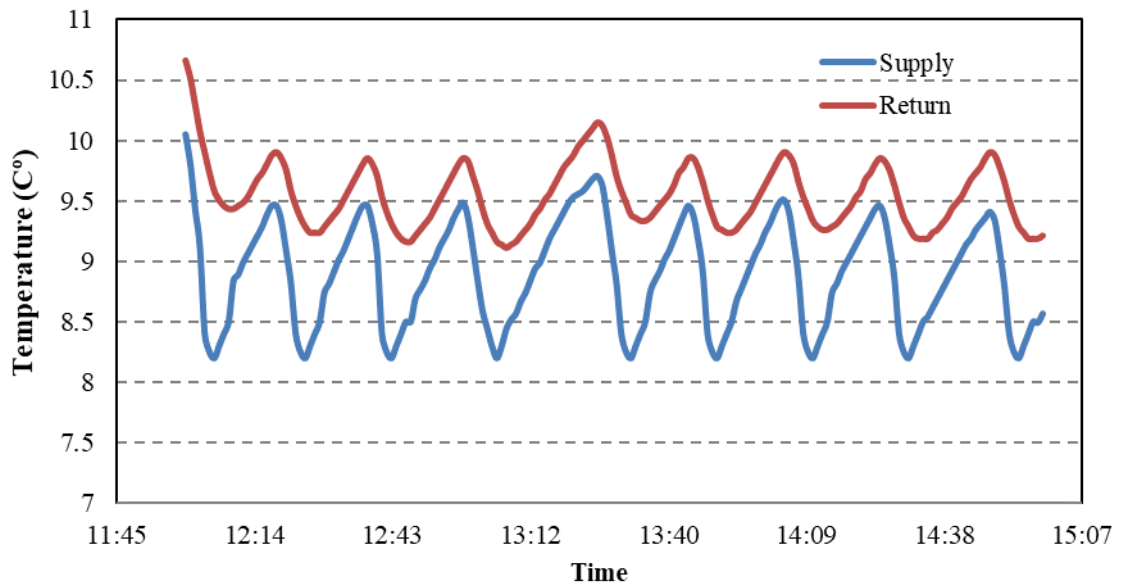
Figure 3-20. Case study 2: Diffuser supply temperatures

Figure 3-21, Figure 3-22 and Figure 3-23 shows graphically the air temperature distribution for case study 2 at the 3 different heights that data were measured with the portable air flow meter. It was observed that the temperature stratification between the three measuring heights followed a steady distribution pattern long wise the production facility. The average temperatures cross all the measuring points for knee, head and ceiling level where 10.1 °C, 10.4 °C and 11.9 respectively.
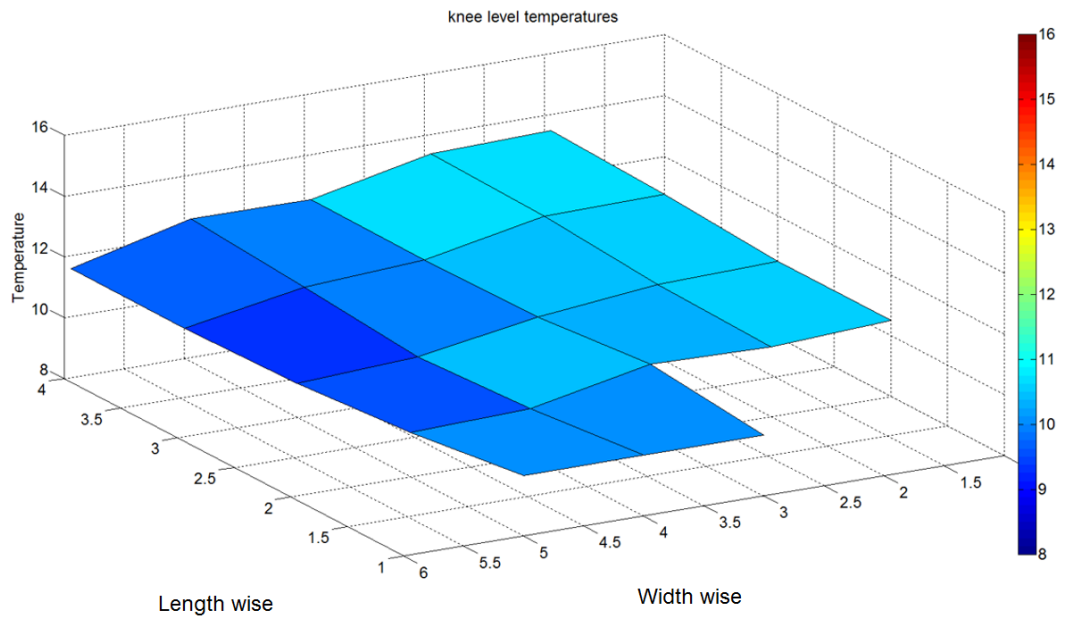
Figure 3-21. Case study 2: Temperature distribution at knee level
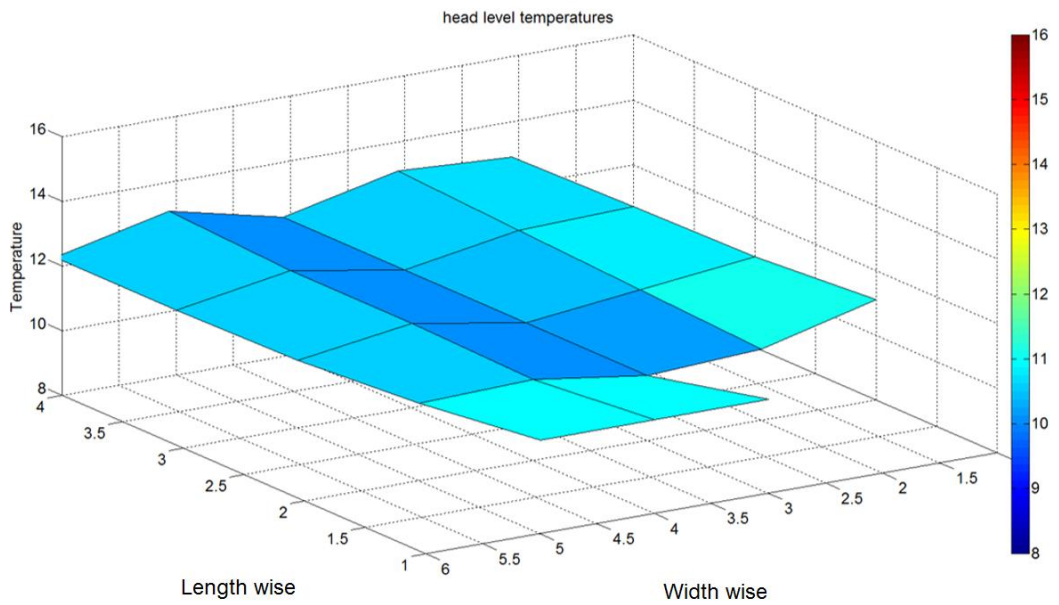
Figure 3-22. Case study 2: Temperature distribution at head level
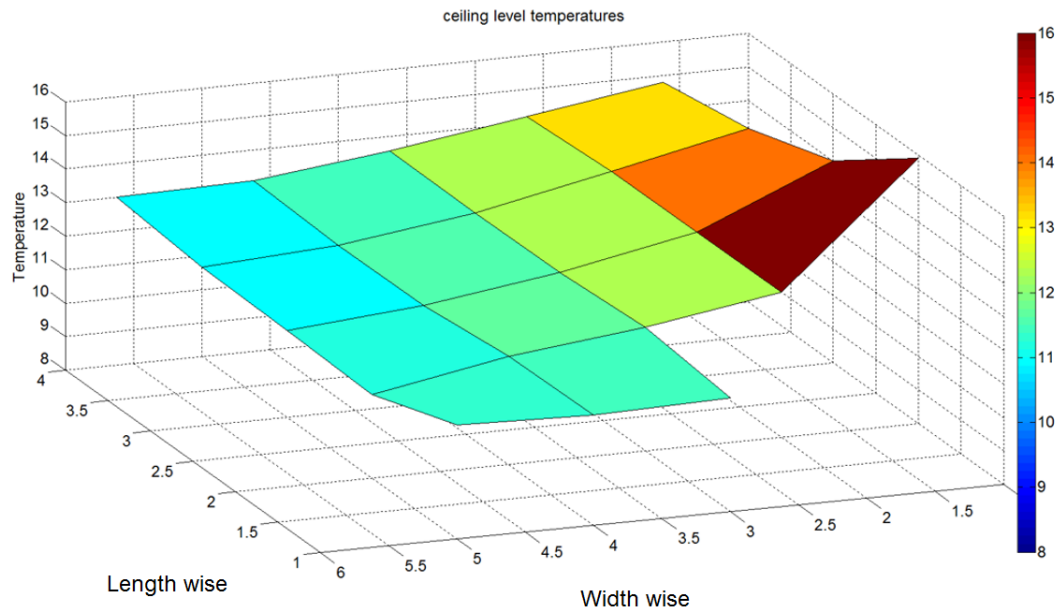
Figure 3-23. Case study 2: Temperature distribution at ceiling level

3.3.2   Case study 2: Air velocity measurements

This sub-section presents an analysis of the thermal environment in terms of air flow for case study 2. The velocity variations over the space of case study 2 facility can be observed in Figure 3-24. In this figure can be noted that the average air velocities taken from the different measurement points varied between 0.05 and 0.35 m.s^{-1} with a variation up to ±0.1 m.s^{-1}. The average velocities cross all the measuring points for knee, head and ceiling level where 0.08 m.s^{-1}, 0.07 m.s^{-1}and 0.11 m.s^{-1} respectively.
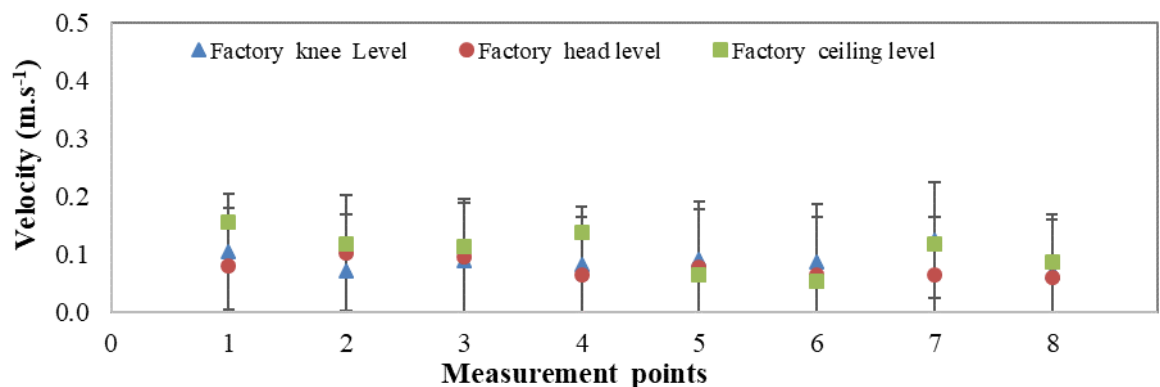
Figure 3-24. Case study 2: Air velocity measurements

In addition, Figure 3-25, Figure 3-26 and Figure 3-27 shows graphically the air velocity distribution along case study 2 at the 3 different heights that data were measured with the

portable air flow meter. Measurements show that air velocities in case 2 were much lower than those in case 1 resulting in a beneficial effect to achieve a partial temperature stratification in the space and reduce the discomfort of the workers produced by the high velocities and low temperatures. With regards to the air flow velocities in case study 2, they were found to vary between 0.05 and 0.15 m.s^{-1} with a variation up to ±0.1 m.s^{-1} and the highest velocities measured at the knee and head level.
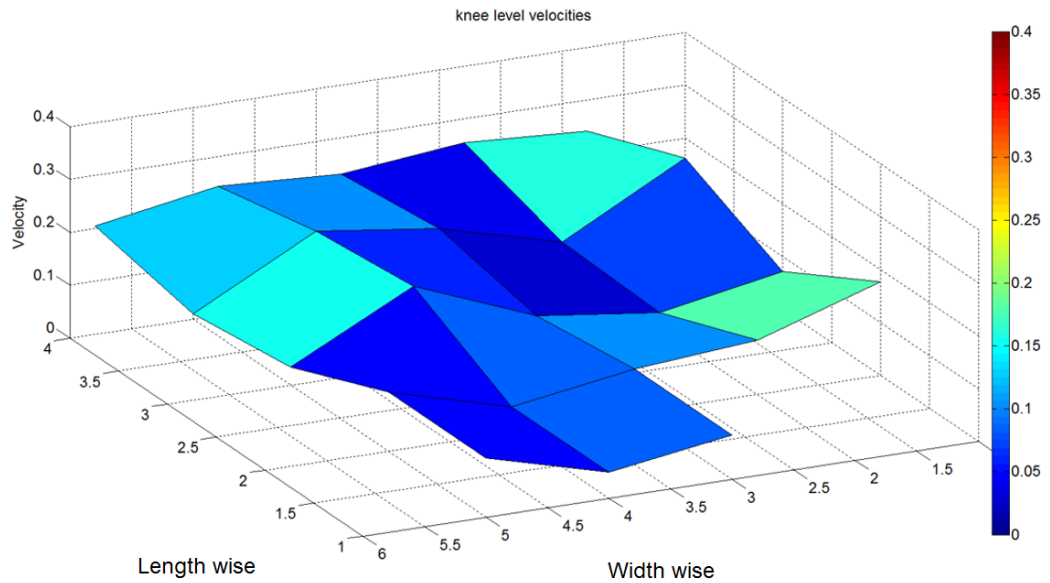
Figure 3-25. Case study 2: Knee level air velocity distribution
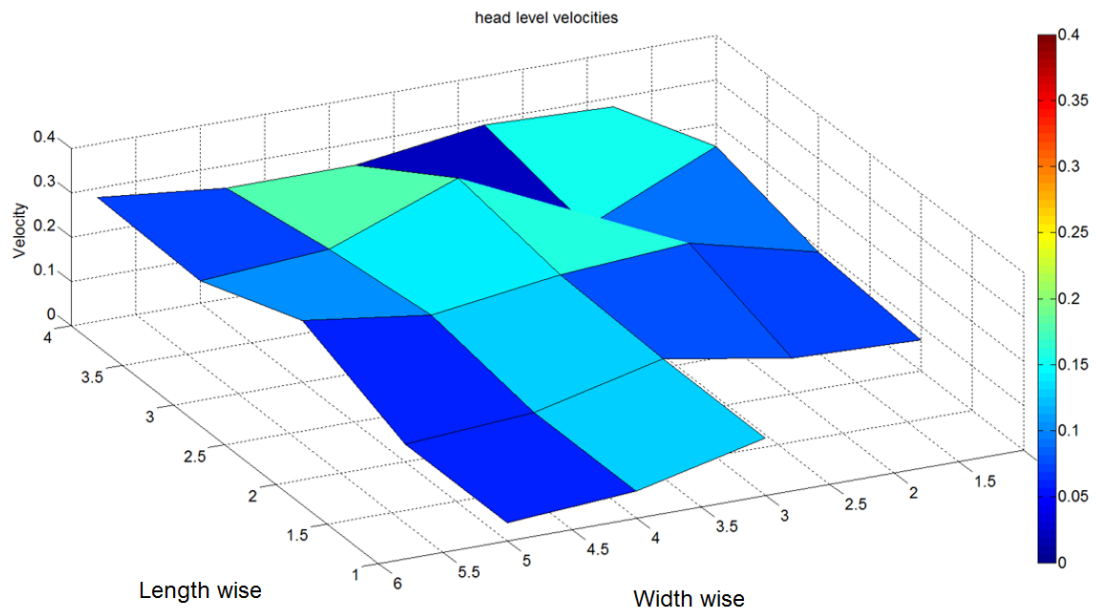
Figure 3-26. Case study 2: Head level air velocity distribution
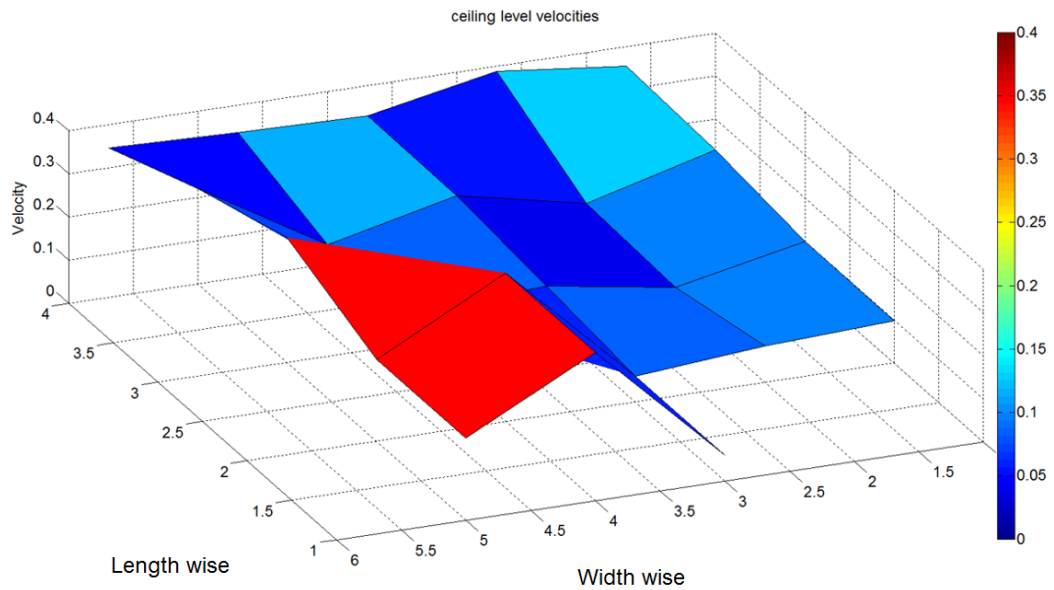
Figure 3-27. Case study 2: Ceiling level air velocity distribution

3.4 Summary of Chapter 3

This chapter focuses on understanding the air flow and the temperature variation in existing chilled food production facilities. Two existing chilled food production facilities (case study 1 and case study 2) using different air distribution systems were monitored. The monitoring of the facilities was implemented in order to understand the temperature and velocity distribution in the space and also to validate the CFD models.

Based on the measured data, the use of fabric ducts appears to be a more appropriate configuration for air distribution in comparison to that in case 1. Fabric ducts employ wider air flow areas covering the production lines and distributing low air flow velocities around the occupied zone. It also seems to facilitate the air temperature stratification around those spaces that are not directly cooled by the air flows from the air distribution system which to some extent may impact in a positive way the energy consumption of the refrigeration system if compared to use of supply/return diffusers. The next chapter will present the development of an experimental setup and testing of an experimental facility representing a section of an actual chilled food factory.

Chapter 4. Experimental set-up and initial monitoring

4.1 Introduction

This chapter deals with the experimental set-up and the initial monitoring of the developed test rig. The experimental set-up was designed and built in order to represent an existing chilled food facility and its air distribution system. In addition, the experimental monitoring implemented was used for the CFD model validation. The work programme involved the following steps:

- Experimental facility setup
- Fabrication of air distribution systems currently used in existing chilled food facilities and apply them at the developed experimental facility. These were:
    - Air distribution via fabric ducts
    - Air distribution via non-ducted evaporator coil
- Monitoring of air temperature and velocity profiles
- Monitoring of refrigeration system and its energy consumption

4.2 Experimental set-up

The experimental test rig was established using an environmental chamber constructed with insulated cold room panels. Measurements of air velocity, air temperature profiles and the energy consumption of the refrigeration system were collected. The chamber dimensions were 2.9 m (H) x 6.6 m (L) x 3.5 m (W). A schematic diagram of the layout of the test rig is shown in Figure 4-1. Cooling in the chamber was provided by an evaporator coil served by a R404a condensing unit situated outside the test rig in the ambient air. The refrigeration system mainly consisted of an evaporator coil in the environmental chamber, a thermal expansion valve, and a packaged condensing unit locate outside the chamber with a reciprocating type compressor. The evaporator unit operated with 100 % recirculated air. For further information regarding the refrigeration system components specifications please refer to Appendix A.

Air temperature measurements in the chamber, using T-type thermocouples, were taken at 4 sections along the length of the chamber (see Figure 4-1) and 4 sections along the width of the chamber (Right-wall, Right-centre, Left-centre and Left-wall) and at three heights: knee level, head level and ceiling level. Temperatures were also measured at the inlet and outlet of each component in the refrigeration system. In total, 58 temperature sensors were installed.

The thermal load from occupants (OC) was simulated by 4 rectangular boxes of 1.6 m^2 surface area each wrapped with trace heater elements, 150W each. The occupan's thermal load was defined by the state of activity (typical metabolic heat generation) based on ASHRAE suggestions (ASHRAE 2013).

Accordingly from the type of lighting fixture, a proportionate internal heat gain is generated through convection and radiation. For the case of chilled food processing areas, which are currently using fluorescent lamps, a fixture surfaces temperature of 28 ºC is generated (value measured experimentally). From this type of lighting the fraction of lighting energy causing internal heat gain is mainly convective. Air velocity measurements were also taken close to the position of each temperature sensor using an air flow meter TSI TA465-P with a thermo-anemometer probe 966 (TSI AIRFLOW INSTRUMENTS Ltd, 2016). A variable speed controller (710-E) was used to control the evaporator fan speed and hence the suction/discharge air volume. The refrigerant mass flow rate was measured using a Coriolis type flow meter Krohne Optimass 7300 C (KROHNE, 2016) placed at the outlet of the condenser. The electrical power consumption of the refrigeration system was recorded by a portable power meter Fluke 435 Series II (FLUKE, 2016).

Figure 4-2 shows Datascan modules 7020 (Measuresoft datascan products and services, 2016) used for the temperature and refrigerant flow data logging. The logging interval of the data was set to 10 s. The time for each test was 17 hrs. Table 4-1 presents the measurement uncertainties of the used sensors. The air temperature in the test chamber was controlled using a temperature controller EKC 102A with the thermostat located at the evaporator air suction side and set to 9.7 ºC.

Table 4-1. Measurement uncertainties of the sensors.

Sensors	Oper. Range	Uncertainty
Thermocouples with TC adapter, (ºC)	-50 to 400	± 0.5 ºC
Thermoanemometer - Air flow meter, (m.s^{-1})	0 to 50	± 3.0 %
Coriolis flow meter - Refrigerant mass flow rate, (kg.h^{-1})	0 to 1230	± 0.10 %
Energy logger - Power consumption, (W)	1 to 400	± 0.5 %

For the initial experiments, the following two air distribution methods used in a large number of chilled food manufacturing facilities were tested:

i) Air distribution using fabric ducts (tests were performed with a duct of 0.4 m diameter and 4.0 m length installed at ceiling level as illustrated in Figure 4-1

ii) Non-ducted evaporator coil.
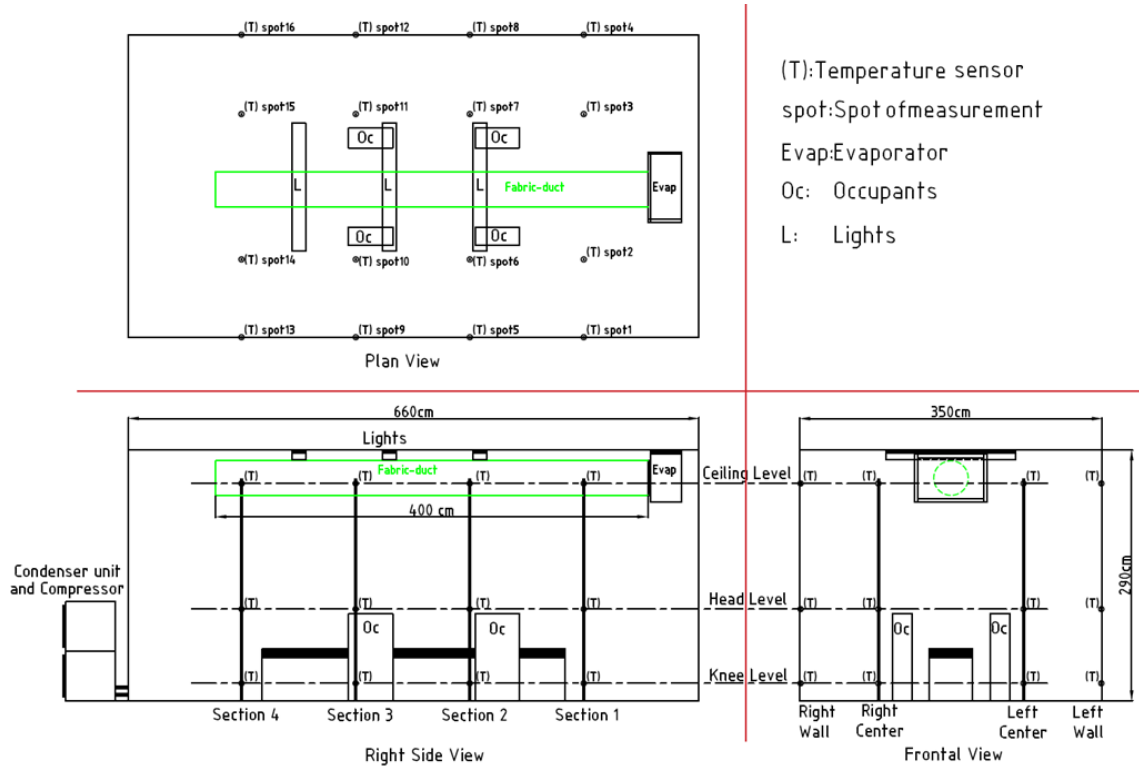
Figure 4-1. Outline of the experimental test facility with air distribution via fabric duct at ceiling level (reference case).

Figure 4-2. Data logging system.

4.3 Air distribution system via circular fabric-duct installed at ceiling level

This section presents the results of experimental measurements of the thermal environment arising from the air distribution system via fabric duct installed at ceiling

level in the experimental facility (Figure 4-3). This configuration corresponds to an actual air distribution system installed in a chilled food processing factory (chilled food facility case study 2). The fabric duct that was used for the initial experimental set-up was fabricated with the 'KE - Low Impulse textile duct fabric' of KE-FIBERTEC (ke-fibertec KE, 2016). The 'KE - Low Impulse textile duct' is the same fabric-duct currently installed in the Case study 2 chilled food facility. The fabric duct measures 40 cm in diameter and 400 cm in length. For further information regarding the fabric duct specifications please refer to Appendix A.

Figure 4-3. Experimental test facility: Air distribution via circular fabric duct.

4.3.1 *Experimental assessment: Air temperature profiles with circular fabric duct at ceiling level*

This sub-section presents an analysis of the thermal environment in terms of air temperature profiles in the space. Figure 4-4 shows the temperature profiles from measurements in the test chamber with air distribution via fabric duct at ceiling level. The evaporator fan velocity was set at 100 % which corresponds to volumetric flow rate of 2825 m³hr^{-1}. Temperature values shown in Figure 4-4 correspond to the average values measured at each position during a day-long test. According to the results, the whole space was kept at low temperatures varying from 8.1 ℃ and 13.9 ℃. The average temperature values measured at knee, head and ceiling level were 9.9 ℃, 10.6 ℃ and 12.4 ℃, with a ±0.5 ℃ variation in each point of measurement, respectively. According to the data recorded, some temperature stratification was obtained with the lowest temperatures measured at knee level and highest at ceiling level. It was also observed that the temperature stratification between the three measuring heights followed an apparent

steady distribution pattern. Furthermore, it can also be noted in Figure 4-4 and Figure 4-5 that the highest temperatures were obtained close to the walls at ceiling level which may be due to the fact that the air around those sections was no directly cooled by the air flowing from the fabric duct. In the case of the central section, the air temperature may have been influenced by the heat gains from the lightings. In addition, it was also observed that the heat gains from the occupants influenced the temperature measurements of the sensors located around the centre of the facility and that the lowest temperatures were recorded close to the walls at knee level.
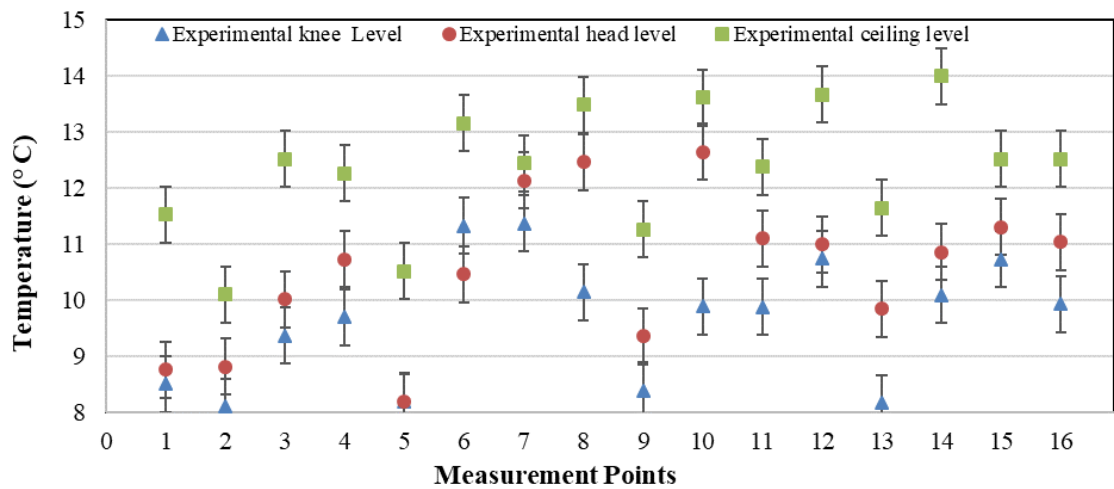
Figure 4-4. Circular fabric duct at ceiling level: Air temperature measurements
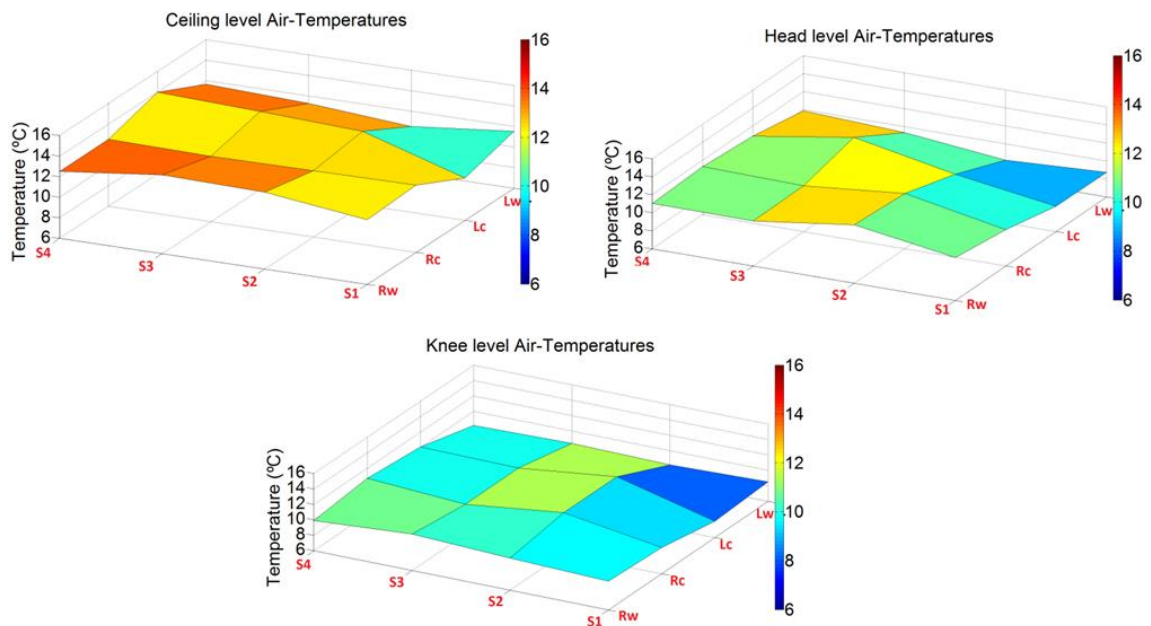
Figure 4-5. Circular fabric duct at ceiling level: Temperature distribution at knee level

The target in a fabric duct is to achieve a constant static pressure inside the duct which will maintain it inflated and will give a uniform discharge air velocity across the whole surface (in the existing chilled food facility was measured at 0.1 m.s^{-1}). The experimental fabric duct surface discharge air velocity was measured around 0.15 $^{-1}$ which agrees with the chilled food facility measured value. Table 4-2 shows a comparison of the average temperature values across all the measurement points at different measuring heights between the experimental and case study 2. The average values of the experimental measurements and case study follow the same pattern.

Table 4-2. Comparison of experimental and case study 2 average temperatures

	Average temperatures (^{o}C)		
	knee level	**head level**	**ceiling level**
Experimental	9.9	10.6	12.4
Case study 2	10.1	10.4	11.9

4.3.2 *Experimental assessment: Air velocity profiles with circular fabric duct at ceiling level*

The air velocity profiles air shown in Figure 4-6. Measured values varied between 0.02 and 0.25 m s^{-1} with highest values recorded at knee level. In this case, the highest velocity values found at knee level may have been caused by return and supply effects of the cooling coil unit which provided recirculation of air in the space. Maximum air velocity close to the fabric duct was found to be 0.17 m s^{-1}. In general, it can be said that the variation of air velocities was within the range expected in air-conditioned spaces and should not create drafts in the space. In addition, Figure 4-7 shows graphically the air velocity distribution along the space at the 3 different Heights that data were measured. The average velocities cross all the measuring points for knee, head and ceiling level where 0.074 m.s^{-1}, 0.044 m.s^{-1} and 0.13 m.s^{-1} respectively.
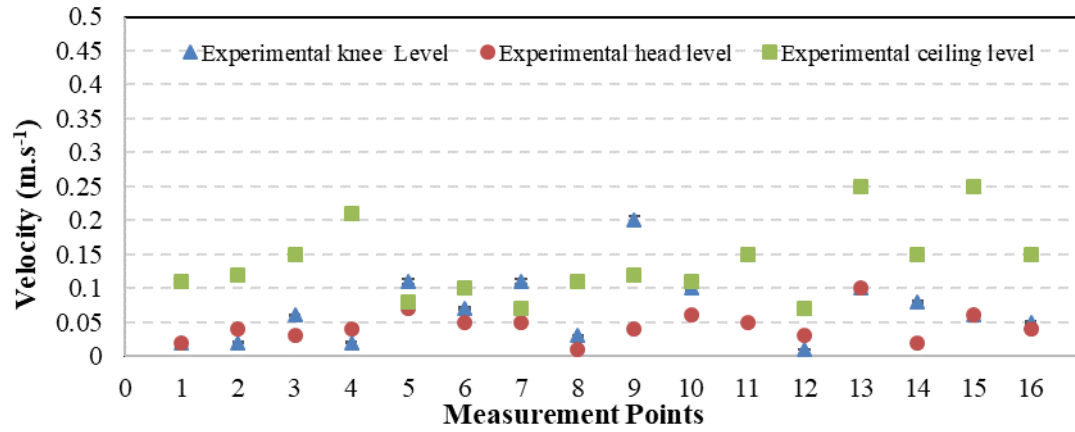
Figure 4-6. Circular fabric duct at ceiling level: Air velocity measurements
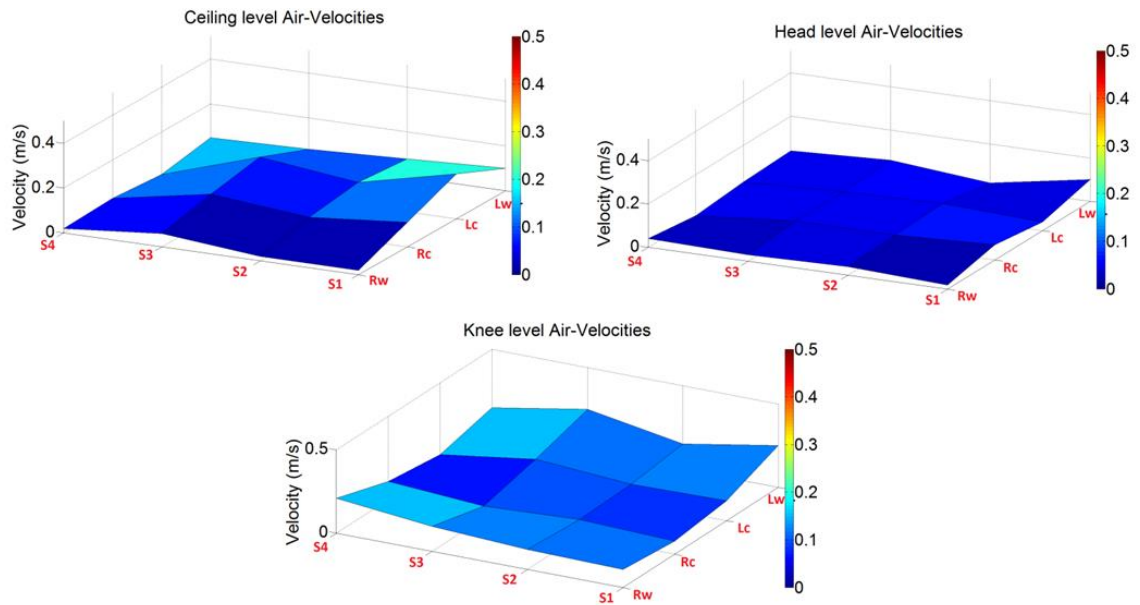
Figure 4-7. Circular fabric duct at ceiling level: Air velocities at knee level

Table 4-3 shows a comparison of the average velocities cross all the measuring point at different measuring heights between the experimental and case study 2. It can be seen that the average values between the experimental and case study follow the same pattern. In general the air distribution via fabric duct is a good method for providing homogeneous and low air flows which therefore reduces the excessive workers discomfort caused by the low temperatures.

Table 4-3. Comparison of experimental and case study 2 averaged velocities

	Average velocities (m.s^{-1})		
	knee level	**head level**	**ceiling level**
Experimental	0.074	0.044	0.13
Case study 2	0.08	0.07	0.11

4.3.3 Experimental assessment: Refrigeration system performance with circular fabric duct at ceiling level

This section presents an analysis of the refrigeration system operating conditions and its energy consumption. The air distribution system used for this part of the analysis was the fabric duct installed at ceiling level. The refrigeration system parameters monitored were the following:

- Refrigerant mass flow rate
- Temperatures at inlet/outlet of each refrigeration system component
- Power consumption

Figure 4-8 shows an example of a thermodynamic cycle on a P-h diagram based on the measured data of the R404a refrigeration system installed in the experimental set-up. States 1, 2, 3 and 4 refer to the condenser inlet, condenser outlet, evaporator inlet and compressor inlet, respectively.
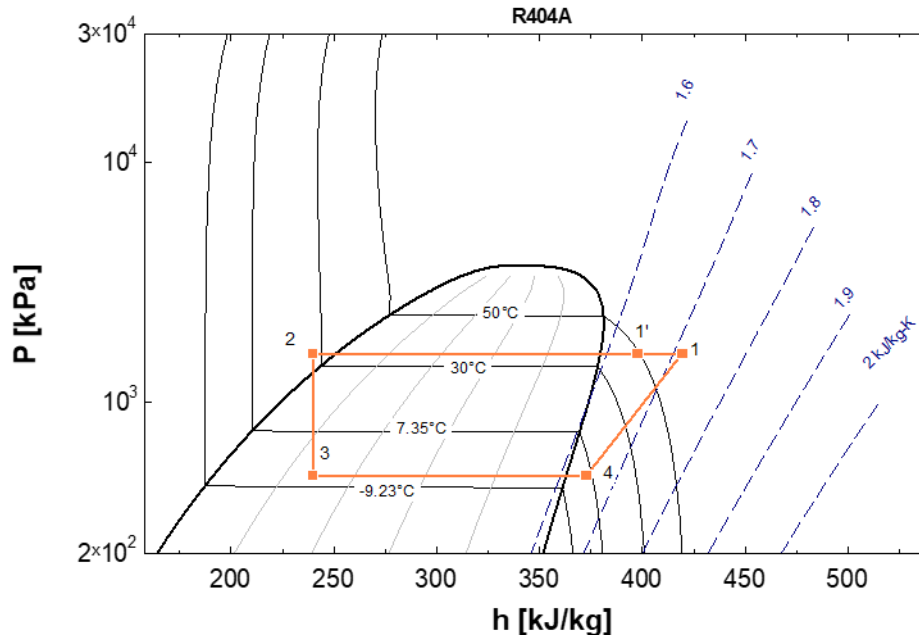
Figure 4-8. Circular fabric duct at ceiling level: R404a refrigeration cycle with the evaporator fan velocity at 100 %.

Table 4-4 and Table 4-5 show the state conditions at each numbered point with fan velocities at 100 % and 60 %, respectively. Also, tables show the thermal load in the evaporator (Q_{evap}) and condenser (Q_{cond}), work of the compressor (W_{comp}), the coefficient of performance of the cycle (COP) and thermodynamic efficiency of the compressor (h_{comp}).

Table 4-4. Circular fabric duct at Ceiling level: State variables in the refrigeration cycle, fan velocity at 100 %.

T_{amb}= 16 °C	P [kPa]	T [°C]	h [kJ/kg]
1	1600	67.82	419.2
2	1600	27.17	239.7
3	499.1	-6.05	239.7
4	499.1	4.7	372.8
Q_{evap} [kJ/s]	Q_{cond} [kJ/s]	W_{comp} [kJ/s]	COP
5.3	7.1	1.8	2.9

Table 4-5. Circular fabric duct at ceiling level: State variables in the refrigeration cycle, fan velocity at 60 %.

T_{amb}= 17°C	P [kPa]	T [°C]	h [kJ/kg]
1	1600	64.62	415.6
2	1600	29.66	243.6
3	499.9	-5.99	243.6
4	499.9	5.02	373.1
Q_{evap} [kJ/s]	Q_{cond} [kJ/s]	W_{comp} [kJ/s]	COP
5.1	6.8	1.7	3.0

4.3.3.1 Refrigerant mass flow rate and power Consumption

An analysis of the refrigeration system power consumption and refrigerant mass flow rate are presented in this section. For each case, data were collected over a 17 hour test period with ambient air temperature of 8 °C. For clarity, power data and mass flow measurements are presented for a period of one hour in Figure 4-9 and 4-10. Data of power consumption and mass flow rate collected for the 17 hours can be found in Appendix B. Power measurements for each system include power drawn by the compressor, condenser fans, evaporator fan and control system. For the circular fabric duct at ceiling level, the fan speed of the evaporator was kept at its nominal value which corresponds to volumetric flow rate of 2825 m³hr^{-1}.

The power consumption (P) of the refrigeration system with each configuration was determined as the summation of the instantaneous power of the refrigeration system during the running period (P_{on}) and power drawn during the off cycle (P_{off}). Data recording was every 10 seconds.

$$P = \sum P_{on} + \sum P_{off} \qquad \text{(W)} \qquad (1)$$

Power measurements showed that by using the fabric duct at ceiling level, the operating time of the refrigeration system was 25.28 minutes per hour with 5.7 operating cycles with an average duration of each cycle of 4.26 minutes. In addition, the peak mass flow rate was 160 kg/hr. Figure 4-10 shows that the average power consumption was at 3.22 kW.
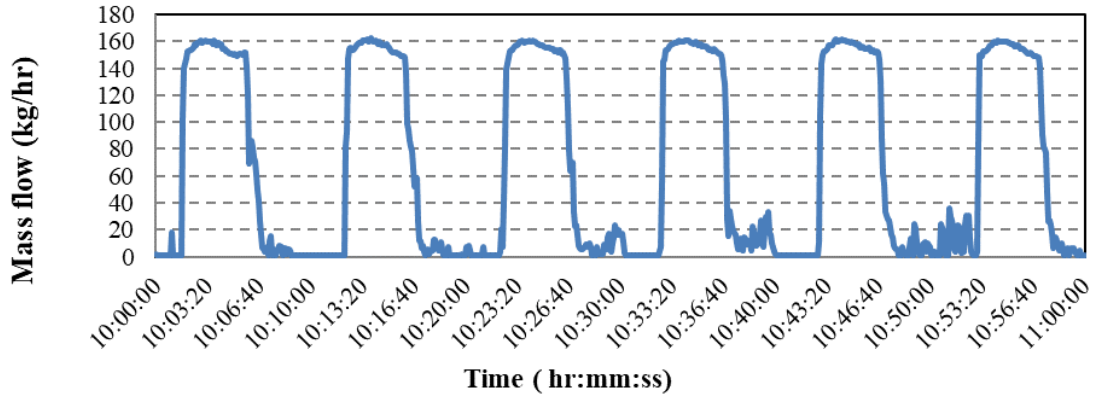
Figure 4-9. Mass flow rate, fabric duct at ceiling level, during a period of 1 hour.
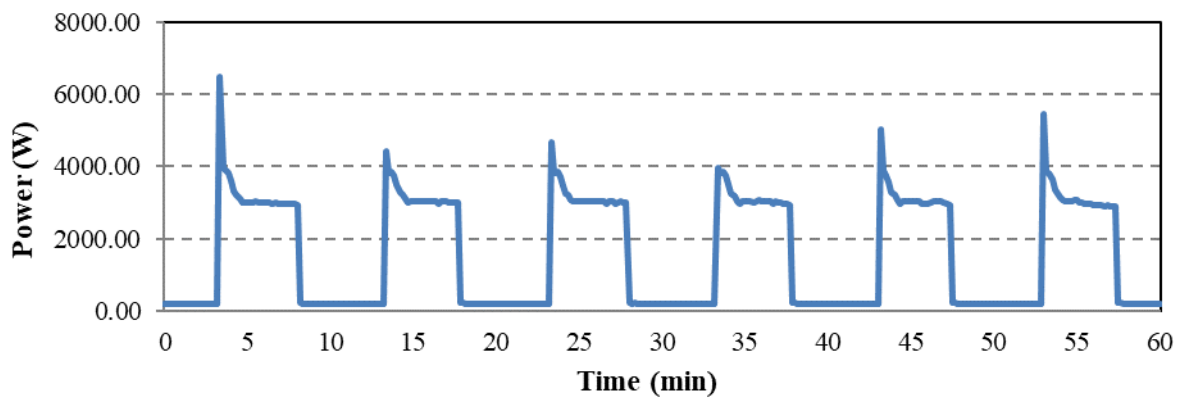
Figure 4-10. Power consumption, fabric duct at ceiling level, during a period of 1 hour.

4.3.3.2   *Refrigerant temperatures at inlet and outlet of each component*

The refrigeration system temperatures with the investigated air distribution configuration (fabric duct at ceiling level) are presented in Figure 4-11 and Figure 4-12. Figure 4-11 shows the refrigerant and air temperatures across the evaporator. During compressor operation, the refrigerant temperatures at the inlet and outlet of the evaporator were -6ºC and +7 ºC respectively. Figure 4-12 shows the refrigerant and air temperatures across the condenser. During compressor operation, the refrigerant temperatures at the inlet and outlet of the condenser were 65ºC and 30 ºC respectively.
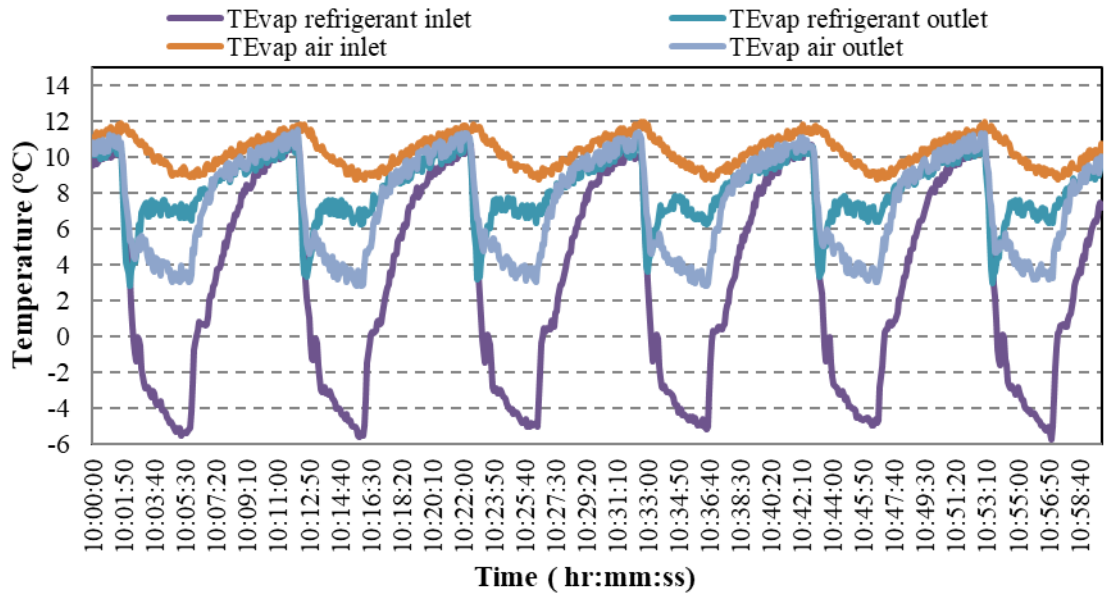
Figure 4-11. Fabric duct at ceiling level: refrigerant and air temperatures at inlet and outlet of the evaporator
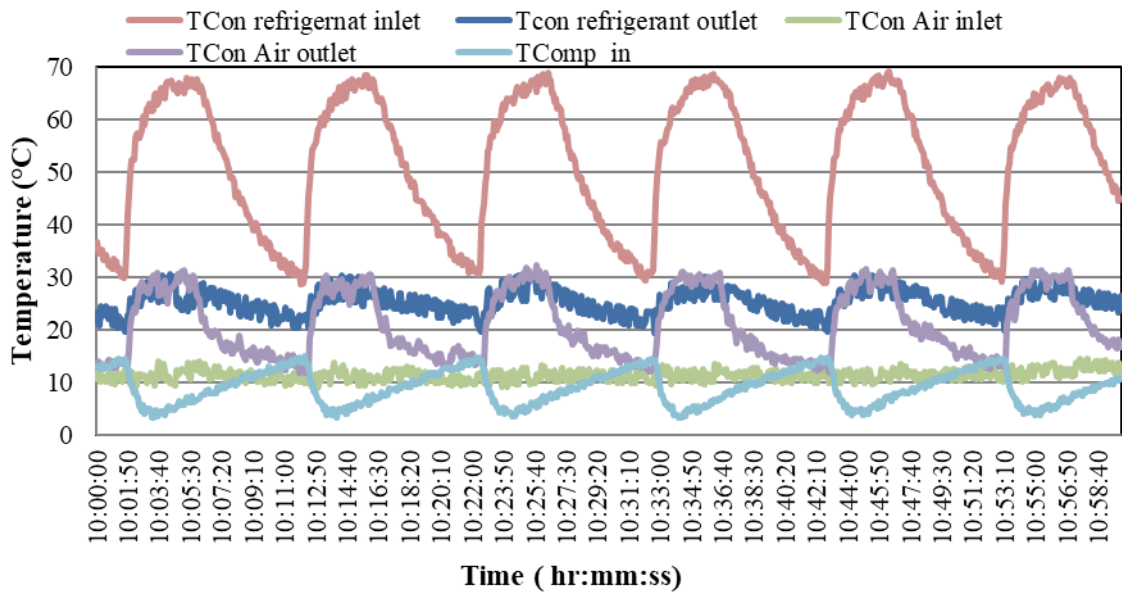
Figure 4-12. Fabric duct at ceiling level: refrigerant and air temperatures at inlet and outlet of the condenser

4.3.3.3 *Air velocity at the evaporator inlet and static pressure into the circular fabric duct*

Figure 4-13 shows air velocity values measured at the inlet of the evaporator and Figure 4-14 shows the static pressure at two different positions (P1 and P2) inside the fabric duct at different fan velocities. Figure 4-13 shows that air velocity values vary from 0.33 (50

% fan capacity) to 1.52 m.s^{-1} (100 % fan capacity). Each value presented was obtained from the average of the air velocity measured at 9 different positions at the inlet of the evaporator.
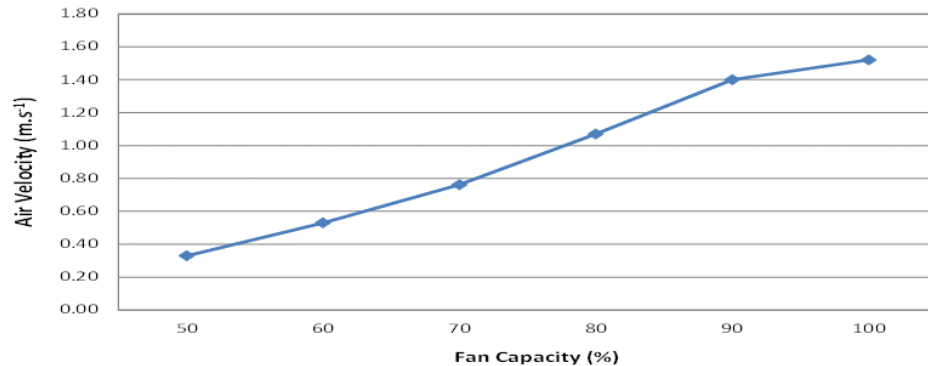
Figure 4-13. Circular fabric duct at ceiling level: Air velocity at the inlet of the evaporator

Position 1 refers to the data measured at the beginning of the fabric duct and position 2 refers to the data measured at the end of the fabric duct. At position 1, the static pressure increased from 0.084 in.H$_2$O (20.91 Pa) to 0.310 in.H$_2$O (77.21 Pa) when the fan velocity was increased from 60 % to 110 %. In the case of position 2, the static pressure increased from 0.060 in.H$_2$O (14.94 Pa) to 0.202 in.H$_2$O (50.31 Pa).
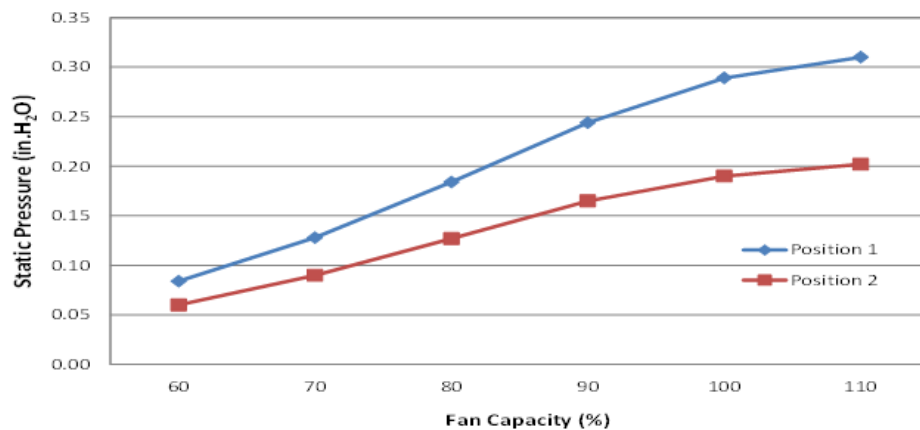
Figure 4-14. Circular fabric duct at ceiling level: Static pressure into the sock at different fan velocities.

4.4 Air distribution with non-ducted evaporator coil

This section presents the results of experimental measurements of the thermal environment arising from air distribution with non-ducted evaporator coil installed at ceiling level in the test rig as shown in Figure 4-15. This configuration corresponds to a cooling system currently applied in a large number of actual chilled food factories and cold rooms. The experimental results depict the investigated space thermal environment.

The main issue with this cooling method is that it tends to cool down uniformly the whole volume of the space. Furthermore, high air velocities are pronounced which, combined with the low operating temperatures can create a negative effect in the working environment in terms of thermal comfort.

Figure 4-15. Experimental test facility: Air distribution via non-ducted evaporator coil

4.4.1 *Experimental assessment: Air temperature profiles with non-ducted evaporator coil at ceiling level*

Figure 4-16 shows the air temperature distribution in the space with a supply air temperature from the evaporator at 7 ℃. The evaporator fan velocity was set at 100 % which corresponds to volumetric flow rate of 2825 m³/hr. Temperature values shown in Figure 4-16 correspond to the average values measured at each position during a 17 hour test.

According to the results, the whole space was kept at low temperatures varying from 6.0 ℃ to 9.1 ℃. The average temperature values measured at knee, head and ceiling level were 7.8 ℃, 7.6 ℃ and 7.2 ℃, respectively. Figure 4-17 represents graphically the temperature profiles at the 3 heights in the chamber. It can be observed that the air temperatures were fairly uniform in the space with no temperature stratification.
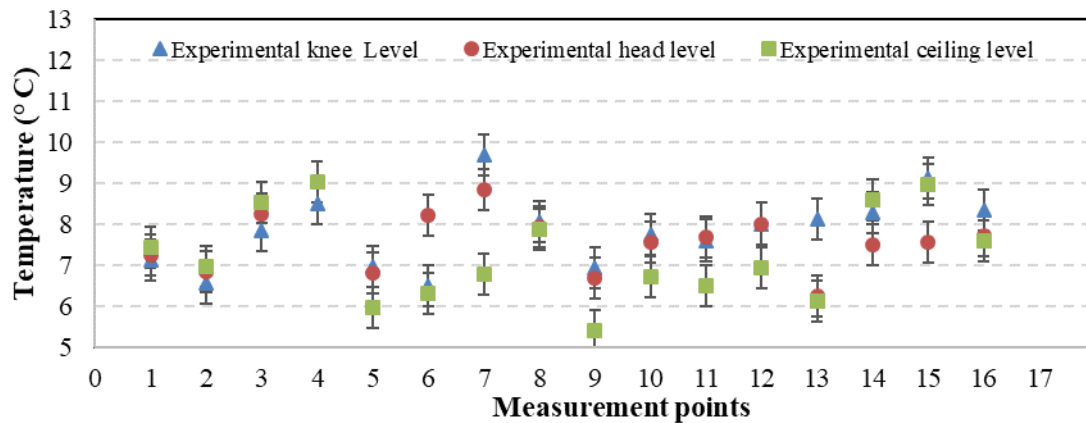
Figure 4-16. Non-ducted evaporator coil: Air temperature measurements
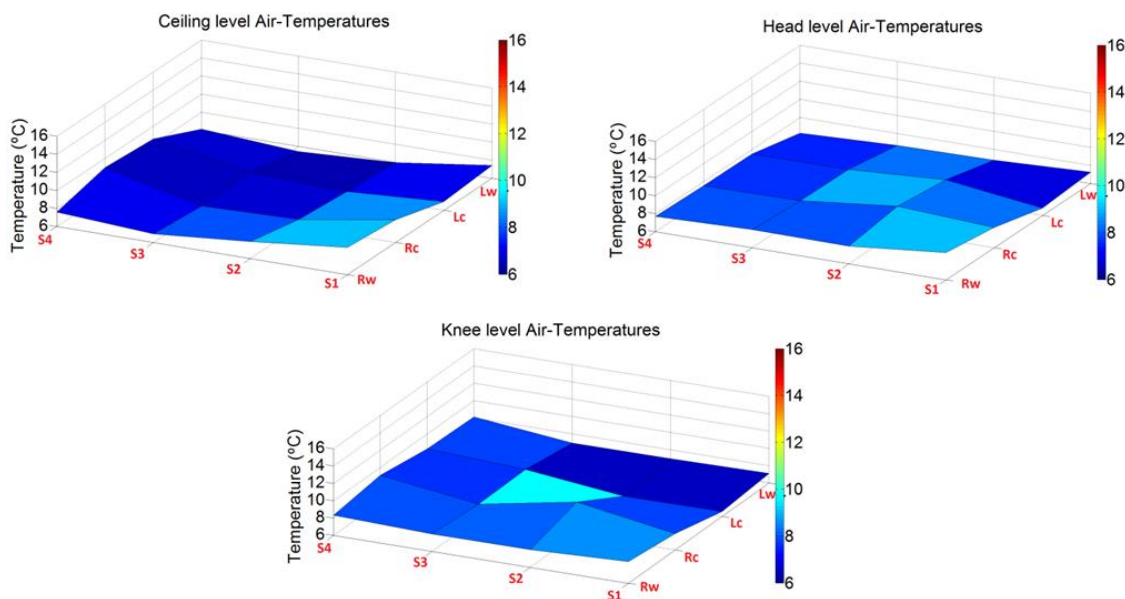
Figure 4-17. Un- ducted evaporator coil: Temperature profiles at different heights, knee Level, head Level and ceiling Level.

4.4.2 *Experimental assessment: Air velocity profiles with non-ducted evaporator coil at ceiling level*

The air velocities with the non-ducted evaporator coil, shown in Figure 4-18, were found to be relatively high ranging from 0.2 to 2.2 m s^{-1}. It can be observed that the highest air velocities were found at ceiling level due to the direct air discharge from the coil. The average velocities across all measurement points for knee, head and ceiling level were 0.45 m.s^{-1}, 0.37 m.s^{-1} and 0.82 m.s^{-1} respectively.

Figure 4-19 shows graphically the air velocity distribution along the space at the 3 different Heights that data were measured. At knee and head level, the velocity in some

locations was high, above 1.0 m s^{-1} which could create an uncomfortable environment for workers in the space.
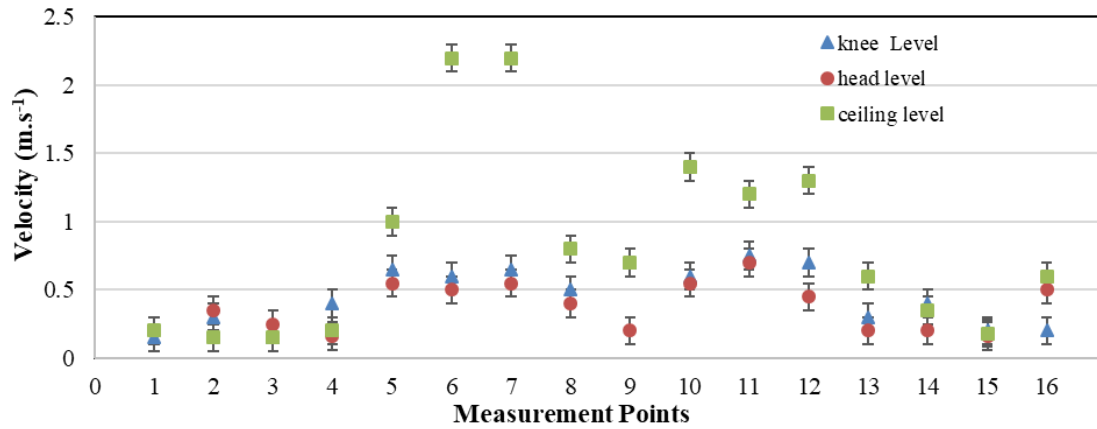
Figure 4-18. Non-ducted evaporator coil: Air velocity measurements
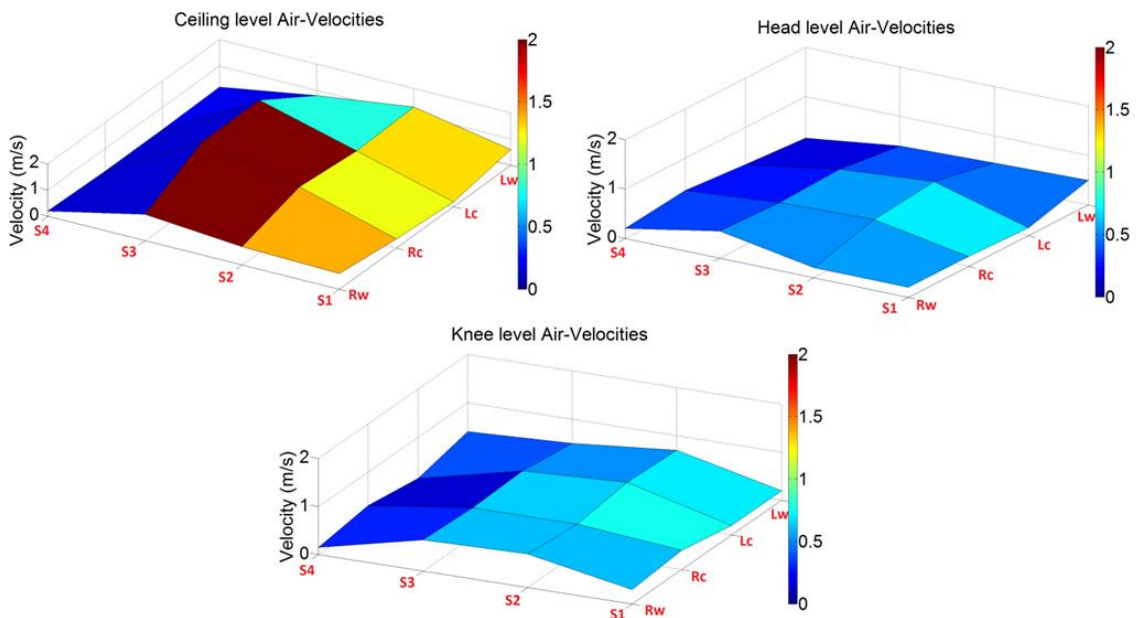
Figure 4-19. Non-ducted evaporator coil: Velocity profiles at different heights, knee Level, head Level and ceiling Level.

4.4.3 *Experimental assessment: Refrigeration system performance with non-ducted evaporator coil at ceiling level*

An analysis of the power consumption and refrigerant mass flow rate with the non-ducted evaporator coil is presented in this section. Data were collected over a 17 hour test period with ambient air temperature of 8 ℃. For clarity, power data and mass flow measurements are presented for a period of one hour in Figure 4-20 and Figure 4-21. Data of power consumption and mass flow rate collected for the 17 hours are given in Appendix B.

Power measurements include the power consumption of the compressor, condenser fans, evaporator fan and control system. For the non-ducted evaporator coil at ceiling level, the fan speed of the evaporator was kept at its nominal value which corresponds to volumetric flow rate of 2825 m³hr-1. The power consumption (P) of the refrigeration system was estimated by equation 1 in sub chapter 4.3.3.1

Power measurements showed that by using the non-ducted evaporator coil at ceiling level leads to higher power consumption compared with the air distribution via fabric duct installed at ceiling level. The operating time of the refrigeration system was 31.9 minutes per hour (fabric duct at ceiling level 25.6 minutes per hour) with 4.2 operating cycles with an average duration for each cycle of 7.6 minutes. The peak mass flow rate was 145kg/hr (Figure 4-20). From Figure 4-21which shows the variation of the refrigeration system power consumption, the average instantaneous power consumption was 3.15 kW.
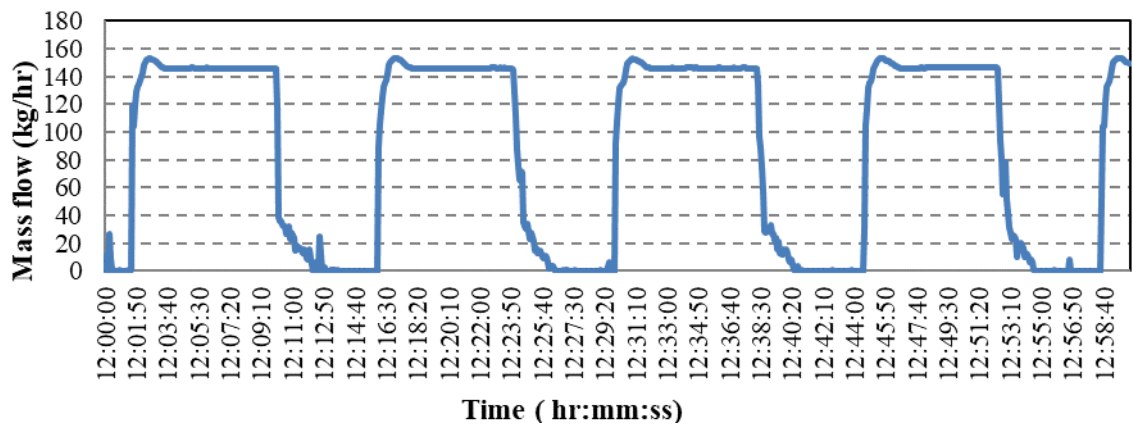
Figure 4-20. Mass flow rate: Non-ducted evaporator coil, during a period of 1 hour.
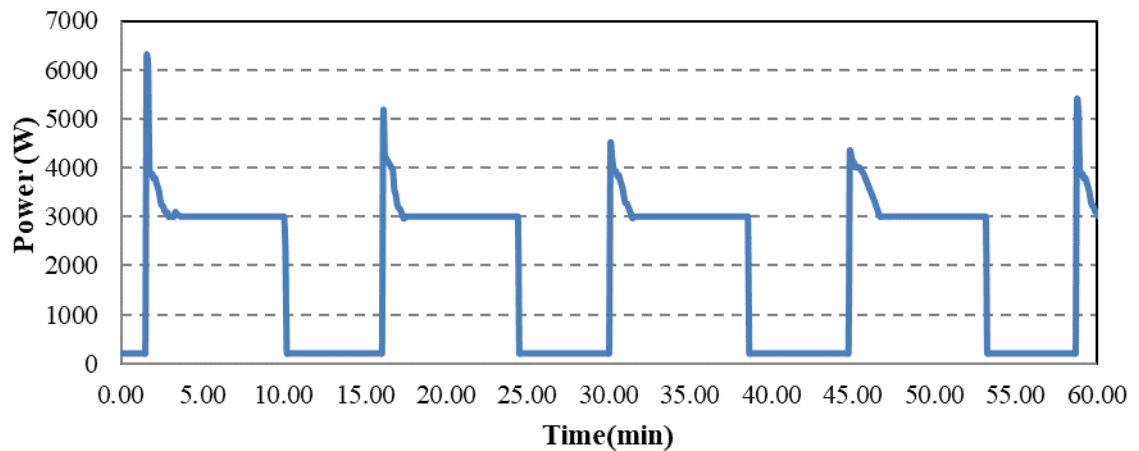
Figure 4-21. Power consumption: Non-ducted evaporator coil, during a period of 1 hour.

4.5   Summary of Chapter 4

This chapter focuses on the development and testing of an experimental facility designed to represent a section of an actual chilled food processing room. The air distribution systems initially tested were the fabric duct installed at ceiling level (case study 2 air distribution system) and the non-ducted evaporator coil. Both air distribution methods are applied in many existing chilled food facilities. The initial monitoring results proved that the developed facility can adequately represent the conditions in chilled food factories in terms of air distribution and the thermal environment in the space.

Comparing the air flow velocities obtained from the air distribution system via non-ducted coil and fabric ducts it can be highlighted that the fabric duct provided much lower air flow velocities. This is beneficial to achieve some temperature stratification in the space and reduce the discomfort of the workers produced by high velocities as seen in the case of the non-ducted coil. Furthermore, it can be concluded that the fabric duct delivered a better environment in the space in terms of air velocity uniformity at the level of the production area. This was mainly due to the lower air velocities in the space obtained with the fabric duct air distribution method. Therefore, there was a clear direct influence of the air flow velocity on the temperature stratification obtained in the space. In addition, the fabric duct resulted in average air temperature stratification in the space of the order of 2.5 °C.

Power measurements showed that by using the non-ducted evaporator coil at ceiling level resulted in higher power consumption compared with the air distribution via fabric duct installed at ceiling level. Power measurements showed that the on-periods for the non-ducted evaporator coil were longer than those for the air distribution with the circular fabric duct. This is primarily due to the high mixing of air in the space and lower temperatures without temperature stratification with the non-ducted coil, which require the refrigeration system to run for a longer time to maintain the temperature in the space. These characteristics result in energy savings of 15% for the circular fabric duct compared to the non-ducted evaporator coil.

Chapter 5 deals with the development of a 3-D CFD air distribution model in order to predict the air temperatures and velocities over the space. In addition, the developed CFD model was validated through measurements taken from the test facility monitoring from Case studies 1 and 2.

Chapter 5. CFD Air distribution model development

5.1   Introduction

A modelling tool based on computational fluid dynamics was developed in order to simulate the air flow and the thermal environment arising from the investigated air distribution methods applied to the experimental facility and the chilled food facilities. The CFD simulations were conducted by developing three-dimensional CFD models.

The validity of the computational models was assessed by comparing modelling results with data obtained from existing chilled food facilities and experimental test facility in the laboratory. This tool was subsequently used to evaluate different air distribution systems and their impact on the air flow and the thermal environment of the space. The case studies that were used for the validation of the CFD Air distribution model were:

- Experimental facility, circular fabric duct at ceiling level
- Experimental facility, non-ducted evaporator coil
- Chilled food facility (Case study 1)
- Chilled food facility (Case study 2)

5.2   CFD Air distribution model simulation solution procedure

The steady state 3-D CFD models detailed in the following sections were solved using the commercial software ANSYS FLUENT®. The simulation process was divided into 3 stages: Pre-processing;, Solving and Post-processing. Figure 5-1 shows the procedure followed in order to implement the CFD simulations.
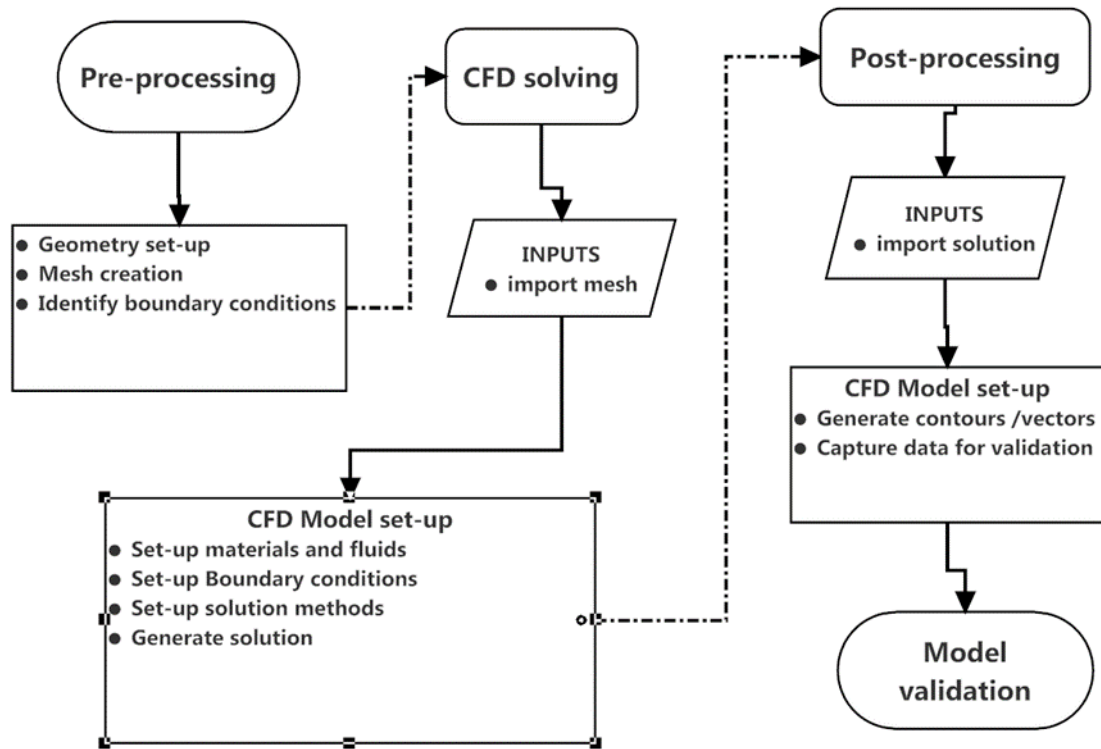
Figure 5-1. Simulation procedure

Initially, the first 3-D model was solved using 6 different turbulence models (Standard k-ε, Realizable k-ε, RNG k-ε, standard k- ω, SST k-ω, and 7 equations Reynolds stress model). The SST-k-ω turbulence model was found to predict actual measured data with better accuracy and reasonable computational time compared to the other turbulence models. The 7 equations Reynolds stress model showed good prediction of the measured data, however, the computational time rose drastically. Furthermore, several computational errors were obtained when the three k-ε models were used and the standard k- ω model was less accurate compared with the SST k-ω model. The SST k-ω model has also been pointed out in open literature as a more accurate model in comparison to the k-ε and k- ω models (Delele et al., 2009, 2013; Stamou and Katsiris, 2006). Based on the previous observations, the 3-D model for the remaining simulations was directly solved using the SST k-ω turbulence model.

The SST-k-ω turbulence model is a two-equation eddy-viscosity model (eq. 1 and 3) which was developed by (Menter 1994) to effectively blend the robust and accurate formulation of the model in the near-wall region. In general, two-equation turbulence models allow the determination of the turbulent length and the time scale by solving two separate transport equations.

The main difference from the turbulent viscosity definition of the standard k-ω turbulence model is that the modelling constants are different and are modified in order to take into account the transport of the turbulent shear stress. The SST-k-ω turbulence model combines the usage of the k-ω formulas for the inner parts of the boundary layers and the usage of the SST formulation to switch the k-ε behaviour in the free-stream. As a result, the SST-k-ω turbulence model can be used as a Low-Re turbulence model without any extra damping functions and combined with the k-ε behaviour avoids the common k-ω problem where the model is too sensitive to the inlet free-stream turbulence properties. The SST-k-ω turbulence model is more accurate and reliable for a wider class of flows than the standard k-ω model (Ansys Fluent 2011 theory guide). The following transport equations define the SST-k-ω turbulence model form. (Ansys Fluent 2011 theory guide)

$$\frac{\partial}{\partial t}(\rho k) + \frac{\partial}{\partial x_i}(\rho k u_i) = \frac{\partial}{\partial x_j}\left\{\Gamma_k \frac{\partial k}{\partial x_j}\right\} + \widetilde{G_k} - Y_k + S_k \tag{2}$$

$$\frac{\partial}{\partial t}(\rho \omega) + \frac{\partial}{\partial x_j}(\rho \omega u_j) = \frac{\partial}{\partial x_j}\left\{\Gamma_\omega \frac{\partial \omega}{\partial x_j}\right\} + G_\omega - Y_\omega + D_\omega + S_\omega \tag{3}$$

$$\widetilde{G_k} = \min(G_k, 10\rho\beta^* k\omega) \tag{4}$$

$$G_\omega = \frac{\alpha}{v_t}\widetilde{G_k} \tag{5}$$

In Eq 3, (G_k)̃ represents the generation of turbulence kinetic energy due to mean velocity gradients. In addition, in Eq. 4, G_ω represents the generation of ω which is calculated similarly to the standard k-ω turbulence model. Γ_k and Γ_ω represent the effective diffusivity of k and ω respectively. Y_k and Y_ω represent the dissipation of k and ω due to turbulence. D_ω is the cross-diffusion term, and S_k and S_ω are user-defined source terms. (G_k)̃ and G_ω are estimated as shown in Eq. 5 and 6, respectively. In Eq. 3, G_k is determined as in the standard k-ω model. α is a factor for turbulent viscosity causing a low-Reynolds number correction.

The effective diffusivities Γ_k and Γ_ω are determined by Eq. 7 and 8. σ_k and σ_ω are the turbulent Prandtl numbers for k and ω, respectively. μ_t refers to the turbulent viscosity. More details of the turbulence model can be found in Ref. (ANSYS FLUENT Theory Guide, 2011; Menter, 1994).

$$\Gamma_k = \mu + \frac{\mu_t}{\sigma_k} \qquad\qquad (6)$$

$$\Gamma_\omega = \mu + \frac{\mu_t}{\sigma_\omega} \qquad\qquad (7)$$

Each 3D model was solved with the pressure based solution algorithm, second order upwind energy and momentum discretization, 'Body-Force' weighted pressure discretization, and SIMPLE pressure-velocity coupling. The second order upwind scheme uses a multidimensional linear reconstruction approach to compute with better accuracy the quantities at cell faces. In addition, the body-force-weighted scheme implements the face pressure computations with the assumption that the normal gradient of the difference between pressure and body forces is constant. The SIMPLE pressure-velocity coupling uses a relationship between velocity and pressure corrections to enforce mass conservation and to obtain the pressure field. More details about how CFD fluent works can be found in ANSYS Fluent Theory Guide (Ansys 2011).

The air inside the food processing area was considered to be compressible and the density was allowed to vary according to the ideal gas law to account for buoyancy effects. The main difference between compressible and incompressible flow is the level of density variation during the flow. A flow is classified as being incompressible when the density of the fluid remains constant throughout flow path-line. Other thermal properties were maintained constant (specific heat, thermal conductivity and viscosity). The raw materials of the food products were not considered in the simulation boundary conditions. The majority of the raw materials are already cooled down prior their entry in to the processing lines. Hence, any affect that the heat gains from the food raw material thermal mass may have on the thermal environment would be negligible and was not included in the modelling.

The thermal boundary conditions of the surrounding walls, ceiling and floor were aproached taking into account the heat flow, temperature profile and thermal resistances (Figure 5-2 and Eqs. 9, 10 and 11) over the interior and exterior of the construction.
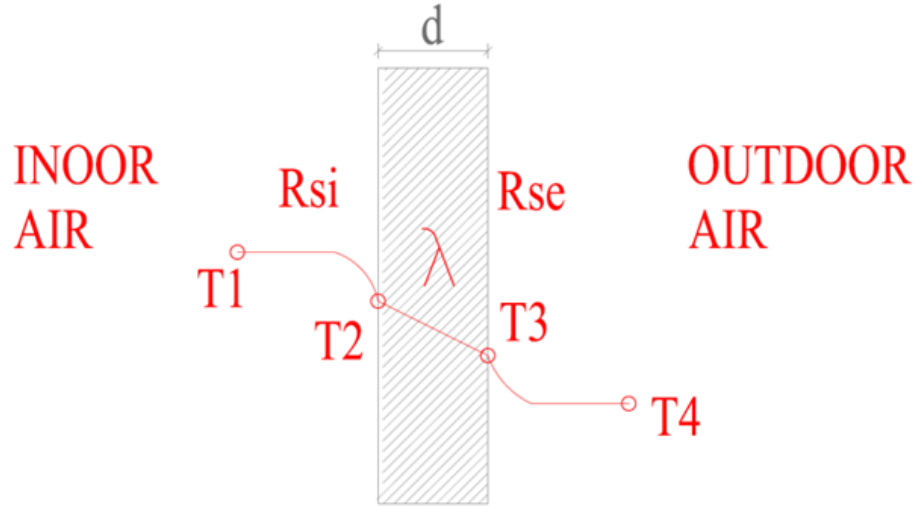
Figure 5-2. Heat flow

$$Ui = \frac{1}{Rsi + R1 + Rse} \left(\frac{W}{m^2 K}\right) \qquad (8)$$

$$R1 = \frac{d}{\lambda} \left(\frac{m^2 K}{W}\right) \qquad (9)$$

Where, $\lambda \left(\frac{W}{m\,K}\right)$, d (m), $Rsi \left(\frac{m^2 K}{W}\right)$, and $Rse \left(\frac{m^2 K}{W}\right)$

$$q = Ui \times \Delta T \left(\frac{W}{m^2}\right) \qquad (10)$$

In Eq 9, Ui represents the overall heat transfer coefficient, and in Eq 10, R1 represents the thermal resistance per unit area of the wall; d represents the thickness and λ the thermal conductivity of the construction. In Eq 9, Rsi and Rse represent the outside and inside surface resistances respectively. Table 5-1 and Figure 5-3 how is the values of the internal and external surface resistances used, depending on the direction of the heat flow.

In Eq 11, q represents the total heat flow per unit area of the construction (BS EN ISO 6946 2007).

Table 5-1. Surface resistance

Surface Resistance	Direction of heat flow		
(m²K / W)	Upwards	Horizontal	Downwards
Rsi	0.10	0.13	0.17
Rse	0.04	0.04	0.04
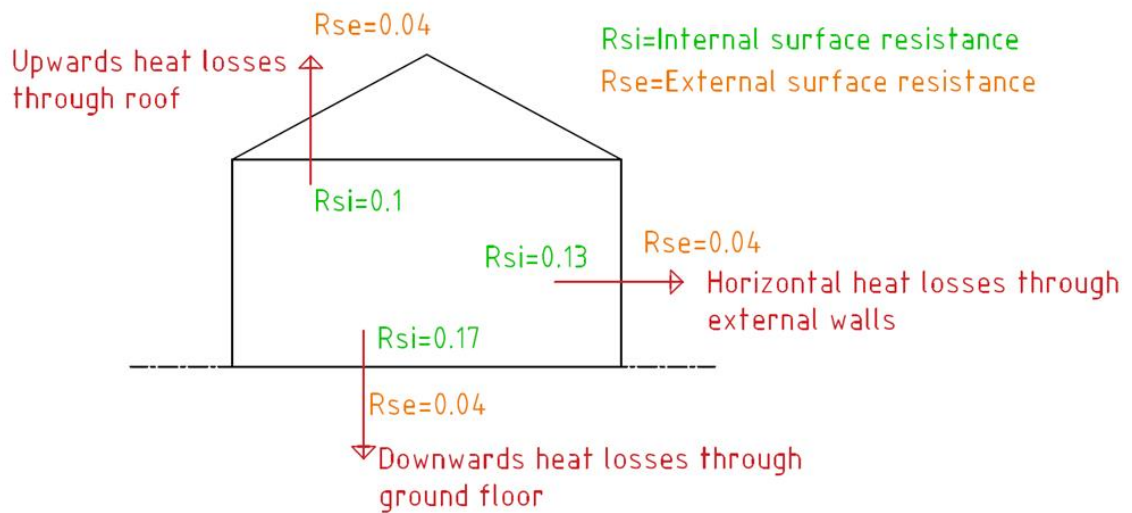
Figure 5-3. Surface resistance graphical representation

5.3 Experimental facility 'Circular fabric duct at ceiling level': CFD Air distribution model

This section discusses the results of the CFD modelling of the thermal environment arising from the air distribution system using the fabric duct at ceiling level. Figure 5-4 shows the developed 3-d CFD model representing the experimental set-up. This model is designed to predict the air temperature and velocity distribution into the investigated space. The experimental facility CFD model was designed using the actual dimensions of the test-room. The actual dimensions and geometry of the experimental facility are shown in Figure 4-1.
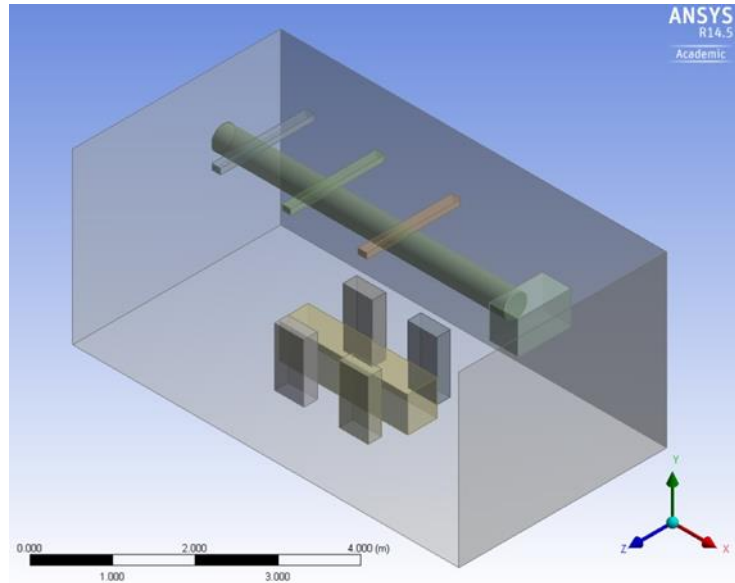
Figure 5-4. Experimental facility with circular fabric duct at ceiling level: 3-D CFD model

5.3.1 CFD Air distribution model meshing

The computational domain was discretized with an automatic mesh method, mainly with tetrahedral and hexahedral cells generated using the in-built ANSYS design modeller meshing algorithm. The mesh density was gradually refined near the internal wall surfaces, internal heat gain sources and the fabric air supply duct. The final mesh size consisted of 9.6 million elements, with element dimensions between 0.02 and 0.06 m. Four inflation layers were employed near the wall surfaces with a first element size of 0.04 m and a growth ratio of 1.2. In addition, a finer mesh was applied by four inflation layers near the internal heat gain surfaces (occupants and lighting) and the air-socks with a first element size of 0.02 m and a growth ratio of 1.2 to capture the effects of the boundary layer. The mesh gradually increased towards the bulk of the air domain producing a maximum element size of 0.06 m.

The final model mesh was generated following a mesh independence study. The convergence criteria for the independence study were set to reach at least a 10-5 residual error for continuity and an average temperature tolerance of $\pm$ 0.5 °C. Mesh refinement was performed by varying all mesh sizes by the same ratio, but maintaining the inflation parameters. The simulation time for each steady-state case was 8 hours, with an average of 3000 iterations, on a 2.5GHz, 64GB RAM, Intel Xeon Processor (2 processors) with 48 parallel threads. Simulation results on the mesh independent grid showed an average y+ value of 6.
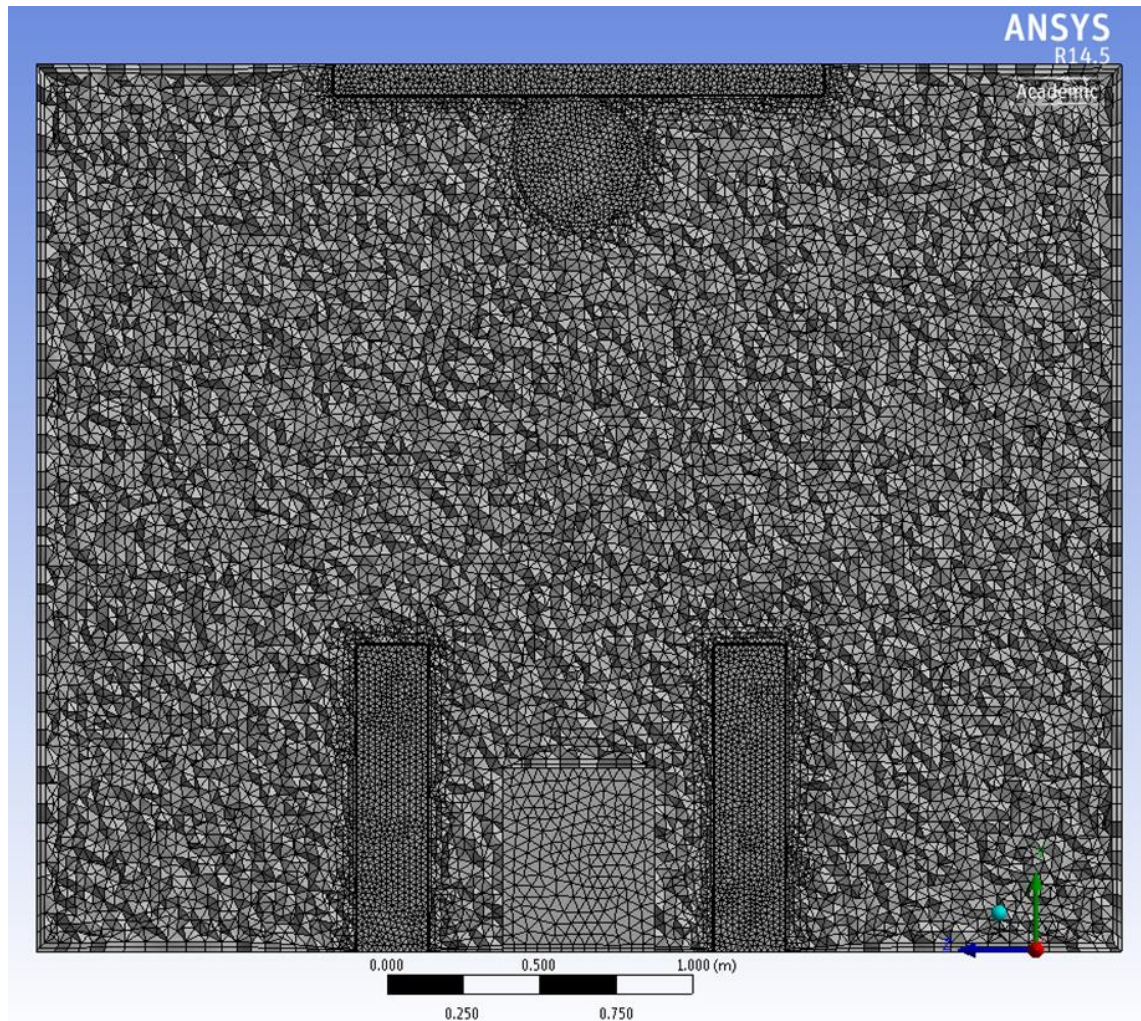
Figure 5-5. Circular fabric duct at ceiling level: Mesh details

Figure 5-6 shows an example of the mesh independency study implemented in order to achieve a mesh independent solution. The convergence criteria for the independency study were set to reach at least a 10-5 residual error for continuity and an average temperature tolerance of ± 0.5 °C. The 3 values of interest were the average temperatures at knee, head and ceiling level height. The initial mesh size was set to 4.6 million cells and the solution convergence criteria at 3000 iterations. Figure 5-5 shows that predicted temperature values of interest were not close to experimental values. Increasing the mesh size to 9.6 million cells the required accuracy was achieved. A further increase to 11.6 million cells did not produce any further improvement and so 9.6 million cells were used for the simulations.
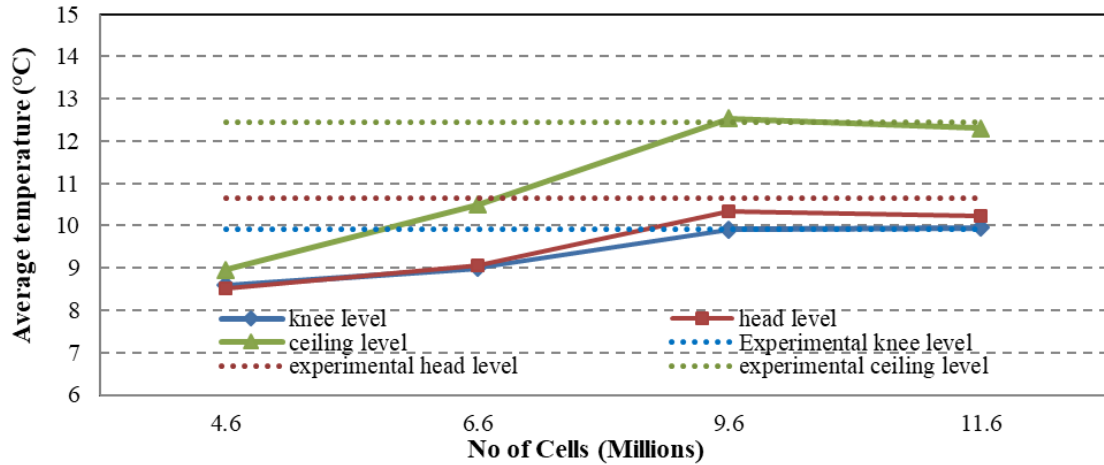
Figure 5-6. Circular fabric duct at ceiling level: Mesh independence study

5.3.2 *CFD Air distribution model boundary conditions*

The air flow supply and return from the evaporator coil were set at 2825 m³hr⁻¹. The target in an air-sock is to achieve a constant static pressure inside the sock which will maintain it inflated and will give a uniform discharge air velocity across the whole surface (normally around 0.1 m.s⁻¹). Due to the density difference between the supplied air and the room air, the supply air descends towards the floor after passing through the sock surface.

For the CFD modelling boundary conditions, the air supply from the air-sock was defined as mass flow inlet setting up the total coil air volume being discharged from the fabric duct surface. The modelling resulted a uniform surface discharge air velocity of 0.15 m.s¹ on the fabric duct surface. In addition, the coil return air boundary condition was defined as mass flow outlet. The boundary conditions for air supply temperature was set at 7 ℃. The occupancy density of the investigated processing area was set at 4 occupants taking into account the experimental facility model area. Each occupant was defined as a rectangular box with 1.57 m² surface area (1.2 m height) with a sensible thermal load of 150 W. The lighting thermal boundary condition was defined with a temperature of 28 ℃ for all the light (value measured experimentally) fixture surfaces. Other heat sources into the processing area were neglected.

The thermal boundary conditions of the surrounding walls were calculated by taking into account the heat flow, temperature profile and thermal resistances (*Rsi, Rw, Rse*) over the interior and exterior of the wall (Figure 5-2 and Eqs. 7,8,9,10 and 11). The wall boundary

condition was estimated considering an outdoor temperature of 20 ℃. The wall thickness was 0.1 m while the thermal conductivity of the wall was 0.023 $W.m^{-1}.K^{-1}$. The exterior and interior wall surface resistances were 0.13 $m^2.K.\ W^{-1}$ and 0.04 $m^2.K.\ W^{-1}$, respectively.

5.3.3   *CFD Air distribution model post-processing*

This subsection presents the results regarding the CFD modelling of the experimental facility using fabric ducts as an air distribution method. Modeling results of the facility are presented below.

Figure 5-7 shows the velocity distribution at 4 cross sections along the space from the modelling of the air distribution system via fabric duct at ceiling level. Modelled air flow velocities in the space were found to be very low and ranging from 0.01 to 0.3 $m.s^{-1}$. It is observed that the highest air flows were found close to the air return section. Figure 5-8 shows the air temperature distribution in the space with a supply air temperature from the fabric duct at 7 ℃. The temperature in the bulk of the space varied between 8.9 ℃ and 13.4 ℃ at the same locations as the measurement points of the experimental tests. This shows that, as it was observed from the experimental measurements, some temperature stratification was obtained with lowest temperatures measured at knee level and highest at ceiling level.
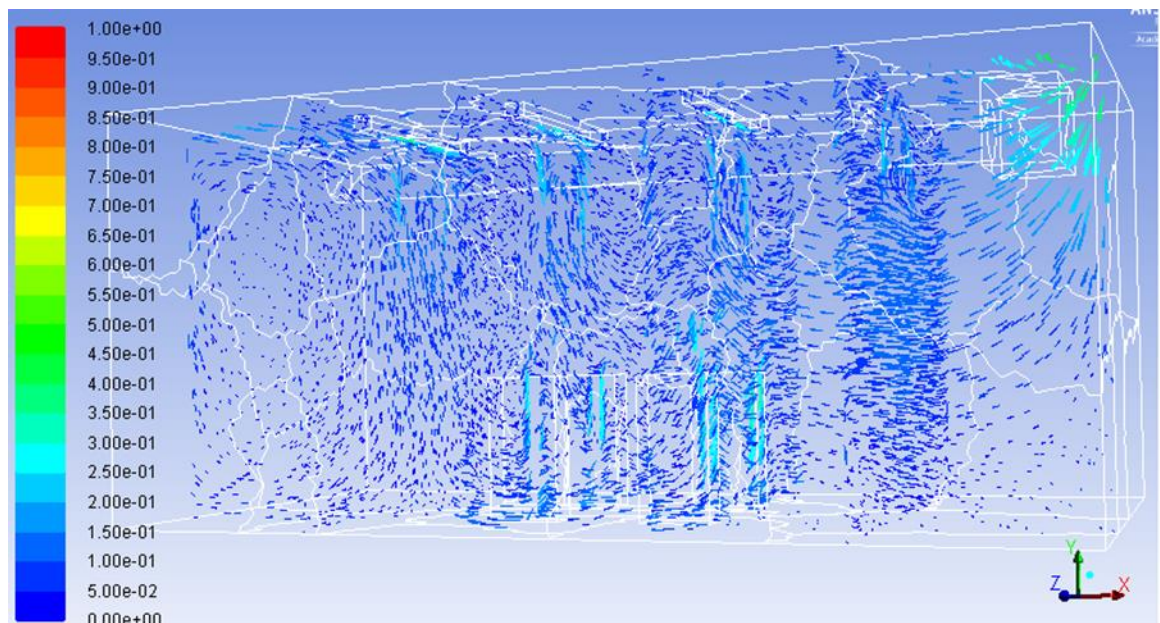
Figure 5-7. CFD Simulation results of air velocity in the space (m.s^{-1}).
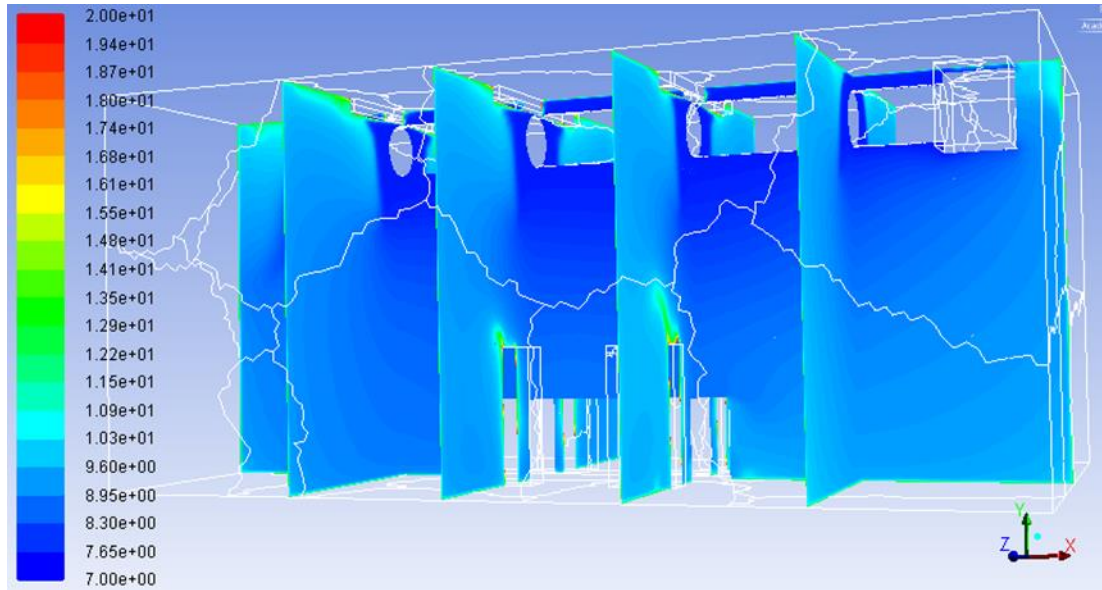
Figure 5-8. CFD Simulation of air temperature in the space (ºC).

5.3.4 CFD Air distribution model validation

This subsection presents the validation of the CFD model using fabric ducts as an air distribution method. The validation of the model was conducted by comparing the monitored air temperatures/velocities (as described in section 4.3) with the CFD predicted temperatures/velocities. Figure 5-9 and Figure 5-10 present the average temperature and velocity data from the experimental measurements, including measurement uncertainty, and comparison with the modelling results. In general, the model shows a good level of prediction for the air temperature distribution and velocity variations achieved in the space. From all results, the average absolute error across all test points in the space was found to be 0.95 ºC and 0.1 m.s^{-1}.
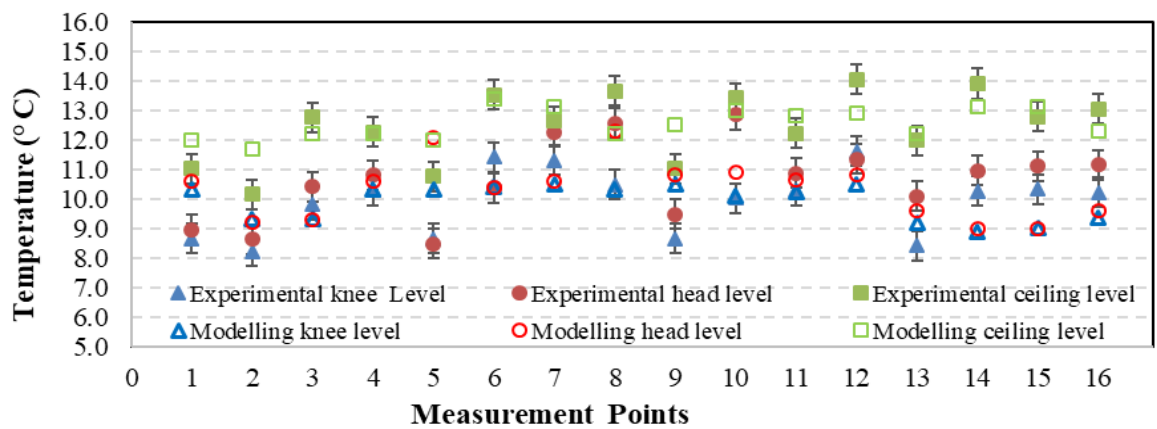
Figure 5-9. Comparison of experimental and CFD modelling results for air temperature
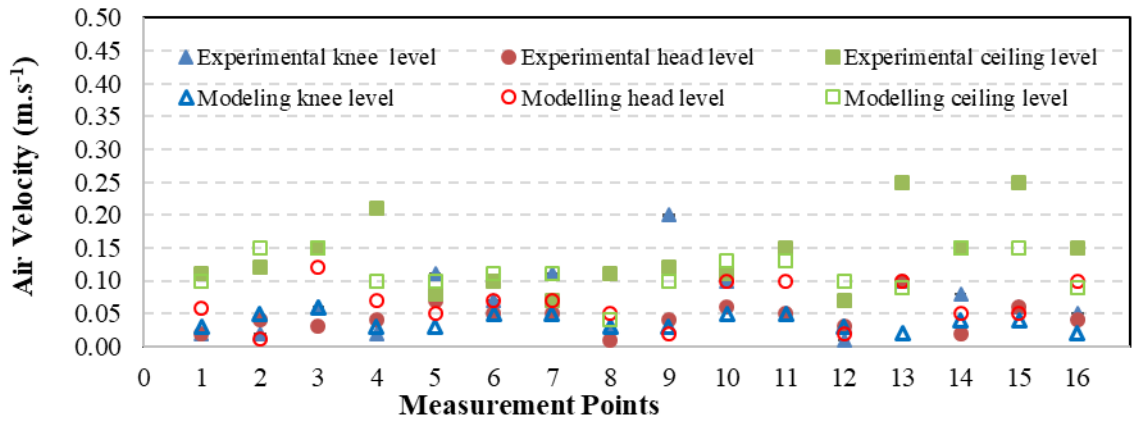
Figure 5-10. Comparison of experimental and CFD modelling results for air velocity

Figure 5-11 shows a comparison between the temperature profiles predicted by the model against temperature measurements in the space. The middle line in the graph indicates the position of 0 ℃ error. The lines above and below indicate the maximum error boundaries. Regarding the positive maximum error boundary line, for each measuring point the maximum positive error is added with the experimental value. The linear tread-line projecting these values represents the positive maximum error boundary line. Equally the negative maximum error boundary line is plotted as a projection of a linear trend-line covering the subtraction of the maximum negative error from the experimental values for each measuring point. The blue points on the graph indicate the modelling values on X axis and experimental value on Y axis. The Distance from the red line depicts the prediction error. Blue spots existing above and below the red line presents a positive and negative prediction error respectively. The absolute average error across all test points in the space was found to be 0.95 ℃ lower than the measured values. The maximum absolute error was found to be 1.7 ℃ lower than the measured value. Considering the measuring equipment uncertainty (± 0.35 ℃) the modelling results validation shows that the predicted air temperatures and their trends are in good agreement with the collected experimental data. The formula used to calculate the absolute error is given in eq. (12).

$$\text{Absolute Error} = |(\text{Experimental Value} \pm \text{CFD Value})| \qquad (11)$$
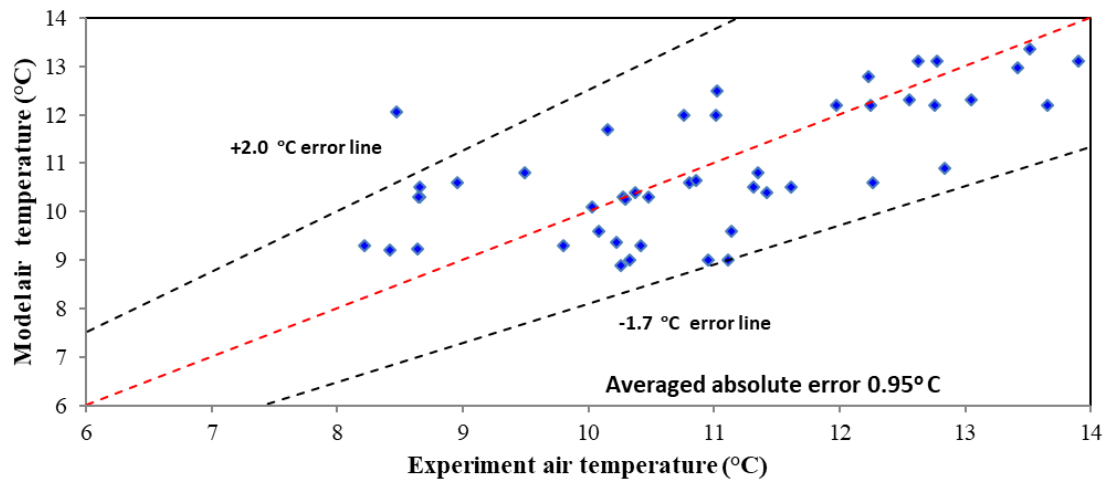
Figure 5-11. Comparison of experimental and CFD modelling results for air temperature.

5.4 Experimental facility 'non-ducted coil': CFD Air distribution model

This section discusses the results of CFD modelling of the thermal environment arising from the air distribution system via the non-ducted evaporator coil at ceiling level. Figure 5-12 shows the 3-D CFD model representation of the experimental sett-up.
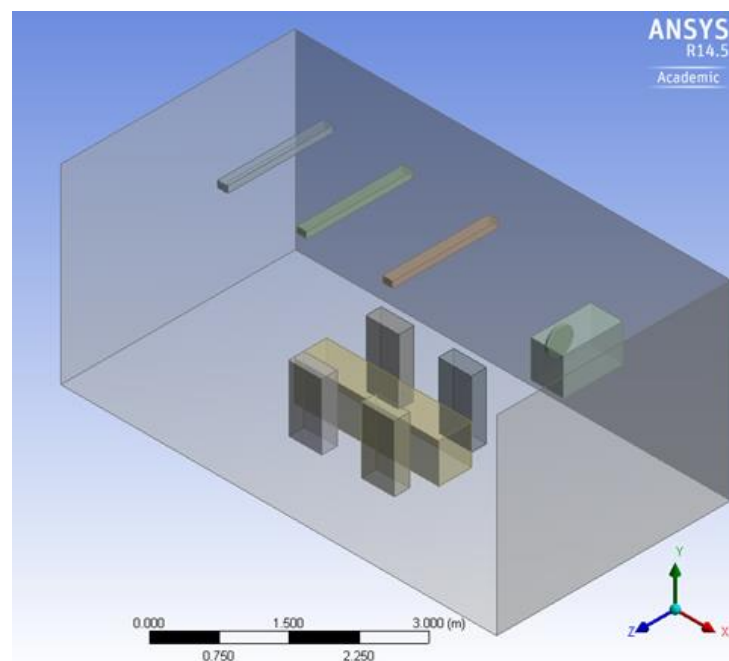
Figure 5-12. CFD model representation of the test facility with non-ducted evaporator coil.

5.4.1 *CFD Air distribution model meshing*

The computational domain was discretized with an automatic mesh method, with mainly tetrahedral cells and hexahedral cells in the boundary layer. The mesh density was gradually refined near the building wall, thermal input surface and the fabric duct. The final mesh size consisted of 9.4 million elements, with element dimensions between 0.02-0.06 m (Figure 5-13). The finer mesh sizes were located near the wall surfaces, where further 4 inflation layers were also employed to capture the effects of the boundary layer. The final model mesh was generated following a mesh independency study, and the simulation time for each steady-state case was 8 hours, with an average of 3000 iterations, on a 2.5 GHz, 64GB RAM, Intel Xeon Processor (2 processors) with 48 parallel threads.
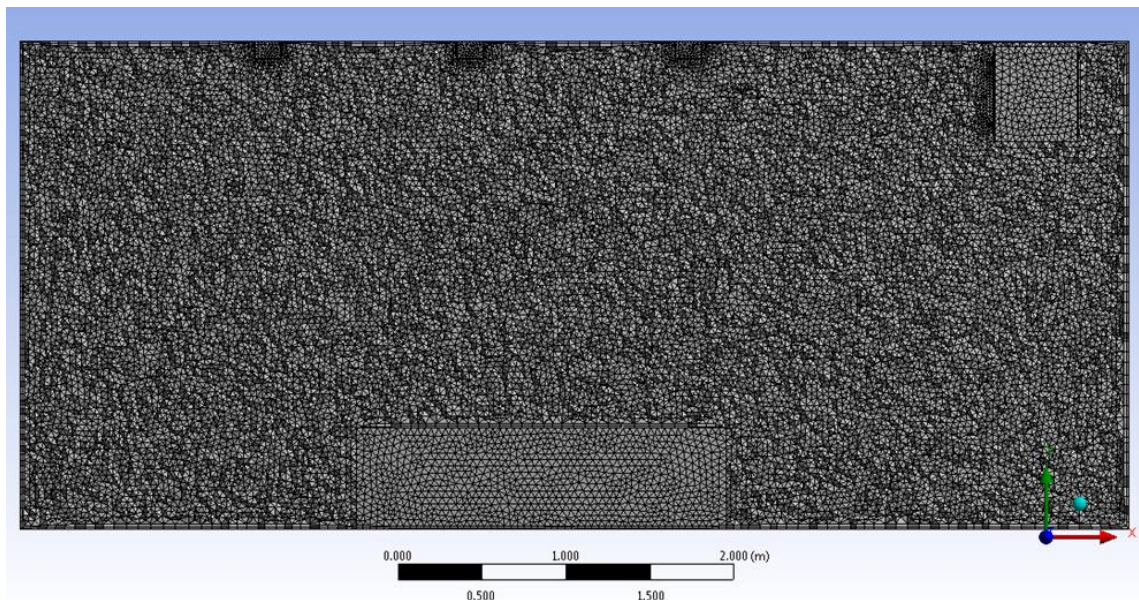
Figure 5-13. Non-ducted evaporator coil: Mesh section

5.4.2 *CFD Air distribution model Boundary conditions*

The air flow supply and return from the evaporator were set at 2825 m³hr^{-1}. The air supply and return air at the coil boundary conditions were defined as mass flow inlets and outlets, respectively. The air supply temperature was set at 7 ℃. The occupancy density was set at 4 occupants. Thermal and internal heat gains boundary conditions were defined as explained in section 5.3.2. Other heat sources into the processing area were neglected.

5.4.3 *CFD Air distribution model post-processing*

This subsection presents the results regarding the CFD modelling of the experimental facility using non-ducted evaporator as an air distribution method. Figure 5-14 shows the

velocity distribution at 4 cross sections along the space. It can be seen that air flow velocities in the space can be high reaching 3.0 m.s^{-1}. As was also observed from the experimental measurements, the highest air velocities were found at ceiling level due to the direct air discharge from coil. In addition, high velocities were also predicted at knee and head level which can lead to excessive discomfort for the occupants.

It can also be observed that the air flow patterns over the space are not uniform. The air flows along the ceiling to the front wall, and then down along the wall to the floor. Recirculation then takes place in an area between floor level and ceiling level. From Figure 5-14 it can also be observed that the air displacement around the space is mainly influenced by the high air flow velocity from the coil rather than buoyancy effects due to heat gains from the workers and equipment.
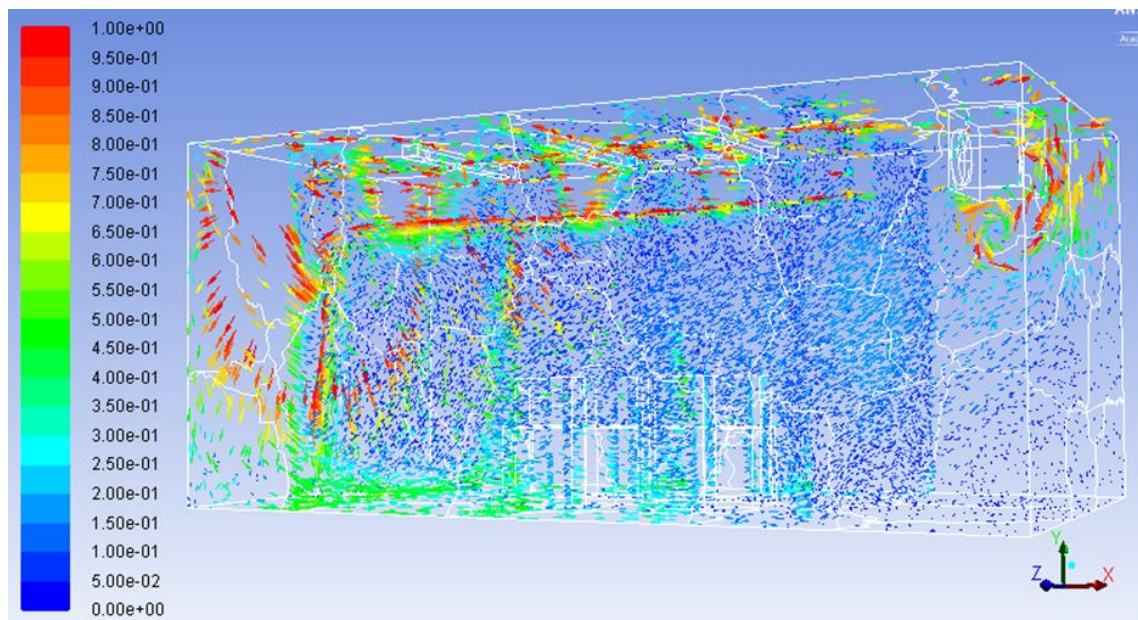
Figure 5-14. CFD Simulation results of air velocity in the space (m.s^{-1}).

Figure 5-15 shows the air temperature distribution in the space with a supply air temperature from the evaporator at 7 ºC. The temperature in the bulk of the space varied between 7.0 ºC and 8.0 ºC at the same positions as the measurement points in experimental tests. As can be seen from Figure 5-15, temperature variation in the space is quite small with slightly higher temperatures only close to the lights and occupant heat sources. This is in agreement with the data from the experimental measurements.

Based on the CFD modelling results and experimental measurements it can be seen that the fan coil distribution system provides mixing and relatively uniform air in the space

arising from the relatively high air velocities. High air velocities at head and knee level, however can lead to excessive discomfort for the occupants and high energy consumption.
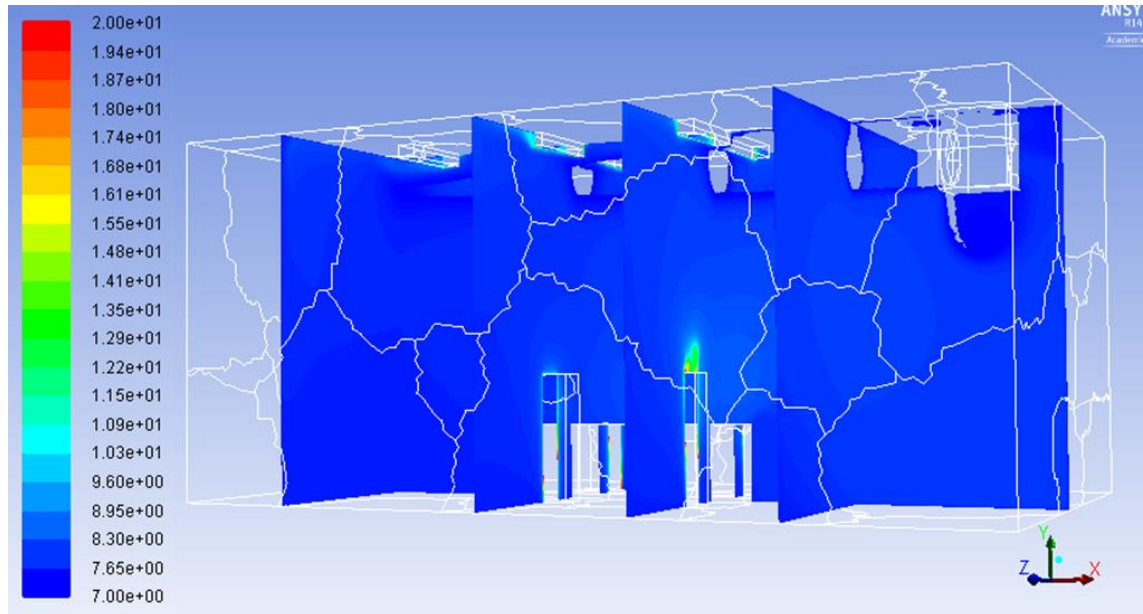
Figure 5-15. CFD Simulation of air temperature in the space (ºC).

5.4.4   CFD Air distribution model validation

This subsection presents the validation of the CFD model of the experimental facility using a non-ducted evaporator coil at ceiling level for air distribution in the space. The validation of the model was conducted by comparing the monitored air temperatures (as described in section 4.4) with the CFD predicted temperatures. Figure 5-16 and Figure 5-17 present the average temperature and velocity data recorded including the measurement uncertainty and the modelling results.

Figure 5-18 shows a comparison between the temperature predictions from the model against temperature measurements from the experimental facility. The middle line in the graph indicates the position of 0 ºC error and the other two lines show the maximum errors of +2.0 and -2.1 ºC respectively. From all results, the average absolute error across all test points in the space was found to be 0.73 ºC and 0.6 ms^{-1}.
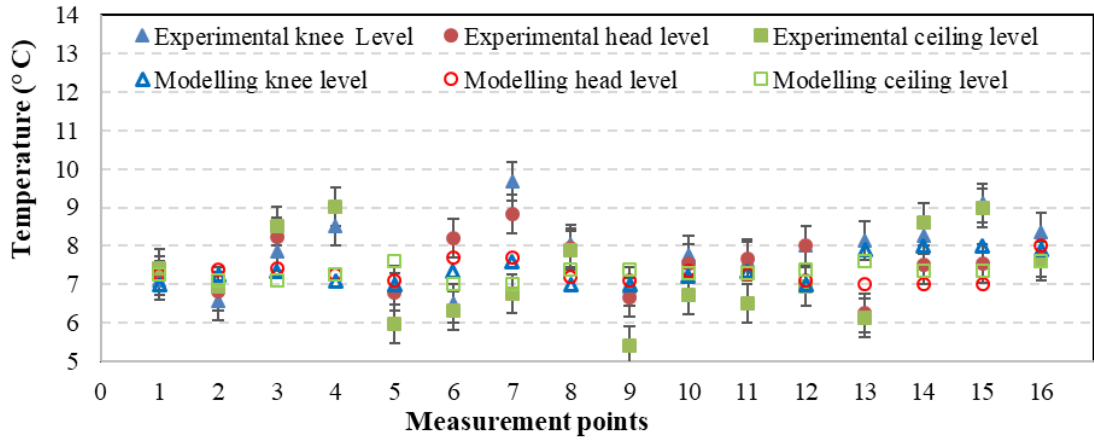
Figure 5-16. Comparison of experimental and CFD modelling results for air temperature
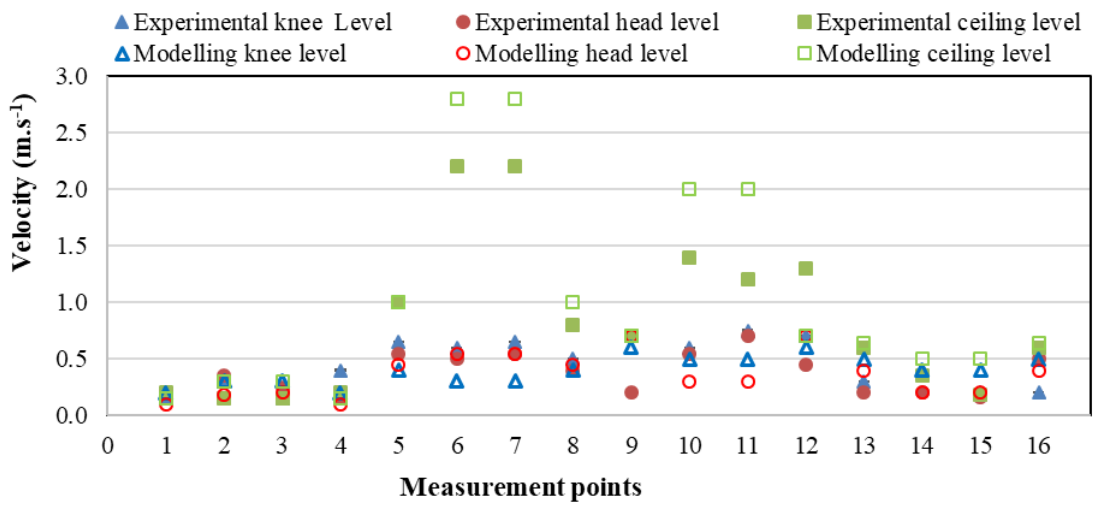
Figure 5-17. Comparison of experimental and CFD modelling results for air velocity.
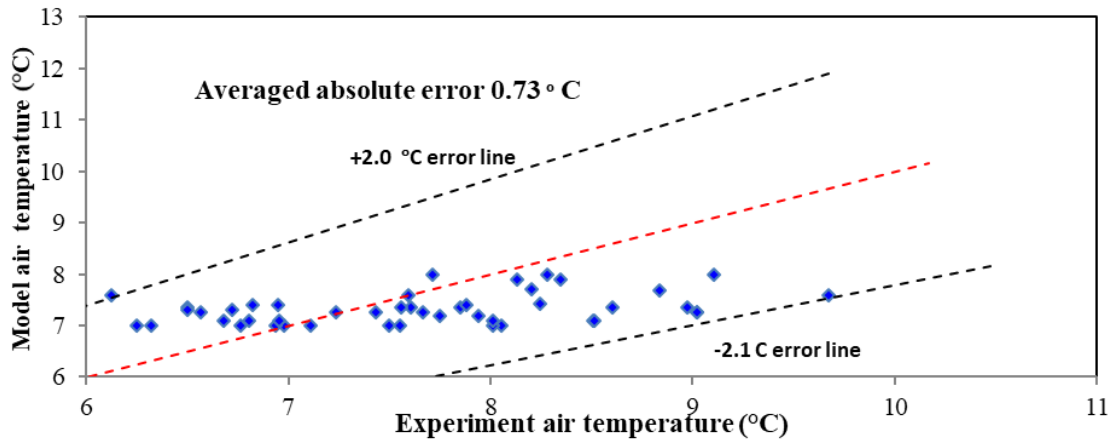
Figure 5-18. Modelling air temperature valuation.

5.5 Case study 1: CFD Air distribution model

This section discusses the results of the CFD modelling of the thermal environment arising from the air distribution system of Case study 1. The CFD model was designed using the actual dimensions of the chilled food processing area. These are detailed in Figure 3-2, Chapter 3.2. Figure 5-19 shows a representation of the developed 3-D CFD model which was designed to predict the air temperature and velocity distribution into the investigated space.
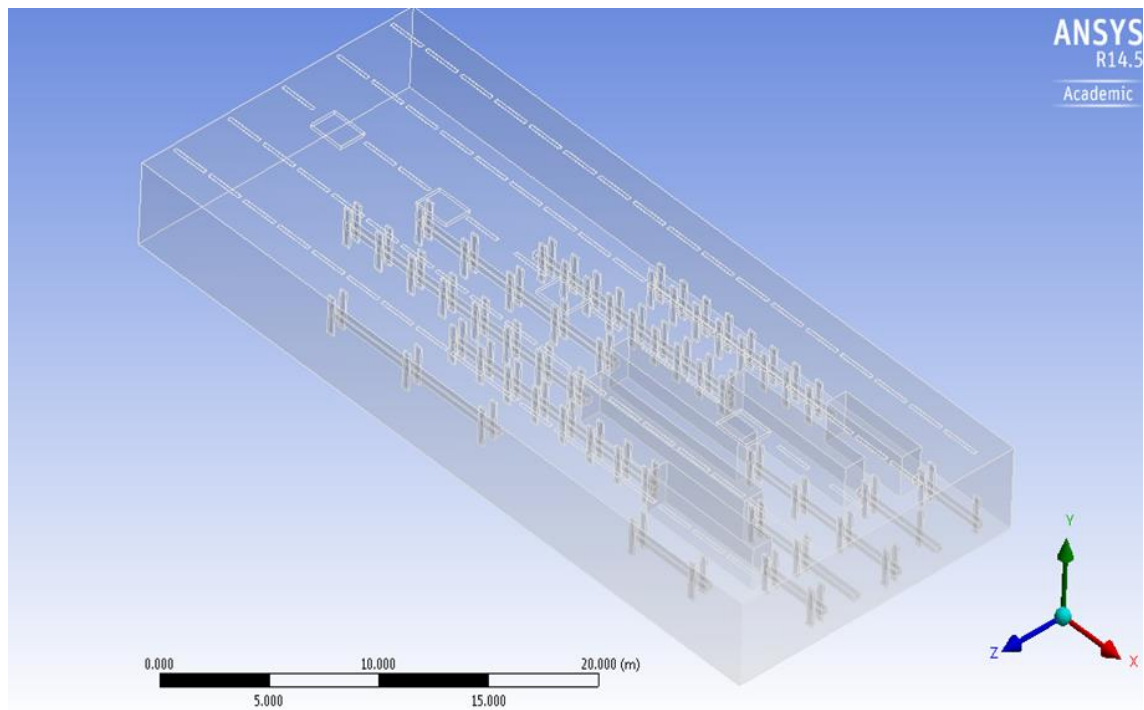
Figure 5-19. Case study 1: 3-D CFD model.

5.5.1 *CFD Air distribution model meshing*

The computational domain was discretized with an automatic mesh method, mainly with tetrahedral and hexahedral cells generated using the in-built ANSYS design modeller meshing algorithm. The resulting mesh comprised of hexahedral cells at the near-wall layers/domain and with tetrahedral and hexahedral cells in the air domain. The mesh density was gradually refined near the building wall, internal heat gains surfaces and the air handling unit supply/return diffusers. The final mesh size consists of 32 million elements, with element dimensions between 0.04-0.15 m. Four inflation layers were employed near the wall surfaces with a first element size of 0.1 m and a growth ratio of 1.2. In addition, a finer mesh was applied by four inflation layers near the internal heat gain surfaces (occupants and lighting) and the air supply/return diffusers with a first

element size of 0.4 m and a growth ratio of 1.2 to capture the effects of the boundary layer. The mesh gradually increases towards the bulk of the air domain producing a maximum element size of 0.15 m.

 The final model mesh was generated following a mesh independence study. The convergence criteria for the independence study were set to reach at least a 10^{-5} residual error for continuity and an average temperature tolerance of $\pm$ 0.5 °C. Mesh refinement was performed by varying all mesh sizes by the same ratio, but maintaining the inflation parameters. The simulation time for each steady-state case was 48 hours, with an average of 1500 iterations, on a 2.6GHz, 32GB RAM, Intel Xeon Processor with 12 parallel threads. Simulation results on the mesh independent grid showed an average y+ value of 6.

5.5.2   *CFD Air distribution model boundary conditions*

The supply and return air flows from each air handling unit were set to a value of 1.4 m³.s⁻¹. The air supply and return air diffuser boundary conditions were defined as mass flow inlets and outlets, respectively. The air supply temperature was set at 7°C. The occupancy density was set to be the maximum of 110 occupants. The occupant positions along both sides of the production lines are indicated in Figure 5-19. This occupant pattern in the space occurs during peak production. Each occupant was defined as a parallelepiped box with a surface area of 1.84 m^2 (based on an average adult) (X: 0.1, Y: 1.8, Z: 0.4) (Zukowska 2012, ASHRAE 2013) and thermal load of 105 W.m^{-2}. The occupant's thermal load was defined by the state of activity (typical metabolic heat generation) based on ASHRAE recommendations (ASHRAE 2013).

The lighting thermal boundary condition was defined with a temperature of 28 ºC for all the lights surfaces (value measured experimentally). The production line motors were defined as surfaces with a temperature of 105 ºC (measured experimentally). The motors are placed at the beginning and end of each production line. In total, 12 motors were used in the model. Other heat sources into the processing area were neglected for this phase of the research.

The surrounding walls were considered adiabatic since the adjoining spaces operated at similar conditions. The thermal boundary conditions of the ceiling and floor were defined as thermal heat flux values calculated by taking into account the temperature profile and

thermal resistances (Figure 5-2 and Eqs. 9, 10 and 11) over the interior and exterior of the construction.

The floor heat flux was calculated assuming a suggested ground temperature of 10.8 ℃ (value recommended by CIBSE, 2015) and an insulated floor with a thermal conductivity of 0.5 W.m^{-1} k^{-1}. In the case of the ceiling boundary, it was assumed an adjoining space temperature of 20 ℃, and the ceiling made of sandwich panels with heat transfer coefficient of 0.28 W.m^{-2} k^{-1}.

5.5.3 *CFD Air distribution model post-processing*

This subsection shows the results from the modelling of the facility with air distribution via the supply/return diffusers discussed in Chapter 3. Figure 5-20 Shows the air temperature distribution at 5 lateral sections along each diffuser and a longitudinal section along the centre line of the space. With a supply temperature from the diffusers of 7 ℃ the temperature in the bulk of the space varied between 10.4 ℃ and 13.2 ℃ at the measurement locations shown in Figure 3-3.

As shown in Figure 5-20, the cooling and air distribution system results only in a very small temperature stratification in the space. It can also be observed that the lowest temperatures were at ceiling level and close to the walls. On the other hand, temperatures slightly higher can be observed around the occupied zone resulting from heat gains from the occupants and electric motors. These results agree with the data collected from the measurements which also showed only small temperature stratification in the space.
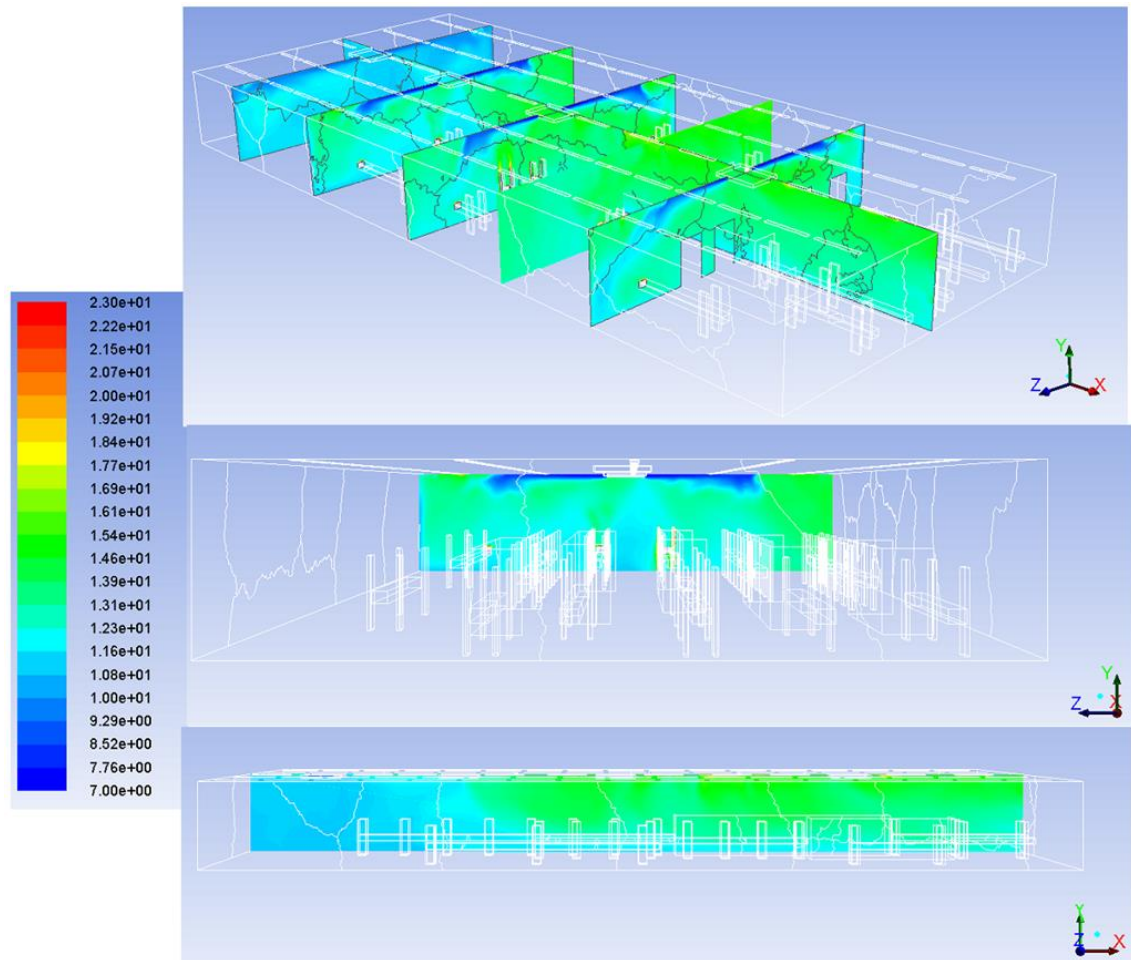
Figure 5-20. Case study 1-CFD modelling of air temperature in the space (°C), (a) 3D view, (b) frontal view, and (c) side view.

Figure 5-21 and Figure 5-22 show the modelled velocity distribution at 4 cross sections from each supply diffuser. According to the modelling results, the air velocities varied between 0.05 and 1.6 m.s^{-1}. The highest air velocities were mainly at ceiling level as could be expected due to the discharge from the cold air supply diffusers.

It can be seen from the Figures that the air flows along the ceiling to the side walls, and then down the wall until it reaches the floor. Then, recirculation takes place in an area between floor and 2.5 m above floor level. There is also some air recirculation between the supply and return grille sections of the combined supply/return diffusers which imply an inefficient use of supply cold air. In Figure 5-22 it can also be noted that the air displacement around the space is mainly influenced by the high air flow velocity from the supply/return diffusers rather than buoyancy effects due to heat gains from the workers and equipment.

The modelling results confirm that this type of air distribution system tends to cool-down the whole volume of the space using the mixing principle which implies high air flow discharge velocities. Cooling of the whole space height can represent significant energy wastage in large food processing facilities while high velocities around the workers in the space may lead to an excessive thermal discomfort.
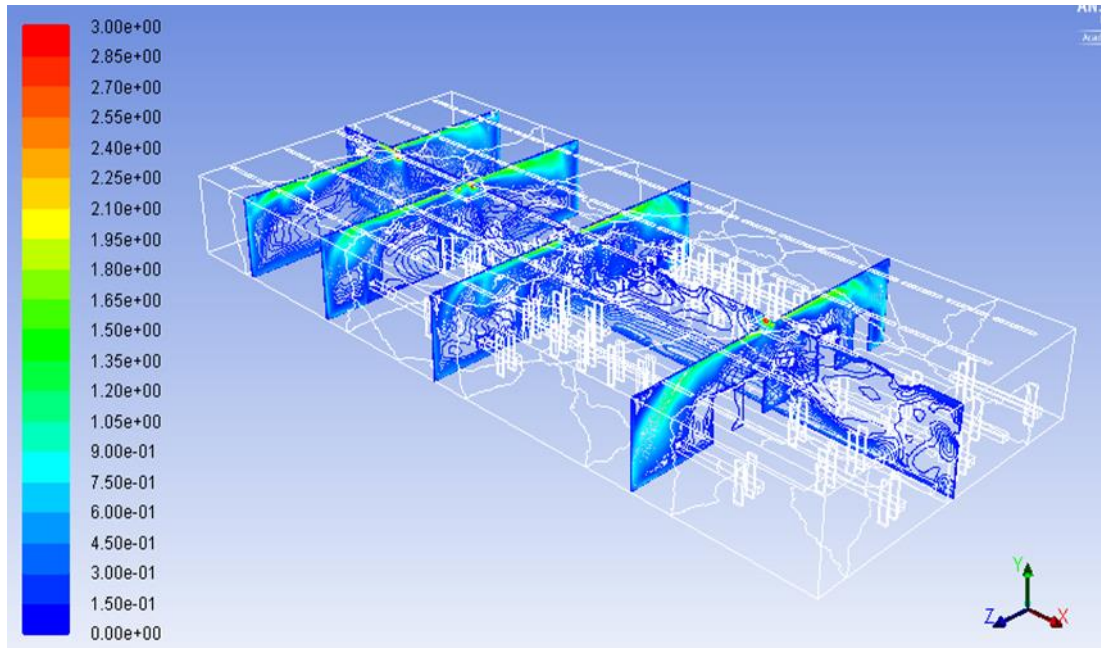
Figure 5-21. CFD modelling results of air velocity intensity in the space (m.s^{-1}).
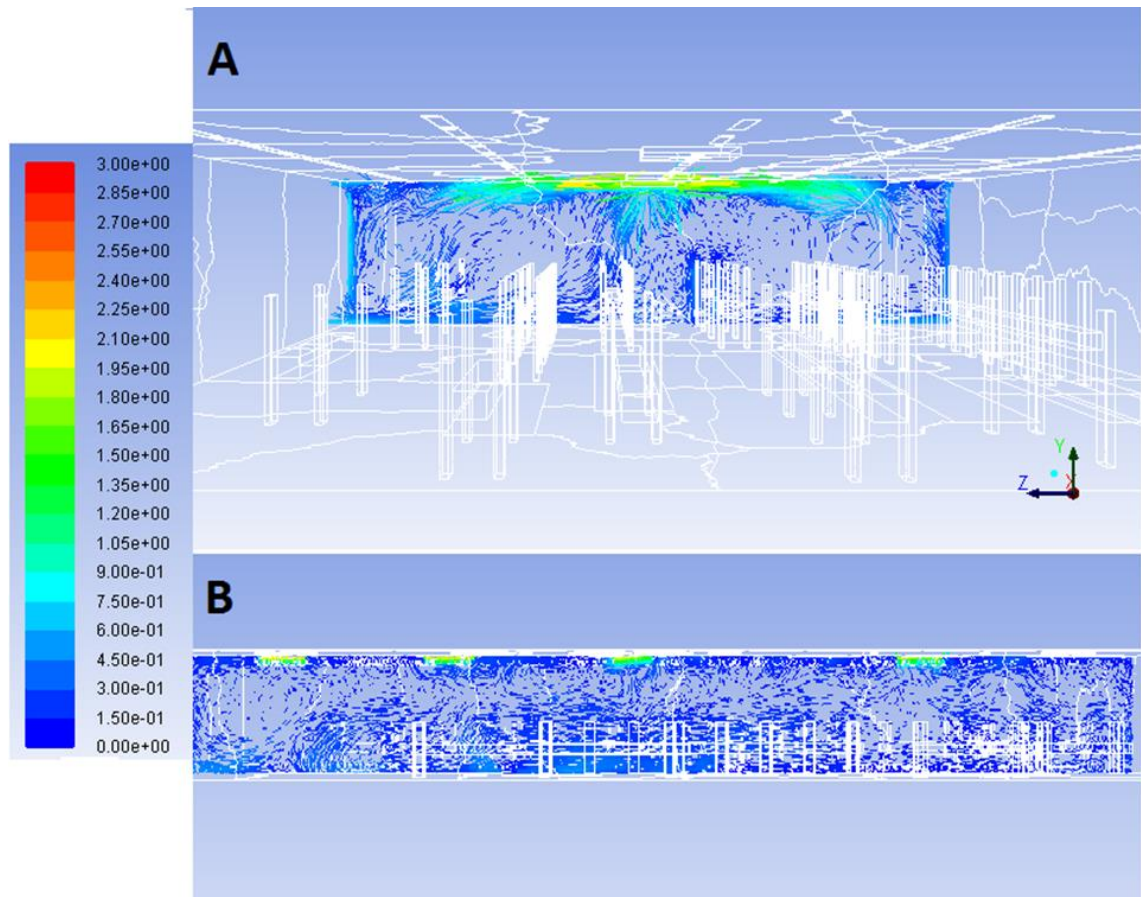
Figure 5-22. CFD modelling results of air velocity vectors at cross sections A (Frontal view) and B (Side view) (m.s^{-1})

5.5.4 *CFD Air distribution model validation*

This subsection shows the validation of the Case study 1 CFD model. The validation of the model was conducted by comparing the monitored air temperatures (as described in Chapter 3-2) with the CFD predicted temperatures.

Figure 5-23 presents a comparison between the average temperature data collected including the measurement uncertainty and the modelling results. The position of each point of measurement can be identified in Figure 3-3. Figure 5-23 shows that the predicted air temperatures are lower at some points and higher at other compared with the measured values. In Case study 1, the CFD 3-d model was developed for fixed fins supply diffusers. However, Case study 1 chilled food facility supply diffusers have adjustable fins that are manipulated by the workers. As a result of the occupant's on-site fins adjustment, this prediction error occurs. Mainly modelling results showed slightly lower temperatures at a low level and higher temperatures at ceiling level compared with experimental measurements. However, the model shows a good level of prediction for the air

temperature trend and distribution achieved in this case study in which very poor temperature stratification in the space was observed.
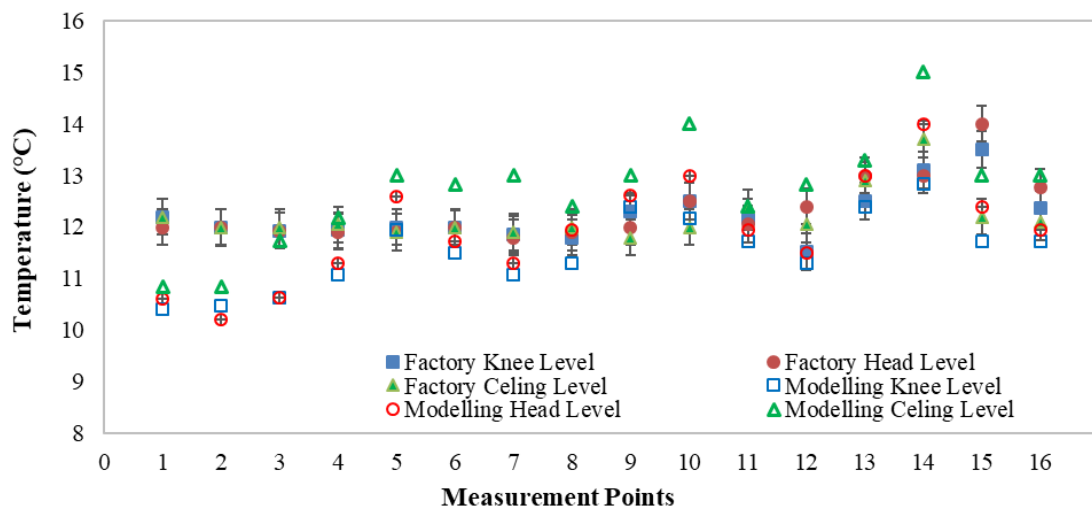
Figure 5-23. Case study 1 air temperature uncertainty analysis.

To determine the validity of the model, the temperature profiles predicted by the model were compared against temperature measurements in the space. Results from this comparison are shown in Figure 5-24. To conclude to the maximum error boundaries (+ 2.0 °C and -1.8 °C error), for each measurement spot all modelling values were subtracted from experimental values. The middle line in the graph indicates the position of 0 °C error. The absolute average error across all test points in the space was found to be 0.8 °C lower than the measured values. The maximum absolute error was found to be 2.0 °C higher than the measured value.
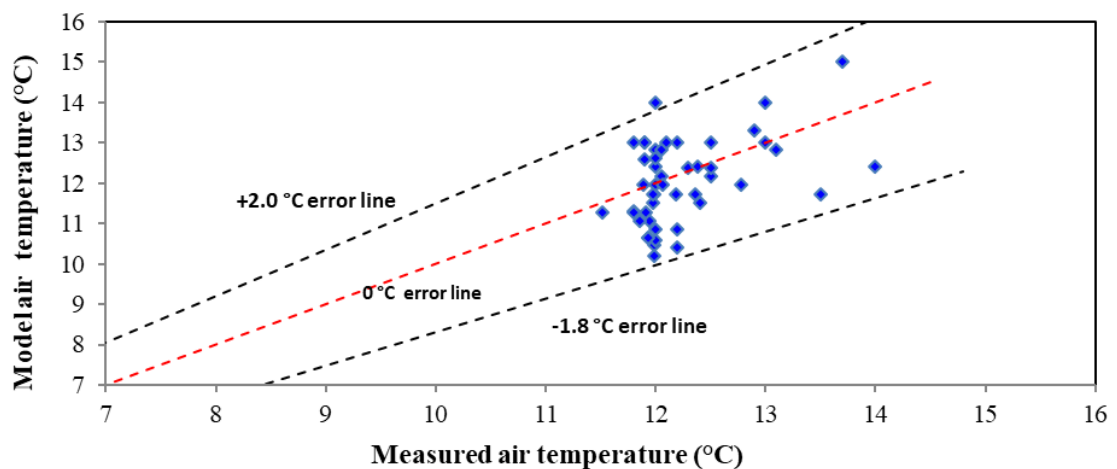
Figure 5-24. Validation of CFD modelling results for air temperature.

5.6   Case study 2: CFD Air distribution model

This section discusses the results of the CFD modelling of the thermal environment arising from the air distribution system of Case study 2. Case study 2 model was designed using the actual dimensions of the chilled food processing area shown in Figure 3-15. Figure 5-25 is a representation of the 3-D CFD model which is designed to model the air temperature and velocity distribution of the chilled food facility.
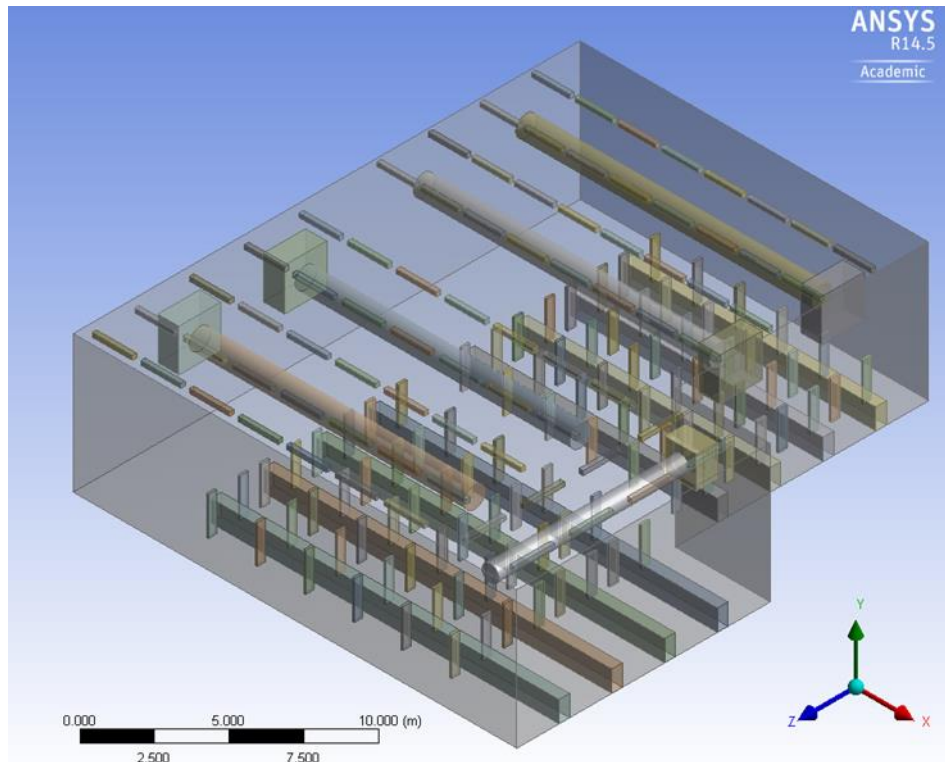
Figure 5-25. Case study 2, 3-D CFD model.

5.6.1   *CFD Air distribution model meshing*

The computational domain was discretized with an automatic mesh method as described in section 5.5.1. The mesh density was gradually refined near the building wall, internal heat gains surfaces and the air-socks. The final mesh size consists of 34 million elements, with element dimensions between 0.04-0.1 m. Four inflation layers were employed near the wall surfaces with a first element size of 0.08 m and a growth ratio of 1.2. In addition, a finer mesh was applied by four inflation layers near the internal heat gain surfaces (occupants and lighting) and the fabric ducts with a first element size of 0.04 m and a growth ratio of 1.2 to capture the effects of the boundary layer. The mesh gradually increases towards the bulk of the air domain producing a maximum element size of 0.1 m. The final model mesh was generated following a mesh independence study. The

convergence criteria for the independence study were set to reach at least a 10^{-5} residual error for continuity and an average temperature tolerance of $\pm$ 0.5 °C. Mesh refinement was performed by varying all mesh sizes by the same ratio, but maintaining the inflation parameters. The simulation time for each steady-state case was 48 hours, with an average of 3000 iterations, on a 2.5GHz (2 processors), 64GB RAM, Intel Xeon Processor with 38 parallel threads.

5.6.2   *CFD Air distribution model boundary conditions*

The supply and return air flow from each evaporator were set at 4.5 $m^3.s^{-1}$. The target in a fabric duct is to achieve a constant static pressure inside the sock which will maintain it inflated and will give a uniform discharge air velocity across the whole surface (normally around 0.1 $m.s^{-1}$). Due to the density difference between the supplied air and the room air, the supply air moves towards the floor immediately after passing through the duct surface. For the CFD modelling boundary conditions, the fabric duct surface was defined as mass flow inlet discharging the air volume of the coil. In addition, the coil return air boundary conditions were defined as mass flow outlets. The air supply temperature from the cooling coil was set at 7 ℃. The occupancy density was set to be the maximum of 96 occupants. The boundary conditions were defined as described in section 5.5.2.

5.6.3   *CFD Air distribution model post-processing*

This subsection details the results from the modelling of the facility with air distribution via fabric ducts. Figure 5-26 and Figure 5-27 present the modelled air temperature distribution at different cross sections along the space. With a supply temperature from the fabric ducts at 7 ℃, the temperature in the bulk of the space varied between 9.5 ℃ and 12.6 ℃ at the same points as the measurement points in Figure 3-18. From all temperatures, the lowest temperature were obtained at knee level and the highest temperatures at ceiling level. From Figure 5-26, it can be seen that a slight stratification results from the air distribution system as it was also the case from the actual measurements.
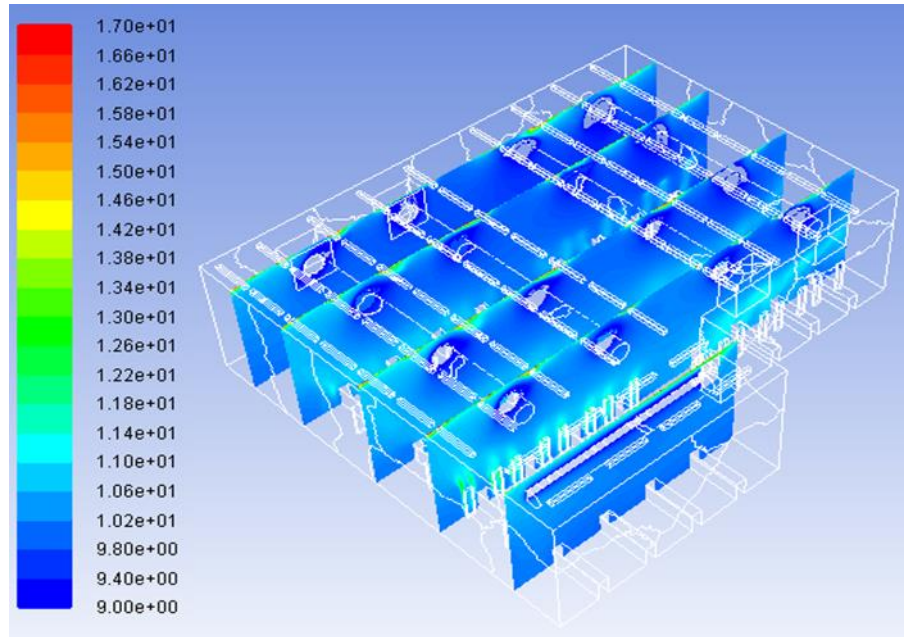
Figure 5-26. Case study 2-CFD results of air temperatures in the space (°C).

Slightly higher air temperatures at low level around the production lines, Figure 5-27, arise mainly from heat gains from the workers.
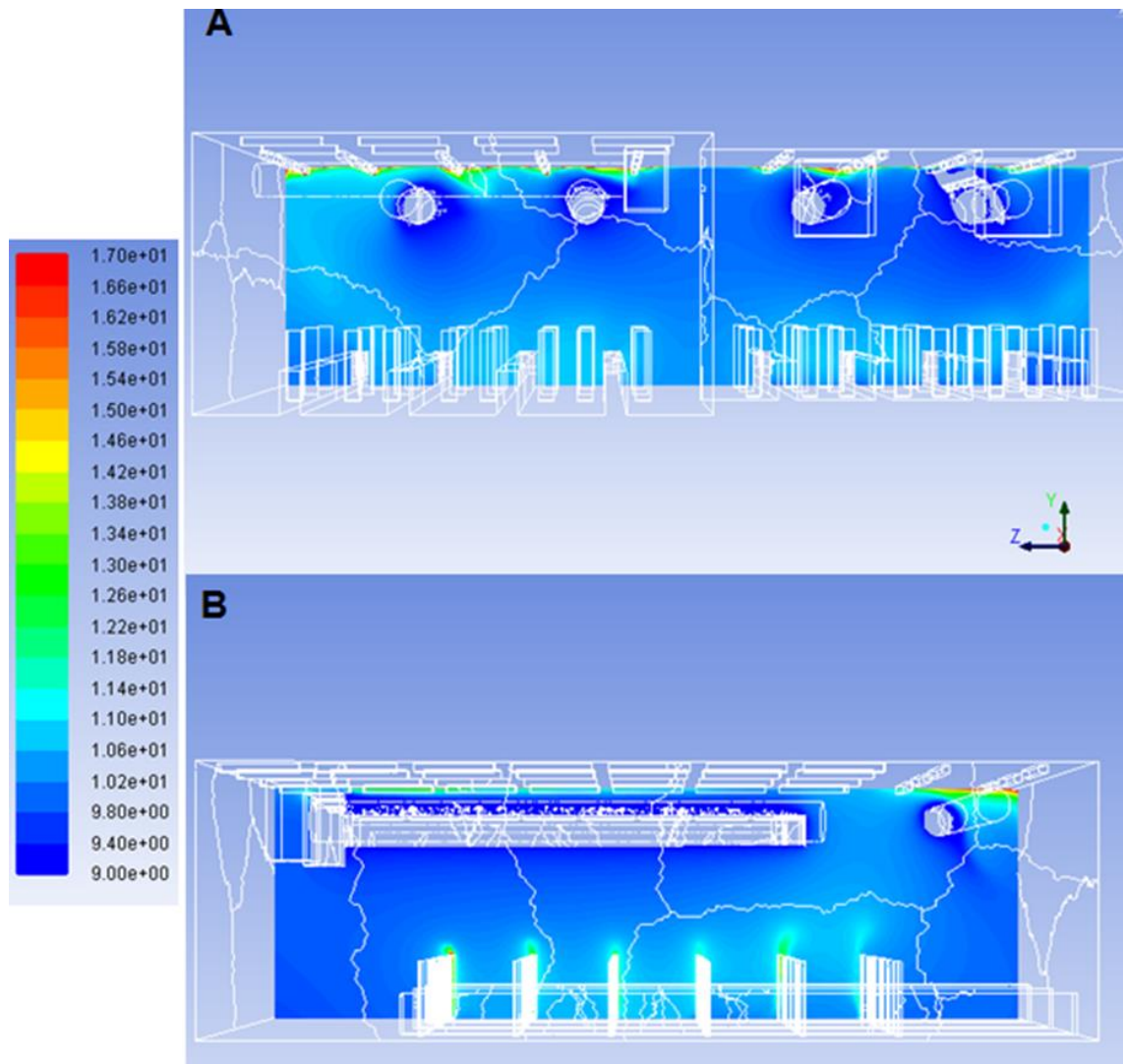
Figure 5-27. Case study 2, CFD modelling of air temperature, cross sections A (Frontal view) and B (Side view) (°C).

Figure 5-29 depicts the modelled air velocity distribution at different cross sections along the space. It can be seen that air velocities at the different measurement points (Figure 3-18) were low and ranged from 0.02 to 0.25 m.s^{-1}. The higher values were close to the evaporator non-ducted air return.

It can also be observed that the use of fabric ducts for air distribution enables a low velocity air distribution over the production zone which is beneficial in reducing thermal discomfort for the workers.
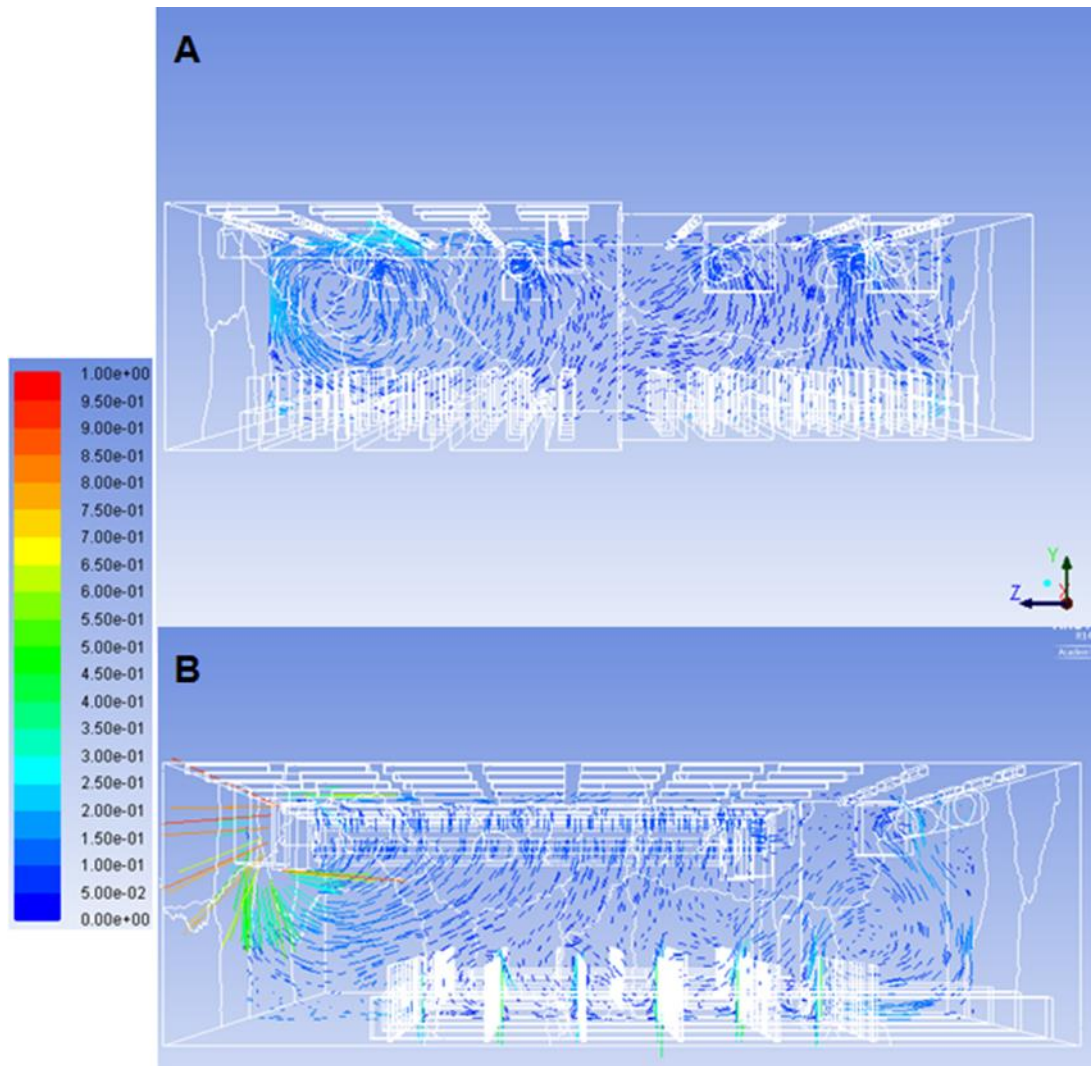
Figure 5-28. Case study 2-CFD modelling of air flow at different cross sections: A (Frontal view) and B (Side view) (m.s⁻¹).
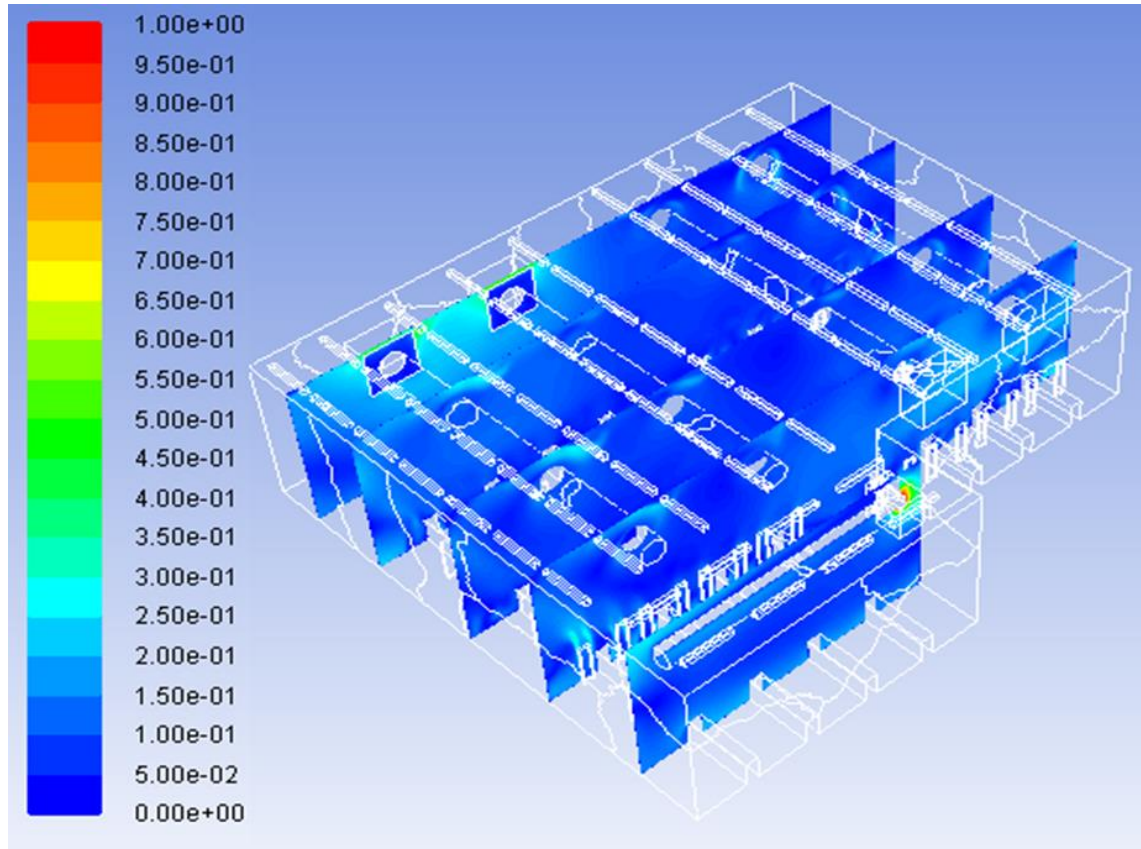
Figure 5-29. Case study 2-CFD modelling of air velocity in the space (m.s⁻¹).

5.6.4   CFD Air distribution model validation

This subsection shows the validation of the Case study 2 CFD model. It was conducted by comparing the monitored air temperatures (as described in Chapter 3) with the CFD predicted temperatures.

Figure 5-30 is presents the comparison between the average temperature data collected including the measurement uncertainty and the modelling results. Figure 5-30 shows that the model under-predicts the air temperatures in comparison to the measured data. In chilled food facilities non steady boundary conditions exist. For example Labourers density change over time depending on the production demand. As a result of the non-steady boundary conditions the predicted results are slightly affected. However, the model shows a good level of prediction and in general a better level of prediction for the air temperature distribution in comparison with that of the case study 1. Figure 5-31 shows that the average absolute error across all test points in the space was found to be 0.6 ℃ lower than the measured values. In addition, the maximum error was found to be 1.7 ℃

lower than the measured value. In any case, predicted air temperatures also show some level of stratification just as observed from the measured data.
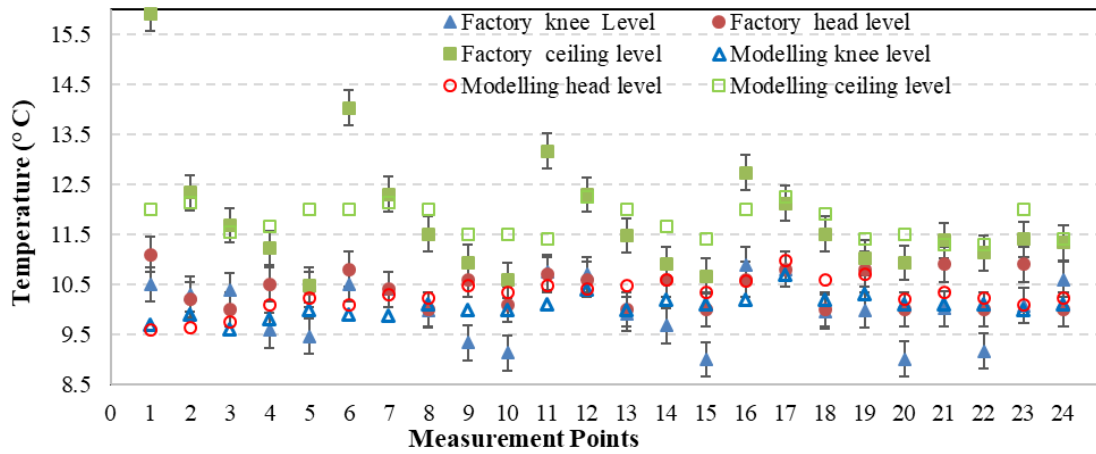
Figure 5-30. Case study 2, air temperature uncertainty analysis
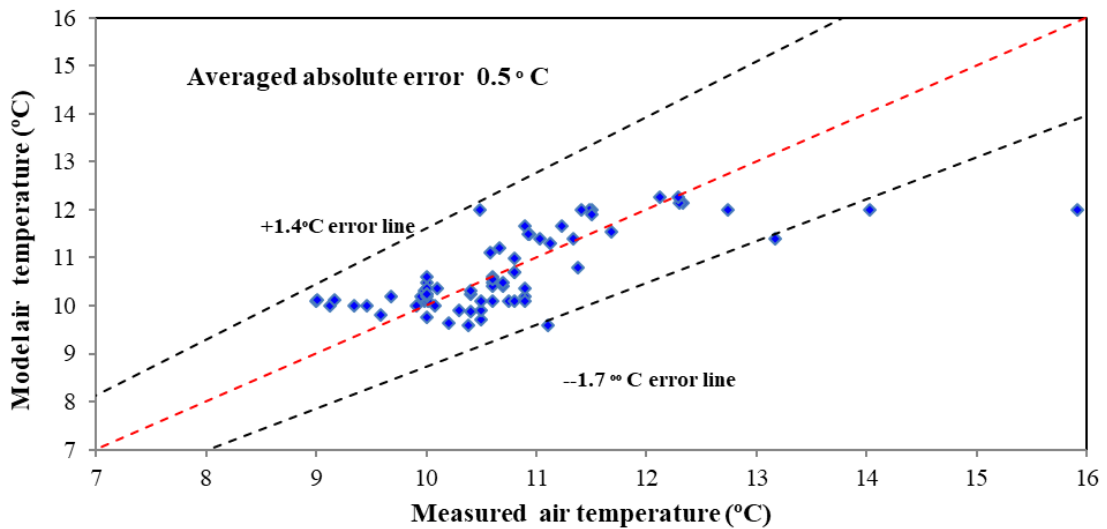
Figure 5-31. Case study 2-Validation of CFD modelling results for space air temperatures

5.7 CFD modelling results overview

This subsection presents an overview of the predicted values form the CFD models compared with temperature measurements from the test and monitored facilities. Tables 5-2 to 5-4, show a comparison between the average measured temperatures (across all the measuring points) at different heights against the averaged predicted values for each height. It can be seen that the average measured temperatures and temperatures predicted by the model follow a similar pattern at the different heights in the space.

In addition, Table 5-6 shows the averaged absolute errors between the temperatures predicted by the model and measured temperatures. From case study 1 and case study 2 the average absolute error across all test points in the space was found to be 0.8 ºC, and 0.5 ºC respectively. In addition, regarding the experimental facility the air distribution method via fabric duct showed 0.95 ºC absolute error whereas the non-ducted evaporator 0.73 ºC absolute error. The modelling results validation shows that the predicted air temperatures and their trends are in good agreement with the collected experimental data. Considering the measuring equipment uncertainty ($\pm$ 0.35 ºC) and the real boundary non-steady conditions of the chilled food factories, these errors are accepted.

Table 5-2. Experimental facility fabric duct at celling level: Comparison of CFD predicted values with measured values overview

Experimental facility: Fabric duct at Ceiling level			
	Average temperatures (ºC)		
	knee level	head level	ceiling level
Predicted	9.9	10.3	12.5
Measured	9.9	10.6	12.4

Table 5-3. Experimental facility non-ducted evaporator coil: Comparison of CFD predicted values with measured values overview

Experimental facility: Non-ducted evaporator coil at Ceiling level			
	Average temperatures (ºC)		
	knee level	head level	ceiling level
Predicted	7.4	7.3	7.3
Measured	7.8	7.6	7.2

Table 5-4. Case study 1: Comparison of CFD predicted values with measured values overview

Case Study 1			
	Average temperatures (ºC)		
	knee level	head level	ceiling level
Predicted	11.7	11.9	12.6
Measured	12.2	12.3	12.1

Table 5-5. Case study 2: Comparison of CFD predicted values with measured values overview

Case Study 2			
	Average temperatures (ºC)		
	knee level	head level	ceiling level
Predicted	10.1	10.2	11.8
Measured	10.1	10.4	11.9

Table 5-6. Validation overview: Averaged absolute errors (°C)

Validation			
	Average absolute error (ºC)		
			Experimental facility	
	Case study 1	Case study 2	Fabric duct	Non-ducted evaporator
Predicted	0.8	0.5	0.95	0.73

5.8   Summary of Chapter 5

This chapter presents the development of a 3-D modelling tool based on computational fluid dynamics. This tool was used to simulate the air flow and temperatures in the investigated chilled food facilities and the experimental test facility. In all cases, a steady state solution was employed using the SST k-ω turbulence model. The model was validated using data from measurements and was shown to predict air temperatures and velocities with a reasonable degree of accuracy.

Based on the measurements and modelling results, it can be highlighted that fabric ducts provide a better environment in the space in terms of air velocity uniformity at the level of the production area in comparison to the use of air supply/return diffusers or non-ducted cooling coils.

Chapter 6 presents results from the use of the developed CFD model to evaluate the performance of more efficient air distribution methods, and their impact on the thermal environment of chilled food processing areas and energy consumption.

Chapter 6.   CFD Modelling study of different air distribution systems

6.1 Introduction

The previous chapter presented the investigation and evaluation of different air distribution systems with the developed 3-D CFD modelling tool. The aim of the current investigation is to identify the most appropriate approaches of providing uniform temperatures and low velocities at horizontal level and temperature stratification from floor to ceiling. Once the CFD model was validated (Chapter 5), it was then used to investigate the air flow and temperature distribution from different air distribution systems. Best air distribution approaches derived from the 3-D CFD modelling investigation were constructed and installed at the experimental facility for further investigation.

Five different air distribution solutions were investigated. The investigation goal was to identify which of the five air distribution solutions is capable to localize cooling only where production takes place. Localizing cooling only where is needed instead of the whole volume of the space will should lead to an improved energy efficient system. The following five air distribution systems were tested:

- 1-Way Lay-in displacement diffuser
- Rectangular 1-Way displacement diffuser
- Semi-circular fabric duct installed at medium level
- Slot diffusers with galvanized duct installed at medium level
- Circular fabric duct installed at medium level

The 3-D CFD model for each investigated air distribution solution was developed based on the experimental facility geometry and boundary conditions. The experimental facility was described in Chapter 4 and the boundary conditions in Chapter 5. Modelling results regarding the predicted air temperature and air velocity profiles are presented below.

6.1.1 *CFD Modelling: Air distribution via 1-way lay in displacement diffuser*

1-way lay-in displacement diffusers are designed to produce a 1-way low velocity air flow from a horizontal installation and discharged air downwards vertically. For the CFD modelling purposes the geometrical characteristics a DF1L 1-way lay-in displacement diffuser from price industries was selected (Price Industries, DF1L Horizontal 1-way displacement diffuser,2014). The DF1L discharges air evenly across the perforated face with minimal turbulence or induction of room air. Figure 6-1 shows an example of the

DF1L 1-way displacement diffuser. Based on Price Engineer displacement ventilation guide (Price Engineer,2013), for the current air distribution method the air flow rate boundary condition was assumed to be 500 m³ hr^{-1}. The air flow was selected to keep the supplied air velocities under 0.2 m.s^{-1}.
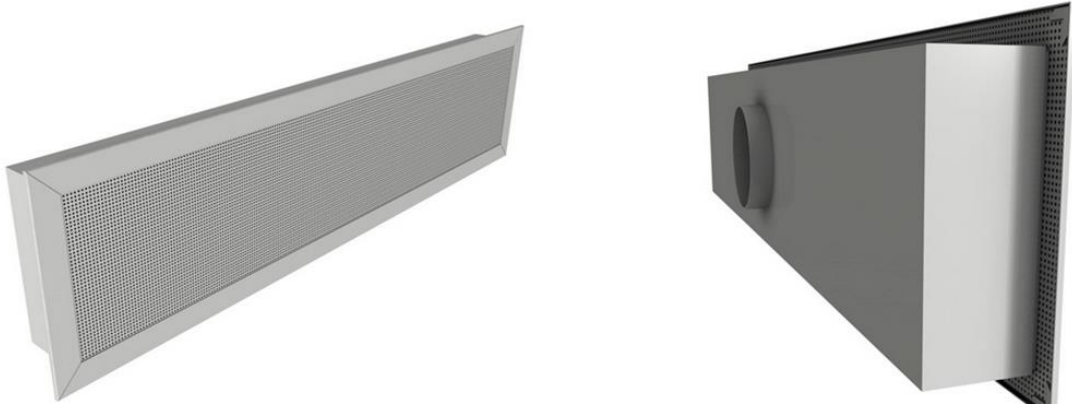
Figure 6-1. 1-way lay-in displacement diffuser

Figure 6-2 shows the developed CFD model using the DF1L 1-way displacement diffuser as an air distribution method. The direction of the supply air flow is shown with the blue arrows which is discharged vertically downwards. In addition, the return air flow to the coil is indicated with the red arrows.
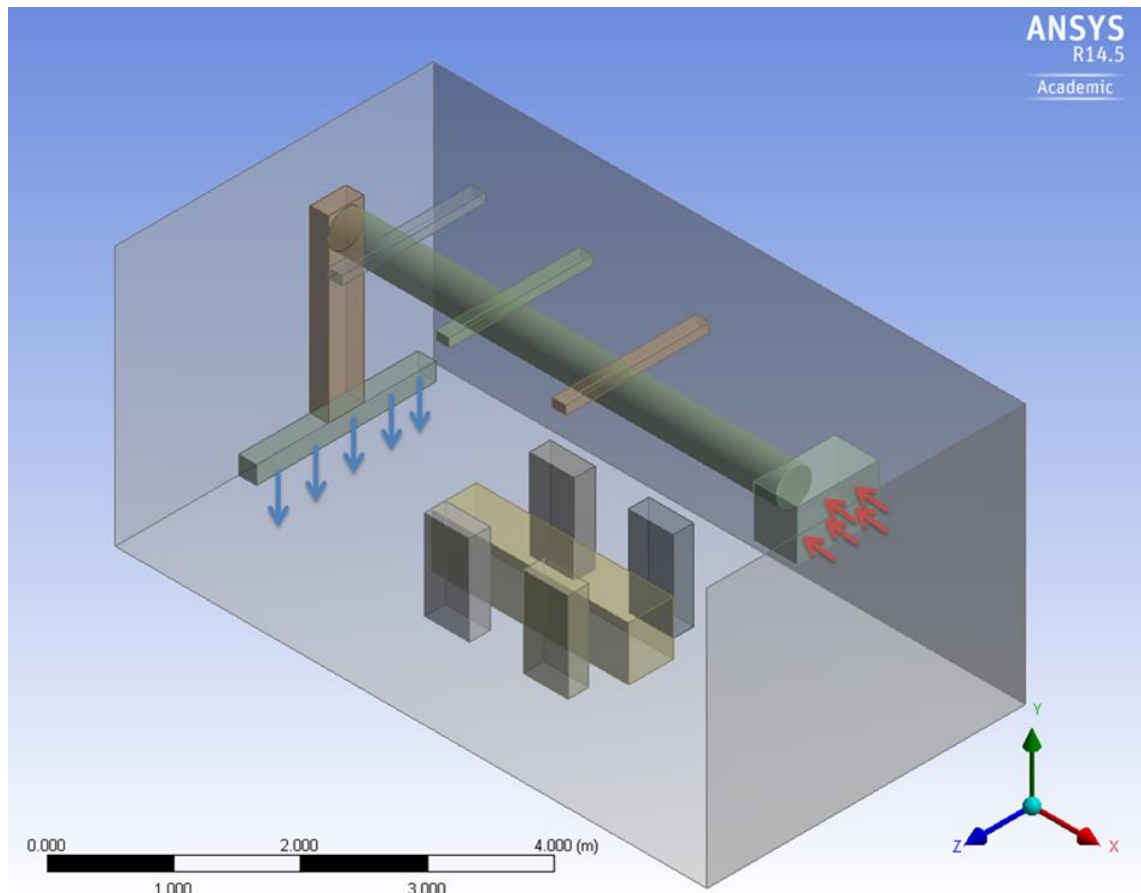
Figure 6-2. CFD model via 1-way lay-in displacement diffuser

Figure 6-3 shows the air temperature distribution at 4 cross sections along the space with air distribution system via displacement ventilation with one DF1L diffuser discharging the supply air vertically downwards. According to the modelling results, the temperature in the bulk of the space varied between 7 ℃ and 13.5℃ with an average temperature at production height of 11.22 ℃.

Temperature stratification occurred with the lowest temperatures close to the diffuser. It was observed that the temperature stratification was driven mainly from buoyancy forces caused by the internal heat gains. A temperature gradient can also be noted at knee level in the horizontal direction which means that the temperature distribution at this level is not uniform.
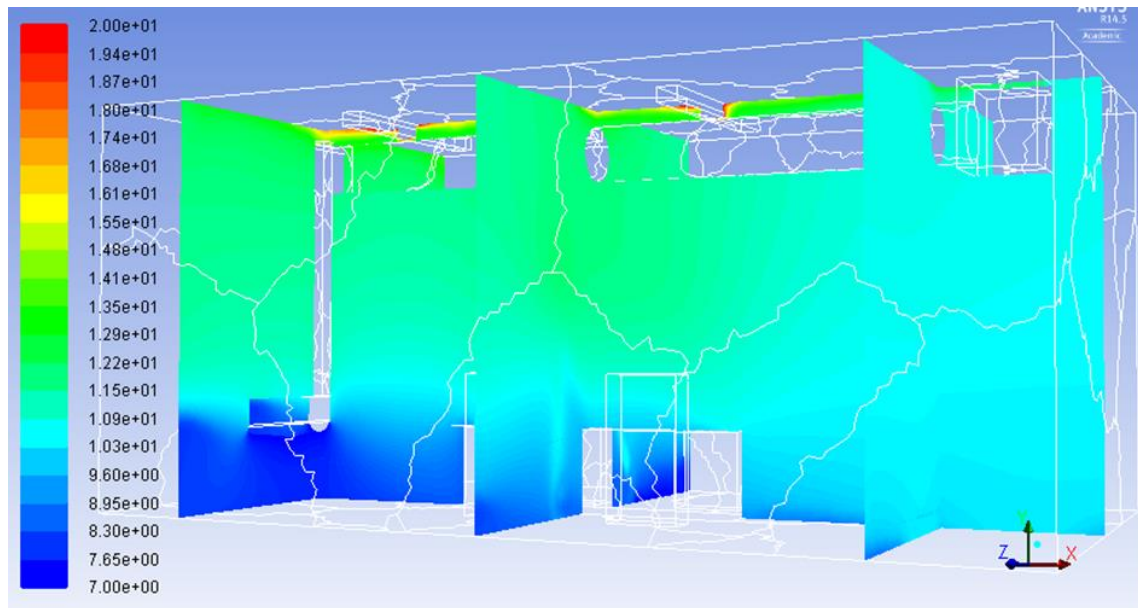
Figure 6-3. Air temperature distribution via displacement ventilation with one diffuser

Figure 6-4 shows the velocity distribution along the space from the air distribution system via displacement ventilation with one DF1L 1-way diffuser. Air velocities from this system were very low, varying between 0.01 and 0.25 m.s^{-1} with the highest velocities close to the diffuser.
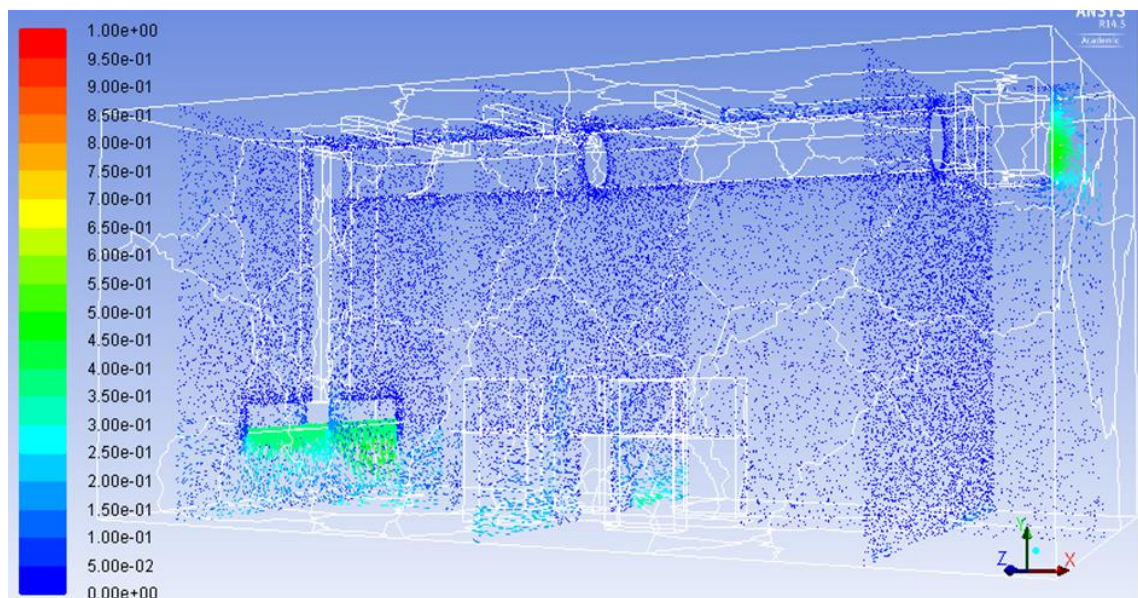
Figure 6-4. Air velocity profiles resulting from displacement ventilation with one diffuser

6.1.2   *CFD Modelling: Air distribution via Rectangular 1-Way Displacement Diffuser*

Rectangular 1-Way Displacement Diffusers are designed to produce a 1-way low velocity air flow, perpendicular to the diffuser face. For the CFD modelling purposes the geometrical characteristics of a DF1 Rectangular 1 way-displacement diffuser from Price

industries was selected (Price Industries, DF1 Rectangular 1-way displacement, 2013). Figure 6-5 shows an example of the Rectangular 1-way displacement diffuser. The DF1 discharges air evenly across its perforated face. The air mass flow rate boundary condition was set, the same as the horizontal diffuser at 500 m³ hr⁻¹.
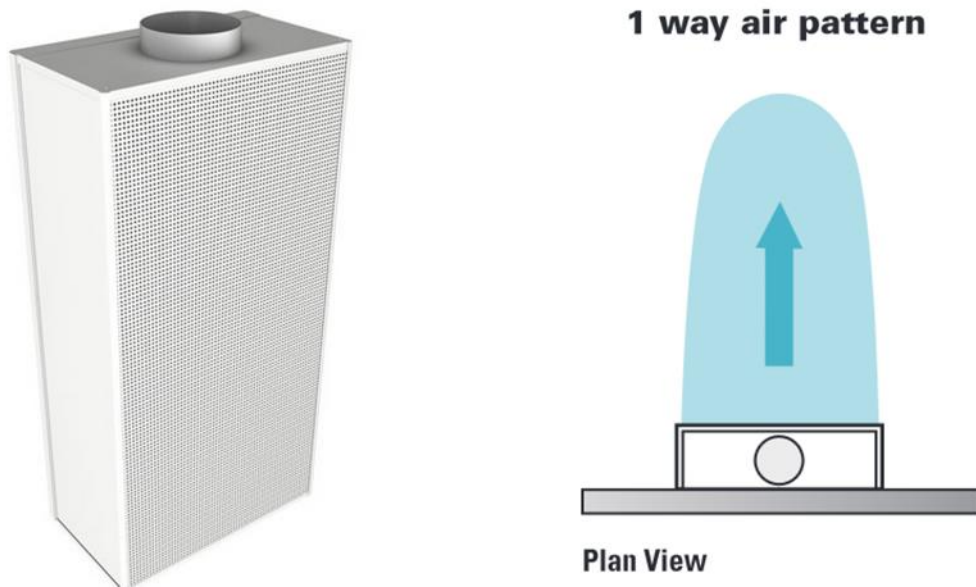
Figure 6-5. Rectangular 1-Way displacement diffuser

Figure 6-6 shows the CFD representation of two Rectangular 1-way displacement diffusers installed at opposite sides of the room as air distribution method. The direction of the supply air flow is shown by the blue arrows and the return air flow to the coil by the red arrows.
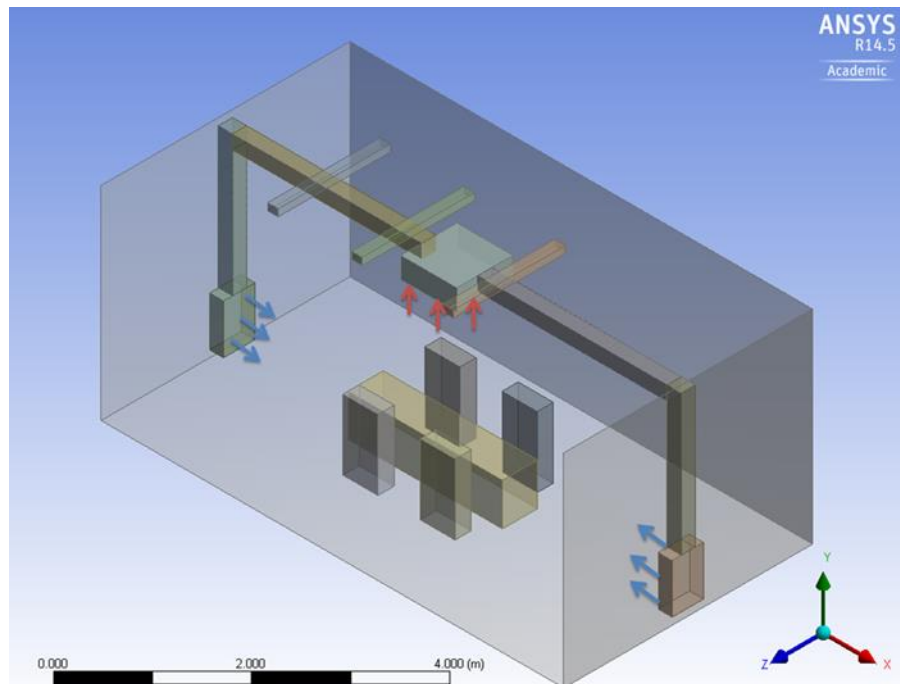
Figure 6-6. CFD model representation of the rectangular 1-Way displacement diffuser

Figure 6-7 shows the air temperature distribution from the arrangement shown in Figure 6-6. For this case, the temperature in the bulk of the space varied between 7 ºC and 15 ºC with an average temperature at production height of 12.0 ºC. With this configuration, the temperature stratification was larger compared to the single displacement diffuser. However, a significant temperature difference can be observed between knee and head level which may cause thermal discomfort from the workers in the space. A significant temperature variation on a horizontal plane at knee level can also be observed with higher temperatures in the centre of the space and minimum temperatures close to the diffuser. This non-uniformity of temperatures will be worse in large spaces as those in food processing areas, making the use of low velocity supply diffusers at low level unsuitable for these applications.
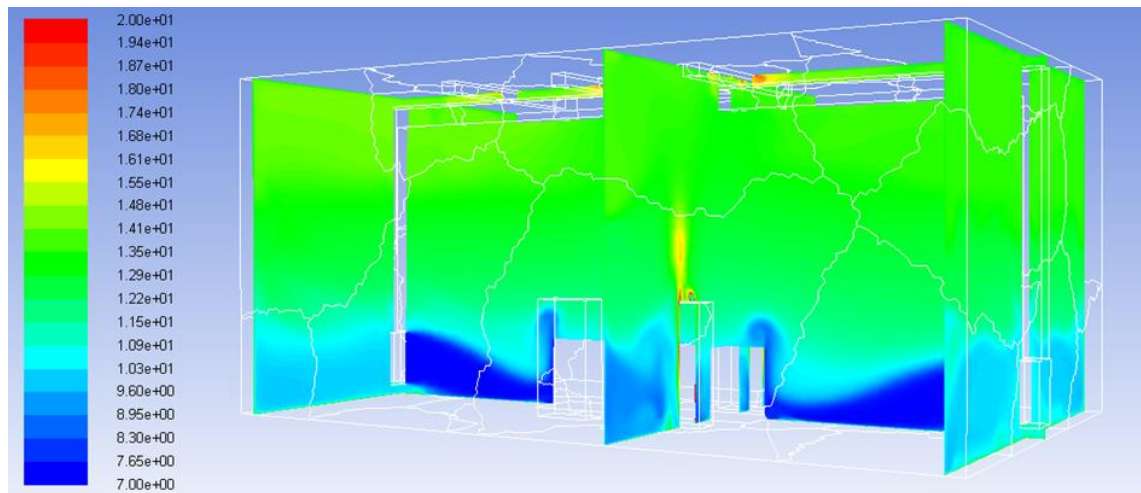
Figure 6-7. Air temperature distribution with two Rectangular 1-way displacement diffusers

Figure 6-8 presents the results for air flow velocity distribution in the space obtained from the CFD model. It can be seen that velocities varied between 0.01 and 0.25 m.s^{-1} with the highest velocities close to the diffusers. Similar velocity values were obtained from the system via displacement ventilation with one horizontal diffuser as described in the previous section.
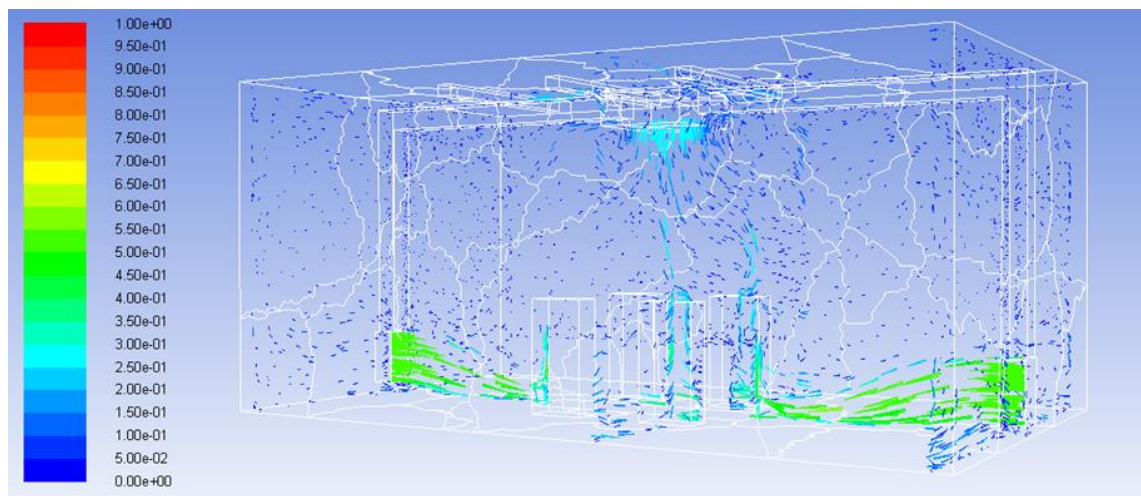
Figure 6-8. Air velocity profiles from air distribution using displacement ventilation system with two Rectangular 1-way displacement diffusers

6.1.3 *CFD modelling: Air distribution with semi-circular fabric duct at a medium level in the space*

With fabric ducts, the cooled air volume is discharged across the whole surface of the duct, allowing the supply of high air volume at low and uniform air velocity. For the CFD modelling purposes the geometrical characteristics of the semi-circular fabric duct are shown in Figure 6-9. The radius was 0.40 m and the length 4.0 m. The only difference to

the reference case is that the centre line of the duct was 1.15 m below ceiling level compared to 0.25 m for the reference case. Based on the KE-fibertec design guide (KE FIBERTEC, KE-Low Impulse, 2013) the air mass flow rate was chosen to be 1400m³ hr[1].
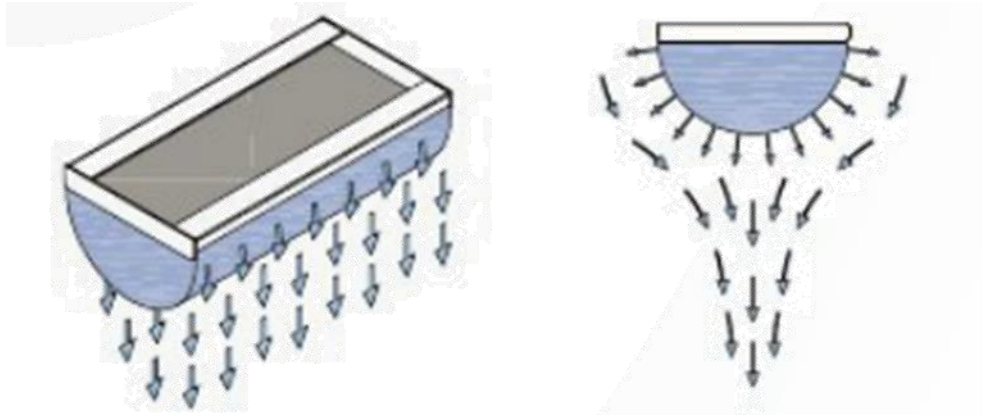
Figure 6-9. Semi-circular fabric duct

Figure 6-10 shows a representation of the semi-circular fabric duct installed at medium level in the space. The direction of the supply air flow is shown by the blue arrows and the return air flow to the coil is shown by the red arrows.
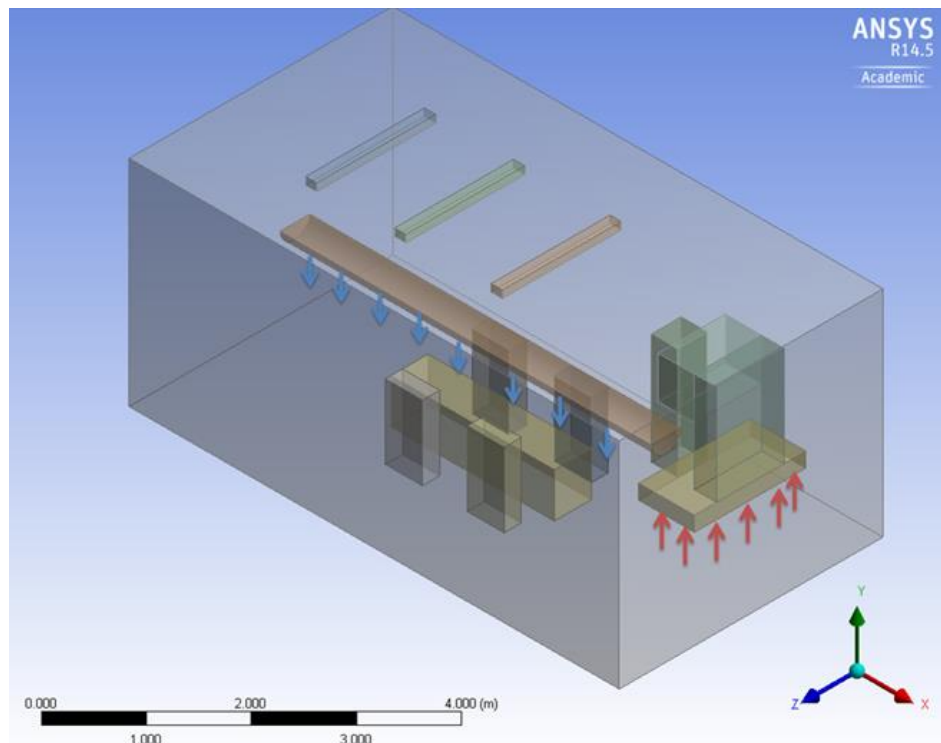
Figure 6-10. Representation of the CFD model with semi-circular fabric duct

Figure 6-11 shows the resulting air temperature distribution with the semi-circular fabric duct installed at a medium level in the space. The temperature in the bulk of the space varied between of 7 ºC and 14.0 ºC with an average temperature at production height of 7.1 ºC. Interesting, the temperature gradients were more pronounced between the head level and the ceiling level keeping the space below the head level at low temperatures.
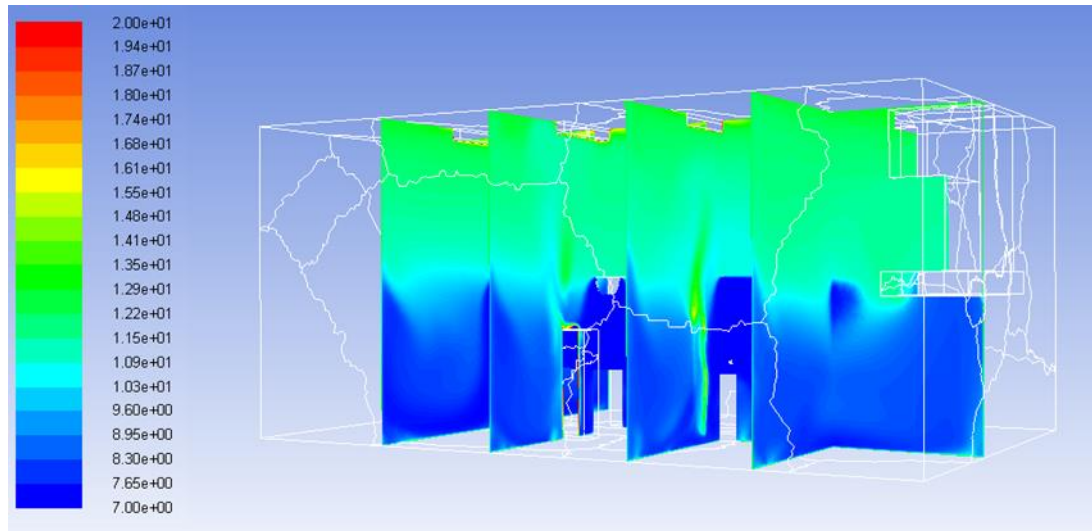
Figure 6-11. Air temperature distribution with semi-circular fabric duct.

From Figure 6-12 can be observed that distribution system via semi-circular fabric duct provides a homogeneous flow pattern along the space with increased temperature stratification and maximum air velocities of 0.3 m.s^{-1} close to the fabric duct and at knee level.
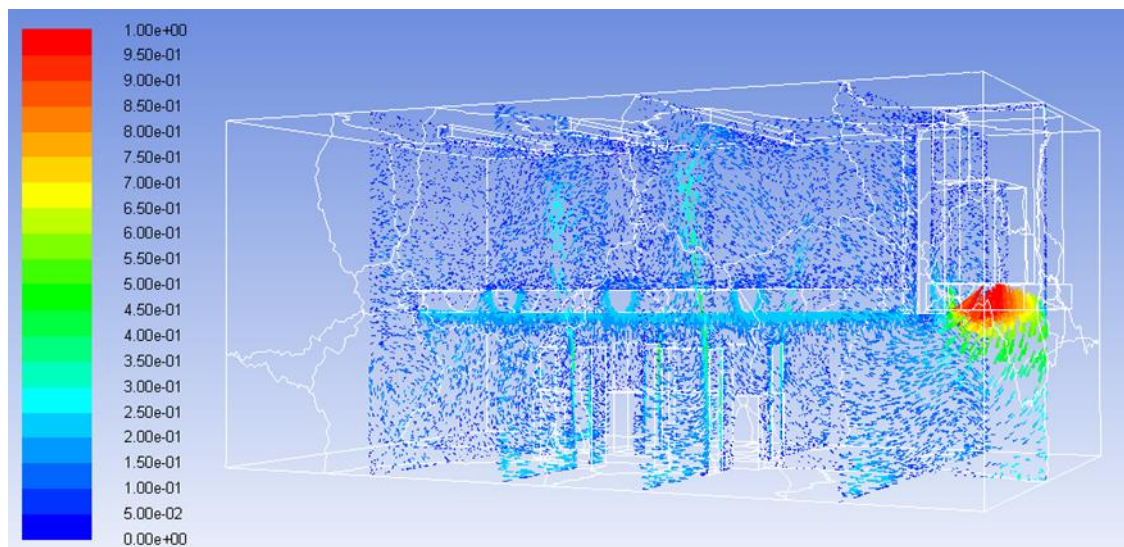
Figure 6-12. Air velocity profiles from air distribution system with a semi-circular duct at medium level in test room

6.1.4 *CFD modelling of air distribution via galvanized metal ducts and 2-slot diffusers*

Slot diffusers are most commonly used for ceiling or sidewall applications. Slot diffusers are flexible to be applied for different air volume applications. For the CFD modelling purposes the geometrical characteristics of a CS-F 2-slot diffuser from Waterloo industries was selected for the study. (Waterloo Air Products Plc., CS-F 2-slot diffuser, 2014). In total four 2-slot diffusers were applied. Figure 6-13 shows an example of the CS-F 2-slot diffuser. The air mass flow rate boundary condition was defined at 1400 m³hr^{-1}.
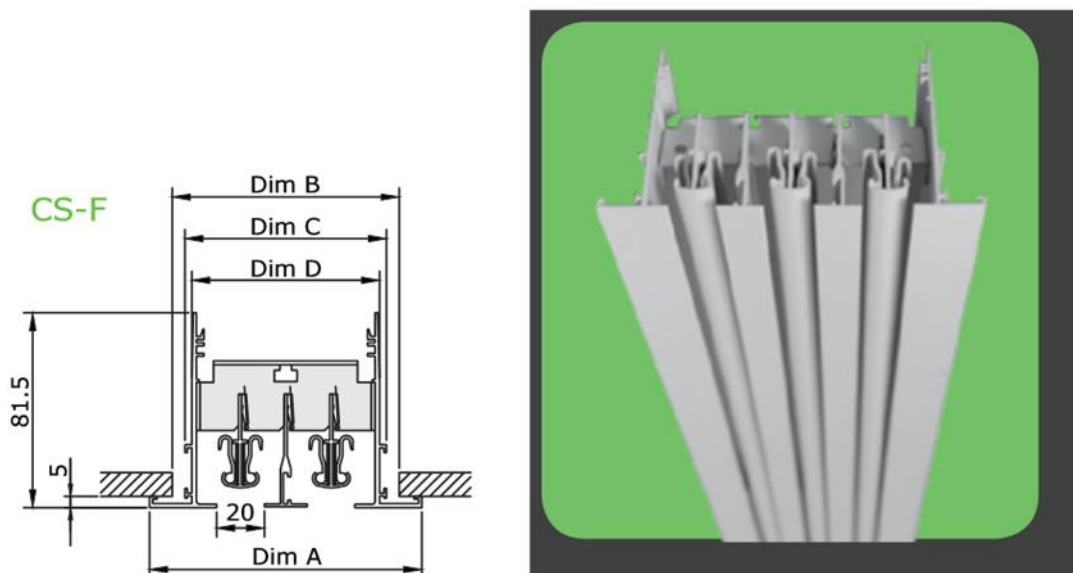
Figure 6-13. Two-slot diffusers

Figure 6-14 shows the geometry for the 2-slot diffusers installed at a medium level in a circular galvanized duct. The direction of the supply air flow to the space is shown with the blue arrows and the return air flow to the coil is indicated with the red arrows.
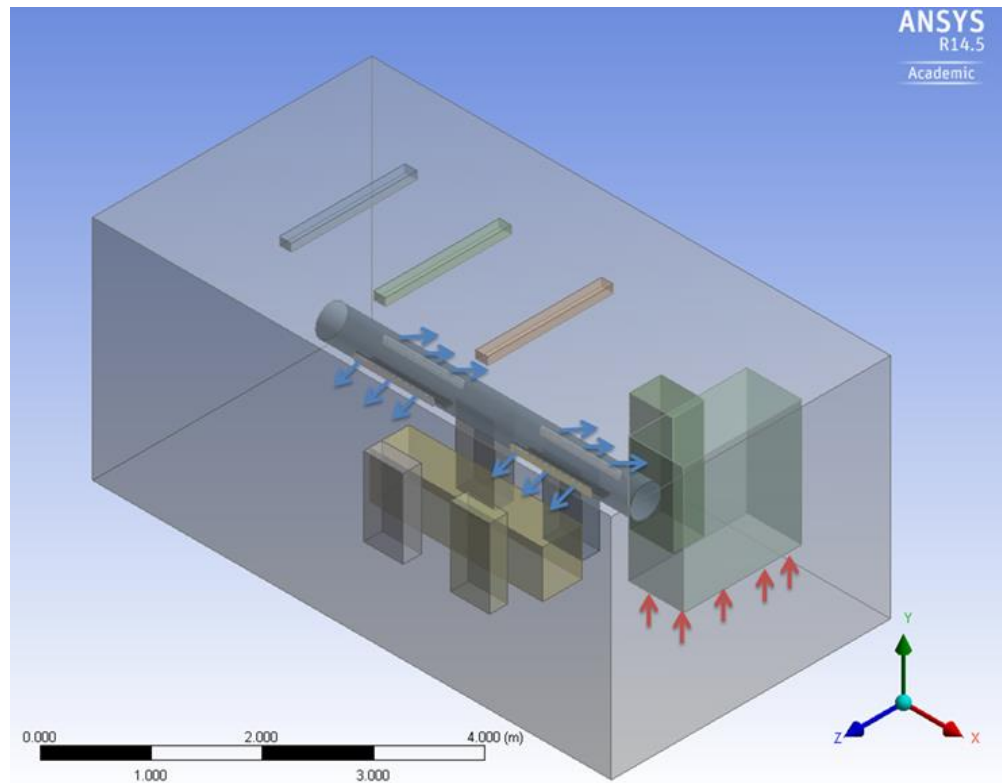
Figure 6-14. CFD model via four 2-slot diffusers

The use of the slot diffusers resulted in temperatures of around 8 ºC at low level and 12.0 ºC at high level very close to the lighting fixtures (Figure 6-15). Stratification, however, between the supply duct and the ceiling away from the lighting fixtures was limited and of the order of 2 °C.

The resulting velocity profiles with the slot diffusers are shown in Figure 6-16. It can be observed that the use of this configuration resulted in high velocities, up to 2.5 ms⁻¹, at low level in the space which will be cause discomfort to the workers in the space.
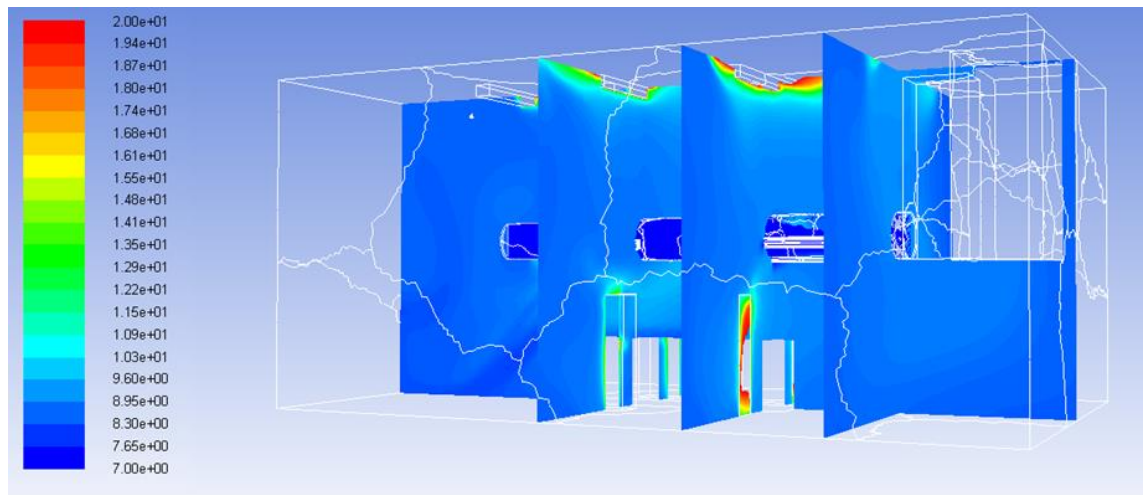
Figure 6-15. Predicted air temperature variation through air distribution with galvanised metal ducts and slot diffusers.
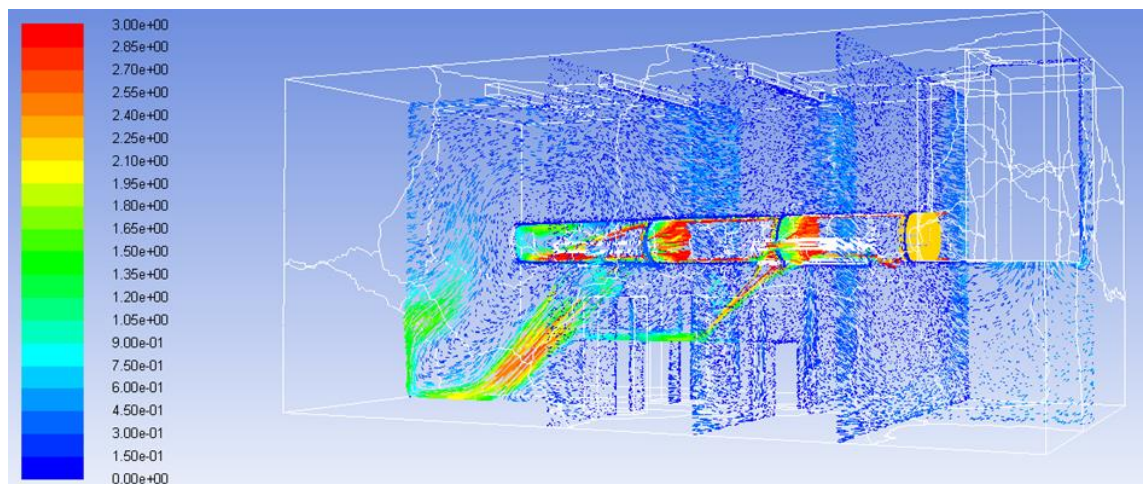
Figure 6-16. Air velocity profiles from air distribution with galvanized metal ducts and slot diffusers

6.1.5 *CFD Modelling of air distribution via circular fabric ducts installed at a medium level in the space*

Figure 6-17 shows an example of a circular fabric duct. The duct had 0.40 m diameter and 4.0 m length. The duct was installed 1.15 m below ceiling level. Using design criteria in the KE-fabrictec design guide (KE FIBERTEC, KE-Low Impulse, 2013) the air mass flow rate boundary condition was selected to be 2825 m³hr^{-1}.
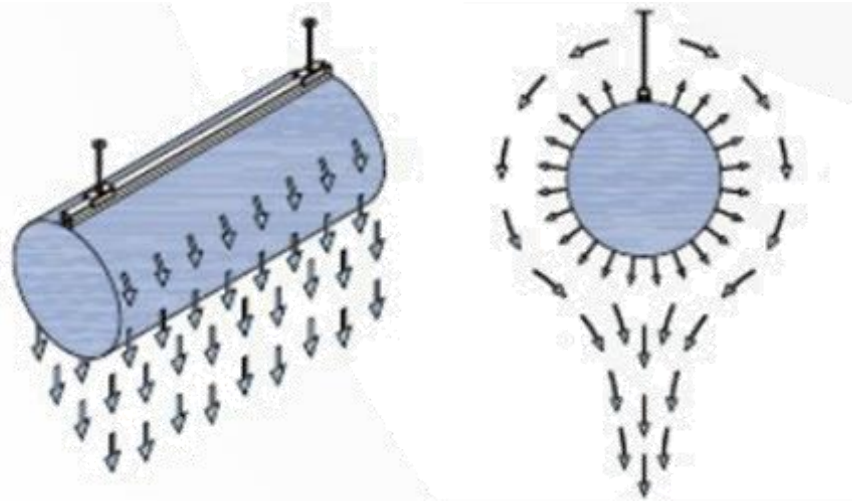
Figure 6-17. Fabric duct

Figure 6-18 shows the CFD model representation. The direction of the supply air flow is shown with the blue arrows and the return air flow path to the coil is indicated with the red arrows.
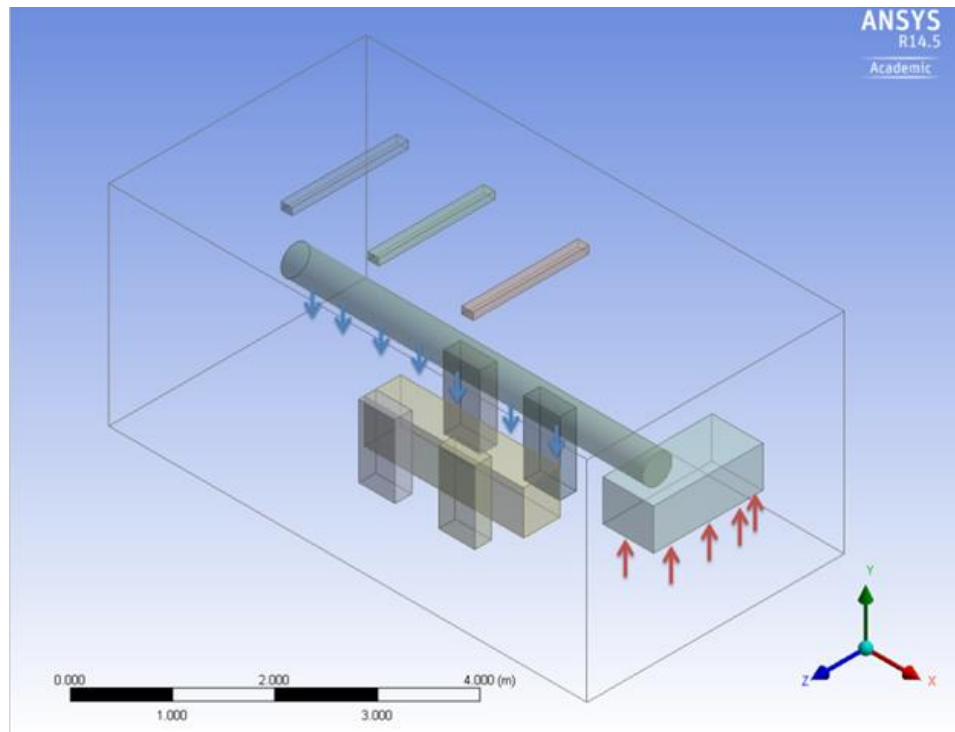
Figure 6-18. CFD model representation for the circular fabric duct installed at medium level.

The air temperature variation in the space resulting from the CFD modelling is shown in Figure 6-19. With a supply temperature from the fabric duct at 7 ℃, the temperature in the space varied from 8.0 ℃ at low level close to the floor to 15 ℃ very close to the ceiling. Temperature stratification between the supply duct and the ceiling was of the order of 5 ℃.
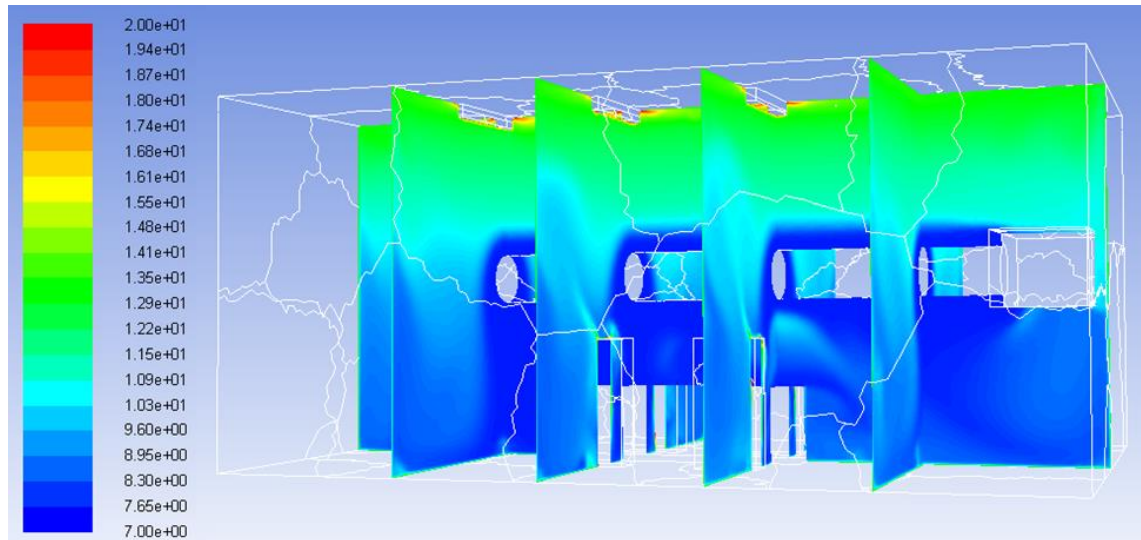
Figure 6-19. Predicted air temperature variation with air supply through a circular fabric duct.

The resulting air velocity distribution in the space is shown in Figure 6-20. It can be seen that the air velocities in the bulk of the space under the supply duct are quite low, between 0.05 and 0.25 m.s⁻¹. This is within the acceptable range to avoid thermal discomfort in cooled spaces.
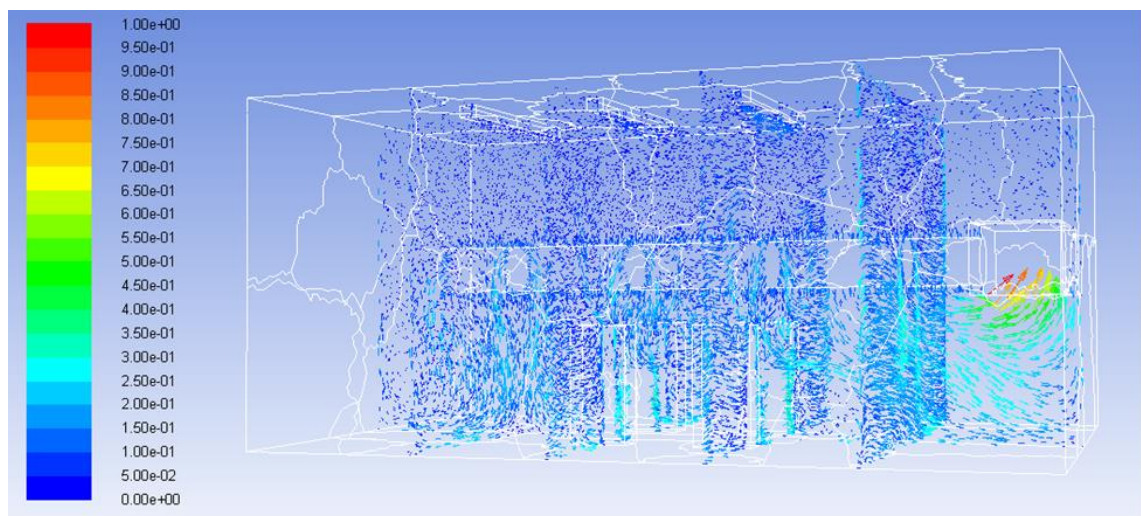
Figure 6-20. Air velocity profiles from air distribution via circular fabric duct at low level.

6.2   Summary of Chapter 6

This chapter presents the investigation and evaluation of different air distribution systems with the developed 3-D CFD modelling tool. From the investigated air distribution solutions, the semi-circular and circular fabric ducts located at medium level have been shown to be the most effective configurations. They both showed to be able to provide good levels of temperature stratification, air flow and temperature uniformity at low levels in the space to cover the production zone and easy implementation in an actual factory. Regarding the 1-way lay in and the rectangular 1-way displacement diffusers solutions, temperature uniformity could be improved around the occupied area by installing additional diffusers in the room. However, due to the large size of a real chilled food production facilities (Chapter 3, Case study 1 and 2) more than 60 diffusers are needed which will interfere to the production space. Furthermore, taking into account chilled food facilities hygiene boundaries and cleaning procedures this two solutions was rejected. During the cleaning process hot water is sprayed into the processing room, which can be trapped into the diffusers and create hygiene problems.

The next chapter deals with experimental investigations and more detailed study of the air distribution solutions with semi-circular and circular fabric ducts located at medium level in the manufacturing space.

Chapter 7. Experimental study of different air distribution systems

7.1 Introduction

The present research stage dealt with the experimental study of different air distribution systems applied in chilled food production facilities. The experimental study was used to identify the most appropriate air distribution approaches. The objective was to achieve low velocities and uniform temperatures at low level to improve thermal comfort for the workers and at the same time achieve temperature stratification between floor and ceiling levels to reduce energy consumption.

Most chilled food factories operate 7 days per week, 24 hours per day with short breaks mainly for cleaning and shift changing. Any modifications or changes to the current air distribution systems need to be implemented during those short breaks in order to avoid any disruption to food production. Therefore, an improved air distribution method needs to provide homogenous air flow throughout the occupied zone and to be easily adaptable to the cooling systems currently installed to an existing chilled food facility without replacement of the existing refrigeration equipment or costly major structural changes.

Taking into account these constraints and the modelling results from the different approaches (Chapter 6.2), air distribution systems via circular fabric duct and semi-circular duct located at medium level were selected for further investigation in the laboratory to establish their effectiveness in providing temperature stratification lead to energy efficiency. Both systems can be easily retrofitted to evaporator coils without ducted air distribution systems placed at ceiling level. The easy implementation of both systems in existing chilled food facilities is therefore a favourable aspect which contributes to their selection. The experimental test rig dimensions and logging system were described in Chapter 4.2.

7.2 Semi-circular -fabric duct at medium level

This section contains the results from experimental measurements and modelling of the thermal environment yielded by the air distribution system via semi-circular fabric duct installed at a medium level height in the scaled test rig. Figure 7-1 shows the experimental set-up for the semi-circular fabric duct installed at a medium level. The semi-circular fabric duct has the same dimensions with the reference case (circular fabric duct at ceiling level Chapter 4.3) and measured 40 cm in diameter and 400 cm in length.

The only difference to the reference case was that the centre line of the duct was 1.15 m below ceiling level compared to 0.25 m for the reference case. In addition, the air was drawn to the evaporator coil through a hood arranged to draw air from the same level as the supply duct. In the case of the semi-circular fabric duct, the volumetric air flow was set to 70% of the total air flow (2825 m³hr^{-1}).

Figure 7-1. Semi-circular fabric duct at medium level

7.2.1 *Experimental assessment: Semi-circular fabric duct at medium level air temperature profiles*

This section presents an analysis of the thermal environment in terms of air temperature. Figure 7-2 shows the temperature profiles measured in the scaled facility from testing the air distribution system via semi-circular fabric duct at medium level.

Temperature values shown in Figure 7-3, Figure 7-4 and Figure 7-5 correspond to the average values measured in each position during a day test. According to the results from testing the semi-circular fabric duct, temperatures values varied from 7.5 ℃ and 15.1 ℃ with average temperature values measured at knee, head and ceiling level of 9.3 ℃, 10.5 ℃ and 14.3 ℃, respectively. Figure 7-2 clearly shows that a significant temperature

gradient was established between the floor and ceiling level, of the order of 5 °C, with colder air flows concentrated at low level in the space localizing the cooling effect at the occupied zone. In addition, most stratification, of the order of 4 °C, takes place between head and ceiling level.
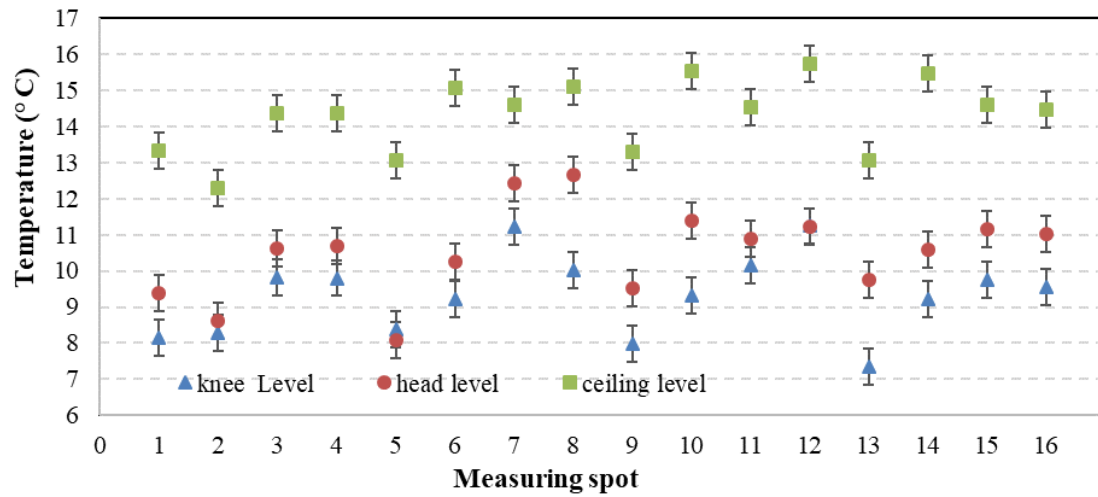
Figure 7-2. Semi-circular fabric duct at medium level: Air temperature measurements
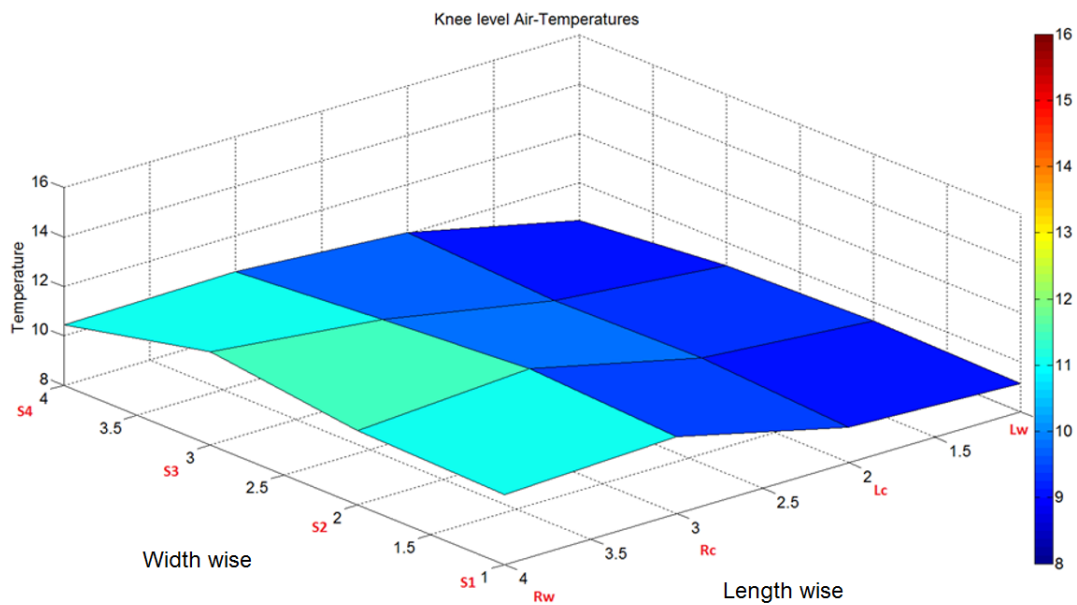
Figure 7-3. Semi-circular fabric duct at medium level: Air temperature at knee level
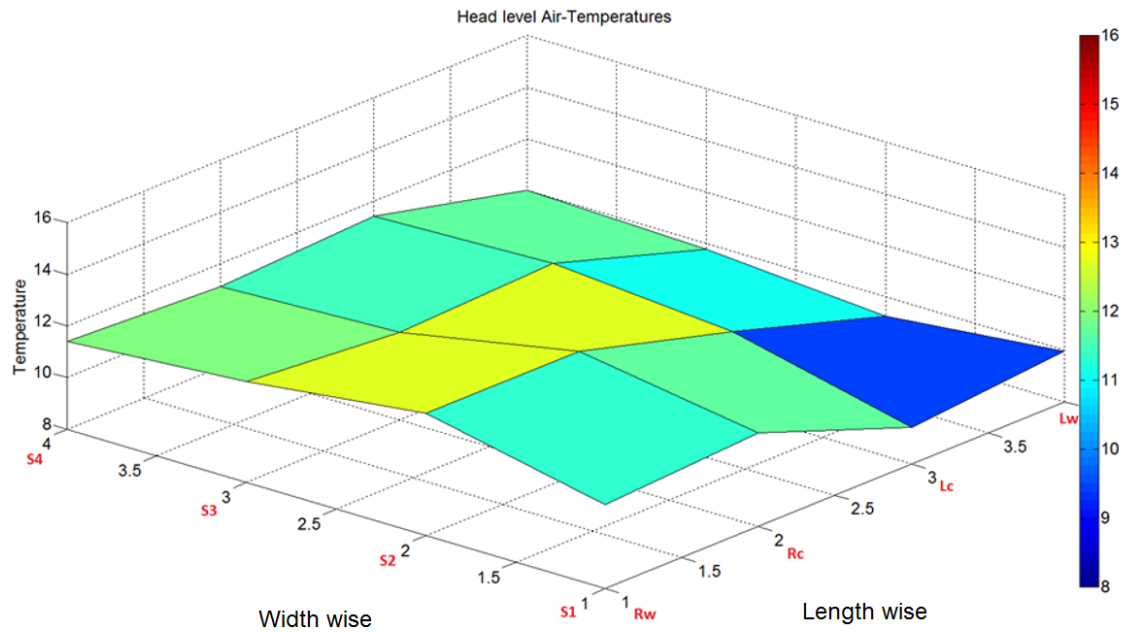
Figure 7-4. Semi-circular fabric duct at medium level: Air temperature at head level
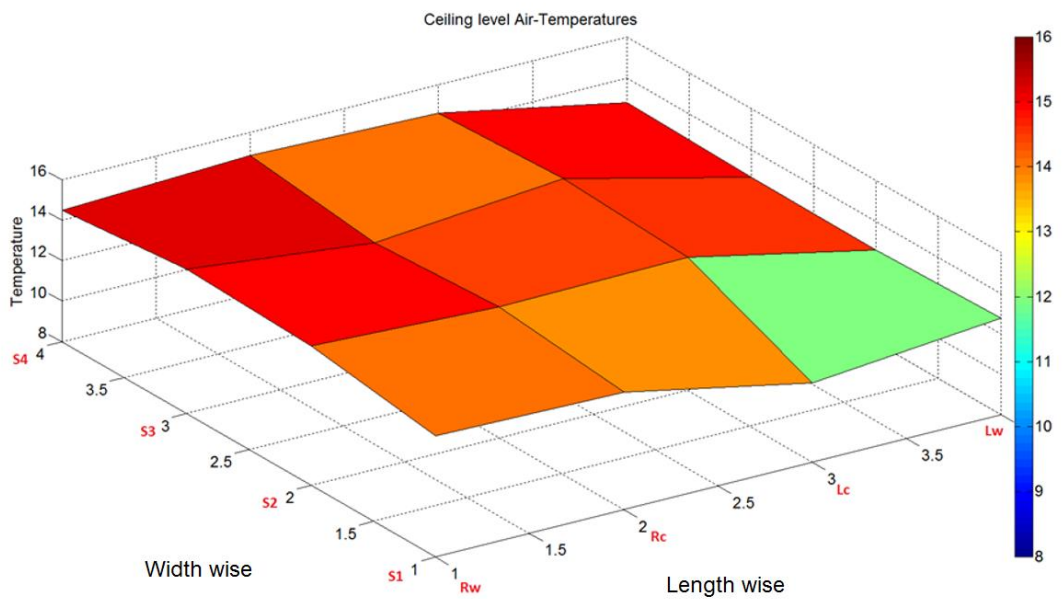
Figure 7-5. Semi-circular fabric duct at medium level: Air temperature at ceiling level

7.2.2 *Experimental assessment: Semi-circular fabric duct at medium level air velocity profiles*

This section presents an analysis of the thermal environment in terms of air velocities. Regarding the measured air velocities, Figure 7-6 shows that values varied between 0.00 and 0.1 m.s^{-1} with the maximum value measured close to the semi-circular fabric duct. In

addition, Figure 7-7, Figure 7-8 and Figure 7-9 show the air velocity distribution along the space at the 3 different Heights that data were measured. It can be observed that air velocities were very low with average velocities cross all the measuring points for knee, head and ceiling level where 0.02 m.s^{-1}, 0.03 m.s^{-1} and 0.00 m.s^{-1} respectively. The very slow air movement at ceiling level maintained high temperatures in this region and created the temperature stratification that can be observed in Figure 7-3, Figure 7-4 and Figure 7-5.
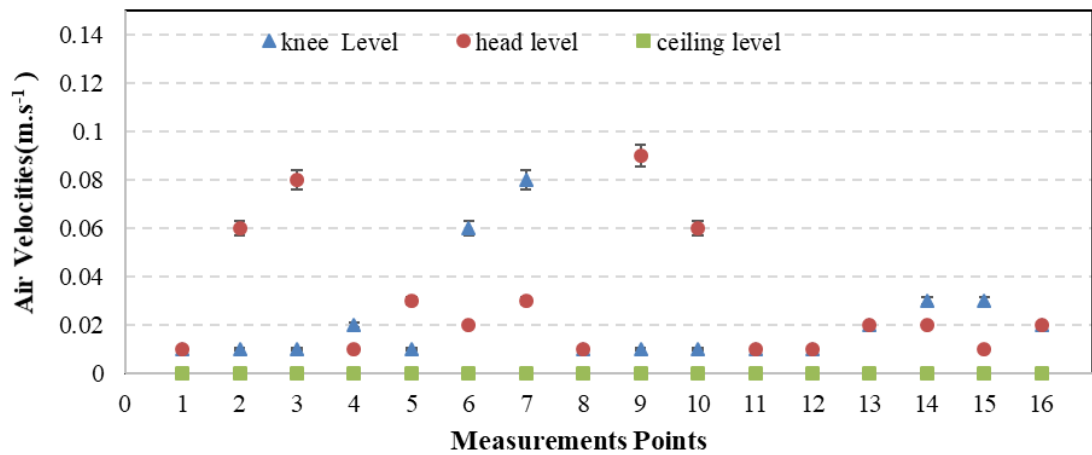
Figure 7-6. Semi-circular fabric duct at medium level: Air velocity measurements
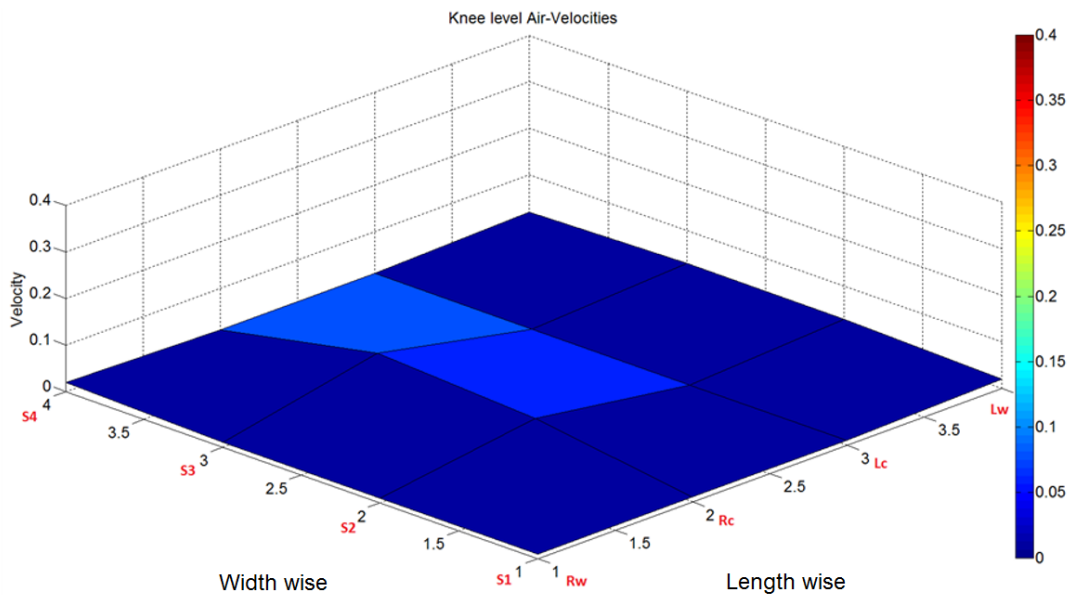
Figure 7-7. Semi-circular fabric duct at medium level: Air velocity at knee level
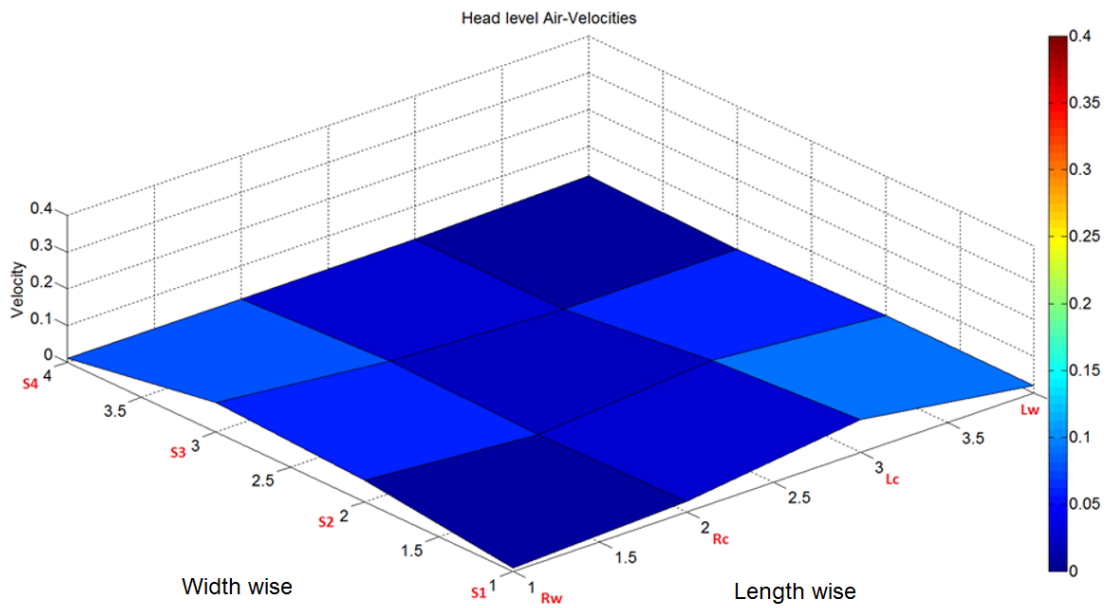
Figure 7-8. Semi-circular fabric duct at medium level: Air velocity at head level
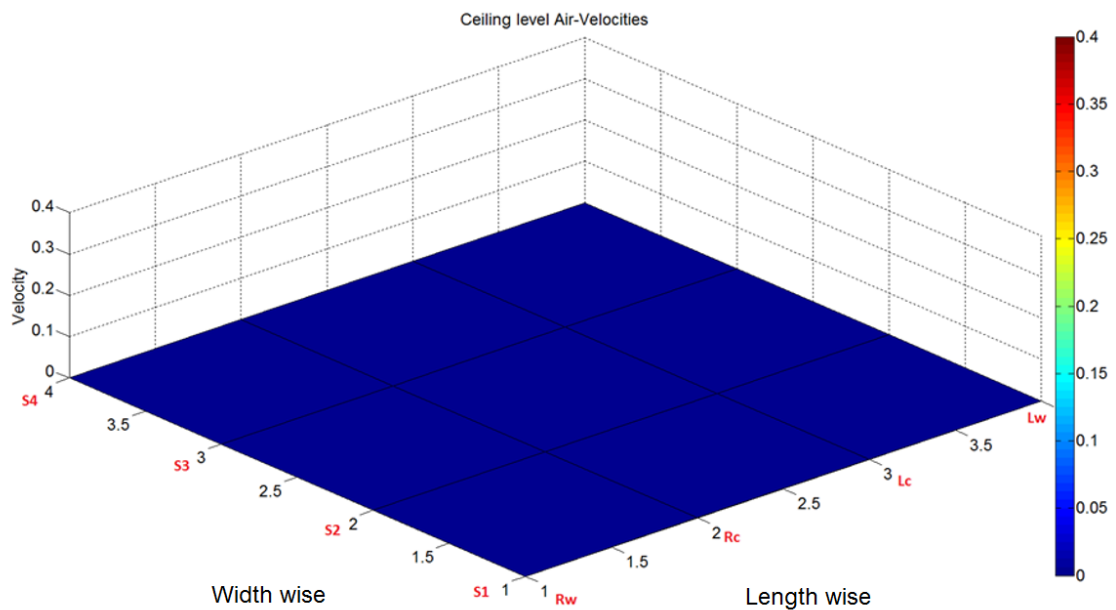
Figure 7-9. Semi-circular fabric duct at medium level: Air velocity at ceiling level

7.2.3 *Experimental facility 'Semi-circular fabric duct at medium level': CFD Air distribution model validation*

This subsection presents the validation of the experimental facility CFD model using semi-circular fabric ducts as an air distribution method. The validation of the model was conducted by comparing the monitored air temperatures with the CFD predicted temperatures (as described in Chapter 6.1.3). Figure 7-10 presents the average temperature data collected including the measurement uncertainty and the modelling

results. In general, the model shows a good level of prediction for the air temperature trend and distribution achieved in the space.
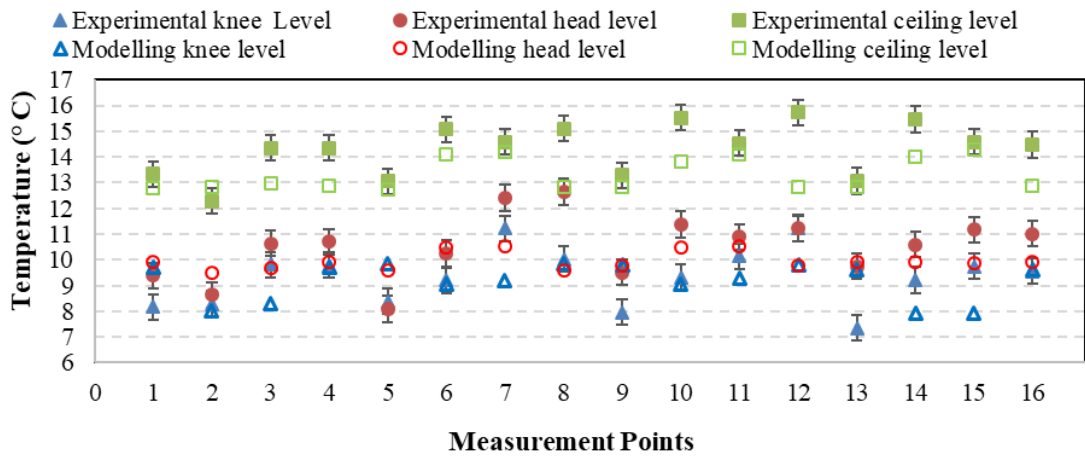
Figure 7-10. Air temperature comparison

To determine the validity of the model, the temperature predictions from the model were compared against temperature measurements obtained from the experimental facility. The results of this comparison are shown in Figure 7-11. The middle line in the graph indicates the position of 0 ℃ error and the other two lines shows the maximum errors of +2.0 and -2.0 ℃ respectively. From all results, the average absolute error across all test points in the space was found to be 0.97 ℃.
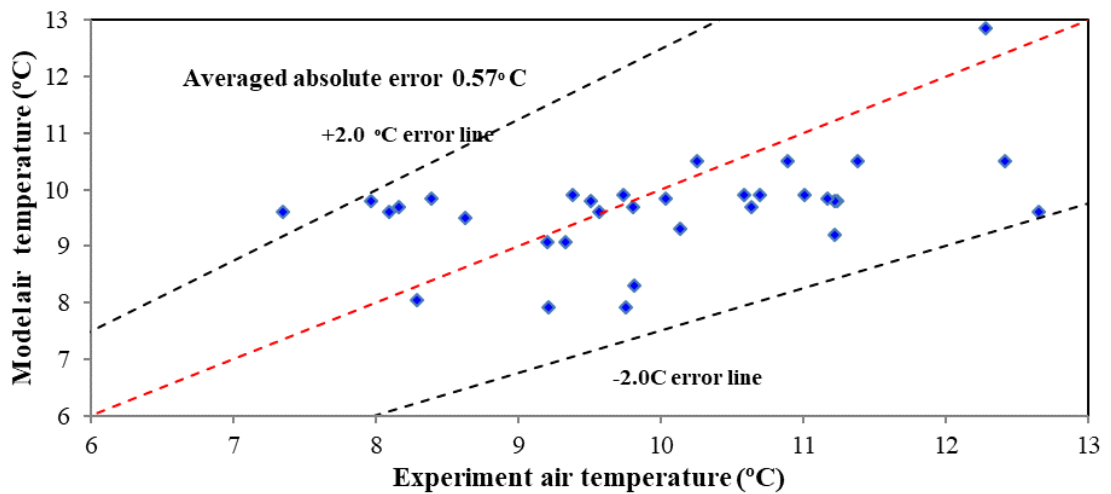
Figure 7-11. CFD modelling air temperature validation: Semi-circular fabric duct at medium level.

7.2.4 *Experimental assessment: Semi-circular fabric duct at medium level refrigerant mass flow rate and power consumption*

An analysis of the refrigeration system power consumption and refrigerant mass flow rate are presented in this section for the investigated air distribution configuration (semi-circular fabric duct at medium level). Data were collected over a 17-hour test period with ambient air temperature around 8 ºC. For clarity, power data and mass flow measurements are presented for a period of one hour in Figure 7-12 and Figure 7-13. Data of power consumption and mass flow rate collected for the 17 hours can be found in Appendix C.

Power measurements include the energy consumption of the compressor, condenser fans, evaporator fan and control system. In the case of the semi-circular duct, the volumetric air flow was set to 70% of the total air flow (2825 m³hr^{-1}). The power consumption (P) of the refrigeration system was estimated by equation 1 in sub section 4.3.3.1

Power measurements showed that by using the semi-circular fabric duct at medium level, the operating time of the refrigeration system was 26.5 minutes per hour with 3 operating cycles with an average duration for each cycle of 7.8 minutes. In addition, the peak instant mass flow rate was 160kg/hr. Figure 7-13 shows that the averaged instant power consumption was at 2.8kW.
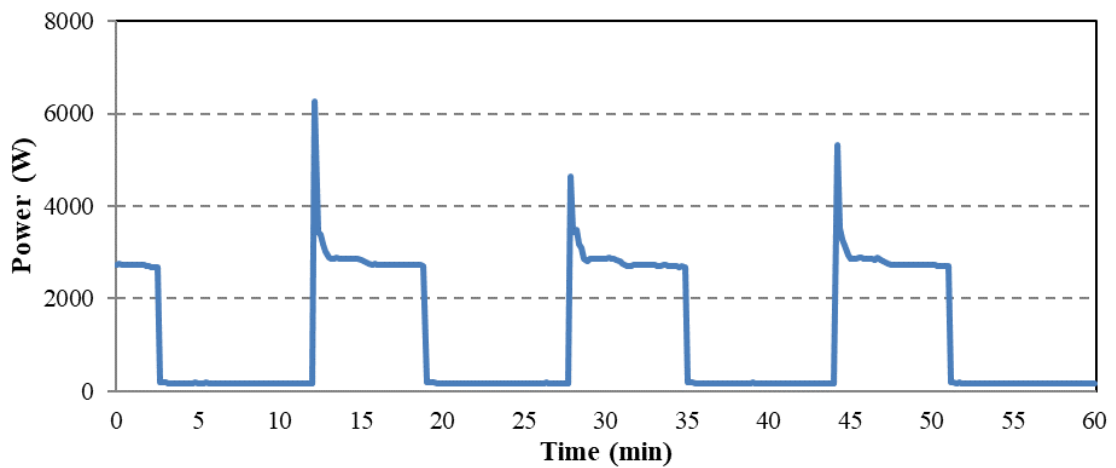
Figure 7-12. Power consumption, semi-circular fabric duct at medium level
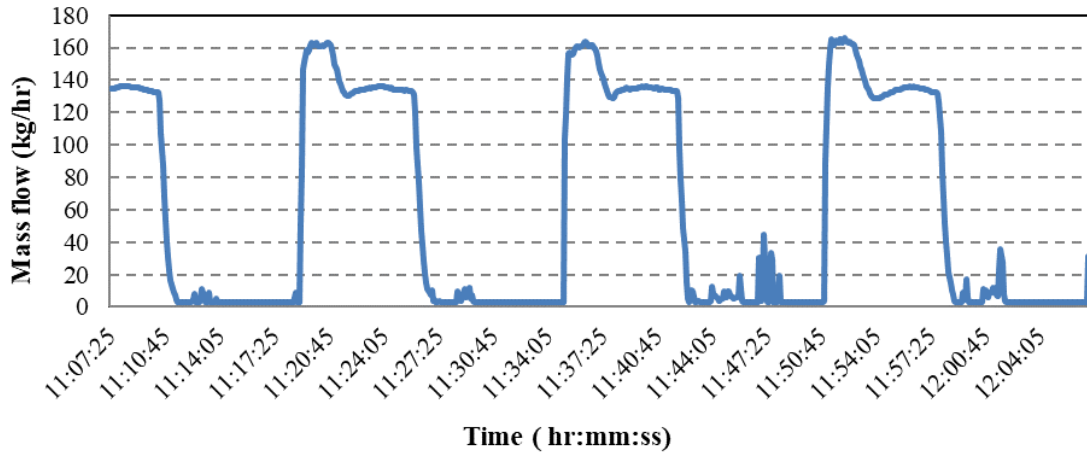
Figure 7-13. Mass flow rate, semi-circular fabric duct at medium level

7.3 Circular fabric duct at medium level

This section contains the results from experimental measurements and modelling of the thermal environment yielded by the air distribution system via circular fabric duct installed at a medium level height in the scaled test rig. Figure 7-14 shows the experimental set-up for the fabric duct installed at a medium level. The circular fabric duct has the same dimensions with the reference case (circular fabric duct at ceiling level Chapter 4.3) and measured 40 cm in diameter and 400 cm in length.

The only difference to the reference case was that the centre line of the duct was 1.15 m below ceiling level compared to 0.25 m for the reference case. In addition, the air was drawn to the evaporator coil through a hood arranged to draw air from the same level as the supply duct. In the case of the circular fabric duct, the volumetric air flow was set to 100% of the total air flow (2825 m³hr-1) likewise the reference case (fabric duct at ceiling level).

Figure 7-14. Circular fabric duct at medium level

7.3.1 *Experimental assessment: Circular fabric duct at medium level air temperature profiles*

This section presents an analysis of the thermal environment in terms of air temperature. Figure 7-15 shows the temperature profiles measured in the scaled facility from testing the air distribution system via circular fabric duct at medium level.

Temperature values shown in in Figure 7-16, Figure 7-17 and Figure 7-18 correspond to the average values measured in each position during a day test. According to the results from testing the circular fabric duct, temperatures values varied from 8.0 ℃ and 16.5 ℃ with average temperature values measured at knee, head and ceiling level of 9.8 ℃, 10.7 ℃ and 15.2 ℃, respectively. Figure 7-15 clearly shows that a significant temperature gradient was established between the floor and ceiling level, of the order of 5 °C, with colder air flows concentrated at low level in the space localizing the cooling effect at the occupied zone. In addition, most stratification, of the order of 4 °C, takes place between head and ceiling level.
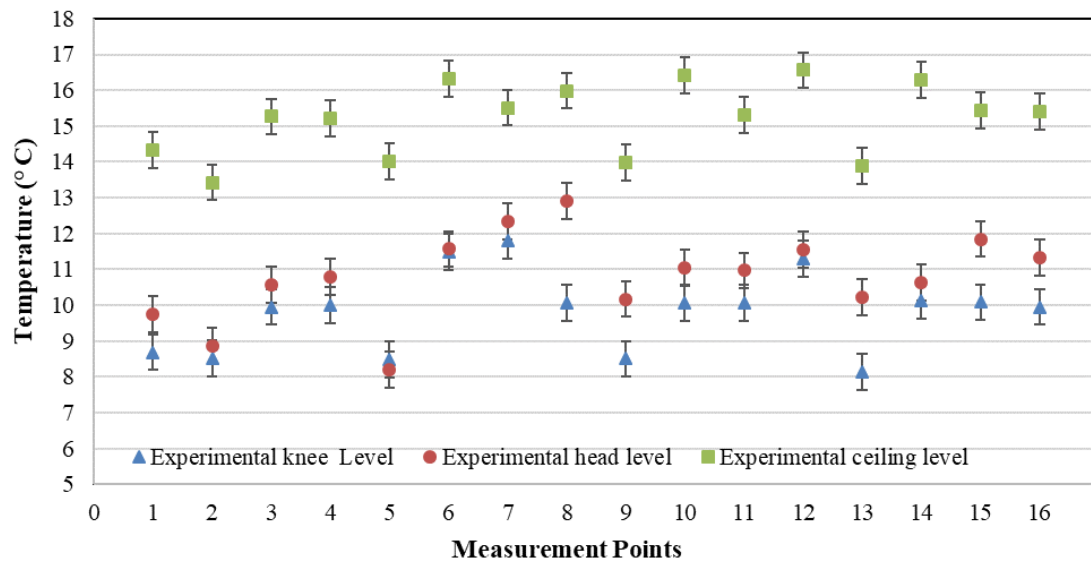
Figure 7-15. Circular fabric duct at medium level: Air temperature measurements
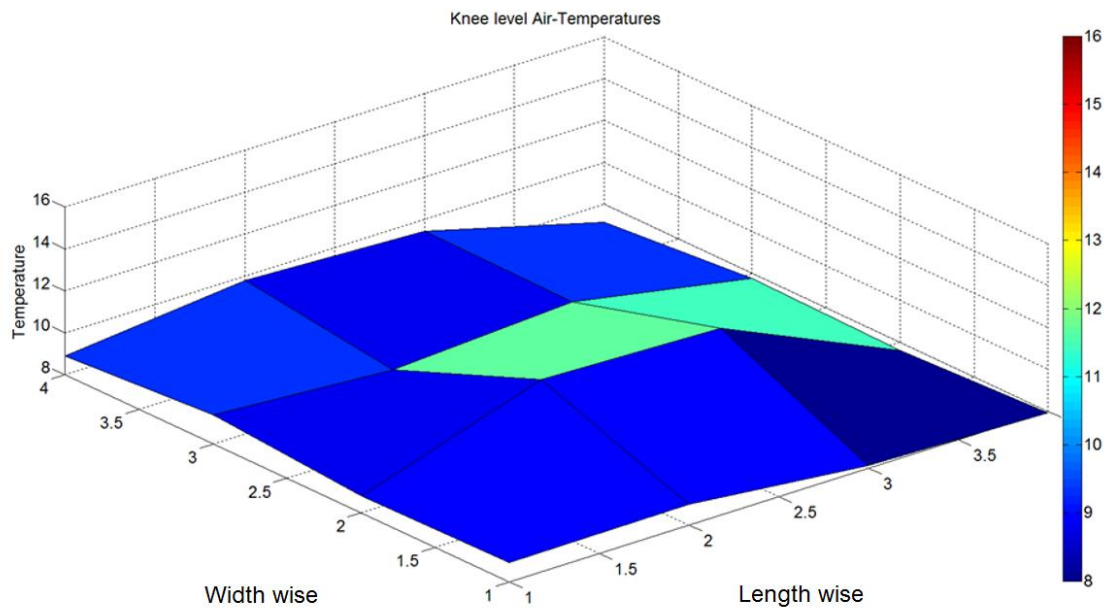
Figure 7-16. Circular fabric duct at medium level: Air temperature at knee level
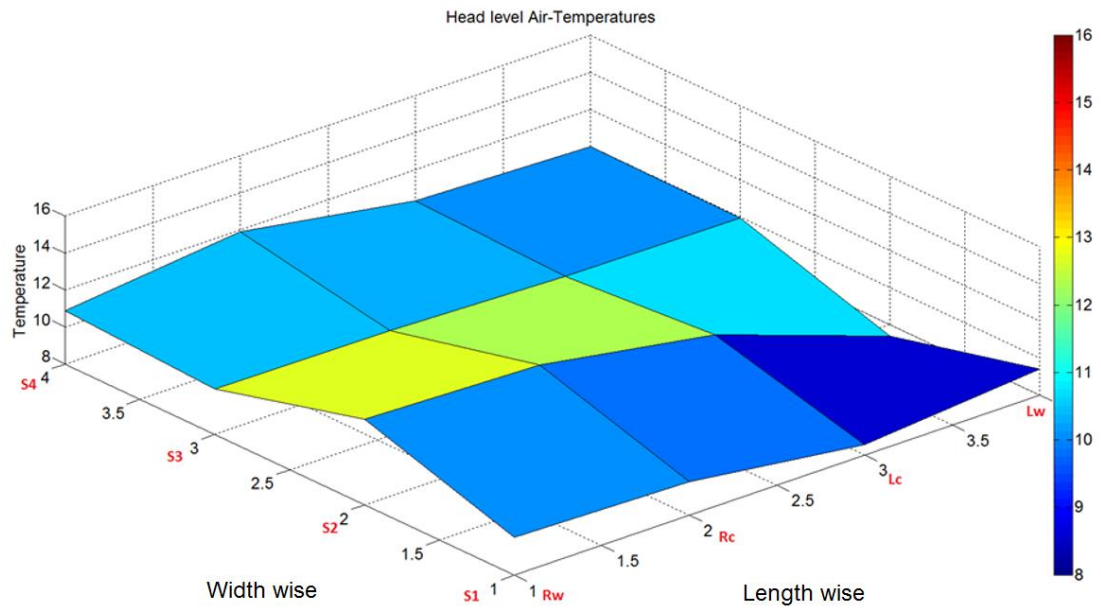
Figure 7-17. Circular fabric duct at medium level: Air temperature at head level
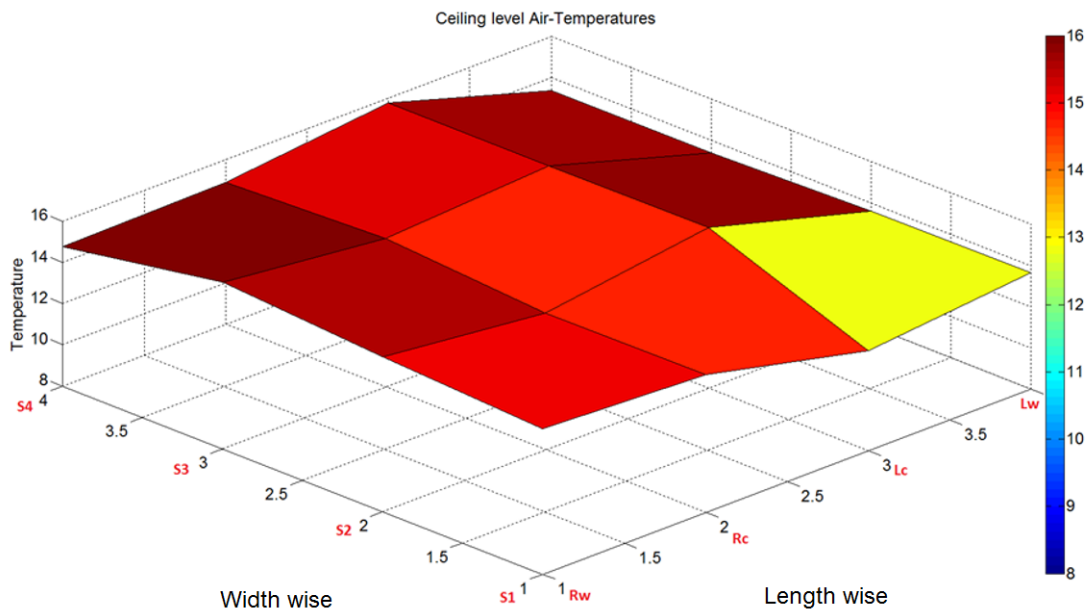
Figure 7-18. Circular fabric duct at medium level: Air temperature measurements

7.3.2 *Experimental assessment: Circular fabric duct at medium level air velocity profiles*

This section presents an analysis of the thermal environment in terms of air velocities. Regarding the measured air velocities, Figure 7-19 shows that values varied between 0.00 and 0.25 m.s^{-1} with the maximum value measured close to the circular fabric duct. In

addition Figure 7-20, Figure 7-21 and Figure 7-22 show the air velocity distribution along the space at the 3 different Heights that data were measured.

It can be observed that air velocities were very low with average velocities cross all the measuring points for knee, head and ceiling level where 0.13 m.s^{-1}, 0.07 m.s^{-1} and 0.00 m.s^{-1} respectively. The very slow air movement at ceiling level maintained high temperatures in this region and created the temperature stratification that can be observed in Figure 7-16, Figure 7-17 and Figure 7-18.
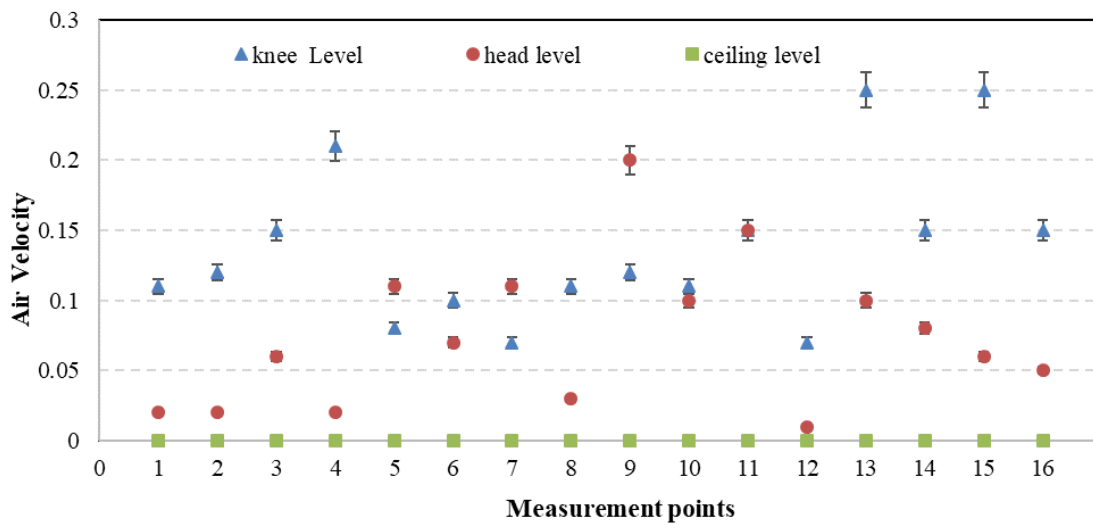
Figure 7-19. Circular fabric duct at medium level: Air velocity measurements
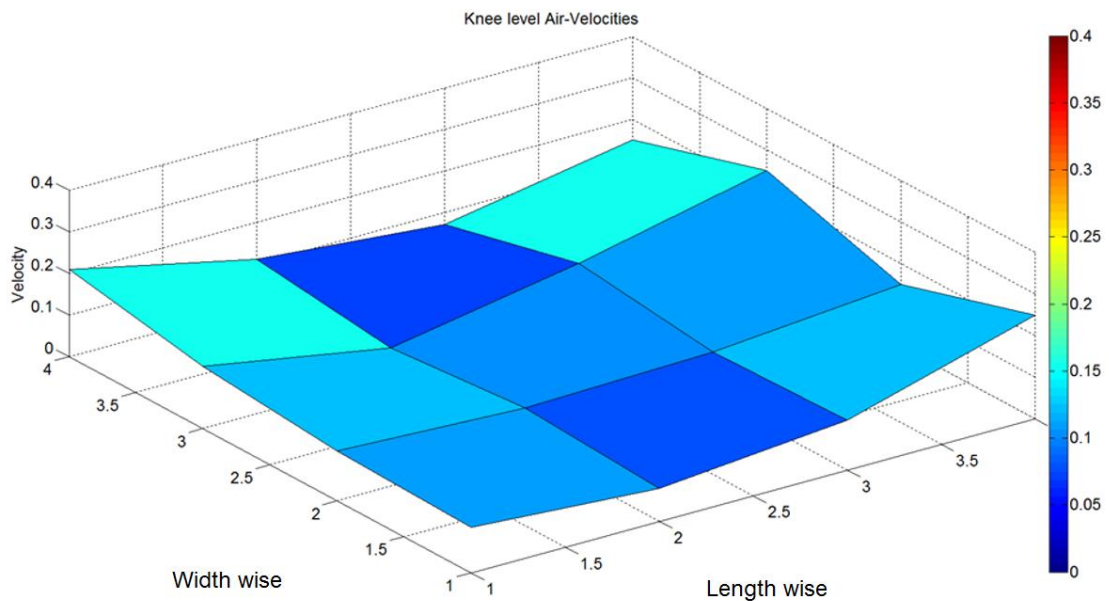
Figure 7-20. Circular fabric duct at medium level: Air velocity at knee level
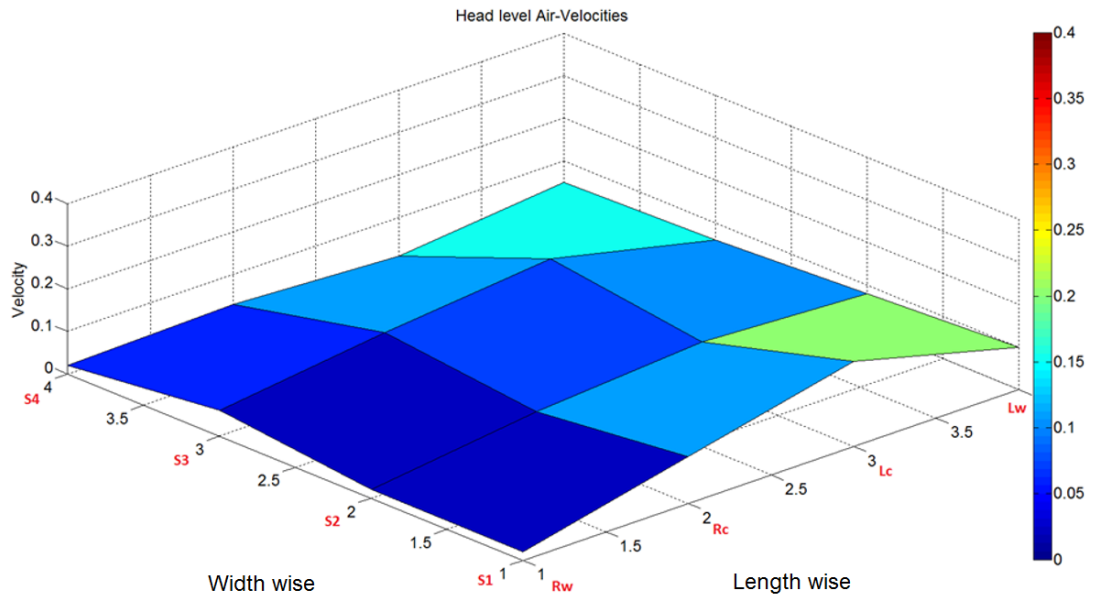
Figure 7-21. Circular fabric duct at medium level: Air velocity at head level
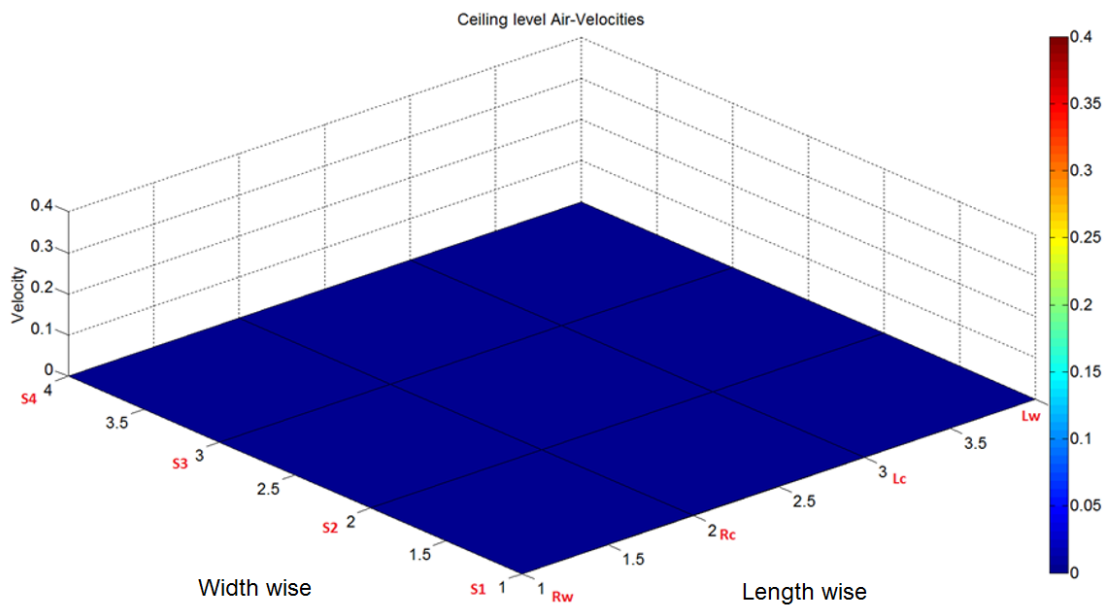
Figure 7-22. Circular fabric duct at medium level: Air velocity at ceiling level

7.3.3 Experimental facility 'Circular fabric duct at medium level': CFD Air distribution model validation

This subsection presents the validation of the experimental facility CFD model using fabric ducts as an air distribution method. The validation of the model was conducted by comparing the monitored air temperatures with the CFD predicted temperatures (as described in section 6.1.5). Figure 7-23 presents the average temperature data collected including the measurement uncertainty and the modelling results. In general, the model

shows a good level of prediction for the air temperature trend and distribution achieved in the space.
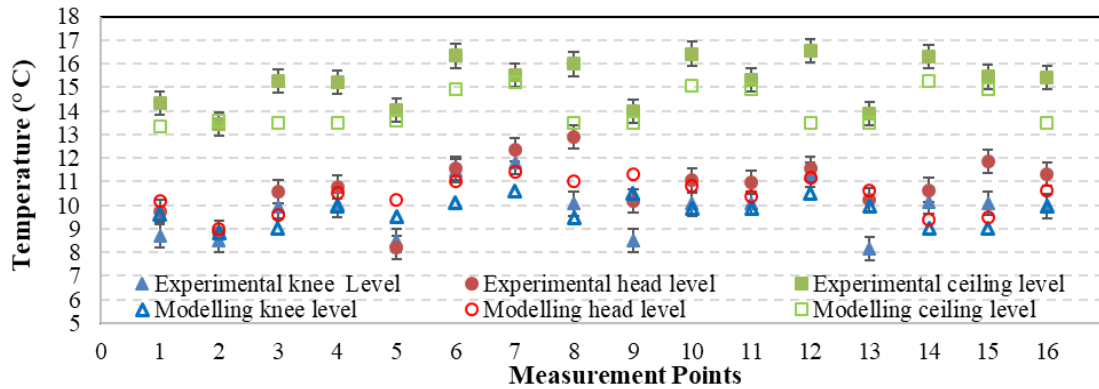
Figure 7-23. Air temperature comparison

To determine the validity of the model, the temperature predictions from the model were compared against temperature measurements obtained from the experimental facility. The results of this comparison are shown in Figure 7-24. The middle line in the graph indicates the position of 0 ℃ error and the other two lines shows the maximum errors of +2.0 and -2.0 ℃ respectively. From all results, the average absolute error across all test points in the space was found to be 0.95 ℃.
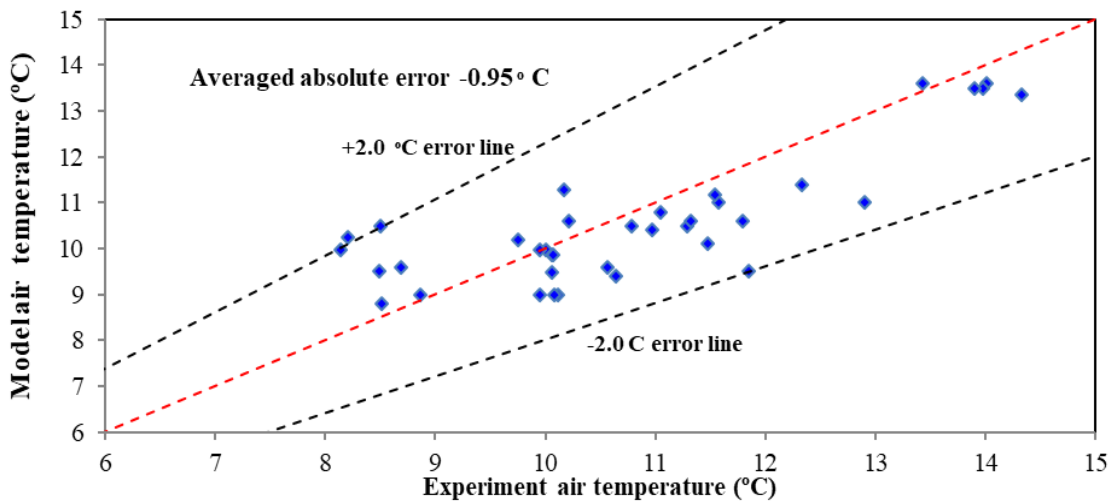
Figure 7-24. CFD modelling air temperature valuation: Circular fabric duct at medium level

7.3.4 *Experimental assessment: Circular fabric duct at medium level refrigerant mass flow rate and power consumption*

An analysis of the refrigeration system power consumption and refrigerant mass flow rate are presented in this section for the investigated air distribution configuration (round-

fabric duct at medium level). Data were collected over a 17-hour test period with ambient air temperature around 8 ºC. For clarity, power data and mass flow measurements are presented for a period of one hour in Figure 7-25 and Figure 7-26 Data of power consumption and mass flow rate collected for the 17 hours can be found in Appendix C. Power measurements include the energy consumption of the compressor, condenser fans, evaporator fan and control system. In the case of the semi-circular duct, the volumetric air flow was set to 100% of the total air flow (2825 m³hr^{-1}). The power consumption (P) of the refrigeration system was estimated by equation 1 in section 4.3.3.1

Power measurements showed that by using the round-fabric duct at medium level, the operating time of the refrigeration system was 21.6 minutes per hour with 7.2 operating cycles with an average duration for each cycle of 3.0 minutes. In addition, the peak instant mass flow rate was 160kg/hr. Figure 7-25 shows that the averaged instant power consumption was at 3.0 kW.
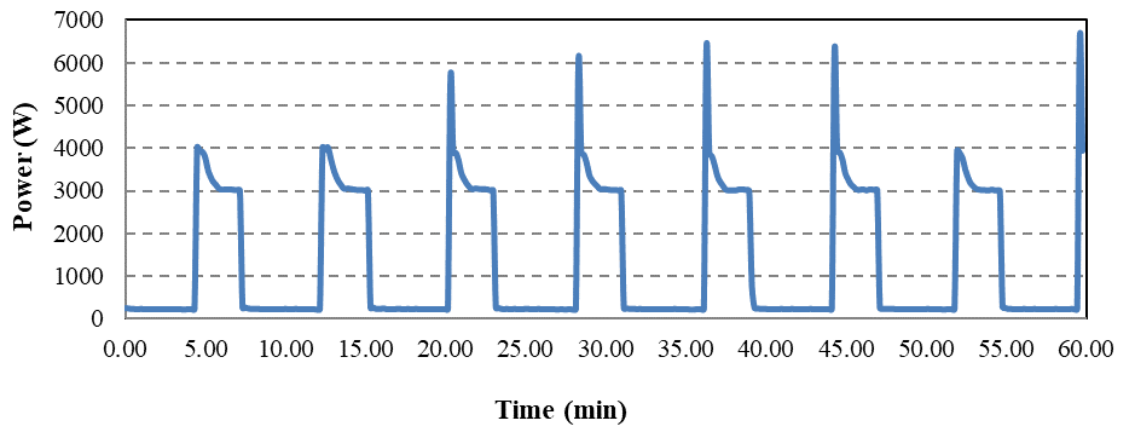
Figure 7-25. Power consumption, Circular fabric duct at medium level
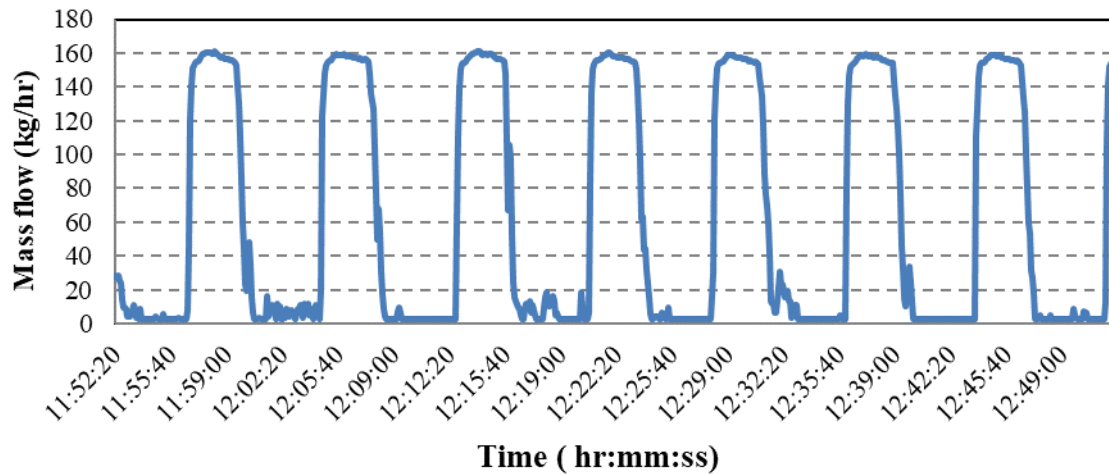
Figure 7-26. Mass flow rate, circular fabric duct at medium level

7.4 Chilled food facility case study 1: Improved air distribution solution CFD modelling

In order to confirm that this chapter experimental findings in terms of localising cooling at low level can exist to a full scale chilled food facility, an improved air distribution solution was numerically applied to case study 2 chilled food facility. Considering the modelling results in Chapter 6 and from experimental results in Chapter 7.2 the circular fabric duct installed at a lower height was introduced as an improved air distribution solution for further investigation.

Therefore, this section presents the results from the further CFD modelling of case study 2 with the improved air distribution system via circular fabric ducts located at a medium level. The 3-D CFD model was implemented with the same boundary conditions and solution procedure as described in Chapter 5.6. The main difference with respect to the reference case is that the fabric ducts and the control thermostats were placed at a medium level. In a real situation, a hood can be added to the evaporator coil in a way that the return air is only driven from the bottom. However, in the present model, the coil was also moved down. As it was mentioned in Chapter 3.3, the space height is 6.5 m and the fabric ducts are currently installed at 6.0 m height. The new installation height for the air distribution modelling is 3.5 m creating a 3.0 m difference with respect to the floor. This is the minimum space allowed so the system does not interfere with the production and cleaning activities. Figure 7-27 shows the model geometry of the air distribution system at a lower level.
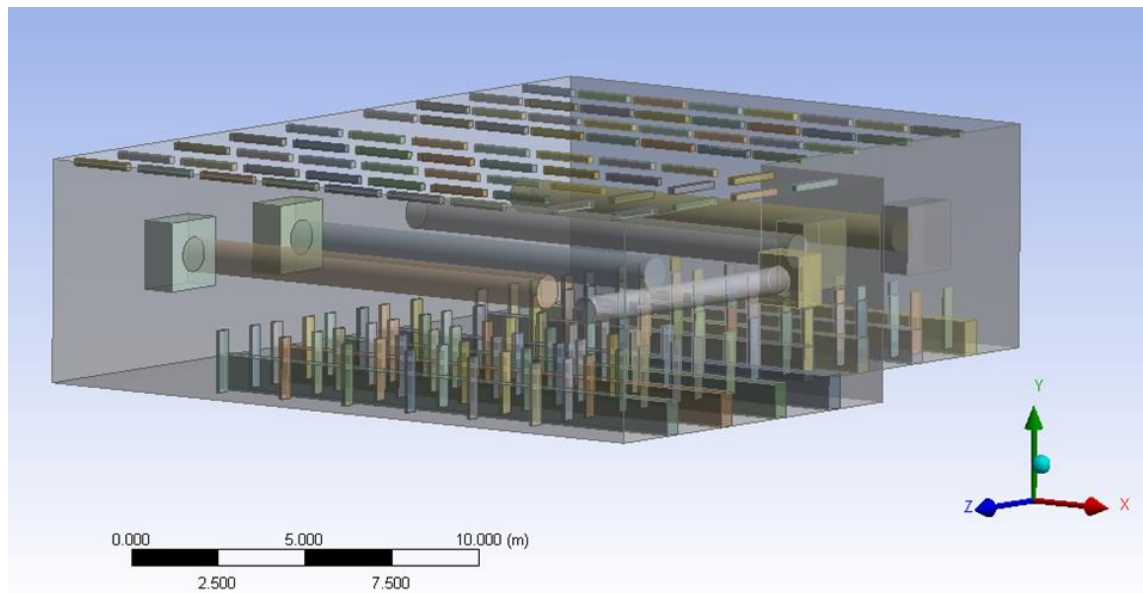
Figure 7-27. Chilled food facility case study 2: Improved air distribution solution modelling

Figure 7-28 shows the temperature profiles from the relocation of the air distribution system via fabric ducts at different cross sections along the space. With a supply temperature from the air socks at 7 ℃ the temperature in the bulk of the space varied between of 9.4 ℃ and 16.9 ℃ considering the same measurement points in Chapter 3.3. As observed in Figure 7-28, the lowest temperatures were obtained at the occupied zone where the temperature difference obtained between the head and knee level was just 0.3 ℃ in average. The average temperature at the occupied zone was 9.9 ℃ while the average temperature at ceiling level was 15.9 ℃. Modelling results also show that the limiting factor to achieving lower temperatures at the occupied zone is the heat released by the occupants. In general, case study 2 improved air distribution solution predicted temperature profiles follows the same pattern with experimental results presented in Chapter 7.2.
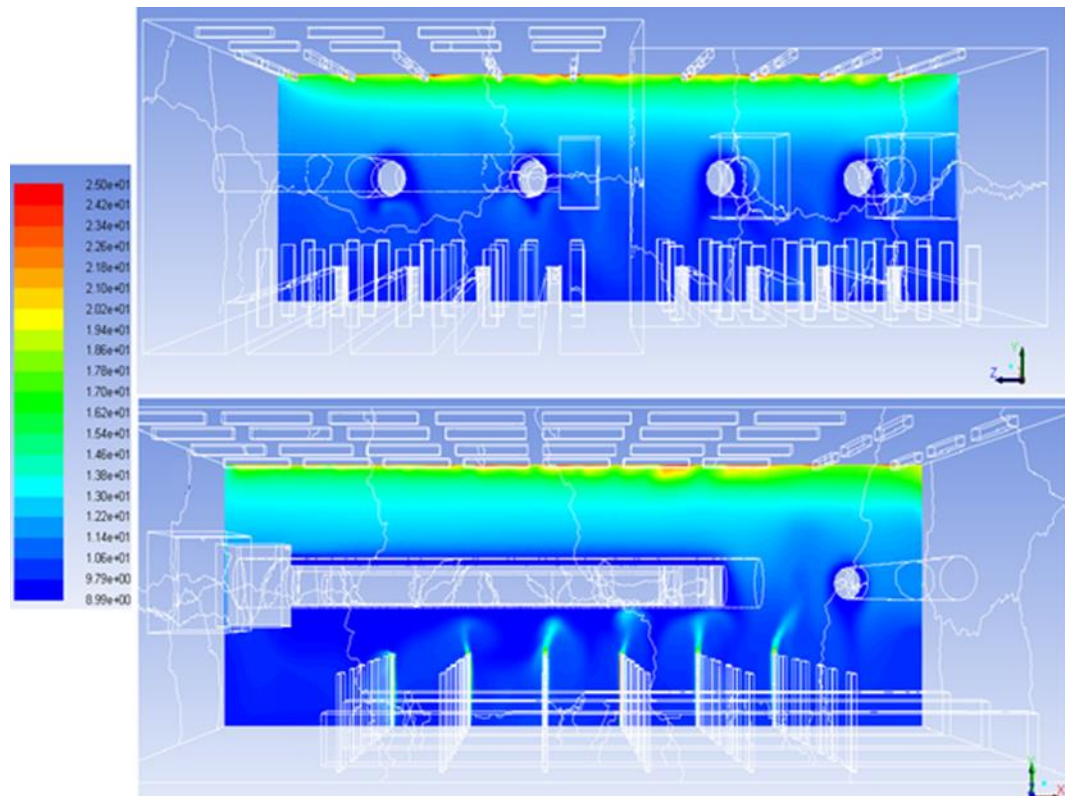
Figure 7-28. Improved air distribution solution: CFD modelling results of air temperature

Meanwhile, Figure 7-29 depicts the modelled velocity distribution at different cross sections along the space. From this figure can be observed that the air velocities were similar to the initial model and to experimental measurements. In this case, velocities varied between 0.02 and 0.35 m.s-1. In Figure 7-29 can also be observed that by locating the air distribution system at a medium level, air displacement is mainly observed at the occupied zone while the air flow at the unoccupied zone is negligible.
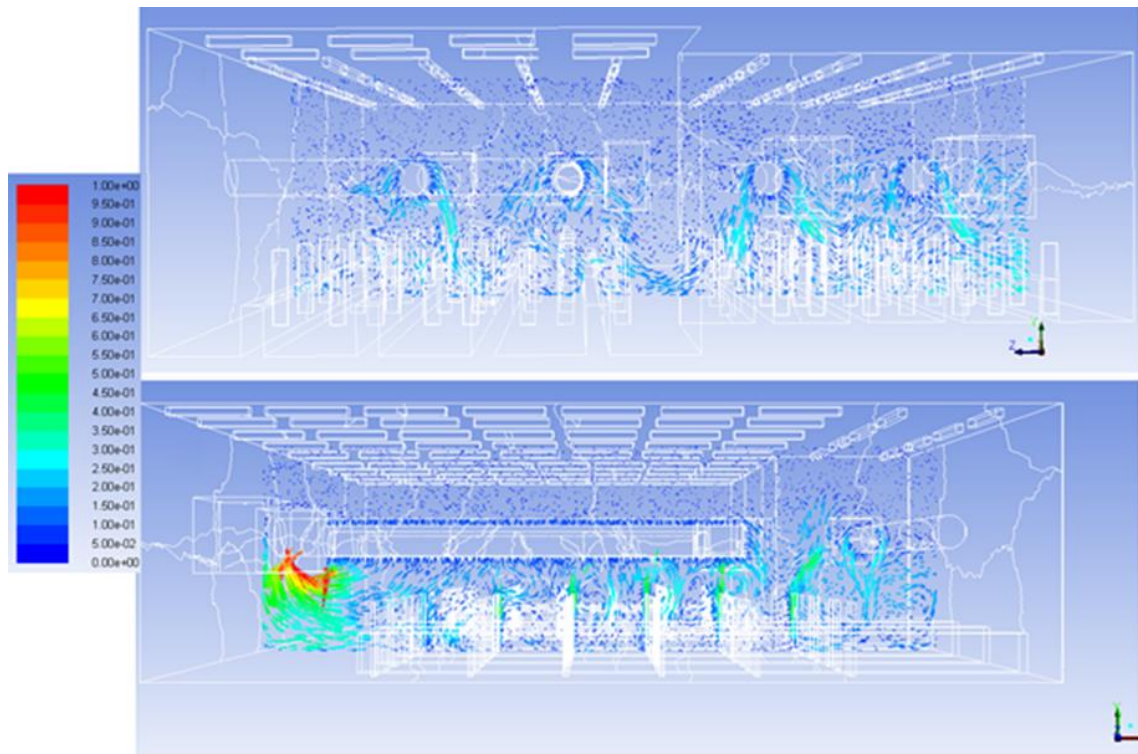
Figure 7-29. Improved air distribution solution: CFD modelling results of air velocity

Moreover, Figure 7-30 presents the comparison between the air temperature profiles obtained from case study 2 and the modified model. The average ceiling level resulting temperatures from the different points of measurement were 11.7 ºC and 15.9 ºC for the initial and modified configurations, respectively. It means that the predicted air temperatures at ceiling level with the modified model are in average 4.1 ºC higher than the initial model. In addition, the average air temperatures at the occupied zone were 10.2 ºC and 9.9 ºC for the initial and modified configurations, respectively. In total, it was obtained an average temperature difference between the unoccupied and occupied zone of 1.5 ºC and 5.9 ºC for the initial and modified cases, respectively.

In general, it is observed that the temperature difference between the knee and the head level from the modified model is as small as that with the initial model. Furthermore, the modified model results show that the temperature difference between the head and ceiling level is significantly increased when lowering the air distribution system which means that the cold air is localized around the production zone at low air flow velocities. This agrees with experimental findings derived in Chapter 7.2.
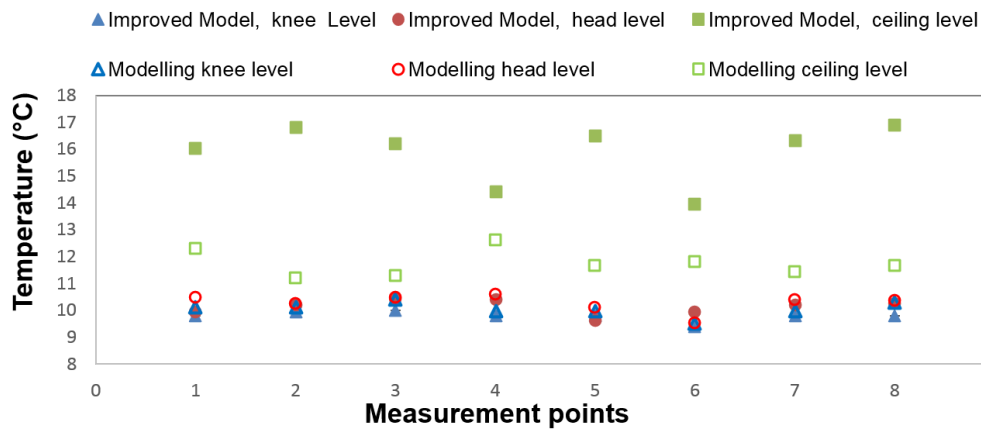
Figure 7-30. Chilled food facility case study 2: Improved air distribution solution temperatures profiles comparison

7.5 Results overview

This subsection presents an overview of the experimental study of different air distribution systems applied in chilled food production facilities. The air distribution systems via fabric duct and semi-circular fabric duct located at medium level were assessed and evaluated at the developed test facility and via CFD modelling for case study 2 chilled food facility. The results overview includes the follow:

- Air temperatures/velocities profiles
- Energy performance

7.5.1 *Results overview: Air temperatures/velocities profiles*

Experimental results confirm that the use of an air distribution system via the fabric ducts located at medium level provides an important temperature gradient along the space if compared with the reference configuration. The fabric ducts located at medium level allow cooling the occupied zone rather than the whole space with a fairly uniform flow pattern around the food processing area. Also, by lowering the fabric duct position at a lower level, air velocities were still kept very low (a maximum of 0.10 m.s^{-1} and 0.25m.s^{1} with the semi-circular fabric duct and the circular fabric duct, respectively). The highest values were observed at knee level and the lowest values at ceiling level. Air velocity values measured at ceiling level were negligible which means that most of the air circulation takes place at the occupied zone. Moreover, CFD modelling results confirms that localising cooling can be succeeded equally to an existing chilled food facility (case

study 2) by moving the fabric ducts to a lower level similarly with the experimental set-up described in Chapter 7.3   Table 7-1 and Table 7-2 show an overview of the average temperature and average velocities cross all the measuring point at different measuring heights for the investigated air distribution methods.

Table 7-1. Results overview: Averaged air temperatures

Average temperatures (ºC)		
knee level	head level	ceiling level
Fabric duct at Ceiling level		
9.9	10.6	12.4
Fabric duct at medium level		
9.8	10.7	15.2
Semi-circular fabric duct at medium level		
9.3	10.5	14.3
Case study 2 chilled food facility: fabric duct at medium level		
9.9	10.5	15.9

Table 7-2. Results overview: Averaged air velocities

Average velocities (m.s^{-1})		
knee level	head level	ceiling level
Fabric duct at Ceiling level		
0.074	0.044	0.13
Fabric duct at medium level		
0.13	0.07	0
Semi-circular fabric duct at medium level		
0.02	0.03	0
Case study 2 chilled food facility: fabric duct at medium level		
0.02	0.035	0

7.5.2 *Results overview: Energy Performance*

The energy consumption of the refrigeration system that provided cooling to the space through each one of the investigated air distribution configurations (non-ducted evaporator coil, circular fabric duct at ceiling level, semi-circular duct and circular fabric duct at medium level) is presented in this sub-section. For each case, experimental data were collected for a week, however, since the condensing unit was in the open, the outdoor temperature was not under control. Therefore, it was selected a 17-hour test period in which case the outdoor air temperature was around 8 °C. For clarity, power data measurements are presented for a period of one hour in Figure 7-31. In addition, Table 7-3 summarises the average operating characteristics of the different systems and the energy consumption results.

Each figure includes the power measurements for each system including the energy consumption of the compressor, condenser fans, evaporator fan and control system. The fan speed of the evaporator was kept at its nominal value in the case of the air distribution via non-ducted evaporator at ceiling level and circular fabric duct at the ceiling and medium level. The power consumption (P) of the refrigeration system with each configuration was then estimated by considering the sum of the instant power consumption of the refrigeration system during the running period (Pon) and the energy consumption of the condenser and evaporator fans and control system during the Stop period (Poff). Data collection was every 10 seconds. (Equation 1 in section 4.3.3.1)

Figure 7-31a shows the power consumption of the refrigeration system with the air distribution via the non-ducted evaporator coil at ceiling level, presented in section 4.4, whereas Figure 7-31b shows the power consumption of the refrigeration system with circular fabric duct air distribution at ceiling level which is presented in section 4.4. Figure 7-31c and Figure 7-31d show the power consumption for air distribution via the circular fabric duct and semi-circular fabric duct at medium level, respectively presented in the current chapter. Comparison of Figure 7-31a and Figure 7-31b depicts that the on-periods for the non-ducted evaporator coil are longer than those for the air distribution with the circular fabric duct. This is primarily due to the high mixing of air in the space and lower temperatures without temperature stratification with the non-ducted coil, as can be seen Figure 4-16, which require the refrigeration system to run for a longer time to maintain on average a lower temperature in the space. These characteristics result in

energy savings of 15% for the circular fabric duct compared to the non-ducted evaporator coil.
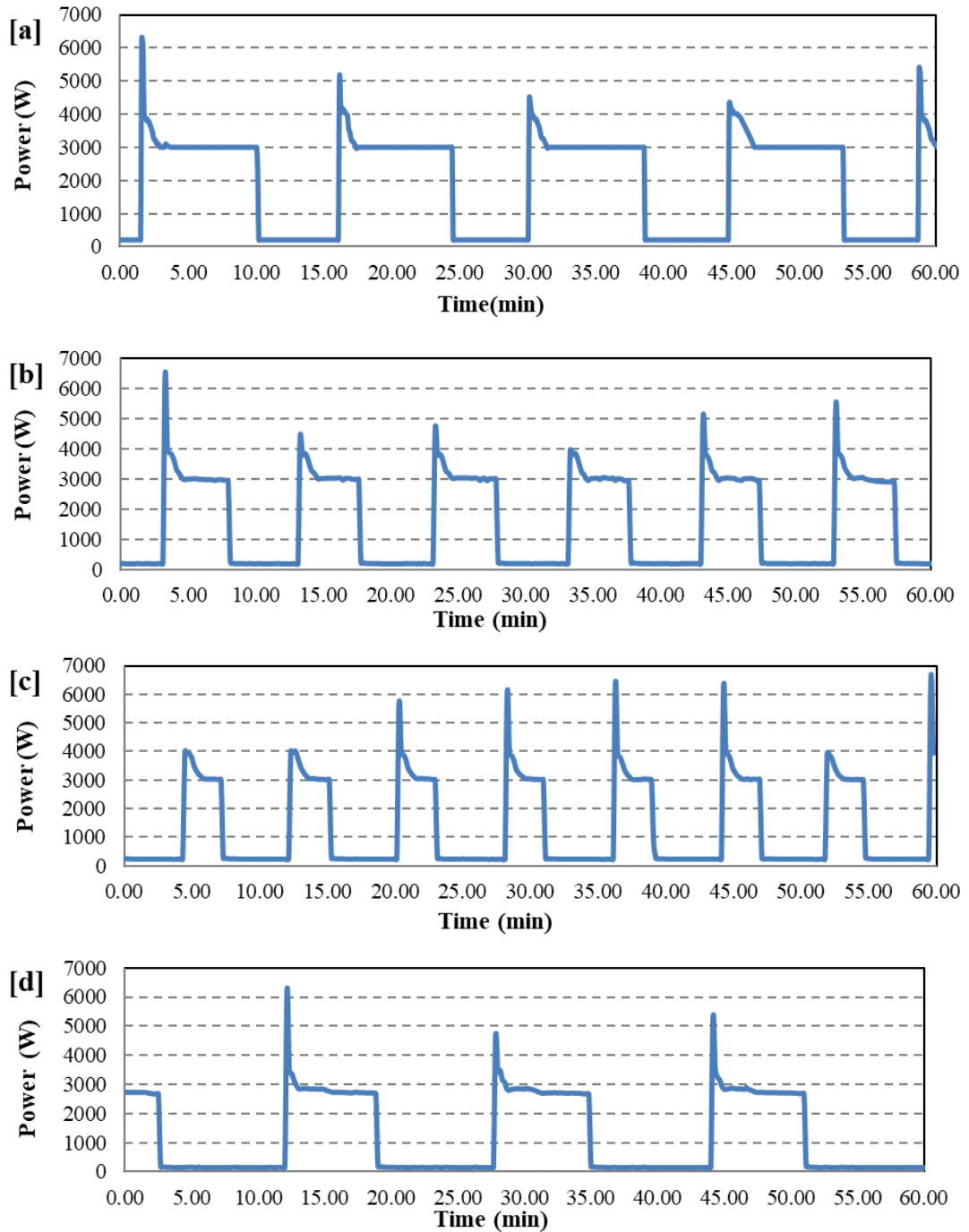
Figure 7-31. Refrigeration system power consumption during a period of 1 hour, [a] non-ducted evaporator at Ceiling level, [b] Circular fabric Duct at Ceiling level, [c] Circular Fabric Duct at Medium level, and [d] Semi-circular Fabric Duct at Medium level.

Comparing the results of the circular fabric duct at ceiling level, Figure 7 31a, and at medium level, Figure 7-31b, it can be observed that with the duct installed at medium level the on periods of the refrigeration system are shorter and the off periods longer. This is because the cooling is concentrated at low level which reduces the area in the space

that is cooled at low temperatures. From Table 7-3, the fabric duct at medium level results in energy demand reduction of 9% compared to ceiling mounted fabric duct and 23% energy demand reduction compared to the non-ducted evaporator coil at ceiling level.

Table 7-3. Operating characteristics and energy consumption of refrigeration system with the different air distribution methods.

Operating characteristics of the refrigeration system for a 17 hours test period						
	Non-ducted evaporator (Rerf.1)	Circular fabric duct at High level (Ref.2)	Circular fabric duct at medium level with hood		Semi-circular fabric duct at medium level with hood	
Total Energy Consumption (kWh)	30.05	25.28	22.88		23.51	
Number of on/off cycles	71.40	102.00	122.40		57.80	
Average 'on' time per cycle (in minutes)	7.60	4.26	3.00		7.80	
Average 'off' time per cycle (in minutes)	6.10	5.70	5.40		9.80	
Average instant power, on period (kW)	3.15	3.22	3.34		2.90	
Average instant power, off period (kW)	0.20	0.20	0.22		0.17	
Operating time per hour (in minutes)	31.92	25.56	21.60		26.52	
Hourly average Energy Consumption(kWh)	1.76	1.49	1.35		1.38	
Energy saving (%)			Ref.1: 23%,	Ref. 2: 9%	Ref. 1: 21%,	Ref.2: 7%

Figure 7-31c and Figure 7-31d show the energy consumption for the round duct and the semi-circular duct installed at medium level. As indicated in Chapter 7.2 the air flow with the semi-circular duct was set at 70% of the air flow with the round duct to ensure similar air supply pressure to the space. Comparing the results in the two cases it can be seen that with the semi-circular duct the on-off cycles of the refrigeration system are reduced significantly compared with the round duct. This is due to the lower flow rate in the space which also results in much lower velocities as can be seen in Figure 7-6 and slightly higher temperature stratification Figure 7-2. From the results in Table 7-3 can be seen that the semi-circular duct results in energy demand reduction of the order of 7%

compared to the circular fabric duct at ceiling level and 21% over the non-ducted evaporator coil at ceiling level.

Based on the power measurements and thermal environment obtained from each air distribution configuration, it has been demonstrated the feasibility of fabric ducts as they can be easily retrofitted onto existing air distribution systems and provide both energy savings and better thermal control conditions in the space through low air velocity supply and thermal stratification.

7.6   Summary of Chapter 7

This chapter presents the experimental analysis of the air distribution system via semi-circular fabric duct and the circular fabric duct at medium level. Experimental and CFD modelling results agreed that by supplying air at medium level in the space through fabric ducts 'socks' it could provide temperature stratification of the order of 7 °C between floor and ceiling level and energy savings in the region of 9% compared to ceiling mounted fabric ducts and 23% over non-ducted cooling coils mounted at ceiling level. Considering this energy reduction percentages, it's possible to achieve important energy savings without replacement of the existing refrigeration equipment or costly major structural changes.

Next chapter deals with the development of a novel integrated EES/CFD model that can be used to the design of an optimum energy efficient air distribution system.

Chapter 8.   Coupled energy and air distribution system modelling

8.1 Introduction

The last stage of this research dealt with the development of a novel dynamic coupled air flow and refrigeration system model to assess the performance of air distribution systems used in chilled food processing areas and their impact on energy consumption.

The coupling model consists of the integration of a CFD air flow/temperature distribution model and a compression refrigeration system model developed in Engineering Equation Solver (EES,2015). After the individual validation of the CFD air distribution model and the EES refrigeration model under steady state conditions, a transient simulation was implemented through the integration of the CFD air distribution model and the EES refrigeration system model. The CFD/EES coupling model can be used to design energy efficient cooled air distribution systems capable of maintaining the required thermal environment in chilled food processing facilities.

8.2 Refrigeration model development using EES

This subsection presents an overview of the developed numerical model in EES in order to simulate the performance of the refrigeration system used in the experimental test-rig. EES is an engineering equation-solving program that can numerically solve non-linear algebraic and differential equations. The advantage of EES is that it includes a library of thermodynamic and transport property data and offers the capability of fast equation solving.

The numerical model developed for the vapour compression refrigeration system is mainly based on correlations for the calculation of the thermodynamic properties of refrigerant R404a (Lemmon, 2003), heat transfer correlations for boiling (Gungor and Winterton, 1986, Kays and London, 1984) and condensation modes (Shah, 2009). Energy balances are carried out considering the state conditions of the refrigerant and air-side flows at the inlet and outlet of each component. The solution procedure follows a step by step process in which energy balances in every component are solved sequentially. The model iterates mainly on the inlet evaporator refrigerant temperature, and also on the degree of sub-cooling at the condenser outlet. Convergence is obtained when the sub-cooling criterion is satisfied. Further information can be found in section 8.2.1.4 and Appendix D.

8.2.1 *Energy Balance equations at each component*

The numerical model developed for the vapour compression refrigeration system is mainly based on correlations for calculating thermodynamic properties, heat transfer coefficients for boiling and condensation modes, and energy balances, which take into account the refrigerant and air-side flows and enthalpies (h) at the inlet and outlet of each component. The actual model was developed using the following assumptions:

- Flow conditions are in a steady state;
- Air flows are distributed uniformly through each section of the coils;
- Refrigerant flow at each cross section of the coils is in thermal equilibrium.
- No condensation or freezing occurs at the evaporator

Figure 8-1 indicates the refrigeration system components and measurements points.
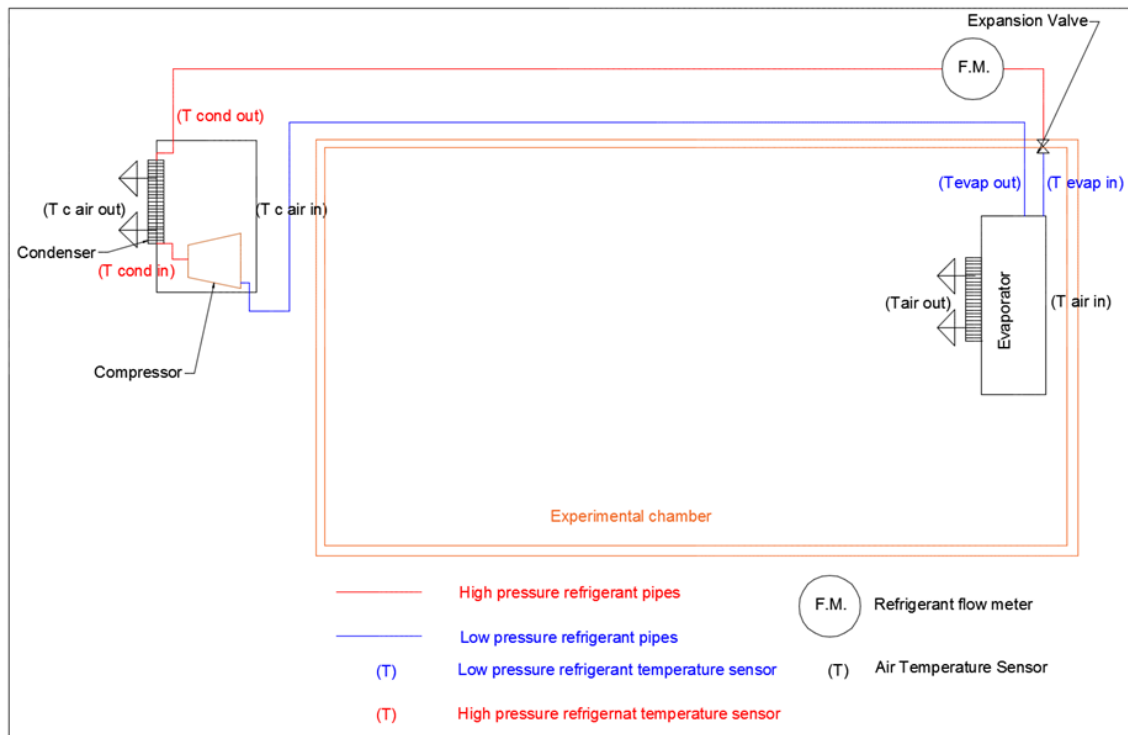
Figure 8-1. Refrigeration system diagram: Components and measurements points

8.2.1.1 Evaporator

The analysis of the evaporator is required in order to determine the inlet evaporation temperature, outlet refrigerant temperature, outlet air-side temperature and refrigerant flow rate. For this, parameters such as evaporator effectiveness and overall heat transfer coefficient need to be determined. Given the thermal load of the evaporator, the inlet

refrigerant evaporation temperature, outlet air-side temperature, and refrigerant flow rate are obtained as follows:

$$Q_{Evap} = C_{min} * \left(T_{Eair_{in}} - T_{Evap_{in}} \right) * \varepsilon_{Evap} \qquad \text{(kW)} \tag{12}$$

$$Q_{Evap} = m_{dot_{air}} * Cp_{air_E} * \left(T_{Eair_{in}} - T_{Eair_{out}} \right) \qquad \text{(kW)} \tag{13}$$

$$Q_{Evap} = m_{dot_{refrig}} * \left(h_{Evap,out} - h_{Evap,in} \right) \qquad \text{(kW)} \tag{14}$$

Where the evaporator effectiveness (ε_{Evap}) for the two-phase region (Eq. 15) and single-phase region (Eq. 16) are obtained as presented by Cengel and Ghajar (2015):

$$\varepsilon_{Evap} = 1 - \exp\left(\frac{-UA_{Evap}}{C_{min}} \right) \tag{15}$$

$$\varepsilon_{Evap} = 1 - \exp\left[NTU^{0.22} \left(\frac{1}{Cr} \right) [\exp(-Cr * NTU^{0.78}) - 1] \right] \tag{16}$$

The overall heat transfer coefficient (U) times the area of the evaporator (A_{Evap}) is determined based in the heat transfer resistances from the bulk refrigerant to the air-side at the inlet and outlet operating conditions (Cengel and Ghajar, 2015).

$$UA_{Evap} = \frac{1}{\left[\left(\frac{1}{\alpha_{int,E} * (Area_{internal})} \right) + (Rw_E) + \left(\frac{1}{\eta_{0,E} * \alpha_{air,E} * Area_{total}} \right) \right]} \qquad \text{(kW/K)} \tag{17}$$

Where η_0 is the air-side overall surface efficiency, $\alpha_{air,C}$ and $\alpha_{int,C}$ are the air-side and refrigerant-side average convective heat transfer coefficients respectively, Rw_E is the conduction resistance, and $A_{internal}$ and A_{total} are the heat transfer areas on the refrigerant and air sides respectively. The refrigerant-side average convective heat transfer coefficient for two phase flow in boiling mode is determined from: (Gungor and Winterton, 1986):

$$\alpha_{Tp} = \left(E * \alpha_{int_{liquid}} \right) + \left(S * \alpha_{int_{pool}} \right) \tag{18}$$

Where,

$$E = 1 + [24000 * (Bo^{1.16})] + 1.37 * \left[\left(\frac{1}{Xtt}\right)^{0.86}\right] \quad \text{"Enhancement factor"} \tag{19}$$

$$S = \frac{1}{1 + 0.00000115 * (E^2) * \left(Re_{liquid}^{1.17}\right)} \quad \text{"Suppression factor"} \tag{20}$$

$$\alpha_{pool} = 55 * (Pr^{0.12}) * (-\log(Pr)^{-0.55}) * (qe^{0.67}) * (M^{-0.5}) \tag{21}$$

$$\alpha_{liquid} = 0.023 * Re_{liquid}^{4/5} * Pr_{refrig[3]}^{0.4} * \frac{k_{refrig[3]}}{D_{tube_{inner}}} \tag{22}$$

And,

$$Bo = \frac{q_e}{Delta_h * G_e} \quad \text{"Boiling number"} \tag{23}$$

$$Xtt = \left[\left(\frac{1-x}{x}\right)^{0.9}\right] * \left[\left(\frac{\rho_v}{\rho_l}\right)^{0.5}\right] * \left[\left(\frac{\mu_l}{\mu_v}\right)^{0.1}\right] \quad \text{"Martinelli Parameter"} \tag{24}$$

The refrigerant-side average convective heat transfer coefficient for the single phase flow is determined as presented by Kays and London (1984):

$$\alpha_{SP} = St * G_{ref} * C_p \tag{25}$$

Where, G_{ref} is the Refrigerant mass flux and St is the Stanton number which is determined from (Kays and London, 1984):

$$St = a * \frac{Re^b}{Pr^{2/3}} \tag{26}$$

The coefficients a and b are based on the flow regime.

For laminar flow (Re<3500), a=1.10647 and b=-0.078992

For transition flow (3500<Re<6000), a=3.5194e-7 and b=1.03804

For Turbulent flow (Re>6000), a=0.2243 and b=-0.385

In the case of the evaporator air-side, the heat transfer coefficient is determined as follows:

$$\alpha_{air_E} = \frac{j_{factor} * Cp_{Air} * G_{Air}}{Pr^{2/3}} \qquad (27)$$

Where the jfactor is determined as presented by McQuiston and Parker (1994).

$$j_{factor} = \left[\frac{[1 - (N_L * 1280 * Re_L^{-1.2})]}{1 - 4 * 1280 * Re_L^{-1.2}} \right] * 0.2675 * JP + 1.325 * 10^{-6} \qquad (28)$$

and the parameter JP is defined as:

$$JP = (Re_D^{-0.4}) * \left(\frac{A_0}{A_t} \right)^{-0.15} \qquad (29)$$

Where A_o is the total air-side heat transfer surface area and A_t is the tube outside surface area. Re_D is the Reynolds number as a function of the outer tube diameter. The air-side overall surface efficiency, is determined from:

$$n_0 = 1 - \left(\frac{Area_{Surface_{fin}}}{Area_{total}} \right) * (1 - n_f) \qquad (30)$$

Where n_f is the efficiency of a single fin.

8.2.1.2   Compressor

The compressor is modelled using the compressor polytropic equations (Cengel and Boles, 2015) in the form of:

$$W_{dot} = \left[m_{dot_{refrig}} * PComp\ in_{pa} * v[Comp\ in] * \left(\frac{n}{n-1} \right) \right] *$$
$$\left[\left[\left(\frac{P[Comp\ out]}{P[Comp\ in]} \right)^{\frac{n-1}{n}} \right] - 1 \right] \qquad (kW) \qquad (31)$$

$$T1_K = \left[\left(\frac{P[Comp\ out]}{P[Comp\ in]} \right)^{\frac{n-1}{n}} \right] * TComp\ in_K \qquad (°C) \qquad (32)$$

Eqs. 32 and 33 allow the calculation of the compressor work and the refrigerant temperature at the outlet of the compressor. The polytropic index 'n' is a crucial parameter which is obtained from Eq. 35 employing the data collected experimentally. Currently, this value is fixed at 1.2. In the case of the electric power supplied to the compressor, this was obtained from setting the efficiency of the compressor to 0.60. This is an average

value obtained experimentally considering the estimated compressor work from the measurements and the isentropic compressor work.

$$\text{Power}_{\text{Comp}} = \frac{\text{m}_{\text{dot}_{\text{refrig}}} * (\text{h}_{\text{Comp,out}} - \text{h}_{\text{Comp,in}})}{\text{eta}_{\text{comp}}} \qquad \text{(kW)} \qquad (33)$$

$$\text{Pcomp\_out} * \text{v}_{\text{Comp}}\text{out}^n = \text{Pcomp\_in} * \text{v\_Comp in}^n \qquad \text{(kW)} \qquad (34)$$

8.2.1.3 Condenser

The analysis of the condenser is required in order to determine the thermal load released to the ambient and refrigerant temperature at the outlet of this component. The thermal load in the condenser is obtained as (Cengel and Ghajar, 2015):

$$Q_{\text{Cond}} = C_{\text{min}} * \left(T_{\text{Cond}_{\text{in}}} - T_{\text{Cair}_{\text{in}}}\right) * \varepsilon_{\text{Cond}} \qquad \text{(kW)} \qquad (35)$$

Where the condenser effectiveness ($\varepsilon_{\text{Cond}}$) for the two-phase region (Eq. 37) and single phase region (Eq. 38) is obtained from:

$$\varepsilon_{\text{Cond}} = 1 - \exp\left(\frac{-\text{UA}_{\text{Cond}}}{C_{\text{min}}}\right) \qquad (36)$$

$$\varepsilon_{\text{Cond}} = 1 - \exp\left[\left(\frac{\text{UA}_{\text{Cond}}}{C_{\text{min}}}\right)^{0.22}\left(\frac{1}{\text{Cr}}\right)\left[\exp\left(-\text{Cr} * \left(\frac{\text{UA}_{\text{Cond}}}{C_{\text{min}}}\right)^{0.78}\right) - 1\right]\right] \qquad (37)$$

The overall heat transfer coefficient (*U*) times the area of the condenser A$_{\text{cond}}$ and is expressed as (Cengel and Ghajar, 2015):

$$\text{UA}_{\text{Cond}} = \frac{1}{\left[\left(\frac{1}{\alpha_{\text{int,C}} * (\text{Area}_{\text{internal}})}\right) + (\text{Rw}_{\text{C}}) + \left(\frac{1}{\eta_{0,\text{C}} * \alpha_{\text{air,C}} * \text{Area}_{\text{total}}}\right)\right]} \qquad \text{(kW/K)} \qquad (38)$$

The refrigerant-side average convective heat transfer coefficient for two phase flow in condensing mode is determined as presented by Shah (2009). For all tube orientations (except upward flow):

In Regime I:

$$\alpha_{\text{Tp}} = \alpha_{\text{L}} \qquad (39)$$

In Regime II:

$$\alpha_{TP} = \alpha_L + \alpha_{Nus} \tag{40}$$

Where,

$$\alpha_L = \alpha_{LT} * \left[\left(\frac{Mu_f}{14 * Mu_g}\right)^n\right] * \left((1 - x)^{0.8} + \frac{3.8 * x^{0.76} * (1 - x)^{0.04}}{Pr^{0.38}}\right) \tag{41}$$

$$\alpha_{Nus} = 1.32 * \left(Re_{LS}^{-1/3}\right) * \left(\frac{\rho_L * (\rho_L - \rho_g) * g * k_f^3}{\mu_f^2}\right)^{\frac{1}{3}} \tag{42}$$

The boundary between Regimes I and II is given by the following relation. Regime I occurs when,

$$Jg \geq 0.98 * (Z + 0.263)^{-0.62} \tag{43}$$

Where J_g is the dimensionless vapour velocity defined as,

$$Jg = \frac{x * G_C}{\left[g * D_{inner} * \rho_g * (\rho_l - \rho_g)\right]^{0.5}} \tag{44}$$

And Z, Shah's correlation parameter,

$$Z = \left[\left(\frac{1}{x}\right) - 1\right]^{0.8} * Pr^{0.4} \tag{45}$$

The refrigerant-side average convective heat transfer coefficient for the single phase flow during the sub-cooling process and the air-side heat transfer coefficient are obtained as presented for the evaporator, (Eq. 26) and (Eq. 28), respectively.

8.2.1.4 Solution procedure of EES model

The solution procedure, shown in Figure 8-2, follows a step by step approach in which energy balances in every component are solved sequentially. The resolution procedure starts from the evaporator, continuing with the immediately next component in the same solution flow direction. The model iterates mainly on the inlet evaporator refrigerant temperature, and also on the degree of sub-cooling at the condenser outlet. Convergence is obtained when the sub-cooling criterion of 5.3°C is satisfied.
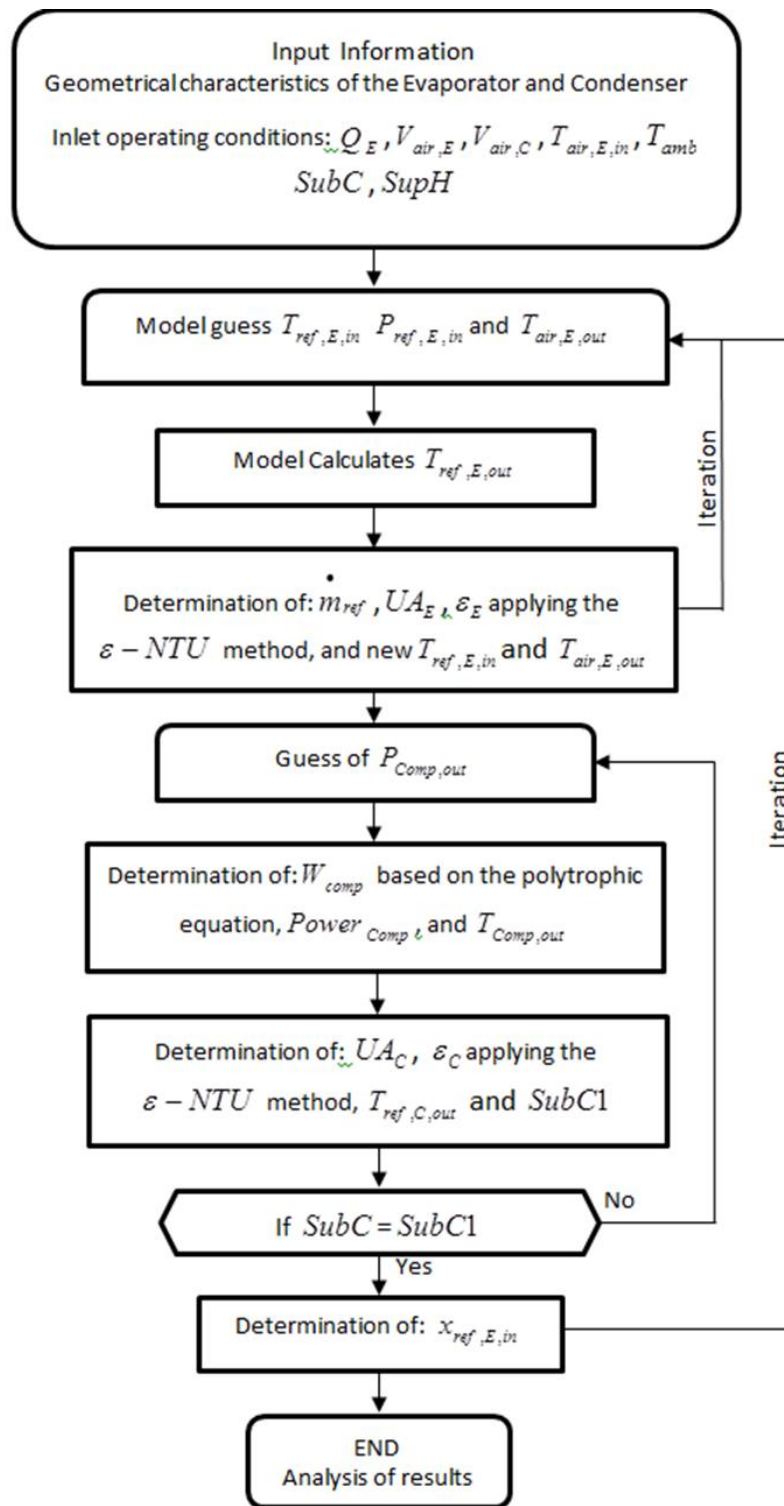
Figure 8-2. Diagram of EES refrigeration model solution procedure.

8.2.2 *Refrigeration system model validation*

Validation was conducted using the data collected from the experimental facility with air distribution using the circular fabric duct at ceiling level presented in Chapter 4.3. The model inputs are the evaporator fan velocity, ambient temperature, inlet air temperature

to the evaporator, evaporator thermal load, Super-heating, sub-cooling and the index n for the compressor. Parameters compared are as follows: Refrigerant flow rate (m_refrig), air-side temperature at the evaporator outlet (Te,air,out), condenser load (Qcond) and electrical instantaneous power input to the compressor (Inst. power). The validation results for the model using R404a as refrigerant are shown in Table 8-1 and Table 8-2

Table 8-1. EES validation comparison.

| **Experimental** | | | | | | | | | | |
runs	Fan Vel %	m_refrig (kg/h)	Te,air,out (ºC)	h1 (kJ/kg)	h2 (kJ/kg)	h3 (kJ/kg)	h4 (kJ/kg)	Qcond (kW)	COP_Elec	Power (kW)
1	70	153.5	-3.3	422.4	239.7	239.7	373.2	7.8	1.9	3
2	80	145.1	-2	423.8	239.4	239.4	369.3	7.4	1.8	3
3	90	145.8	0.7	417.9	242.8	242.8	371.5	7.1	1.8	3
Model										
1	70	146.7	-4.4	411.3	229.4	229.4	369.2	7.4	2.3	2.5
2	80	138	1.1	405.1	233.4	233.4	370	6.6	2	2.7
3	90	128.9	3.2	403.3	228.3	228.3	373.8	6.3	2.2	2.5

Table 8-2. EES validation comparison.

Error	m_refrig	Te,air,out	h1	h2	h3	h4	Qcond	COP_Elect	Power
1	4.40%	1	2.60%	4.30%	4.30%	1.10%	4.90%	18.40%	14.80%
2	4.90%	3.1	4.40%	2.50%	2.50%	0.20%	11.50%	10.70%	8.20%
3	11.60%	2.5	3.50%	6.00%	6.00%	0.60%	11.60%	24.40%	18.10%

The larger errors, are for the compressor power consumption and COP of the refrigeration system which are dependant. The errors may be due to the simplified modelling of the refrigeration system which, in its current form, does not account for condensation of water vapour of the evaporator coil.

8.3   EES-TRNSYS-CFD coupling

The CFD/EES coupling dynamic model was achieved with the usage of TRNSYS platform and FORTRAN programming. As described in section 5.3, CFD modelling was used to simulate the air-distribution in the space, whereas the EES model was developed to simulate the refrigeration system. The dynamic coupling was achieved within the TRNSYS platform. TRNSYS (TRNSYS, 2015) is a flexible graphically based software used to simulate the behaviour of dynamic transient systems. TRNSYS consists of two

parts, the kernel and the in-build components library. The kernel is the part that reads and processed input files and solves dynamic problems. The components in the library include various models of components, (approximately 150), such as those of pumps, multi-zone building, wind turbines, weather data etc. The advantage of TRNSYS is that models are developed in such a way that the user can modify existing components. In addition, users can write their own component model programs, via coding languages such as FORTRAN or C++ which can be compiled and integrated with the Dynamic Link Library (DLL).

In this research the TRNSYS platform was used to control the simulation procedure and exchange data between CFD and EES at the end of each time step. In order to achieve this, a TRNSYS component was programmed in FORTRAN and compiled in TRNSYS (Appendix E). This component was used for the communication between CFD-TRNSYS which occurred via script and results files. TRNSYS generates a script file (*.in) which contains all the journal information needed to set up the CFD model dynamic boundary conditions. When Fluent completes the required transient iterations, a results file is created that contains the data that are imported back to TRNSYS. In addition, TRNSYS-EES coupling was achieved through data exchange via clipboard as indicated in Figure 8-3.
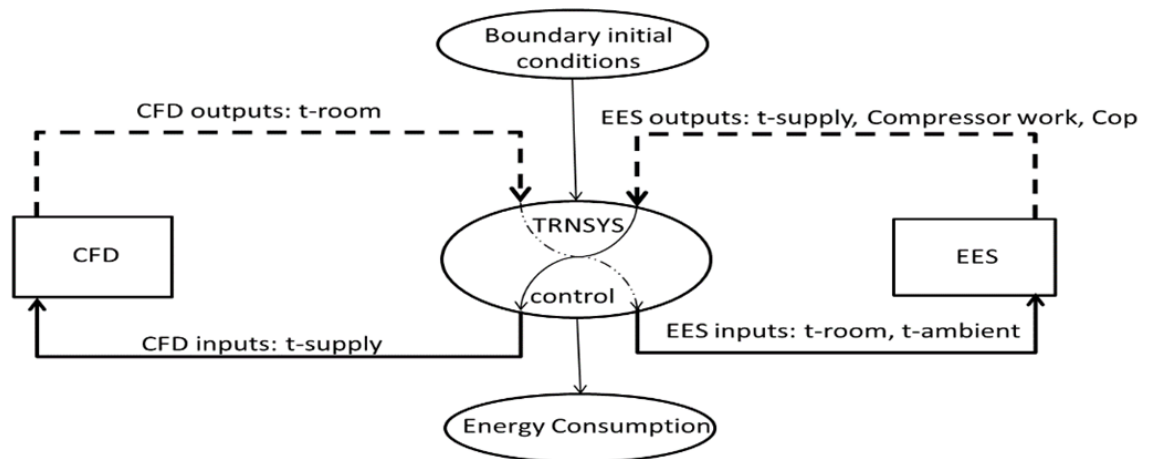
Figure 8-3. CFD-TRNSYS-EES dynamic simulation data exchange

Figure 8-4 shows a flow chart, data exchange and solution procedure. The time step interval and the simulation duration are set in TRNSYS. TRNSYS controls the procedure, calling and exchanging data between CFD and EES for each time step until the simulation duration is completed. Within the simulation duration, TRNSYS calls CFD in order to

model the air distribution in the space. Once the CFD modelling is completed, TRNSYS calls EES in order to model the refrigeration system. If the room temperature is higher than the set point, EES calculates the new supply temperature and the work done (power input) to the refrigeration system.
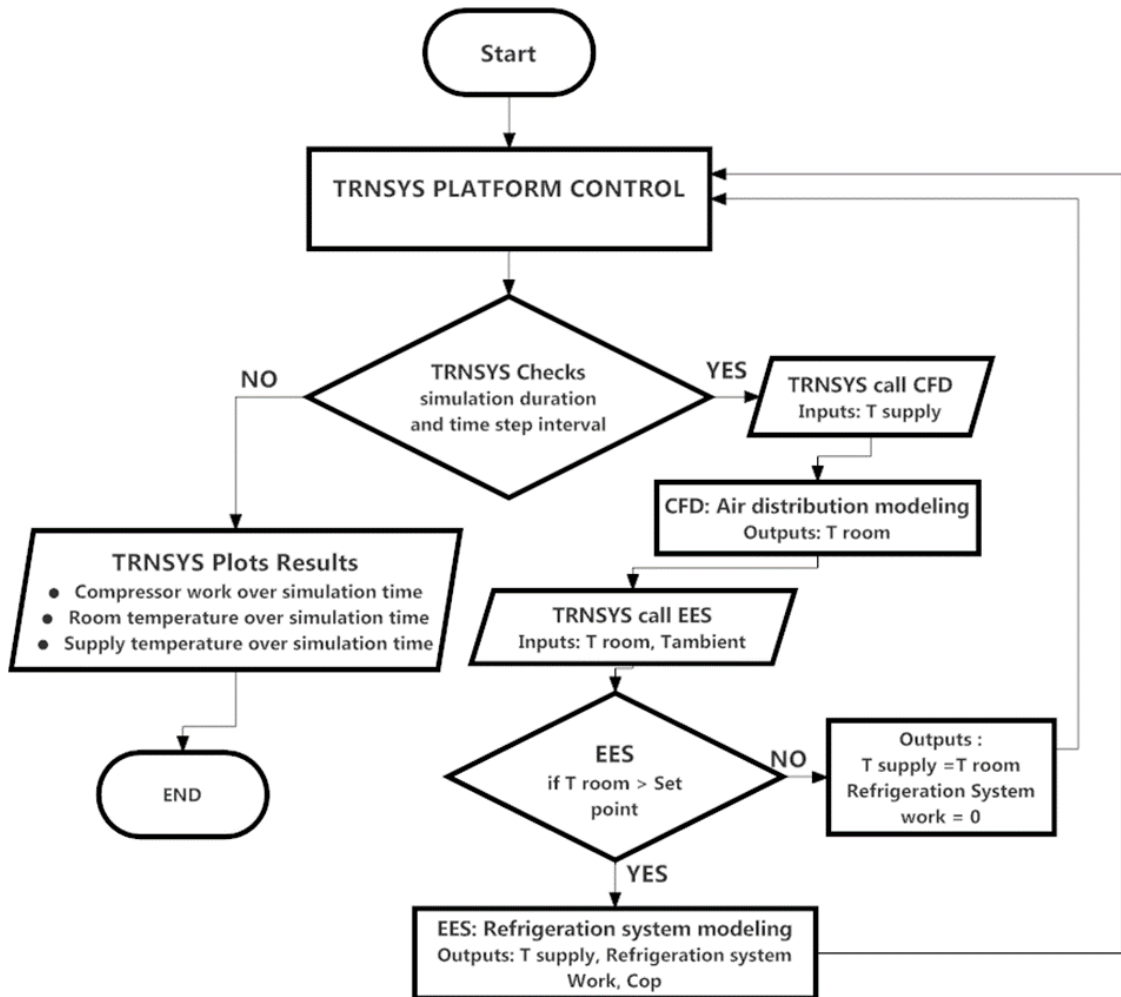
Figure 8-4. Diagram of the integrated EES/CFD model flow chart.

8.3.1 *EES/CFD coupling validation*

The CFD-EES coupling model was validated using the power consumption of the refrigeration system in the test facility and the air temperature measurements carried out. Due to high computational time, the transient simulation was conducted for 1 hour of real time operation. Figure 8-5. shows a comparison between predicted and experimental values for the air supply temperature, room temperature (return temperature) and instant power consumption. Modelling results show that supply and return air temperatures vary over time from 5° C- 12 ° C and 9.5° C- 12 ° C respectively. Experimental values show

the variation of the supply temperature to be from 4° C- 11.5 ° C and that of the return temperature between 9.0° C- 12 ° C.

In addition, the predicted running power consumption estimated at 2.95 kW shows a good agreement compared with the experimentally measured running power consumption. Figure 8-5.b shows that the power at the start of each on-cycle has a peak, rising to 5.0 kW and then dropping to the running power consumption of around 3.0 kW. This happens with every refrigeration system with an on-off controlled compressor. Figure 8-5.a shows that as expected, the developed EES model could not predict the start-up power of the compressor. The inability of predicting the start-up power produces a small error in the overall energy consumption prediction. Nevertheless for comparison of the power consumption and estimation of energy savings between two systems, (both predicted with EES) the results are not significantly affected from the inability to determine that instantaneous start-up power.
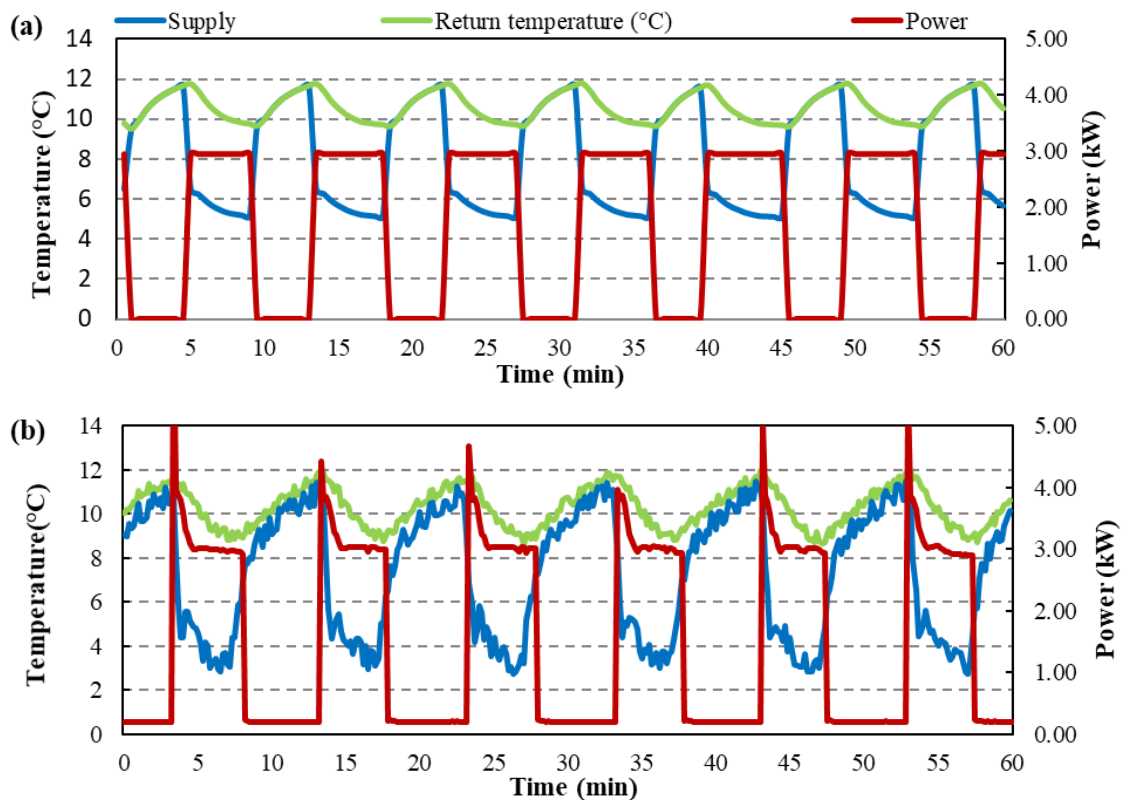
Figure 8-5. Model validation: (a) CFD/EES Modelling results (b) Experimental values.

The energy consumption (P) of the refrigeration system during the running period, was estimated by considering the sum of the instantaneous power consumption of the refrigeration system, including fans and controls, during the running period (P_{on}) and the

energy consumption of the condenser and evaporator fans and control system during the compressor of-cycle (P_{off}). Data collection was every 10 seconds. (Eq. 2).

Comparing the results, the number of operation cycles and their duration are in a good agreement. Table 8-3 shows that the predicted hourly consumption was 1.57 kWh whereas experimental measurements showed an average hourly energy consumption of 1.49 kWh. In general, the integrated CFD/EES modelling showed a good agreement with the measured data.

Table 8-3. CFD/EES coupling model validation.

One hour running time

	Experimental		Modelling		Error
Number of on Cycles	6	cycles	6.3	cycles	
Refrigeration System 'on' Period	4.26	minutes	4.5	minutes	5.60%
Hourly Consumption (kWh)	1.49	kWh	1.57	kWh	5.30%
Instant Power Consumption during operation (kW)	3.22	kW	2.9	kW	9.90%

8.3.2 *EES-CFD Dynamic modelling: Case study 2 chilled food facility*

After the EES-CFD dynamic model validation, the coupling tool was applied to the Case study 2 facility in order to evaluate the energy performance of the improved air distribution system described in Chapter 7.4. Due to extensive computational time, this integrated tool was applied only to a section of the chilled food facility. Figure 8-6 shows the section of the facility that was used for further modelling analysis. The following two CFD models were developed based on Figure 8-6.

- Fabric duct at ceiling level
- Fabric duct at medium level

25
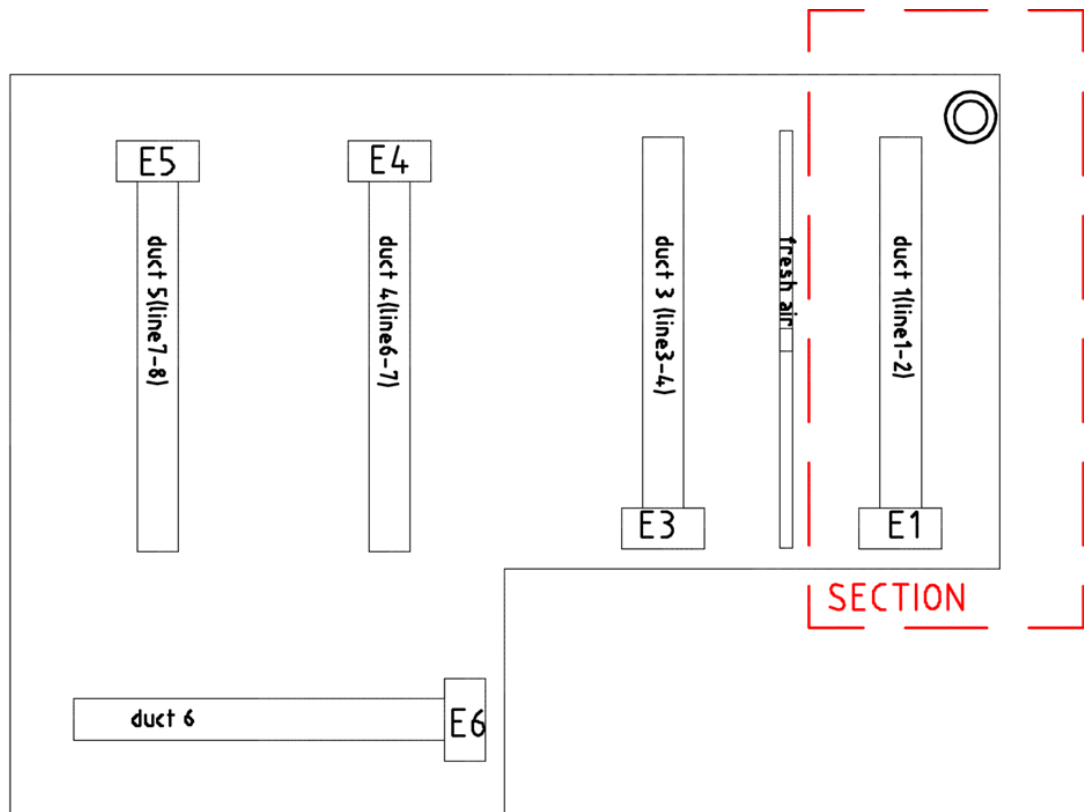
Figure 8-6. Chilled food facility Case study 2, modelled section

Figure 8-7 shows the improved air distribution system construction plans and its easiness to be retrofitted to the existing refrigeration system of the chilled food facility. With minor costs for construction works and without interfering with the production, the improved air distribution system is feasible to be installed in the existing chilled food facility. A single row safe track supported by threated rods can relocate the existing fabric duct to a lower level. In addition, a plenum box needs to be installed at the back to the evaporator coil in a way that the coil return air will occur at the same height that air is supplied.
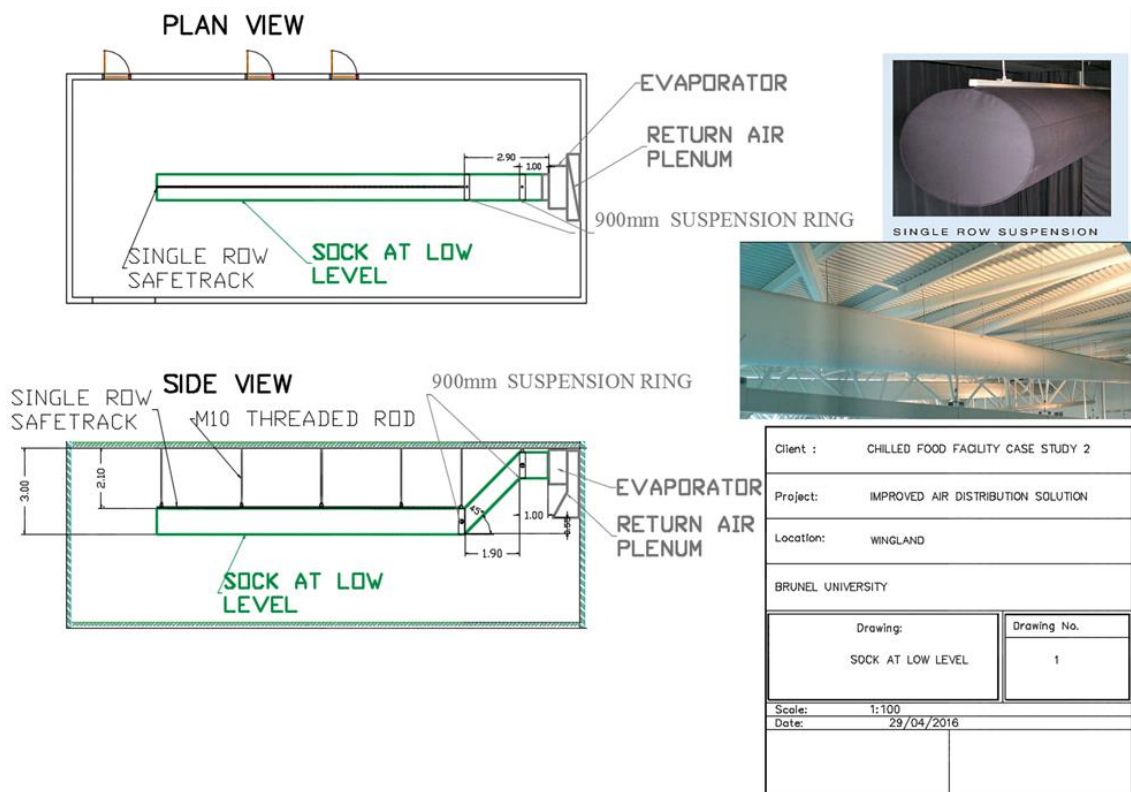
Figure 8-7. Improved air distribution system retrofit to existing refrigeration system

8.3.2.1 Case study 2 chilled food facility: Improved air distribution system CFD modelling

As described in Chapter 7.4 the main difference between the improved air distribution solution and the reference case is that the fabric ducts and the control thermostats were placed at medium level. Furthermore, as mentioned in Chapter 3.3, the height, floor to ceiling of the chilled food facility was 6.5 m and the fabric ducts were installed at 6.0 m height.

The new installation height for the air distribution modelling, shown in Figure 8-9 was 3.5 m. The boundary conditions, meshing and simulation procedure used were the same as those described in Chapter 5.6.
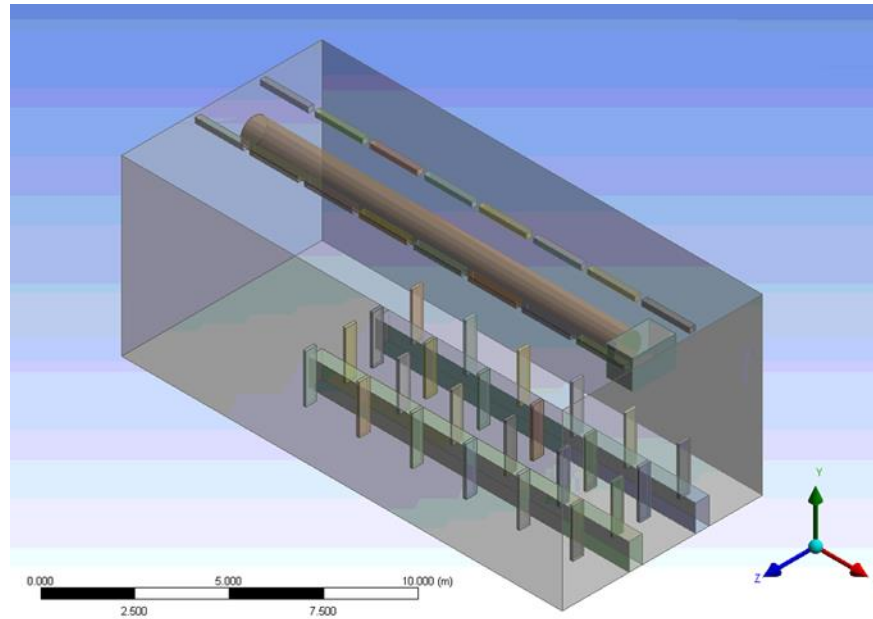
Figure 8-8. Chilled food facility Case study 2 (single duct section). Existing air distribution solution modelling
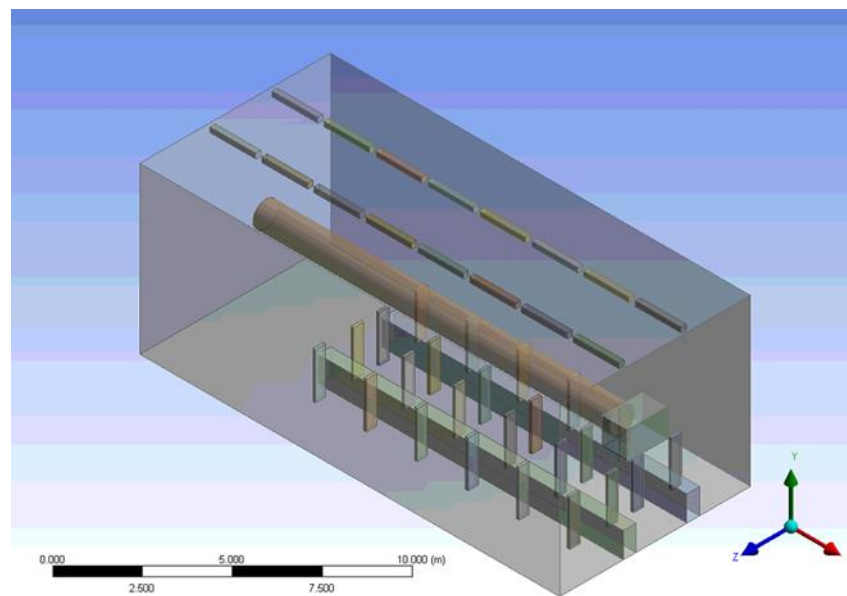
Figure 8-9. Chilled food facility Case study 2 (single duct section): Improved air distribution model representation

Figure 8-10 and 8-11 present modelling results of air temperature distribution at different cross sections along the space for the Case study 2 (section in the factory) with air distribution systems using fabric duct at ceiling level and medium level respectively. Figure 8-10 shows that the fabric duct at ceiling level produces similar average temperatures as those for the whole refrigerated space presented in chapter 5.6.3. With a supply temperature from the fabric ducts at 7 ºC, the temperature in the bulk of the space varied between 8.9 ºC and 12.1 ºC. Similarly, Figure 8-11 depicts the modelled air

temperatures with the fabric duct at medium level. The average temperature at the occupied zone was 9.1 ℃ while the average temperature at ceiling level was 14.2 ℃ which agrees with modelling results on chapter 7.4.
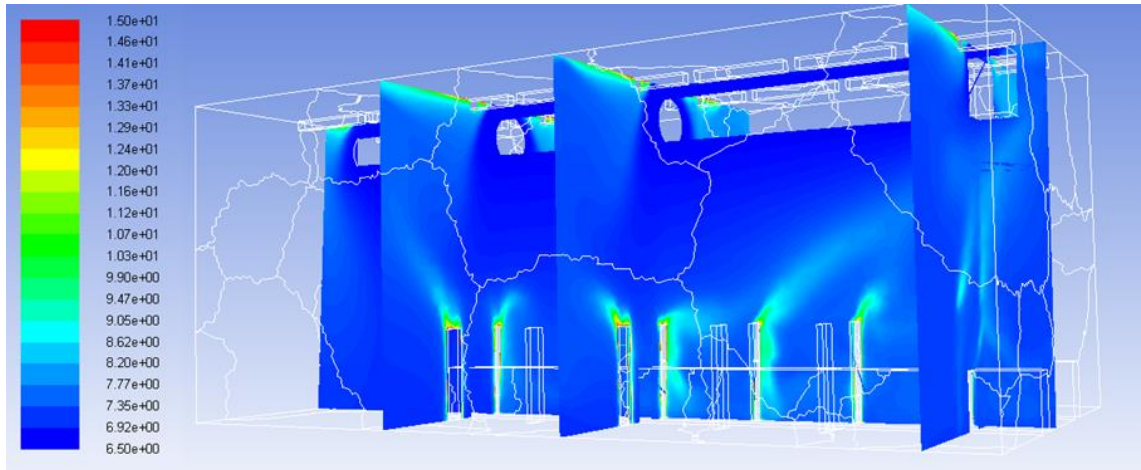
Figure 8-10. Case study 2 section- fabric duct at ceiling level CFD results of air temperatures in the space (°C).
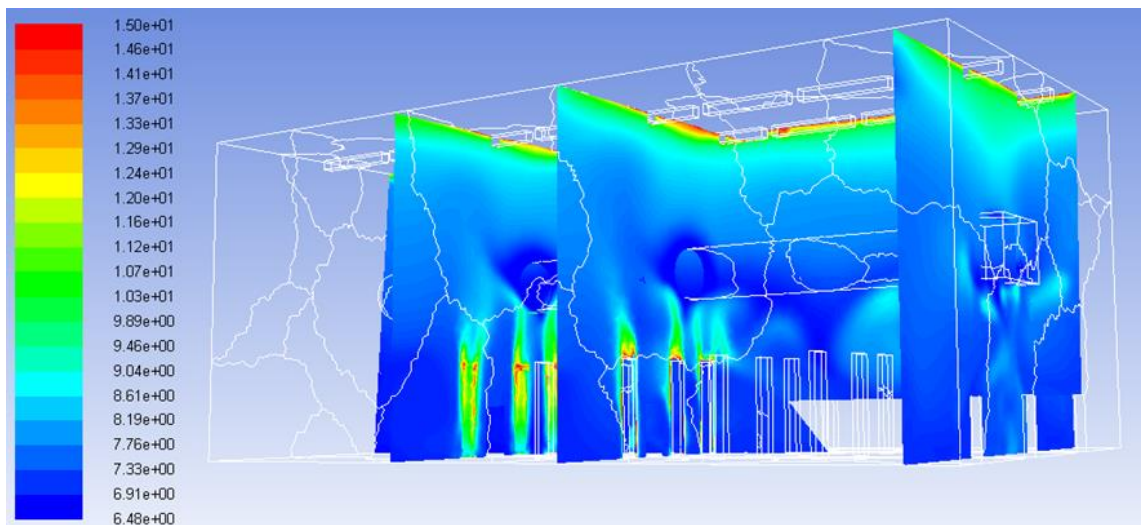
Figure 8-11. Case study 2 section-fabric duct at medium level CFD results of air temperatures in the space (°C).

Figure 8-12 and 8-14, show the modelled velocity distribution at different cross sections along the space. From these figures it can be observed that the air velocities varied between 0.02 and 0.35 m.s-1 which were similar to the initial model. In Figure 8-13 it can also be observed that by locating the air distribution system at a medium level, air circulation mainly takes place at low level in the production area allowing more stagnant air at high level towards the ceiling
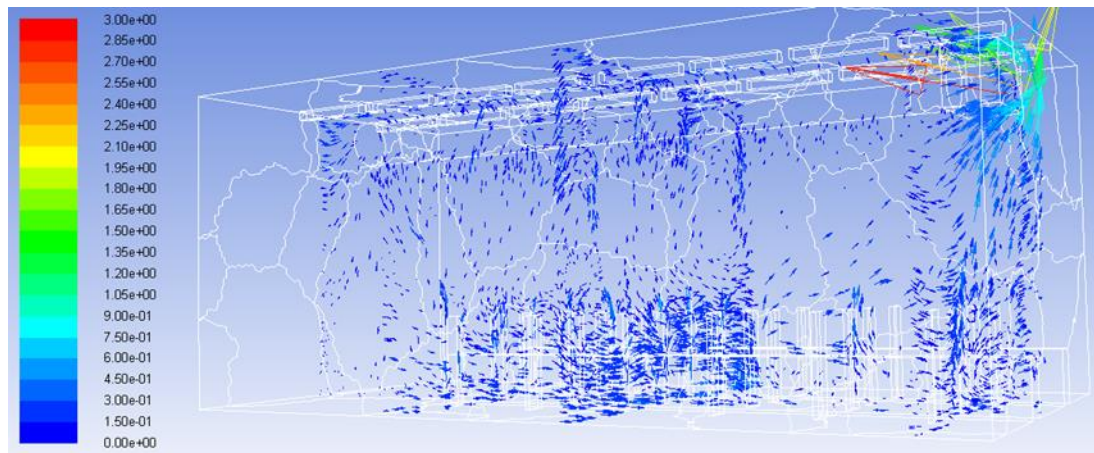
Figure 8-12. Case study 2 section-fabric duct at ceiling level CFD results of air velocity in the space (m/s).
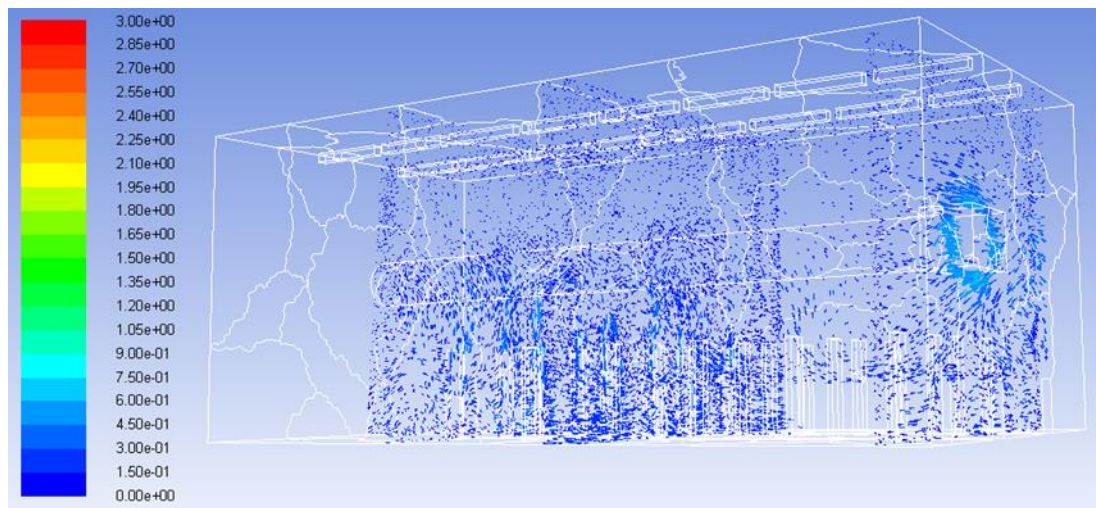
Figure 8-13. Case study 2 section-fabric duct at medium level CFD results of air velocity in the space (m/s).

8.3.2.2 Case study 2 chilled food facility section: EES-CFD coupling to investigate energy consumption

The CFD-EES coupling model was implemented in order to predict the energy efficiency of the improved air distribution system applied in the chilled food facility section. Due to high computational time, the transient simulation was conducted for one hour only. Figure 8-14 and 8-15 show the predicted values for the air supply temperature, room temperature (return temperature) and instantaneous power consumption for the air distribution systems via circular fabric ducts at ceiling and medium level respectively. The refrigeration system control parameter was defined in TRNSYS with a return air temperature at 10.8 ° C for both cases. The supply air temperatures for the steady CFD

model described in Chapter 7.4 was defined as a steady state condition at 7.0 ° C. However in dynamic conditions the supply air temperature fluctuates over time which was predicted in the integrated model. Modelling results show that supply and return air temperatures are fluctuating over time from 4° C- 11 ° C and 9.0° C- 11.5 ° C respectively for the fabric duct at ceiling level and 4.5° C- 11 ° C and 9.0° C- 11.8 ° C for the fabric duct at medium level. The 0.5 ° C lower supply air temperatures, for the case of circular fabric duct at ceiling level, was resulted mainly due to the longer refrigeration system 'on' cycles.
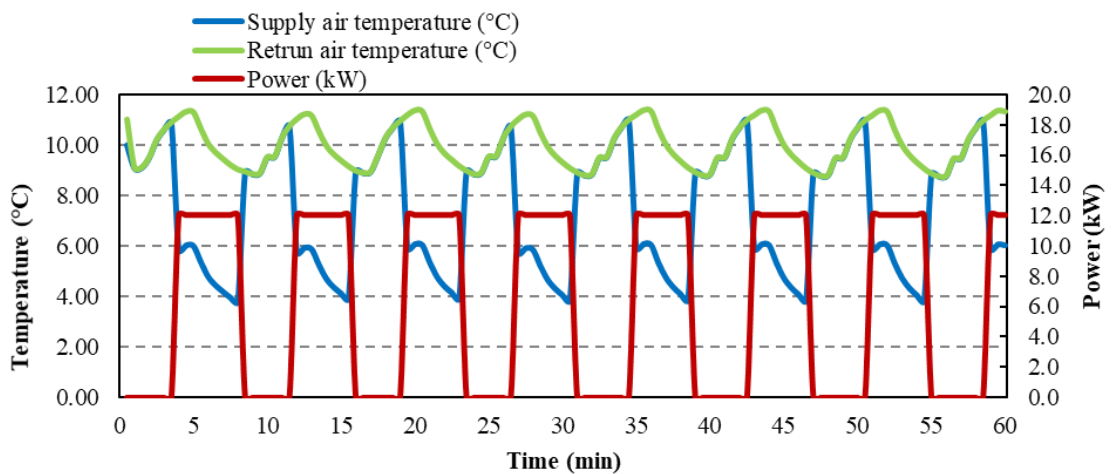
Figure 8-14. CFD-EES dynamic model: Chilled food facility case study 2 section, circular fabric duct at ceiling level
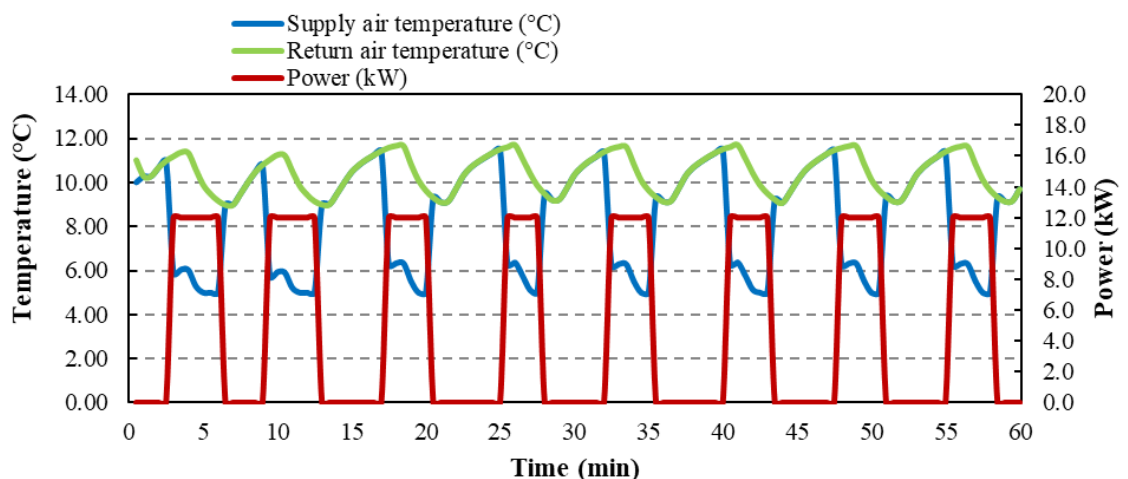
Figure 8-15. CFD-EES dynamic model: Chilled food facility case study 2 section, circular fabric duct at medium level

The power consumption (P) of the refrigeration system was estimated as described in Chapter 8.3.1. Data collection was every 30 seconds and the predicted instantaneous power consumption was around 12.0 kW. Comparison of Figure 8-14 and Figure 8-15 shows that the on-periods for the circular fabric duct at ceiling level are longer than those for the fabric duct at medium level. On the other hand, the off periods are longer for the circular duct installed at medium level. This is primarily due to the mixing of air in the whole volume of the space with a small temperature stratification with the fabric duct at ceiling level, which require the refrigeration system to run for a longer time to maintain the required temperature in the space. With the fabric duct at medium level, cooling is concentrated at low level which reduces the area in the space that is cooled at low temperatures. These characteristics result in a predicted energy saving of 14.3% for the circular fabric duct at medium level compared to the circular fabric duct at ceiling level as shown in Table 8-4.

Table 8-4. CFD-EES dynamic coupling: Air distribution systems energy efficiency prediction

1 Hour CFD-EES dynamic simulation		
	circular duct at ceiling level	circular duct at medium level
Total consumption (kWh)	5.6	4.8
Number of 'on' cycles	7	8
Average 'on' time per cycle (in minutes)	4	3
Average 'off' time per cycle (in minutes)	4	4.5
Average instant power, on period (kW)	12	12
Total operating time (in minutes)	28	24
Energy Saving (%)		14.3

8.4 Summary

A CFD/EES coupling model was developed with the usage of the TRNSYS platform and FORTRAN programming. The integrated CFD/EES model was validated against experimental results showing a good prediction of the measured data. The validated CFD-EES dynamic model was applied for a section of chilled food facility, Case study 2, to evaluate the energy efficiency of the circular fabric duct installed at medium level. Based on the predicted power measurements and thermal environment obtained from each air

distribution configuration, it has demonstrated the feasibility of fabric ducts of being easily retrofitted to existing air distribution systems and provide both energy savings and better thermal control conditions in the space through low air velocity supply and thermal stratification.

The integrated CFD/EES model can be used for further investigation and design of an optimum energy efficient air distribution system that will create an environment capable of maintaining the food product quality and provide a good environment in terms of reduced thermal discomfort. Chapter 9 presents a summary of concluding remarks of this research and recommendations for further studies to extend the research and enable actual evaluation of the benefits of the proposed air distribution system in the factory.

Chapter 9. Conclusions and Recommendation for Future Work

9.1 Introduction

In recent years, chilled food manufacturing in the UK has experienced annual increases of around 10 %. Chilled food manufacturing is energy intensive and to reduce the Greenhouse Gas Emissions of the industry the Chilled Food Association (CFA) has set an ambitious goal to reduce the CO_2 emissions of the industry by 30% by 2020 compared to 1990 levels and 40% by 2023. The chilled food chain relies heavily on refrigeration for the maintenance of low temperatures during processing, transportation and retail of chilled food products. In chilled food processing facilities, refrigeration can account for up to 60 % of the total energy consumption of the facility and hence reduction of the energy required to provide refrigeration is a priority for chilled food manufacturers.

Chilled food manufacturing facilities are constructed with high ceilings where normally are cooled by fan coil units located at ceiling level in a similar way to cold rooms, resulting in high velocities, uncomfortable environments for the workers and high energy consumption. The high energy consumption arises from the fact that the refrigeration systems cool the air in the entire space even though the food manufacturing lines are located at low level in the space. This thesis describes the numerical and experimental procedures employed to improve the cold air-temperature distribution in chilled food processing areas. The objective was to achieve low velocities and uniform temperatures at low level to improve thermal comfort for the workers and at the same time localize cooling at the occupied zone to provide chilled food safety and reduce energy consumption.

Objectives set in the beginning of this research work were achieved as follows:

Objective 1:

A detailed literature review covering the background of this study is presented in Chapter 2. This literature includes the understanding of air distribution in cold rooms and food regulation regarding temperature control. In addition, the literature reviews available tools for predicting air temperatures and velocity profiles in cold rooms and large spaces.

Objective 2:

Chapter 3 focuses on understanding the air flow and the temperature variation in existing chilled food production facilities. Two existing chilled food production facilities (case

study 1 and case study 2) using different air distribution systems were monitored. The monitoring of the facilities was implemented also for the CFD model validation.

Objective 3:

Chapter 4 deals with the experimental set-up and the initial monitoring of the developed test rig. The experimental set-up was designed and built in order to represent an existing chilled food facility and its air distribution system. The initial monitoring results proved that the developed facility can adequately represents the conditions in chilled food factories in terms of air distribution and thermal environment in the space. The effectiveness of the CFD air distribution models for the prediction of the air flow and the thermal environment of chilled food facilities has been explored in chapter 5.

Objective 4:

Employing the CFD validated model to investigate and evaluate different air distribution systems was established in Chapter 6. In addition, chapter 7 presented the experimental evaluation of alternate air distribution solutions. A primary objective was to demonstrate the feasibility of flexible systems that can be easily retrofitted onto existing air distribution systems and provide both energy savings and better thermal control conditions in the space through low air velocity supply and thermal stratification.

Objective 5:

A coupled air flow and refrigeration system model was developed in order to assess the performance of air distribution systems used in chilled food processing areas and its energy consumption impact. The model was tested and validated using experimental data collected from the scaled air distribution test rig built in an environmental chamber showing a good agreement with the measured data. The coupling model consists of integration of a CFD air flow/temperature distribution model and a compression refrigeration system model developed in EES. The CFD/EES coupling model can be used to design energy efficient cooled air distribution systems capable of maintaining the required thermal environment in chilled food processing facilities. This is described in Chapter 8.

9.2 Concluding remarks

The section below summarises concluding remarks arising from the research.

1. According to the literature, very little work has been reported on air distribution in chilled food factories where the objective is to maintain the temperature at low levels for food safety and quality. General points extracted from the literature are:

    a. Temperature control is critical in providing chilled food safety, freshness and quality. Depending on the type of product chilled, food processing takes place in facilities that are normally maintained at temperatures in the range between +4 to +12°C.

    b. Air-temperature control in chilled food facilities is normally provided by convection heat transfer systems. Air distribution patterns can be obtained from experimental results and from numerical models.

    c. CFD is an important tool that is used to predict air distribution in cold rooms. In general, CFD numerical studies applied for different refrigerated spaces showed a good level of agreement with experimental data. The SST k-ω model has been reported as a more accurate model in comparison to k-ε and k- ω models. In addition, the 7 equations Reynolds stress model was reported to increase drastically the computational time.

    d. In general, numerical studies involving stratified air temperatures in air conditioned spaces demonstrated the potential to achieve better environment in terms of thermal comfort and savings in commercial buildings in comparison to systems working on the mixing principle.

    e. In order to improve thermal comfort the following 3 parameters must be considered during the design stage of an air distribution system:

        i. Position of inlets/outlets of the air distribution system in relation to occupants, and sources of heat gains and losses in the space.

        ii. Air flow direction from air distribution inlets/outlets. Air velocities need to be kept at low levels.

        iii. Minimize draughts at occupied level.

2. The conclusions which can be drawn from the investigation into air distribution systems and thermal environment control in two existing chilled food processing facilities are as follows:

a. Enabled the understanding of temperature and air velocity distribution of chilled food manufacturing facilities with alternative air distribution systems. The monitoring of the two case studies provided evidence of the air-temperature distribution issues (such as high velocities, poor temperature distribution and cooling of the whole space).

b. Air distribution via supply/return diffusers in case 1 was effective in maintaining the required temperature condition in the space but provided excessively high air flow velocities. According to the recorded data, velocity in some locations was as high as 0.6 m s^{-1} which together with the low temperatures it can lead to excessive discomfort.

c. The air distribution system via fabric ducts, case study 2, was found to be a more appropriate method to provide adequate and uniform air flows, including relatively low air velocities, in the range 0.05 and 0.35 m s^{-1} in the space. Fabric ducts employ wider air flow areas covering the production lines and distributing low air flow velocities around the occupied zone. It also seems to facilitate some air temperature stratification which may impact in a positive way on the energy consumption of the refrigeration system when compare to systems with supply/return diffusers. CFD modelling showed that air temperature stratification in the food processing facility can be achieved by relocating the circular fabric ducts at a lower level in order to localize the coldness around the production zone.

d. Data gathered enabled the development and validation of CFD models for the simulation of air flows in chilled food manufacturing halls. The SST-k-ω turbulence model was found to predict actual measured data with better accuracy and reasonable computational time compared to the other turbulence models.

3. The experimental and CFD modelling results conducted for the developed experimental test facility indicated the following conclusions:

a. Numerical and experimental results agreed that air distribution through fabric ducts result in lower air velocities and better thermal environments in chilled food manufacturing facilities compared to ceiling mounted non-ducted systems.

b. Experimental results confirm that the use of an air distribution system via the fabric ducts located at medium level provides an important temperature gradient along the space if compared with the non-ducted evaporator coil. Even when mounted at ceiling level fabric ducts develop a temperature stratification in the space with a temperature gradient up to 2.5 ℃ between knee and ceiling level. According to the experimental results with the circular fabric duct at medium level, temperatures values varied from 8.0 ℃ and 16.5 ℃ with average temperature values measured at knee, head and ceiling level of 9.8 ℃, 10.7 ℃ and 15.2 ℃, respectively. In contrary, experimental results with the non-ducted evaporator coil showed fairly uniform air temperatures in the space with average temperature values measured at knee, head and ceiling level were 7.8 ℃, 7.6 ℃ and 7.2 ℃, respectively. Meanwhile, with the fabric duct at medium level, most of the air circulation takes place at the occupied zone. Numerical and experimental results proven that the fabric ducts located at medium level allow cooling the occupied zone rather than the whole space with a fairly uniform flow pattern around the food processing area.

c. Power measurements confirms that when the air entering the cooling coil is drawn from a lower level in the space the system can lead to energy demand reduction and savings of the order of 15%. Furthermore, cooling and supplying at medium level was identified to be the best system with respect to energy consumption and energy demand reduction. The results from medium level supply showed energy savings of the order of 23% over a non-ducted evaporator coil at ceiling level and 9% over a circular fabric duct distribution system mounted at ceiling level. Experimental results agreed that with the circular fabric duct installed at medium level the on periods of the refrigeration system are shorter and the off periods longer compared with the tested air distribution solutions installed at ceiling level.

d. In general, modelling and experimental results demonstrate the feasibility of flexible systems which can be easily retrofitted onto existing air distribution systems and could provide both energy savings and better thermal control conditions in the space through low air velocity supply and thermal stratification. Fabric duct air distribution systems are very flexible

and easily adaptable for the cooling of large high ceiling places. However, an issue with their application in chilled food factories particularly when mounted at low level is the risk of wetting from cleaning the space on a daily basis. To address this issue, alternative materials of construction that can provide similar air distribution properties but which can be easily cleanable need to be identified.

4. The conclusions that can be drawn from the development of the integrated CFD/EES model are the following:

   a. Firstly, an EES simulation model capable of predicting the energy consumption and performance characteristics of refrigeration systems was developed. Validation was conducted with data collected from the experimental facility using the circular fabric duct at ceiling level as an air distribution system. It was shown that the model could predict the power consumption of the refrigeration system with a mean error of 12%.

   b. A novel CFD/EES dynamic coupling model was developed with the usage of the TRNSYS platform and FORTRAN programming. The TRYNSYS platform was used to control the simulation procedure and exchange data between CFD and EES. CFD modeling was used in order to simulate the air-distribution in the space, whereas the EES model was developed to simulate the refrigeration system. The dynamic coupled model is capable of assessing the performance of air distribution systems and their impact on energy consumption. After the design principles and modelling tools were established and proven, the integrated CFD/EES model was validated against experimental results showing a good prediction of the measured data.

   c. The integrated model was applied for a section of the case study 2 chilled food facility. Modelling results demonstrated that by lowering the circular fabric duct to a lower level (3.5m new installation height) could produce 14.3% energy savings compared to the circular fabric duct installed at ceiling level (6.0 m height). The integrated CFD/EES model can be used for further investigation and to design optimum energy efficient air distribution systems for chilled food facilities.

9.3   Recommendations for Future work

A primary objective of the project was to demonstrate the feasibility of flexible systems that can be easily retrofitted into existing air distribution systems and provide both energy savings and better thermal control conditions in the space through low air velocity supply and thermal stratification. Future work needs to be done to arrive at an ideal air distribution system in terms of material selection, cost reduction and ease of retrofit for roll-out to food manufacturing facilities.

Alternative materials of construction with the fabric ducts, that can provide similar air distribution properties but which can be easily cleanable need to be identified. In addition, the design and development of an air distribution prototype that can be install in the monitored chilled food facilities can be implemented in future work which will allow to test and evaluate its performance. The prototype requirements drawn from this study are:

a) The alternate material should have a low risk of dirt and water accumulation and growth of bacteria and should be easy to clean.

b) The prototype should be designed in a way to avoid condensation.

c) The ducting should be easy to retrofit with low cost and lead to energy savings greater than 10%.

d) Provide a reasonable thermal environment for workers in the space. Minimise draughts at occupied level.

e) Localise cooling at the occupied space by supplying the air at a lower level.

In general the findings of this study provide useful guidelines for the design of a food-safe energy efficient air distribution system for chilled food manufacturing facilities. In terms of thermal comfort improvement, this research proposed energy efficient air distribution system designs that can minimize draughts and air velocities. Nevertheless, more work can be done for a more detailed investigation into thermal comfort. The thermal conditions that are used in chilled food factories in order to ensure food quality and safety, are different from those required for the workers' comfort. The prolonged exposure to cold environments increases health and safety risks for the occupant.

The integrated CFD/EES model is a powerful tool that can be used to design an optimum energy efficient air distribution system without compromising food quality. This powerful tool can be applied to evaluate different air distribution scenarios and their

impact on the thermal environment and the energy efficiency. However, due to extensive computational time, this integrated tool was applied only for the scaled experimental test rig and a section of the case study 2 chilled food facility for only one hour of simulation period. In the near future with more powerful computers this integrated approach could be applied for a full scaled chilled food manufacturing facility and for longer simulation periods. This will provide a better prediction of the energy savings that could arise for system design optimization and control. In addition, due its complexity and the need for powerful computers, application is currently rather limited to academic research. In order to promote its application to industry, a more practical tool that requires less computational time should be developed.

References

Ambaw, A., Delele, M.A., Defraeye, T., Ho, Q.T., Opara, L.U., Nicolaï, B.M. & Verboven, P. 2013, "The use of CFD to characterize and design post-harvest storage facilities: Past, present and future", Computers and Electronics in Agriculture, vol. 93, no. 0, pp. 184-194.

ANSYS FLUENT 2011., "Theory Guide" in ANSYS, ed. ANSYS, Release 14.0 edn, ANSYS, .

ASHRAE 2013, "2013 Ashrae Handbook Fundamentals", Handbook Editor ASHRAE 1791 Tullie Circle Atlanta, GA 30329 USA, .

ASHRAE 2010, "Thermal Properties of Foods " in Handbook-Refrigeration, pp. 19.1.

ASHRAE Standard 55 2010, Thermal enviroment conditions for human occupancy, America Society of Heating Refrigeration and Air Conditioning Engineers.

Becker, B.R. & Fricke, B.A. 2004, "Heat transfer coefficients for forced-air cooling and freezing of selected foods", International Journal of Refrigeration, vol. 27, no. 5, pp. 540-551.

British Standard (ed) 2005, Ergonomics of the thermal environment —Analytical determination and interpretation of thermal comfort using calculation of the PMV and PPD indices and local thermal comfort criteria, BS EN ISO 7730:2005 edn.

Bryan Hackett and Sandra Chow 2005, " Energy Efficiency Opportunities in Fresh Fruit and Vegetable Processing/Cold Storage Facilities ", ACEEE Summer Study on Energy Efficiency in Industry, .

Cernela, J., Heyd, B., Keller, S., Bailleul, J.L., Maillard, M.N., Bonazzi, C. & Broyart, B. 2015, "Experimental study of heat and mass transfer phenomena during the contact heating of solid food models", Journal of Food Engineering, vol. 146, no. 0, pp. 99-106.

Cengel .Y and Ghajar A. (ed) 2015, Heat and Mass Transfer: Fundamentals and Applications, 5th Edition edn.

Cengel Y., B.A. 2015, THERMODYNAMICS AN ENGINEERING APPROACH , 8th EDITION SOLUTION MANUAL edn, McGraw-Hill Education, University of Nevada.

CFA 2012, , Climate Change Agreement - Chilled Food Sector Progress and Barriers. Available:
http://www.chilledfood.org/Media/campaigns/Climate+Change+Agreement+-+Chilled+Food+Sector+Progress+and+Barriers.htm [2013, 28/11].

Chanteloup, V. & Mirade, P. 2009, "Computational fluid dynamics (CFD) modelling of local mean age of air distribution in forced-ventilation food plants", Journal of Food Engineering, vol. 90, no. 1, pp. 90-103.

Cheng, Y., Niu, J., Liu, X. & Gao, N. 2013, "Experimental and numerical investigations on stratified air distribution systems with special configuration: Thermal comfort and energy saving", Energy and Buildings, vol. 64, pp. 154-161.

Chourasia, M.K. & Goswami, T.K. 2007, "Simulation of Effect of Stack Dimensions and Stacking Arrangement on Cool-down Characteristics of Potato in a Cold Store by Computational Fluid Dynamics", Biosystems Engineering, vol. 96, no. 4, pp. 503-515.

Chourasia, M.K. & Goswami, T.K. 2007, "Steady state CFD modeling of airflow, heat transfer and moisture loss in a commercial potato cold store", International Journal of Refrigeration, vol. 30, no. 4, pp. 672-689.

Chourasia, M.K. & Goswami, T.K. 2007, "Three dimensional modeling on airflow, heat and mass transfer in partially impermeable enclosure containing agricultural produce during natural convective cooling", Energy Conversion and Management, vol. 48, no. 7, pp. 2136-2149.

CIBSE 2015, "Guide A" in Guide A, Environmental design, ed. Chartered Institution of Building Services Engineers, Eighth edition edn, pp. Appendix 3.A4.

Croitoru, C. 2011, "Airflow And Heat Transfer Modeling For A Human Body By Computational Fluid Dynamics", Mathematical Modeling in Civil Engineering, , no. 1/2, pp. 77.

Darby S. & White R. 2005, "Thermal Comfort", Environmental Change Institute University of Oxford, .

Darmawan A 1999, "Adaptive Thermal Comfort A Multiclultural Issue", Annex 35: Hybrid Ventilation in New and Retrofitted Office Buildings, .

David Butler 2003, "Air Conditioning using displacement ventilation to maximize free cooling", BRE's Enviromental Engineering Center, [Online], , pp. 19/11/2013.

Defra 2012;, "Food and Rural Affairs" in Food Statistics Pocketbook , ed. Department of Environment, pp. 86.

Delele, M.A., Ngcobo, M.E.K., Getahun, S.T., Chen, L., Mellmann, J. & Opara, U.L. 2013, "Studying airflow and heat transfer characteristics of a horticultural produce packaging system using a 3-D CFD model. Part I: Model development and validation", Postharvest Biology and Technology, vol. 86, no. 0, pp. 536-545.

Delele, M.A., Schenk, A., Tijskens, E., Ramon, H., Nicolaï, B.M. & Verboven, P. 2009, "Optimization of the humidification of cold stores by pressurized water atomizers based on a multiscale CFD model", Journal of Food Engineering, vol. 91, no. 2, pp. 228-239.

Delgado, A.E. & Sun, D. 2001, "Heat and mass transfer models for predicting freezing processes – a review", Journal of Food Engineering, vol. 47, no. 3, pp. 157-174.

Duret, S., Hoang, H.-., Flick, D. & Laguerre, O. 2014, "Experimental characterization of airflow, heat and mass transfer in a cold room filled with food products", International Journal of Refrigeration, vol. 46, no. 0, pp. 17-25.

Fathollahzadeh, M.H., Heidarinejad, G. & Pasdarshahri, H. 2015, "Prediction of thermal comfort, IAQ, and energy consumption in a dense occupancy environment with the under floor air distribution system", Building and Environment, vol. 90, pp. 96-104.

F-Chart Software 2015, EES, V10.097-3D edn, Box 44042 Madison, WI 53744.

Feng, Y., Downey, G., Sun, D., Walsh, D. & Xu, J. 2015, "Towards improvement in classification of Escherichia coli, Listeria innocua and their strains in isolated systems based on chemometric analysis of visible and near-infrared spectroscopic data", Journal of Food Engineering, vol. 149, no. 0, pp. 87-96.

Ficarella, A., Perago, A., Starace, G. & Laforgia, D. 2003, "Thermo-fluid-dynamic investigation of a dryer, using numerical and experimental approach", Journal of Food Engineering, vol. 59, no. 4, pp. 413-420.

FLUKE , Fluke 435 Series II Power Quality and Energy Analyzer. Available: http://en-us.fluke.com/products/power-quality-analyzers/fluke-435-ii-power-quality.html [2016, MAY].

Food Standards Agency 2007, "Guidance on Temperature Control Legislation in the United Kingdom: EC Regulation 852/2004 ", The Food Hygiene Regulations 2006, .

Foster, A.M., Barrett, R., James, S.J. & Swain, M.J. 2002, "Measurement and prediction of air movement through doorways in refrigerated rooms", International Journal of Refrigeration, vol. 25, no. 8, pp. 1102-1109.

Gonçalves, J.C., Costa, J.J., Figueiredo, A.R. & Lopes, A.M.G. 2012, "CFD modelling of aerodynamic sealing by vertical and horizontal air curtains", Energy and Buildings, vol. 52, no. 0, pp. 153-160.

Gungor K.E. and Winterton R. H. S. 1986, "A general correlation for flow boiling in tubes and annuli", Int. Journal of Heat And Mass Transfer, vol. 29, no. (3), pp. 351.

H Skistad, 2003, "Displacement Ventilation and Air Curtain Zoning", Efficient Ventilation, [Online], , pp. 19/11/2013.

Halton 2013, , Displacement ventilation system. Available: http://www.halton.com/halton/cms.nsf/www/newspublicationsindoors [2013, 15,11].

Ho, S.H., Rosario, L. & Rahman, M.M. 2010, "Numerical simulation of temperature and velocity in a refrigerated warehouse", International Journal of Refrigeration, vol. 33, no. 5, pp. 1015-1025.

Hoang, M.L., Verboven, P., De Baerdemaeker, J. & Nicolaï, B.M. 2000, "Analysis of the air flow in a cold store by means of computational fluid dynamics", International Journal of Refrigeration, vol. 23, no. 2, pp. 127-140.

HSE 2007, Workplace health, safety and welfare: A short quide for managers, rev2 edn, Health and Safety Executive.

HSE (ed) 1999, Thermal comfort in the workplace: Guidance for employers, ISBN 0 7176 2468 4 edn, Health & Safety Executive.

International Organization for Standardization 20014, "Building components and building elements -- Thermal resistance and thermal transmittance -- Calculation method", ISO 6946:2017, vol. ICS : 91.060.01 Elements of buildings in general 91.120.10 Thermal insulation of buildings.

J L M Hensen and M J H Hamelinck 1995, "Energy Simulation of Displacement Ventilation in Offices", Building Services Engineering and Technology, vol. 16(2), no. 77-81, pp. 1.

J L M Hensen, M J H Hamelinck and M G L C Loomans 1996, "Modelling Approaches for Displacement Ventilation", Proceeding of the 5th International Conference Roomvent, , no. Yohohama University of Tokyo, pp. 1-8.

Jose de Castro, S., Mederos, B. J. T., & Rossi, L. A. 2014, "Simulation of air flow in cold chambers using the openfoam® computational fluid dynamics (CFD) software", African Journal of Agricultural Research, vol. 9, no. 1, pp. 1-7.

Jurelionis, A., Gagytė, L., Prasauskas, T., Čiužas, D., Krugly, E., Šeduikytė, L. & Martuzevičius, D. 2015, "The impact of the air distribution method in ventilated rooms on the aerosol particle dispersion and removal: The experimental approach", Energy and Buildings, vol. 86, pp. 305-313.

Kays W. M. and London A. L. 1984, Compact Heat Exchangers, 3rd Edition edn, , New York.

KE FIBERTEC , KE-Low Impulse System. Available: https://www.ke-fibertec.com/en/products/range-of-products/ke-low-impulse-system/ [2013, 6/7].

KE-fabrictec , KE-fabrictec design guide . Available: http://www.ke-fibertec.com/en/products/design/ [2014, June].

ke-fibertec , KE - Low Impulse textile duct fabric. Available: http://www.ke-fibertec.com/uk [2016, MAY].

Kondjoyan, A. 2006, "A review on surface heat and mass transfer coefficients during air chilling and storage of food products", International Journal of Refrigeration, vol. 29, no. 6, pp. 863-875.

K. Zhang, X. Zhang, S. Li, Simplified model for desired airflow rate in underfloor air distribution (UFAD) systems, Applied Thermal Engineering 93 (2016) 244–250.

KROHNE , Krohne Optimass 7300 C . Available: http://krohne.com/en/products/flow-measurement/mass-flowmeters/optimass-7000/optimass-7000-tantalum-application/ [2016, MAY].

Laguerre, O., Duret, S., Hoang, H.M., Guillier, L. & Flick, D. 2015, "Simplified heat transfer modeling in a cold room filled with food products", Journal of Food Engineering, vol. 149, no. 0, pp. 78-86.

Laguerre, O., Hoang, H.M. & Flick, D. 2013, "Experimental investigation and modelling in the food cold chain: Thermal and quality evolution", Trends in Food Science & Technology, vol. 29, no. 2, pp. 87-97.

Lau J and Chen Q 2006, "energy analysis for workshops with floor-supply displacement ventialtion under U.S. climates", Energy and Buildings, vol. 38(10), no. 1212-129.

Lemmon E. 2003, "Pseudo-pure fluid equations of state for the refrigerant Blends R410A, R404A, R507A, and R407C", International Journal of Thermophysics, vol. 24, no. (4).

Lin, Y.J.P. & Tsai, T.Y. 2014, "An experimental study on a full-scale indoor thermal environment using an Under-Floor Air Distribution system", Energy and Buildings, vol. 80, pp. 321-330.

Malcolm Cook , Tong Yang , and Paul Cropper 2011, "Thermal comfort in naturally ventilated classrooms: application of coupled simulation models", Proceedings of Building Simulation 2011: 12th Conference of International Building Performance Simulation Association, Sydney, 14-16 November., vol. 12, pp. 2257-2262.

McQuiston Faye C., Jerald D. Parker, Jeffrey D. Spitler Heating, Ventilating and Air Conditioning: Analysis and Design, 6th Edition edn, 2004, Oklahoma State University.

Measuresoft datascan products and services , Datascan modules 7020 . Available: http://datascan.measuresoft.com/products/analog-modules/7020-16-channel-analog-input-module/ [2016, MAY].

Menter FR J 1994, "Two-equation eddy-viscosity turbulence models for engineering applications", AIAA, vol. 32, pp. 1598–1605.

Mirade, P.S. & Daudin, J.D. 1998, "A new experimental method for measuring and visualising air flow in large food plants", Journal of Food Engineering, vol. 36, no. 1, pp. 31-49.

Mirade, P.S., Daudin, J.D. & Arnaud, G. 1995, "Simulation en deux dimensions de l'aéraulique de deux tunnels de réfrigération des viandes", International Journal of Refrigeration, vol. 18, no. 6, pp. 403-412.

Mirade, P., Kondjoyan, A. & Daudin, J. 2002, "Three-dimensional CFD calculations for designing large food chillers", Computers and Electronics in Agriculture, vol. 34, no. 1–3, pp. 67-88.

Moureh, J. & Flick, D. 2005, Airflow characteristics within a slot-ventilated enclosure.

Moureh, J., Tapsoba, S., Derens, E. & Flick, D. 2009, Air velocity characteristics within vented pallets loaded in a refrigerated vehicle with and without air ducts.

Moureh, J., Tapsoba, M. & Flick, D. 2009, Airflow in a slot-ventilated enclosure partially filled with porous boxes: Part I – Measurements and simulations in the clear region.

Moureh, J., Tapsoba, M. & Flick, D. 2009, Airflow in a slot-ventilated enclosure partially filled with porous boxes: Part II – Measurements and simulations within porous boxes.

Nahor, H.B., Hoang, M.L., Verboven, P., Baelmans, M. & Nicolaï, B.M. 2005, "CFD model of the airflow, heat and mass transfer in cool stores", International Journal of Refrigeration, vol. 28, no. 3, pp. 368-380.

Nick Cullen "High Performance Displacement Ventialtion using Fabric Diffusers-A Case Study", SPC Coil Products Limited, [Online], vol. App Notes 001, , pp. 21/11/2013.

Nicol JF and Humphreys M 2002, "Adaptive thermal comfort and sustainable thermal standards for buildings.", Energy and Buildings, .

Ning, M., Mengjie, S., Mingyin, C., Dongmei, P. & Shiming, D. 2016, "Computational fluid dynamics (CFD) modelling of air flow field, mean age of air and CO_2 distributions inside a bedroom with different heights of conditioned air supply outlet", Applied Energy, vol. 164, pp. 906-915.

Parpas, D., Amaris, C., Sun, J., Tsamos, K.M. & Tassou, S.A. 2017a, "Numerical study of air temperature distribution and refrigeration systems coupling for chilled food processing facilities", Energy Procedia, vol. 123, pp. 156-163.

Parpas, D., Amaris, C. & Tassou, S.A. 2017b, Experimental investigation and modelling of thermal environment control of air distribution systems for chilled food manufacturing facilities. Applied Thermal Engineering 127C (2017) pp. 1326-1339

Parpas, D, S.A. TASSOU, B.L. GOWREESUNKER, A.H. RAEISI "Air Distribution and Temperature Control in Chilled Food Manufacturing Facilities" IIR 2014 / 23rd – 25th June, St Mary's University College, Twickenham, London

Parpas, D, C. Amaris, S.A. Tassou, B.L Gowreesunker "Investigation into air distribution systems and temperature control in chilled food manufacturing facilities" SusTEM 2015 Sustainable Thermal Energy Management Network, 3rd Sustainable Thermal Energy Management Int. Conf., Newcastle upon Tyne, UK, 7-8 July, (2015) 110-119.

Pasut, W., Bauman, F. & De Carli, M. 2014, "The use of ducts to improve the control of supply air temperature rise in UFAD systems: CFD and lab study", Applied Energy, vol. 134, pp. 490-498.

Price Engineer's 2013, , Displacement Ventilation Engineering Guide. Available: http://www.price-hvac.com/Handbook/ [2013, 10/11/2013].

Price Engineer's 2007, , Displacement Ventilation DESIGN GUIDE. Available: http://www.price-hvac.com/Handbook [2013, 22/11].

Price Indistries , Displacement ventilation engineering guide . Available: https://www.priceindustries.com/content/uploads/assets/literature/engineering-guides/displacement-ventilation-engineering-guide.pdf [2015, May].

Price Industries , DF1 - Rectangular 1 Way Displacement Diffuser. Available: https://www.priceindustries.com/products/details/df1-rectangular-1way-displacement-diffuser [2013, 5/12].

Price Industries , DF1L - 1 Way Lay-In Displacement Diffuser. Available: https://www.priceindustries.com/products/details/df1l-1way-layin-displacement-diffuser [2013, 5/14].

Rees, S.J. & Haves, P. 2013, "An experimental study of air flow and temperature distribution in a room with displacement ventilation and a chilled ceiling", Building and Environment, vol. 59, pp. 358-368.

Rhee, K., Shin, M. & Choi, S. 2015, "Thermal uniformity in an open plan room with an active chilled beam system and conventional air distribution systems", Energy and Buildings, vol. 93, pp. 236-248.

Richard Meskimmon 2004, "Application of heat Pipes to Displacement Ventialtion/Chilled Ceiling Systems", S&p Coil Products Limited, vol. Application Notes 001.

S.A.Tassou, B.L. Gowreesunker, D. Parpas, A. Raeisi. Modelling cold food chain processing and display environments, In Modelling Food Processing Operations. 185-208, Elsevier, April 2015, ISBN-139781782422846.

Shah M 2009, "An improved and extended general correlation for heat transfer during condensation in plain tubes", Hvac &R Research, vol. 15, no. (5), pp. 889-913.

Simon J. Rees Philip Haves 2012, " An experimental study of air flow and temperature distribution in a room with displacement ventilation and a chilled ceiling ", Building and Environment 59 (2013) 358e368, .

Smale, N.J., Moureh, J. & Cortella, G. 2006, "A review of numerical models of airflow in refrigerated food applications", International Journal of Refrigeration, vol. 29, no. 6, pp. 911-930.

SOHAS 2007, Working to Prevent and Alleviate the effects of work on helath: Cold work.

Stamou, A. & Katsiris, I. 2006, "Verification of a CFD model for indoor airflow and heat transfer", Building and Environment, vol. 41, no. 9, pp. 1171-1181.

Tassou, S.A. & Xiang, W. 1998, "Modelling the environment within a wet air-cooled vegetable store", Journal of Food Engineering, vol. 38, no. 2, pp. 169-187.

TEMPCON , HOBO U12-013 Temp/RH/2xExt Data Logger. Available: https://www.tempcon.co.uk/shop/data-loggers/onset-hobo-data-loggers/hobo-u12-013-hobo-u12-temp-rh-2xext-logger-u12-013 [2016, MAY].

TSI AIRFLOW INSTRUMENTS Ltd. , TSI TA465-P . Available: http://www.tsi.com/airflow-instruments-multi-function-anemometer-ta465-p/ [2016, may].

Thermal Energy System Specialists, LLC 2015, TRNSYS, 17.02.0004 edn, 22 North Carroll Street, Suite 370 Madison, WI 53703 USA.

Wang, H. & Touber, S. 1990, "Distributed dynamic modelling of a refrigerated room", International Journal of Refrigeration, vol. 13, no. 4, pp. 214-222.

Waterloo Air Products Plc. , CS-F 2- Aluminium Linear slot diffuser . Available: http://www.waterloo.co.uk/product-models/cs-aluminium-linear-slot-diffusers/ [2014, July].

Work Safe Victoria 2008, A handbook for workplaces: Safe operation of cold storage facilities, 1st edn.

Xie, J., Qu, X., Shi, J. & Sun, D. 2006, "Effects of design parameters on flow and temperature fields of a cold store by CFD simulation", Journal of Food Engineering, vol. 77, no. 2, pp. 355-363.

Zukowska, D., Melikov, A. & Popiolek, Z. 2012, "Impact of geometry of a sedentary occupant simulator on the generated thermal plume: Experimental investigation", HVAC&R Research, vol. 18, no. 4, pp. 795-811.

Appendix A - Experimental Set-up

This appendix provides supporting information used in the development of the experimental set-up described in Chapter 4.

Appendix A.1 Industrial evaporator: Kobol CR39

Constructed using copper tubes of ½'' diameter and aluminium corrugated fins. Staggered arrangement of the copper tubes is used across self-spaces fins. Fin spacing is 4.5mm. A single-phase fan with external rotor is used. Manufacturer data are shown in T-A 1 and F-A 1

T-A 1. Kobol CR 39 manufacturer specification

CR SERIES
Fin spacing : 4,5 mm.   **R-404A**

MODELO MODEL	CAPACIDAD CAPACITY	ENV 328 COND.2	Tev = −5ºC				SUPERFICIE SURFACE	CAUDAL DE AIRE / AIR FLOW	DARDO AIR THROW	VOL. INT. INT. VOL.	PESO WEIGHT
			DT1 = 5	DT1 = 7	DT1 = 8	DT1 = 10	m2	m3/h	m³	dm3	kg
CR-39	W	3.201	2.385	3.617	4.417	5.890	18,03	2.825	20	5,2	24
	kcal/h		2.051	3.111	3.799	5.065					

COMMON FEATURES

MODELO MODEL		VENTILADORES FANS		CONSUMO ENERGÉTICO Y DE CORRIENTE / POWER & CURRENT CONSUMPTION		DIMENSIONES (mm) / DIMENSIONS (mm)					ENTRADA INLET	SALIDA OUTLET	RESISTENCIAS HEATERS 400V	
		N	Ø (mm)	W	230 V (A)	A	B	C	D	E	Ø	Ø	W	A
CR-39	CC-27	1	350	145	0,73	905	685	490	450	565	1/2"	5/8"	2.436	5,1
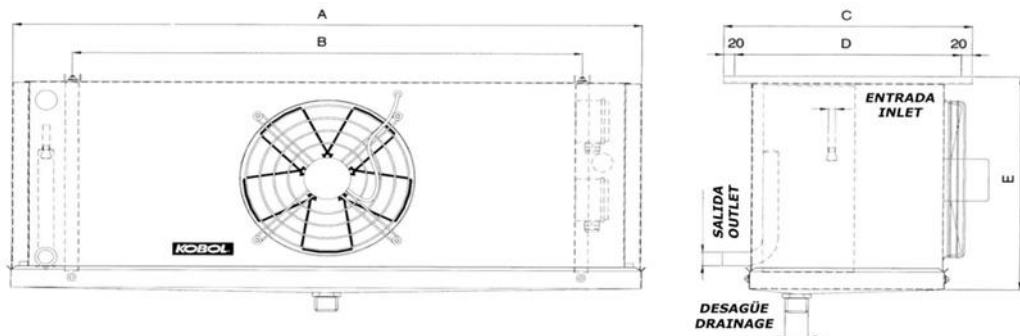
F-A 1. Kobol CR39 Dimensions

Tecumseh Silensys 3 phase condensing unit (R404A)

The Tecumseh Silensys 3-phase condensing unit is using a R404A reciprocating type compressor (TAG4546Z). Manufacturer technical data and dimensions are shown in F-A 2 and F-A 3.

TAG4546Z	Tension T : 400V 3~ 50Hz / 440V 3~ 60 Hz		R404A	N°227CU-T	Ind g

Les performances sont données dans les **conditions EN 12900** : Gaz aspirés : 20°C
Elles sont certifiées uniquement en 50 Hz   Sous refroidissement : 0°K

The performance data are in **EN 12900 conditions** : Return gas : 20°C
They are only certified in 50 Hz   Subcooling : 0°K

50 Hz R404A

4 |T condensation	5 |T évaporation	(°C)	-25	-20	-15	-10	-5	0	5	10	15
30	1 | P frigorifique	(W)	3296	4578	6126	7972	10149	12690	15628	18995	22823
	2 | P absorbée	(W)	1863	2196	2500	2781	3042	3288	3525	3757	3988
	3 | I absorbée	(A)	3.97	4.39	4.8	5.18	5.55	5.91	6.24	6.56	6.87
40	1 | P frigorifique	(W)		3394	4721	6287	8125	10267	12746	15595	18846
	2 | P absorbée	(W)		2168	2558	2916	3247	3555	3846	4124	4394
	3 | I absorbée	(A)		4.35	4.86	5.35	5.83	6.29	6.73	7.16	7.57
50	1 | P frigorifique	(W)			3370	4646	6134	7867	9878	12198	14861
	2 | P absorbée	(W)			2497	2951	3371	3761	4125	4469	4797
	3 | I absorbée	(A)			4.78	5.37	5.96	6.52	7.07	7.6	8.12
60	1 | P frigorifique	(W)				3109	4238	5552	7084	8866	10931
	2 | P absorbée	(W)				2846	3374	3864	4321	4749	5154
	3 | I absorbée	(A)				5.25	5.94	6.61	7.27	7.9	8.53

F-A 2. Silensys 3-phase condensing unit: technical data
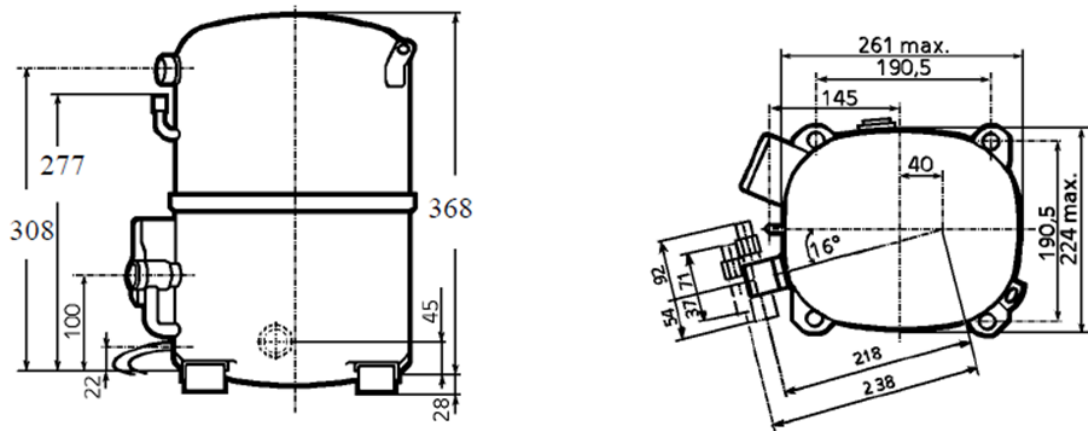
F-A 3. Silensys 3-phase condensing unit: compressor dimensions

Temperature controller - EKC 102

The controller is used for temperature control refrigeration appliances and cold rooms. The controller contains one relay output and one temperature control signal where the signal is defined and received from the temperature sensor. The sensor is placed in the cold air flow after the evaporator or in the warm air flow just before the evaporator. The controller functions include temperature control at start/stop of compressor and Natural defrost at stop of compressor. Manufacturer data are shown in F-A 4.

Data

Supply voltage	230 V a.c. +15/-15 %. 1,5 VA	
Sensors	Pt 1000 or PTC (1000 ohm / 25°C) or NTC-M2020 (5000 ohm / 25°C)	
Accuracy	Measuring range	-60 to +99°C
	Controller	±1 K below -35°C ±0,5 K between -35 to +25°C ±1 K above +25°C
	Pt 1000 sensor	±0.3 K at 0°C ±0.005 K per grad
Display	LED, 3 digits	
Digital inputs	Signal from contact functions Requirements to contacts: Gold plating Cable length must be max. 15 m Use auxiliary relays when the cable is longer	
Electrical connection cable	Max.1,5 mm² multi-core cable on supply and relays. Max. 1 mm² on sensors - and DI inputs. Terminals are mounted on the circuit board	
Relays	Refrigeration	SPDT, Imax. = 10 A ohmic/ 6 A AC 15* inductive
	Alarm/ Defrost/ Refrigeration 2	(It is a 16 A relay, but conductor lanes and derating mean that 10 A must not be exceeded).
Environments	0 to +55°C, During operations -40 to +70°C, During transport	
	20 - 80% Rh, not condensed	
	No shock influence / vibrations	
Density	IP 65 from front. Buttons and packing are imbedded in the front.	
Approvals	EU Low Voltage Directive and EMC demands re CE-marking complied with LVD tested acc. EN 60730-1 og EN 60730-2-9, A1, A2 EMC tested acc. EN50082-1 og EN 60730-2-9, A2	

* AC 15 load to EN 60947-5-1
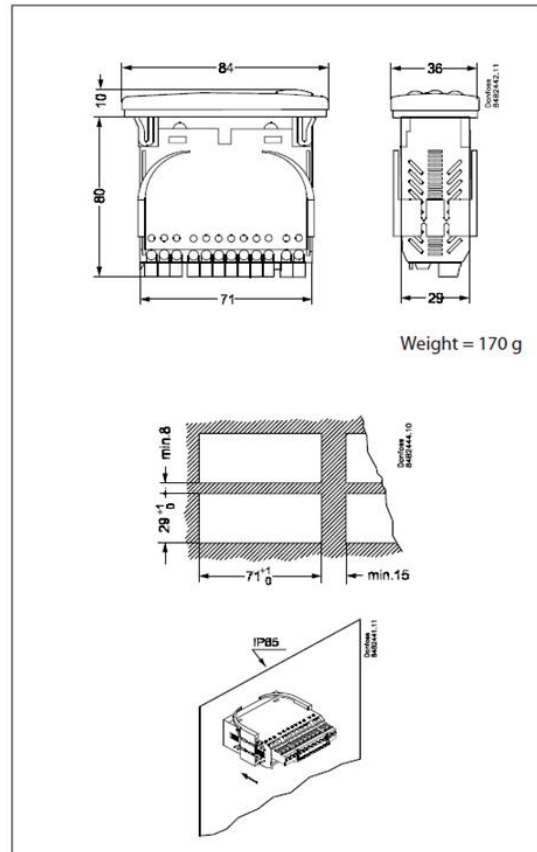
F-A 4. Temperature controller - EKC 102: Manufacturer data

KE - Low Impulse textile duct

The KE - Low Impulse textile duct is an ideal solution for the delivery and distribution of cooled air, particularly suitable for hygiene, comfort and temperature control. KE Fibertec's textile based low impulse systems are woven from Trevira CS polyester yarn, and the textile surface acts as a fine mesh, allowing the supply of air to pass through the surface at a very low uniform discharge velocity. KE - Low Impulse textile duct is produced using round ducts (Ø). Because of the density differential, with the cooled air being heavier than the warmer air in the room, the room air is displaced below the duct while the supply air continues moving towards the floor. The warm air is driven up to high level where it will not cause discomfort. Low impulse textile duct systems are only suitable for cooling purposes. Manufacturer data are shown in F-A 5.
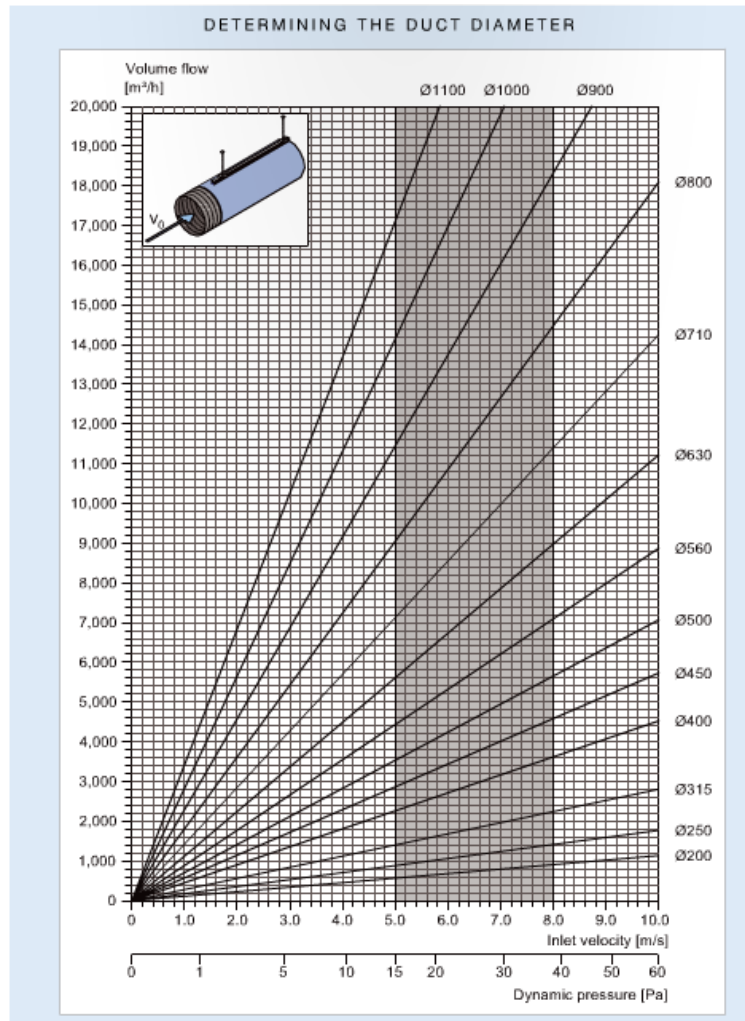
F-A 5. KE Fabric Duct: manufacturer data

Appendix B - Experimental Set-up Initial monitoring

This appendix provides supporting information regarding the monitoring of the initial experimental set-up described in Chapter 4. The air distribution system used in the initial experiments was the fabric duct installed at ceiling level.

Appendix B.1 Refrigeration system monitoring

This section presents data of power consumption collected for 17 hours. In addition, refrigerant and air temperatures at the inlet and outlet of each component of the refrigeration system are presented.
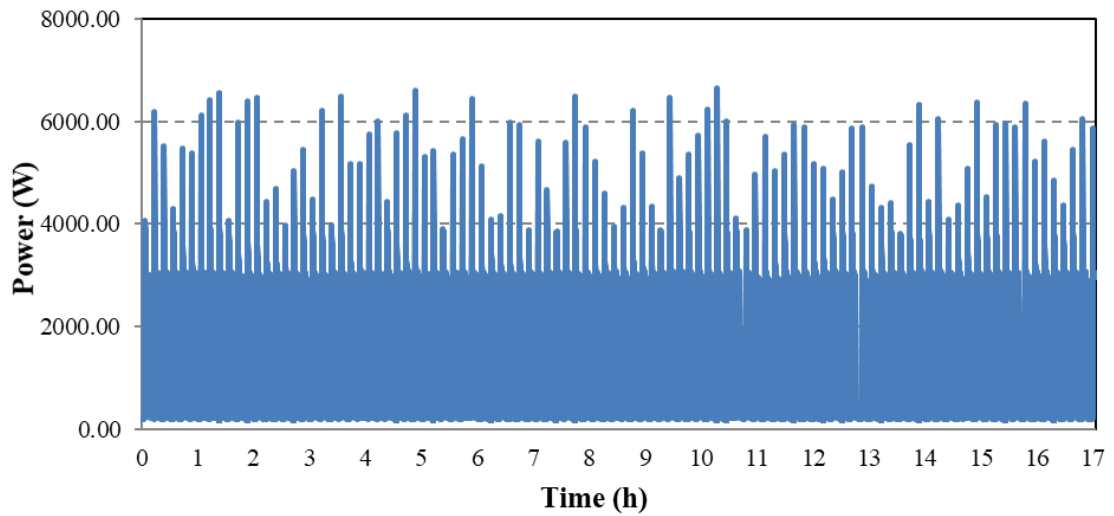
F-A 6. Power consumption, Fabric Duct at Ceiling level, during a period of 17 hours.
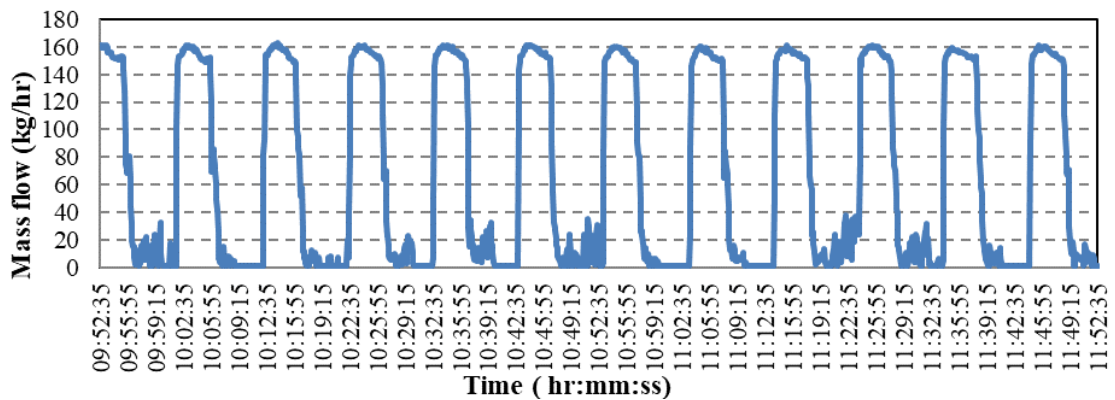
F-A 7. Refrigerant mass flow rate, Fabric Duct at Ceiling level, during a period of 2 hours.

Appendix C - Experimental study of different air distribution systems

This appendix provides supporting information regarding the monitoring of the air distribution systems via circular fabric duct and semi-circular fabric duct located at medium level described in Chapter 7.

Semi-circular fabric duct located at medium level Refrigeration system monitoring

This section presents an analysis of the refrigeration system refrigerant and air temperatures at the inlet and outlet of each component. The refrigeration system temperatures with the investigated air distribution configuration are presented in F-A 8 and F-A 9. The data of power consumption collected for 17 hours are shown in F-A 10.
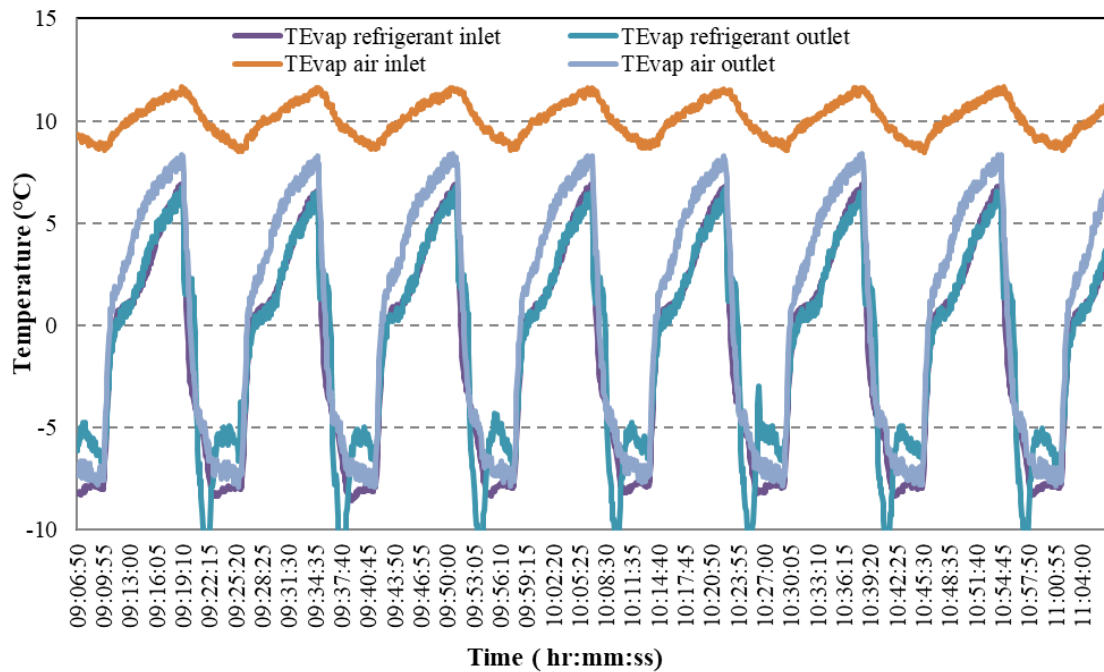
F-A 8. Semi-circular -fabric duct at medium level: refrigerant-air temperatures at inlet/outlet of evaporator
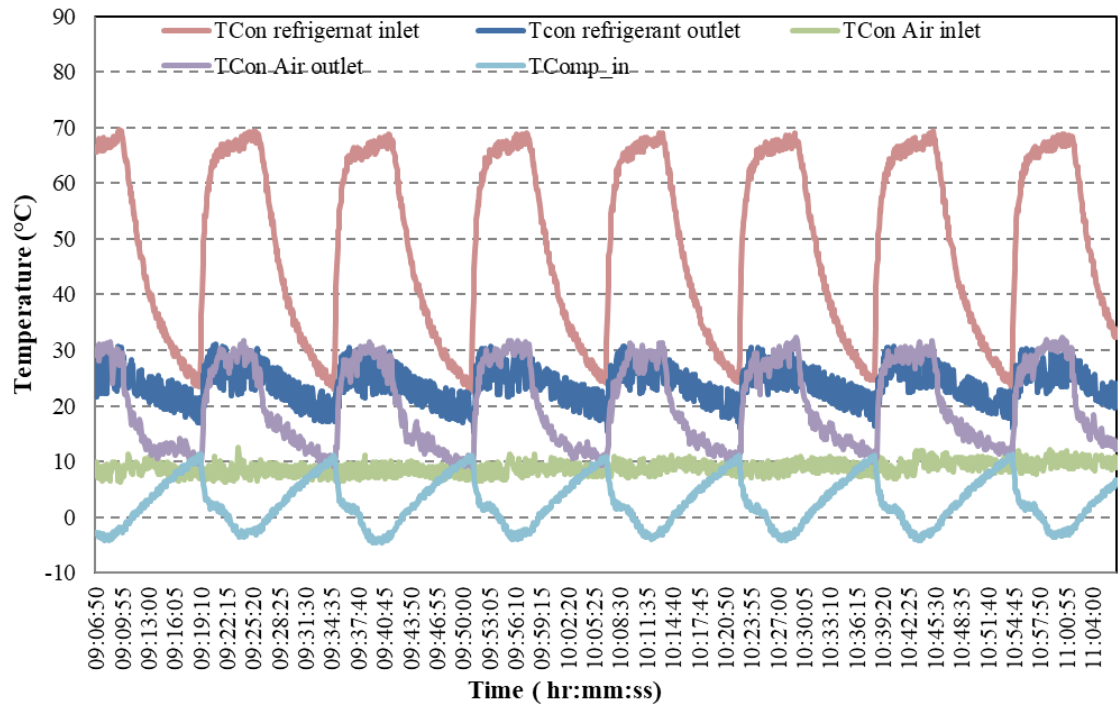
F-A 9. Semi-circular fabric duct at medium level: refrigerant-air temperatures at inlet/outlet of evaporator
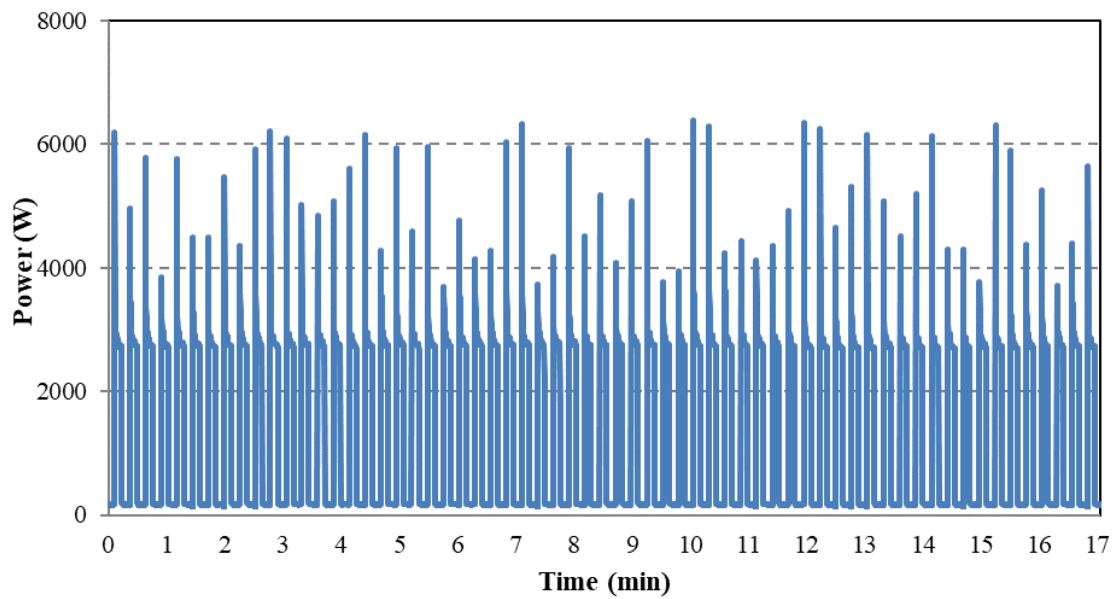
F-A 10. Power consumption, semi-circular - Fabric Duct at medium level, during a period of 17 hours.

fabric duct located at medium level Refrigeration system monitoring

This section presents an analysis of the refrigeration system refrigerant and air temperatures at the inlet and outlet of each component. The refrigeration system temperatures with the investigated air distribution configuration are presented in F-A 11 and F-A 12. The data of power consumption collected for 17 hours are shown in F-A 13.
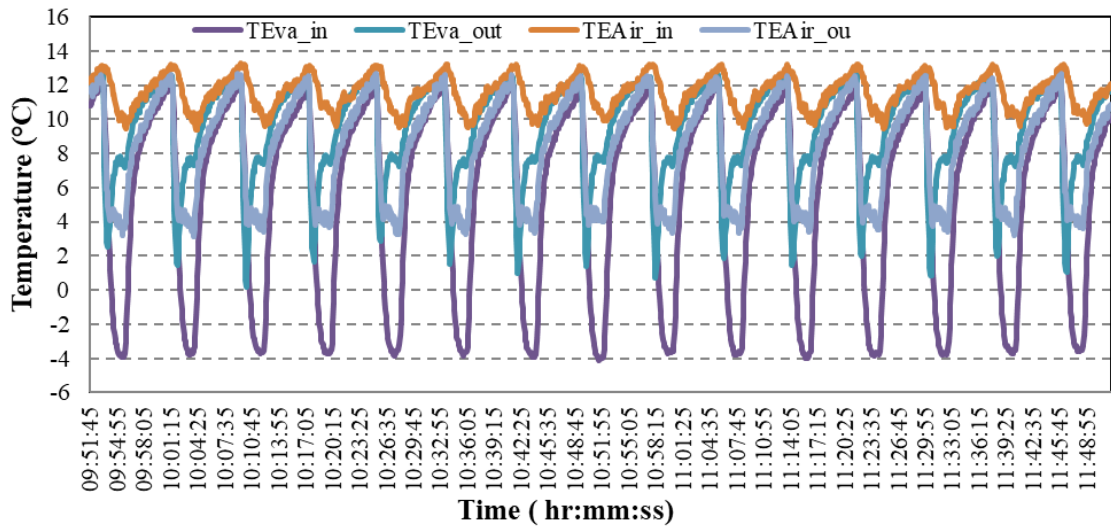
F-A 11. Fabric duct at medium level: refrigerant-air temperatures at inlet/outlet of evaporator
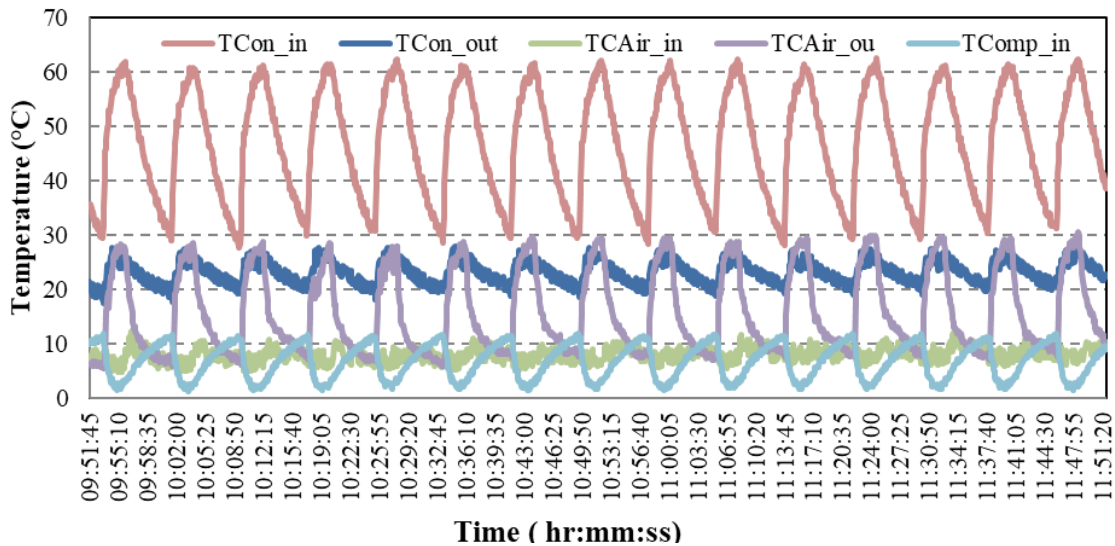
F-A 12. Fabric duct at medium level: refrigerant-air temperatures at inlet/outlet of evaporator
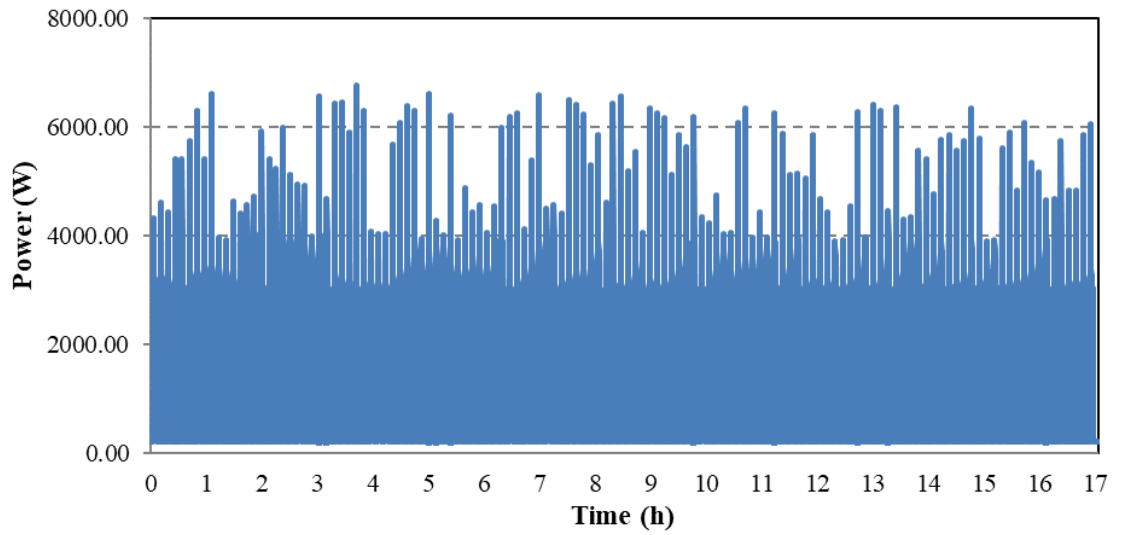
F-A 13. Power consumption, Fabric Duct at medium level, during a period of 17 hours.

Appendix D - EES refrigeration model

This appendix provides supporting information regarding the developed EES refrigeration model described in Chapter 8. The EES programming was implemented as follow:

```
procedure        Results(Cop_real,tempa,W_power_Comp,        T_Eair_out,T_Eair_in:Cop_temp,
tempb,W_comp_temp,T_Eair_out_temp)

 IF (T_Eair_in>=11.7) then  "if statement to identify if the air conditioning system will work"

    W_comp_temp =W_power_Comp
    T_Eair_out_temp=T_Eair_out
    Cop_temp=Cop_real
     tempa=1
else
IF (T_Eair_in<9.7) then
    W_comp_temp=0
    T_Eair_out_temp=T_Eair_in
    Cop_temp=0
else
W_comp_temp =0
    T_Eair_out_temp=T_Eair_in
    Cop_temp=0

endif
endif


tempb=tempa

end




"Nusselt for the Refrigerant"
Procedure Nus_Refrigerant(Re_refrig,L_tube,N,Lt,Pr_refrig,D_tube_inner:Nus_refrig)
IF (Re_refrig<2300) and (Lt>N*L_tube/2) then
Gz_D_refrig = D_tube_inner*Re_refrig*Pr_refrig/(N*L_tube)
Nus_refrig = 3.66 + 0.0668 * Gz_D_refrig/(1+0.04*Gz_D_refrig^(2/3))
else
if (Re_refrig<2300) and (Lt<N*L_tube/2) then
Nus_refrig = 3.66
else
if (Re_refrig>2300) then
Nus_refrig = 0.023*Re_refrig^(4/5)*Pr_refrig^0.4
endif
endif
endif
end




Procedure
PropertiesAir(T_air_in,T_air_out,T_tube_in,T_tube_out,S_T,S_L,D_tube,Vel_air:Vel_max_air,rho_air,mu_air,Pr_air,Pr_air_s,k_air,cp_air,h_air_in,h_air_out,v_air_in,v_air_out,Re_air,Nus_air)
"Air thermophysical properties"
P_air=101.325  "kPa"
```

```
T_m_air=(T_air_in+T_air_out)/2
T_air_s=(T_tube_in+T_tube_out)/2
Vel_max_air=(S_T/(S_T-D_tube))*Vel_air          "since 2*A_D>A_T"
rho_air=Density(Air,T=T_m_air,P=P_air)              "kg/m^3"
mu_air=Viscosity(Air,T=T_m_air)                     "kg/m-s"
Pr_air=Prandtl(Air,T=T_m_air)
Pr_air_s=Prandtl(Air,T=T_air_s)
k_air=(Conductivity(Air,T=T_m_air))/1000
cp_air=Cp(Air,T=T_m_air)
h_air_in=Enthalpy(Air_ha,T=T_air_in,P=P_air)
h_air_out=Enthalpy(Air_ha,T=T_air_out,P=P_air)
v_air_in=Volume(Air_ha,T=T_air_in,P=P_air)
v_air_out=Volume(Air_ha,T=T_air_out,P=P_air)
Re_air=(rho_air*Vel_max_air*D_tube)/mu_air


"Zukauskas correlations, 1987"
IF (Re_air>0) and (Re_air<500) then
Nus_air=1.04*(Re_air^0.4)*(Pr_air^0.36)*((Pr_air/Pr_air_s)^0.25)
 else
IF (Re_air>500) and (Re_air<1000) then
Nus_air=0.71*(Re_air^0.5)*(Pr_air^0.36)*((Pr_air/Pr_air_s)^0.25)
else
IF (Re_air>1000) and (Re_air<200000) then
Nus_air=0.35*((S_T/S_L)^0.2)*(Re_air^0.6)*(Pr_air^0.36)*((Pr_air/Pr_air_s)^0.25)
else
IF (Re_air>200000) and (Re_air<2000000) then
Nus_air=0.031*((S_T/S_L)^0.2)*(Re_air^0.8)*(Pr_air^0.36)*((Pr_air/Pr_air_s)^0.25)
endif
endif
endif
endif

End


Procedure h_singlephase(ref$,D, m_dot_r, T1, T2, P:h_SP)
{Single phase refrigerant heat transfer coefficient for the sub-cooled and superheated portion of
the condenser, Kays & London (1984)}
Area=(D/2)^2*pi
G=m_dot_r/Area
Tav=(T1+T2)/2
rho=density(ref$, T=Tav,P=P)
c_p=specheat(ref$, T=Tav, P=P)
mu=viscosity(ref$, T=Tav, P=P)
Re=m_dot_r*D/(Area*mu)
Pr=prandtl(ref$, T=Tav, P=P)
If Re<3500 then
a=1.10647
b=-.078992
endIF
if (Re>3500) and (Re<6000) then
a=3.5194e-7
b=1.03804
ENDIF
if Re>6000 then
a=.2243
b=-.385
endif
St=a*Re^b/(Pr^(2/3))
h_SP=St*G*C_p
end
```

```
Procedure h_TwoPhaseCondenser(ref$,D_tube_inner_C,m_dot_refrig,P1,P2:alpha_TP_C)
g=9.806
Mu_prime2=Viscosity(ref$,P=P2,x=0)
Mu_prime1=Viscosity(ref$,P=P1,x=1)
Pr_refrig2=Prandtl(ref$,P=P2,x=0)
Pr_refrig1=Prandtl(ref$,P=P1,x=1)
k_refrig2=Conductivity(ref$,x=0,P=P2)/1000
k_refrig1=Conductivity(ref$,x=1,P=P1)/1000
rho2=Density(ref$,x=0,P=P2)
rho1=Density(ref$,x=1,P=P1)
Pcrit=P_crit(ref$)
Pr_C=P1/Pcrit "reduced pressure,  definition by M.M. Sham 1978"
G_C=(4*m_dot_refrig)/(pi*D_tube_inner_C^2)
nn=0.0058+0.557*Pr_C
xx=0.4 "x assumed as 0.4, average vapor quality"
Z=(((1/xx)-1)^0.8)*Pr_C^0.4
Re_refrig_c_vapor  =  (4*m_dot_refrig)/(pi*D_tube_inner_C*Mu_prime1)         "Reynolds  GT,
assuming total mass flowing as vapor "
Re_refrig_c_ls  =  ((4*m_dot_refrig)*(1-xx))/(pi*D_tube_inner_C*Mu_prime2)      "Reynolds  LS,
assuming liquid phase flowing alone"
Re_refrig_c_liquid= (4*m_dot_refrig)/(pi*D_tube_inner_C*Mu_prime2)  "Reynolds LT, assuming
total mass flowing as liquid "

Nusselt_refrig_c_liquid= 0.023*Re_refrig_c_ls^(4/5)*Pr_refrig2^0.4    "Dittus-Boelter correlation
with Re_refrig_c_ls "
Nusselt_refrig_c_lt= 0.023*Re_refrig_c_liquid^(4/5)*Pr_refrig2^0.4     "Dittus-Boelter correlation
with Re_refrig_c_liquid "

alpha_int_c_lt=k_refrig2*Nusselt_refrig_c_lt/D_tube_inner_C "kW/m2.k, heat transfer coefficient
for the liquid-phase only"
alpha_TP_C1=alpha_int_c_lt*(((1-xx)^0.8)+((3.8*(xx^0.76)*((1-xx)^0.04))/(Pr_C^0.38)))
"Correlation reported by M.M. Sham 1978, Old Correlation"
alpha_L_c=alpha_int_c_lt*((Mu_prime1/(14*Mu_prime2))^nn)*(((1-xx)^0.8)+((3.8*(xx^0.76)*((1-
xx)^0.04))/(Pr_C^0.38))) "found in An improved and extended general correlation for heat transfer
during condensation, M.M. Shah 2009, New Correlation"
alpha_Nus=1.32*(Re_refrig_c_ls^(-1/3))*((rho2*(rho2-
rho1)*g*(k_refrig2^3))/(Mu_prime2^2))^(1/3)

J_g=(xx*G_C)/(g*D_tube_inner_C*rho1*(rho2-rho1))^0.5 "dimensionless vapor velocity"
J_g1=0.98*(Z+0.263)^(-0.62) "for horizontal tubes"

if (J_g>J_g1) then "regime I"
alpha_TP_C=alpha_L_c
else "regime II"
alpha_TP_C=alpha_L_c+alpha_Nus
Endif
End

Procedure h_airside(hf, eta,t,L, ma, mu, D_o, Ao,At, Cp, Pr, n:ha)
{Returns air-side heat transfer coefficient based on McQuiston Method}
{h_bar_a- external heat transfer coefficient (btu/hr-ft^2-R)}
A_min=(hf/2)*(1/eta-t) "[ft^2]"
Gmax=ma*(1/eta-t)/(A_min*L) "[lbm/hr-ft^2]"
Re_D=Gmax*D_o/m
Re_L=Gmax*hf/mu
dum1=(Ao/(At))
JP=Re_D^(-.4)*(Ao/(At/(1-t*eta)))^(-.15)
j4=.2675*JP+1.325*10^(-3)
jn=(1-n*1280*Re_L^(-1.2))*j4/(1-4*1280*Re_L^(-1.2))
```

```
ha=jn*Cp*Gmax/(Pr^(2/3))*convert(1/s,1/hr)
end


Procedure geteuler(Re, h_f, dep_f, D, nrow:Eu)
{finds Euler number for staggered banks of tubes}
{Modify Euler number to account for non- equilateral geometry
find correction factor k1 to account for a/b ratio, use k1 with other relationships to correct Euler # for row
spacing}
a=dep_f/D
b=h_f/D
Check1=1
Check2=1
Check3=1

spacerat=a/b
Eu=0
k1=0
If (spacerat>.5) and (spacerat<1.2) and (re>=1000) and (Re<10000) then {this relationship is stated
for Re=1000, not the range 1000<Re<10000}
k1=spacerat^(-.048)
k2=1.28-.708/spacerat+.55/(spacerat^2)-0.113/(spacerat^3)
k1=(k2-k1)/(10000-1000)*(Re-1000)+k1
endIF
if (spacerat>1.25) and (spacerat<3.5) and (Re>1000) and (Re<10000) then
k1=.951*spacerat^.284
k2=1.28-.708/spacerat+.55/(spacerat^2)-0.113/(spacerat^3)
k1=(k2-k1)/(10000-1000)*(Re-1000)+k1
endIF
If (spacerat>.45) and (spacerat<3.5) and (Re>=10000) and (Re<100000) then {stated for Re=10000}
k1=1.28-.708/spacerat+.55/(spacerat^2)-0.113/(spacerat^3)
k2=2.016-1.675*spacerat+.948*spacerat^2-.234*spacerat^3+.021*spacerat^4
k1=(k2-k1)/(100000-10000)*(Re-10000)+k1
endif
If  ((spacerat>.45)  and  (spacerat<3.5)  and  (Re>=100000))  or  ((spacerat>.45)  and  (spacerat<1.6)  and
(Re>=1000000)) then {stated for Re=100000}
k1=2.016-1.675*spacerat+.948*spacerat^2-.234*spacerat^3+.021*spacerat^4
endIF
if (spacerat>1.25) and (spacerat<3.5) and (Re>100) and (Re<1000) then
k1=.93*spacerat^.48
k2=spacerat^(-.048)
k1=(k2-k1)/(1000-100)*(Re-100)+k1
endIF
if (spacerat=1.155) then
k1=1
endif
If k1=0 then check1=0
If (a>=1.25) and (a<1.5) and (Re>3) and (re<1000) then
{Stated for a=1.25}
Eu1:=(.795+247/re+335/(re^2)-1550/Re^3+2410/Re^4)
eu2:=(.683+1.11e2/re-97.3/Re^2+426/re^3-574/re^4)
Eu=(Eu2-Eu1)/(1.5-1.25)*(a-1.25)+Eu1
endif
If (a>=1.25) and (a<1.5) and (Re>1000) and (Re<2e6) then
Eu1:=(.245+3390/Re-9.84e6/Re^2+1.32e10/re^3-5.99e12/Re^4)
Eu2:=(.203+2480/re-7.58e6/re^2+1.04e10/re^3-4.82e12/re^4)
Eu=(Eu2-Eu1)/(1.5-1.25)*(a-1.25)+Eu1
endif
If (a>=1.5) and (a<2) and (Re>3) and (Re<100) then
eu1:=(.683+1.11e2/re-97.3/Re^2+426/re^3-574/re^4)
Eu2:=(.713+44.8/Re-126/Re^2-582/Re^3)
Eu=(Eu2-Eu1)/(2-1.5)*(a-1.5)+Eu1
endif
If (a>=1.5) and (a<2) and (Re>100) and (Re<1000) then
eu1:=(.683+1.11e2/re-97.3/Re^2+426/re^3-574/re^4)
Eu2:=(.343+303/re-7.17e4/re^2+8.8e6/re^3-3.8e8/Re^4)
Eu=(Eu2-Eu1)/(2-1.5)*(a-1.5)+Eu1
```

```
endif
If (a>=1.5) and (a<2) and (Re>1000) and (Re<10000) then
Eu1:=(.203+2480/re-7.58e6/re^2+1.04e10/re^3-4.82e12/re^4)
Eu2:=(.343+303/re-7.17e4/re^2+8.8e6/re^3-3.8e8/Re^4)
Eu=(Eu2-Eu1)/(2-1.5)*(a-1.5)+Eu1
endif
If (a>=1.5) and (a<2) and (Re>10000) and (Re<200000) then
Eu1:=(.203+2480/re-7.58e6/re^2+1.04e10/re^3-4.82e12/re^4)
Eu2=(.162+1810/Re+7.92e7/re^2-1.65e12/Re^3+8.72e15/re^4)
Eu=(Eu2-Eu1)/(2-1.5)*(a-1.5)+Eu1
endif
If (a>=2) and (a<2.5) and (Re>7) and (Re<100) then
Eu1:=(.713+44.8/Re-126/Re^2-582/Re^3)
Eu2:=(.33+98.9/re-1.48e4/Re^2+1.92e6/re^3-8.62e7/re^4)
Eu=(Eu2-Eu1)/(2.5-2)*(a-2)+Eu1
endif
If (a>=2) and (a<2.5) and (Re>100) and (Re<5000) then
Eu1:=(.343+303/re-7.17e4/re^2+8.8e6/re^3-3.8e8/Re^4)
Eu2:=(.33+98.9/re-1.48e4/Re^2+1.92e6/re^3-8.62e7/re^4)
Eu=(Eu2-Eu1)/(2.5-2)*(a-2)+Eu1
endif
If (a>=2) and (a<2.5) and (Re>5000) and (Re<10000) then
Eu1:=(.343+303/re-7.17e4/re^2+8.8e6/re^3-3.8e8/Re^4)
Eu2:=(.119+498/Re-5.07e8/Re^2+2.51e11/Re^3-4.62e14/re^4)
Eu=(Eu2-Eu1)/(2.5-2)*(a-2)+Eu1
endif
If (a>=2) and (a<2.5) and (Re>10000) and (Re<2000000) then
Eu1:=(.162+1810/Re+7.92e7/re^2-1.65e12/Re^3+8.72e15/re^4)
Eu2:=(.119+4980/Re-5.07e7/Re^2+2.51e11/Re^3-4.62e14/re^4)
Eu=(Eu2-Eu1)/(2.5-2)*(a-2)+Eu1
endif
If (a>=2.5) and (Re>100) and (Re<5000) then
Eu:=(.33+98.9/re-1.48e4/Re^2+1.92e6/re^3-8.62e7/re^4)
endif
If (a>=2.5) and (Re>5000) and (Re<2000000) then
Eu:=(.119+4980/Re-5.07e7/Re^2+2.51e11/Re^3-4.63e14/re^4)
endif
If Eu=0 then Check2=0
{Modify for less than 4 rows}
z=1
C=0
c_z=0
if nrow<10 then
repeat
If z>=3 then
c_z=1
else
IF Re>=10 THEN
c_z1=1.065-(.180/(z-.297))
c_z2=1.798-(3.497/(z+1.273))
c_z=(c_z2-c_z1)/(100-10)*(Re-10)+c_z1
endif
IF Re>=100 THEN
c_z1=1.798-(3.497/(z+1.273))
c_z2=1.149-(.411/(z-.412))
c_z=(c_z2-c_z1)/(1000-100)*(Re-100)+c_z1
endif
IF Re>=1000 THEN
c_z1=1.149-(.411/(z-.412))
c_z2=.924+(.269/(z+.143))
c_z=(c_z2-c_z1)/(10000-1000)*(Re-1000)+c_z1
endif
IF Re>=10000 THEN
c_z1=.924+(.269/(z+.143))
c_z2=.62+(1.467/(z+.667))
c_z=(c_z2-c_z1)/(100000-10000)*(Re-10000)+c_z1
endif
```

```
IF Re>=100000 THEN
c_z=.62+(1.467/(z+.667))
endif
endif
z=z+1
C=C+c_z
until z>nrow
C=C/nrow
If C=0 then Check3=0
endif
Eu=Eu*C*k1
end

FUNCTION T_adjusted(Ts)
If (Ts =0) THEN
T_adjusted = 0.1
ELSE
T_adjusted = Ts
ENDIF
END
rho_air_in_C=Density(Air,T=T_Cair_in,P=P_air)
rho_air_in_E=Density(Air,T=T_Eair_in,P=P_air)
```

"Procedure AirSidePressureDrop"
f_fin_C=10*1.7*Re_L_C^(-0.5) "frinction factor expressed by Rich 1973"
delta_PFin_C=((f_fin_C*v_air_in_C*((G_Air_C^2)/2)*(Area_Surface_1fin_C/A_air_min1_C)))/1000 "KPa"
P_T_C=S_T_C/D_tube_C
P_L_C=S_L_C/D_tube_C
P_C=P_T_C/P_L_C
x_c=1"Taking into account P=1.2, incropera pag. 473 "
{delta_PTubes_C=(N_C*x_c*((rho_air_C*(Vel_max_air_C^2))/2)*f_fin_C)/1000 "KPa"
delta_P_C=delta_PFin_C+delta_PTubes_C}
W_fan_C=(Vel_air_C*Frontal_area_C*delta_PAir_C/0.55)*N_units

{Re_a_C=(G_Air_C*D_hC)/mu_air_C}
delta_PAir_C=(v_air_in_C*((G_Air_C^2)/2)*(f_fin_C*(Area_Surface_1fin_C/A_air_min1_C)+((1+sigma_C^2)*(rho_air_in_C/rho_air_C))))/1000

f_fin_E=10*1.7*Re_L^(-0.5)
delta_PFin_E=((f_fin_E*v_air_in_E*((G_Air_E^2)/2)*(Area_Surface_1fin/A_air_min1)))/1000 "KPa"
P_T=S_T/D_tube
P_L=S_L/D_tube
P=P_T/P_L
x_e=1"Taking into account P =1.2, incropera pag. 473 "
{delta_PTubes_E=(N*x_e*((rho_air_E*(Vel_max_air_E^2))/2)*f_fin_E) /1000 "KPa"
delta_P=delta_PFin_E+delta_PTubes_E}
W_fan_E=Vel_max_air_E*Frontal_area*Delta_PAir_E*0.1

Delta_PAir_E=(v_air_in_E*((G_Air_E^2)/2)*(f_fin_E*(Area_Surface_1fin/A_air_min1)+((1+sigma^2)*(rho_air_in_E/rho_air_E))))/1000
"**"

"!This is a testing simulation of calling ees from trnsys "

"The following variables come from TRNSYS via the clipboard:
T_1_ambient, T_2_roomtemp
"

"To test the file, copy the following numbers to the clipboard:

1.05 302 0.005 5 360 0.288 1.3
"
{ Import inputs from the clipboard}
$Import 'CLIPBOARD' T_amb_trnsys, T_Eair_in_trnsys, tempa_trnsys

"! Unit Conversion from TRNSYS"

{"The EES file is set to use Kelvin for temperature "

T_amb = convertTemp(C,K,T_amb_trnsys)
T_Eair_in = convertTemp(C,K,T_Eair_in_trnsys)}

T_amb = T_amb_trnsys
T_Eair_in = T_Eair_in_trnsys
tempa=tempa_trnsys

g=9.806 "m/s2, acceleration due to gravity"

"Evaporator details"
{Call AirVelocity(E_Fan_vel%:Vel_air_E) "Mean velocity at the inlet of the evaporator, m/s"}
D_tube=0.011   "diamater of the tubes, m"
D_tube_inner=D_tube-0.002   "inner diameter of the tubes, m"
L_tube=0.67   "length of the tubes, m"
L_tube_Total=L_tube*N
H_e=0.5   "Height of the evaporator, m"
N_L=4   "number of rows"
N_T=16   "tubes per rows"
N=N_L*N_T   "total number of tubes"
N_units=2   "Evaporator units"
S_T=0.03   "transverse pitch, vertical m"
S_L=0.025   "longitudinal pitch, horizontal m"
P_air=101.325   "Air_pressure"
S_D=sqrt((S_L^2)+((S_T/2)^2))   "diagonal pitch, m"
A_1=S_T*L_tube   "Flow area 1, m2"
A_T=(S_T-D_tube)*L_tube   "Flow area 2, m2"
A_D=(S_D-D_tube)*L_tube   "Flow area 3, m2"
N_fins=143   "number of fins"
fins_height=0.007   "from the tube surface to the fin tip, m"
fins_thickness=0.00015   "m"
fins_separation=0.0045   "m"
Total_Surface_Area=18.03   "m2"
Area_internal=pi*D_tube_inner*L_tube*N
Frontal_area=L_tube*H_e
D_DepE=((2*fins_height)+D_tube)*N_L
Area_external_tube=pi*D_tube*L_tube*N
Area_external_occupedbyfins=pi*D_tube*(fins_thickness*N_fins)*N
Area_external_tube_nofins=Area_external_tube-Area_external_occupedbyfins
Frontal_area_fins=H_e*fins_thickness*N_fins*2
Area_Surface_1fin=((S_T*S_L)-(pi*(D_tube/2)^2))*2
Area_Surface_fin=18.03-(Area_external_tube_nofins){(((0.03*0.025)-(pi*(D_tube/2)^2))*2*N_fins*N}
Area_total=18.03 "m2"

A_air_min1=(fins_separation-fins_thickness)*S_T "minimum free flow area"
sigma=A_air_min1/Frontal_area

Ratio_int_ext=Area_internal/Area_total

"Condenser details"
Vel_air_C=0.6   "Mean velocity at the inlet of the condenser, m/s"
D_tube_C=0.008   "diamater of the tubes, m"
D_tube_inner_C=D_tube_C-0.002   "inner diameter of the tubes, m"
L_tube_C=0.585   "length of the tubes, m"
L_tube_Total_C=L_tube_C*N_C
H_e_C=0.605   "Height of the condenser, m"
N_L_C=2   "number of rows"
N_T_C=24   "tubes per rows"
N_C=N_L_C*N_T_C   "total number of tubes"
N_C_units=2   "condenser units"
S_T_C=0.03   "transverse pitch, vertical m"
S_L_C=0.025   "longitudinal pitch, horizontal m"
S_D_C=sqrt((S_L_C^2)+((S_T_C/2)^2)) "diagonal pitch, m"
A_1_C=S_T_C*L_tube_C   "Flow area 1, m2"
A_T_C=(S_T_C-D_tube_C)*L_tube_C   "Flow area 2, m2"
A_D_C=(S_D_C-D_tube_C)*L_tube_C   "Flow area 3, m2"
N_fins_C=140   "number of fins"
fins_height_C=0.008   "from the tube surface to the fin tip, m"
fins_thickness_C=0.0001   "m"
fins_separation_C=0.0018   "m"

Area_internal_C=pi*D_tube_inner_C*L_tube_C*N_C
Frontal_area_C=L_tube_C*H_e_C
D_DepC=((2*fins_height_C)+D_tube_C)*N_L_C "Depth of the condenser"

Area_external_tube_C=pi*D_tube_C*L_tube_C*N_C
Area_external_occupedbyfins_C=pi*D_tube_C*(fins_thickness_C*N_fins_C)*N_C
Area_external_tube_nofins_C=Area_external_tube_C-Area_external_occupedbyfins_C
Frontal_area_fins_C=H_e_C*fins_thickness_C*N_fins_C*2
Area_Surface_1fin_C=((S_T_C*S_L_C)-(pi*(D_tube_C/2)^2))*2
Area_Surface_fin_C=((S_T_C*S_L_C)-
(pi*(D_tube_C/2)^2))*2*N_fins_C*N_C+Frontal_area_fins_C
Area_total_C=Area_Surface_fin_C+Area_external_tube_nofins_C
Ratio_int_ext_C=Area_internal_C/Area_total_C

A_air_min1_C=(fins_separation_C-fins_thickness_C)*S_T_C "minimum free flow area"
sigma_C=A_air_min1_C/Frontal_area_C   "Ratio of the minimum free-flow area to the frontal area"

A_air_min1_C1=(S_T_C/2)*(1/fins_separation_C-fins_thickness_C)

"Compressor details"
frecuency=50   "HZ, o 60"
Frec=frecuency*60   "1 HZ=60 Rpm"
V_cil=90.2/1000000   "cm3 to m3, Displacement_capacity"
V_dot_comp=V_cil*Frec/60   "m3/s"
V_dot_refrig_4=m_dot_refrig*v[4]
eta_comp_vol=V_dot_refrig_4/V_dot_comp   "Volumetric efficiency"
eta_ideal_comp=eta_comp_vol/eta_comp

"Operating Conditions, R404A Refrigeration Cycle"
ref$ = 'R404A'
m_dot_refrigerant=142.71 "kg/h"
m_dot_refrig=m_dot_refrigerant/3600 "kg/s"

"Inputs"
E_Fan_vel%=100

```
Volumetric_air_flow=(2825 "m3/h"*E_Fan_vel%/100)
Fabric_duct_diameter=0.40 "m"
Vel_air_E=((Volumetric_air_flow/(pi*(Fabric_duct_diameter/2)^2)))/3600 "m/s"


Q_evap=5.1 "kJ/s"
{T_Eair_in= 11            "Air-side temperature at the intlet of the Evaporator"
T_amb= 4}            "Air-side temperature at the intlet of the Condenser"
T_sb=5.25
Super_heating=10    "C, averange data taken from experiments"

Sub_Cooling = T_adjusted(T_sb)

T[1]=T_Cond_in     "Refrigerant temperature at the intlet of the Condenser"
T[2]=T_Cond_out "Refrigerant temperature at the outlet of the Condenser"
T[3]=T_Evap_in     "Refrigerant temperature at the intlet of the Evaporator"
T[4]=T_Evap_out "Refrigerant temperature at the outtlet of the Evaporator"
T_Cair_in=T_amb "Ambient temperature, Air temperature at the inlet of the compressor"

T_Evap_in=-5

"Energy Balance on the Evaporator"
T_Evap_out=T_Evap_in+Super_heating                    "Determination of Refrigerant
temperature at the outlet of the evaporator taking into account the super heating"
m_dot_air=rho_air_E*Vel_max_air_E*(N_T*S_T*L_tube)          "Air-side flow rate in the
evaporator"
C_min=m_dot_air*Cp_air_E
epsilon_Evap=1-exp((-UA_Evap)/(C_min))                "Determination of efficiency
of the evaporator during phase change, NTU method"
{Q_evap=(C_min*(T_Eair_in-T_Evap_in))*epsilon_Evap}             "$$Determination of the
refrigerant temp at the inlet of the Evaporator"
{Q_evap=m_dot_air*Cp_air_E*(T_Eair_in-T_Eair_out)*epsilon_Evap}
epsilon_Evap =(T_Eair_in-T_Eair_out)/(T_Eair_in-T_Evap_in)      "$$Determination of Air-side
Temperature at the outlet of the Evaporator"

Q_Evap=m_dot_refrig*(h[4]-h[3])                          "Determination of the
refrigerant flow rate"
{Q_Evap=m_dot_air*Cp_air_E*(T_Eair_in-T_Eair_out1)}

{m_dot_air_TP=rho_air_E*Vel_max_air_E*(N_T*S_T*L_tube)*(A_TP/Area_total)
C_min_CP=m_dot_air_TP*Cp_air_E*(A_TP/Area_total)

Q_Evap_TP=m_dot_refrig*(L_TP/L_tube_Total)*(h_sat[4]-h[3])
Q_Evap_SP=m_dot_refrig*(L_SP/L_tube_Total)*(h[4]-h_sat[4])
Q_evap=Q_Evap_TP+Q_Evap_SP
Q_Evap=m_dot_refrig*((L_TP+L_SP)/L_tube_Total)*(h[4]-h[3]) }

P[3]=Pressure(ref$,T=T[3],x=0.277{x[3]})
P[4]=P[3]
h[4]=Enthalpy(ref$,T=T[4],P=P[4])
s[4]=Entropy(ref$,h=h[4],T=T[4])
s_prime[1]=s[4]

k=1.2                "Compressor politropic index"
{T_initial[1]=35}
P[1]=Pressure(ref$,T=T_initial[1],x=1)
Pressure_ratio=P[1]/P[4]
P4_pa= P[4]*convert(kpa,pa)
P1_pa= P[1]*convert(kpa,pa)
v[4]=Volume(ref$,T=T[4],P=P[4])
```

```
W_dot=((m_dot_refrig*P4_pa*v[4]*(k/(k-1))*(( (P[1]/P[4])^((k-1)/k))-1)))/1000          "Compressor
work equation, value similar to the isentropic work"
T4_K=T[4]+274.15
T1_K = ((P[1]/P[4])^((k-1)/k))*T4_K
T[1] = T1_K - 274.15
h[1]=Enthalpy(ref$,T=T[1],P=P[1])


h_prime[1]=Enthalpy(ref$,P=P[1],s=s_prime[1])
W_comp_ise=m_dot_refrig*(h_prime[1]-h[4])          "kJ/s, Isentropic work"

W_dot_Comp=m_dot_refrig*(h[1]-h[4])
eta_comp=W_dot/W_dot_Comp                "Compresor efficiency"
Power_comp=W_dot_Comp/eta_ideal_comp "Determination of electrical power "

T_prime[1]=temperature(ref$,P=P[1],h=h_prime[1])
P[1]=P[2]

h[2]=h[3]
x[3]=Quality(ref$,P=P[3],h=h[3])

T[2] = temperature(ref$, P=P[2], h=h[2])    "Determination of the Temperature in state 2"
T3[3] = temperature(ref$, P=P[3], h=h[3])

Cop_thermod=Q_Evap/W_dot_Comp  "Thermodynamic Cop"
Cop_real=Q_Evap/Power_comp          "COP taking into account the eletrical power"
{Cop_eletr_total=Q_Evap/Power_total
Power_total=W_fan_E+W_fan_C+Power_comp }
T_prime[3]=temperature(ref$,P=P[3],h=h[3])




T_sat[2]=temperature(ref$,P=P[2],x=0)
T_sat[1]=temperature(ref$,P=P[2],x=1)
T_sat[4]=temperature(ref$,P=P[4],x=1)
h_sat[2]=Enthalpy(ref$,x=0,P=P[2])
h_sat[1]=Enthalpy(ref$,x=1,P=P[1])
h_sat[4]=Enthalpy(ref$,x=1,P=P[4])



"Energy Balance on the Condenser"
m_dot_air_C=rho_air_C*Vel_max_air_C*(N_T_C*S_T_C*L_tube_C)
C_min_C=m_dot_air_C*Cp_air_C
epsilon_Cond=(1-exp((-UA_Cond)/(C_min_C)))                  "Determination of efficiency of
the Condenser during phase change, NTU method"
Q_Cond=(C_min_C*(T_Cond_in-T_Cair_in))*epsilon_Cond          "Determination of Condenser
thermal load during phase change, NTU method"
Q_Cond_Sh=m_dot_refrig*(h[1]-h_sat[1]) " load in the Superheated portion of condenser"
Q_Cond_Tp=m_dot_refrig*(h_sat[1]-h_sat[2]) " load in the twophase portion of condenser"
Q_Cond_Sc=m_dot_refrig*(h_sat[2]-h[2]) " load in the Sub-cooled portion of condenser,
Determination of the enthalpy in state 2"
Q_Cond1=Q_Cond_Sh+Q_Cond_Tp+Q_Cond_Sc "kJ/s"     "Total Condenser load"
Q_Cond=m_dot_air_C*Cp_air_C*(T_Cair_out-T_Cair_in)




P[4]=P_high
```

P[2]=P_low

s[1]=Entropy(ref$,h=h[1],T=T[1])
s[2]=Entropy(ref$,h=h[2],T=T[2])
s[3]=Entropy(ref$,h=h[3],T=T[3])

s[6]=s[4]
P[6]=P[1]
T[6]=temperature(ref$,P=P[6],s=s[6])
h[6]=Enthalpy(ref$,T=T[6],s=s[6])

h[5]=h[1]
T[5]=T[1]
s[5]=s[1]
P[5]=P[1]

cp[4]=Cp(ref$,T=T[4],P=P[4])
cv[4]=Cv(ref$,T=T[4],P=P[4])

v[1]=Volume(ref$,T=T[1],P=P[1])

T_prime[4]=temperature(ref$,P=P[4],x=1)

T_subcoo_act =T_sat[2] - T[2]
T_subcoo_act = Sub_Cooling

"£££££££££££££££££££££££££££££££££££££££   EVAPORATOR
£££"
Call
PropertiesAir(T_Eair_in,T_Eair_in,T_Evap_in,T_Evap_out,S_T,S_L,D_tube,Vel_air_E:Vel_max
_air_E,rho_air_E,mu_air_E,Pr_air_E,Pr_air_s_E,k_air_E,cp_air_E,h_air_in_E,h_air_out_E,v_ai
r_in_E,v_air_out_E,Re_air_E,Nus_air_E)

"Internal flow convection coeficient in the evaporator"
T_m_e=(T[4]+T[3])/2
Mu_prime[3]=Viscosity(ref$,P=P[3],x=0)
Mu_prime[4]=Viscosity(ref$,P=P[4],x=1)
v_prime[3]=Volume(ref$,P=P[3],x=0)
v_prime[4]=Volume(ref$,P=P[4],x=1)
Pr_refrig[3]=Prandtl(ref$,P=P[3],x=0)
Pr_refrig[4]=Prandtl(ref$,P=P[4],x=1)
k_refrig[3]=Conductivity(ref$,x=0,P=P[3])/1000
k_refrig[4]=Conductivity(ref$,x=1,P=P[4])/1000
rho[3]=Density(ref$,x=0,P=P[3])
rho[4]=Density(ref$,x=1,P=P[4])
h_prime[3]=Enthalpy(ref$,x=0,P=P[3])
h_prime[4]=Enthalpy(ref$,x=1,P=P[4])
Delta_h=h_prime[4]-h_prime[3] "kJ/kg, Latent heat"
T_mm=(((T_Evap_in+T_Evap_out)/2)+((T_Eair_out+T_Eair_in)/2))/2
k_wall=Conductivity(Aluminum, T=T_mm)/1000
k_fin=Conductivity(Aluminum,T=T_amb)/1000
Pcrit=P_crit(ref$)
Pr=P[3]/Pcrit "reduced pressure, definition by M.M. Sham 1978"

v=v_prime[3]+(x[3]*(v_prime[4]-v_prime[3]))   "Specific volumen"
(1/Mu_refrig_E)=((x[3]/Mu_prime[4])+((1-x[3])/Mu_prime[3]))   "viscusity of the
refrigerant, McAdams (1954)"
V_dot_refrig_E=m_dot_refrig*v[4]   "Volumetric flow"

Vel_Refrig_E=(m_dot_refrig)/(((rho[3]+rho[4])/2)*(pi*(D_tube_inner/2)^2))   "Velocity of the Refrigerant"
Re_refrig_e_liquid = (4*(m_dot_refrig))/(pi*D_tube_inner*Mu_prime[3])   "Reynolds number"

Nusselt_refrig_e_liquid=   0.023*Re_refrig_e_liquid^(4/5)*Pr_refrig[3]^0.4   "Dittus-Boelter correlation"
alpha_int_liquid=k_refrig[3]*Nusselt_refrig_e_liquid/D_tube_inner   "kW/m2.k, heat transfer coefficient for the liquid-phase only"

Xtt=(((1-x[3])/x[3])^0.9)*((rho[4]/rho[3])^0.5)*((Mu_prime[3]/Mu_prime[4])^0.1)   "Martinelli Parameter"

q_e=Q_evap/Area_internal "kW/m2, heat flux"
G_e=Vel_Refrig_E*((rho[3]+rho[4])/2) "kg/s.m2, Mass flux"
Bo=q_e/(Delta_h*G_e) "Boiling number"
E=1+(24000*(Bo^1.16))+1.37*((1/Xtt)^0.86) "Enhancement factor"
S=1/(1+0.00000115*(E^2)*(Re_refrig_e_liquid^1.17))   "Suppression factor"
Log=log10(Pr)
M=MolarMass(ref$)
alpha_int_pool=55*(Pr^0.12)*((-log)^(-0.55))*(q_e^0.67)*(M^(-0.5))   "Correlation for saturated boiling"
alpha_int_e=(E*alpha_int_liquid)+(S*alpha_int_pool) "refrigerant heat transfer coefficient, A general correlation for flow boiling in tubes and annuli, GUNGOR and R. H. S. WINTERTON, 1986"
alpha_int_e1=(1+(3000*(Bo^0.86)))+1.12*((x[3]/(1-x[3]))^0.75)*((rho[3]/rho[4])^0.41))*alpha_int_liquid   "Gungor K.E. and Winterton R.H.S. Simplified general correlation for saturated flow boiling and comparisons of correlation with dat', Chem. Eng. Res. & des. , Vol.65, March 1997., found in Comparison Of Energy Consumption Of Ventilated And Natural Convection Evaporators Of Refrigerators And Freezers, Zoughaib and Clodic, 2002"
Call h_singlephase(ref$,D_tube_inner,m_dot_refrig,T[4],T_sat[4], P[4]:alpha_SupH_E)

Rw=(ln(D_tube/D_tube_inner))/(2*k_wall*L_tube*N) "Wall Resistence"

"External flow convection coeficient at the evaporator"
G_Air_E=Vel_max_air_E*rho_air_E "kg/s.m2, Mass flux"
mm =SQRT(2*alpha_air_E/(k_fin*fins_thickness)) "Incropera pag 166, ed.7 "
Lc = fins_height + (fins_thickness/2)
n_f =tanh(mm*Lc)/(mm*Lc)
n_0=1-(Area_Surface_fin/Area_total)*(1-n_f)
D_he=(4*A_air_min1*D_DepE)/Area_total

Re_L=G_Air_E*S_L/mu_air_E "Reynolds number based on the row spacing S_L"
JP=(Re_air_e^(-0.4))*((4*S_T*S_L*sigma)/(pi*D_he*D_DepE))^(-0.15)
j4=0.2675*JP+1.325*10^(-6) "Colburn j-factor for a 4-row finned-tube heat exchanger, McQuiston (McQuiston and Parker, 1994)"
air_j_factor=((1-(N_L*1280*Re_L^(-1.2)))*j4)/(1-4*1280*Re_L^(-1.2))   "j-factor for heat exchangers with four or fewer rows"
{air_j_factor1 = 0.2675*JP+0.000001325}
alpha_air_E=(air_j_factor*Cp_air_E*G_Air_E)/(Pr_air_E^(2/3)) "Pag. 58, Enhanced finned-tubbe condenser...2003, Susan White Stewart"
{F_E=0.89 "correction factor for an evaporator with 4 rows, Zukauskas, 1987"
Nusselt_air_E=F_E*Nus_air_E}
{alpha_air_E2=(Nusselt_air_E*k_air_E/(D_tube))}

UA_Evap=1/ ((1/(alpha_int_e*(Area_internal)))+(Rw) + (1/(n_0*alpha_air_E*Area_total)))

"££   CONDENSER
££"
Call
PropertiesAir(T_Cair_in,T_Cair_in,T_Cond_in,T_Cond_out,S_T_C,S_L_C,D_tube_C,Vel_air_C:
Vel_max_air_C,rho_air_C,mu_air_C,Pr_air_C,Pr_air_s_C,k_air_C,cp_air_C,h_air_in_C,h_air_o
ut_C,v_air_in_C,v_air_out_C,Re_air_C,Nus_air_C)

T_m_c=(T[1]+T[2])/2

Mu[1]=Viscosity(ref$,P=P[1],T=T[1])
Mu[2]=Viscosity(ref$,P=P[2],T=T[2])
Delta_h_C=h_sat[1]-h_sat[2] "kJ/kg, Latent heat"
T_mm_c=(((T_Cond_in+T_Cond_out)/2)+((T_Cair_in+T_Cair_out)/2))/2
k_wall_C=Conductivity(Aluminum, T=T_mm_c)/1000
k_fin_C=Conductivity(Aluminum,T=T_amb)/1000

Call
h_TwoPhaseCondenser(ref$,D_tube_inner_C,m_dot_refrig/N_C_units,P[1],P[2]:alpha_TP_C)
"Two phase heat transfer coefficient during condensation"
Call   h_singlephase(ref$,D_tube_inner_C,m_dot_refrig/N_C_units,T[1],T_sat[1],
P[1]:alpha_SupH_C) "single phase heat transfer coefficient in the condenser for the superheated
region"
Call   h_singlephase(ref$,D_tube_inner_C,m_dot_refrig/N_C_units,T[2],T_sat[2],
P[2]:alpha_SubC_C) "single phase heat transfer coefficient in the condenser for the subcooled
region"

Rw_C=(ln(D_tube_C/D_tube_inner_C))/(2*k_wall_C*L_tube_C*N_C) "Wall Resistence"

"External flow convection coeficient at the Condenser"
G_Air_C=Vel_max_air_C*rho_air_C
mm_C =SQRT((2*alpha_air_C)/(k_fin_C*fins_thickness_C)) "Incropera pag 166, ed.7 "
Lc_C = fins_height + fins_thickness/2

B=S_T_C/2   "since S_L_C>S_T_C/2"
r_t=D_tube_C/2 " tube ratio"
psi=B/(r_t)
H=(1/2)*sqrt(((S_T_C/2)^2)+(S_L_C^2))
BETA=H/B
R_e=r_t*1.27*psi*((BETA-0.3)^(1/2))
phi=(R_e/r_t-1)*(1+0.35*ln(R_e/r_t))

n_f_C = tanh(mm_C*Lc_C)/(mm_C*Lc_C)
{n_f_C1 =((tanh(mm_C*R_e*phi))/(mm_C*R_e*phi))}
n_0_C=1-(Area_Surface_fin_C/Area_total_C)*(1-n_f_C)

Re_L_C=G_Air_C*S_L_C/mu_air_C   "Reynolds number based on the row spacing S_L_C"
D_hC=(4*A_air_min1_C*D_DepC)/Area_total_C
JP_C=(Re_air_c^(-0.4))*((4*S_T_C*S_L_C*sigma_C)/(pi*D_hC*D_DepC))^(-0.15)
{j4_C=0.2675*JP_C+1.325*10^(-6)
air_j_factor_C1=((1-(N_L_C*1280*Re_L_C^(-1.2)))*j4_C)/(1-4*1280*Re_L_C^(-1.2)) "j-factor for
heat exchangers with four or fewer rows"}
air_j_factor_C = 0.2675*JP_C+0.000001325"Colburn j-factor for a 4-row finned-tube heat
exchanger, McQuiston (McQuiston and Parker, 1994)"
alpha_air_C=(air_j_factor_C*Cp_air_C*G_Air_C)/(Pr_air_C^(2/3)) "Pag. 58, Enhanced finned-
tubbe condenser...2003, Susan White Stewart"

UA_Cond=1/ ((1/(alpha_TP_C*(Area_internal_C)))+(Rw_C) + (1/(n_0_C*alpha_air_C*Area_total_C)))

UA_Cond_TP=1/ ((1/(alpha_TP_C*(Area_internal_C)))+(Rw_C) + (1/(n_0_C*alpha_air_C*Area_total_C)))
UA_Cond_Sh=1/ ((1/(alpha_SupH_C*(Area_internal_C)))+(Rw_C) + (1/(n_0_C*alpha_air_C*Area_total_C)))
UA_Cond_Sb=1/ ((1/(alpha_SubC_C*(Area_internal_C)))+(Rw_C) + (1/(n_0_C*alpha_air_C*Area_total_C)))

Q_Cond_Tp=(C_min_C*(T_sat[1]-T_Cair_in))*epsilon_Cond_TP
{epsilon_Cond_TP=(1-exp((-UA_Cond_TP)/(C_min_C))) }

{Area_internal_C_TP=pi*D_tube_inner_C*(L_TP/L_tube_C)*N_C}

{Area_total_C_TP=Area_Surface_fin_C_TP+Area_external_tube_nofins_C_TP}

CALL Results(Cop_real,tempa,Power_comp, T_Eair_out,T_Eair_in:Cop_temp,tempb,W_comp_temp,T_Eair_out_temp)

"! TRNSYS outputs"

out1 = W_comp_temp
out2 = T_Eair_out_temp
out3=tempb
out4=Cop_temp

$Export 'CLIPBOARD' out1,out2,out3,out4

$Warnings Off

Appendix E - CFD/EES dynamic coupling

This appendix provides supporting information regarding the developed CFD/EES dynamic coupling described in Chapter 8. TRYNSYS platform was used to control the simulation procedure and exchange data between CFD and EES at the end of each time step. In order to succeed that, a TRNSYS component was programmed in FORTRAN and compiled in TRNSYS. F-A 14 show TRNSYS platform environment back round. In addition, F-A 15 shows the coupling results into TRNSYS platform.
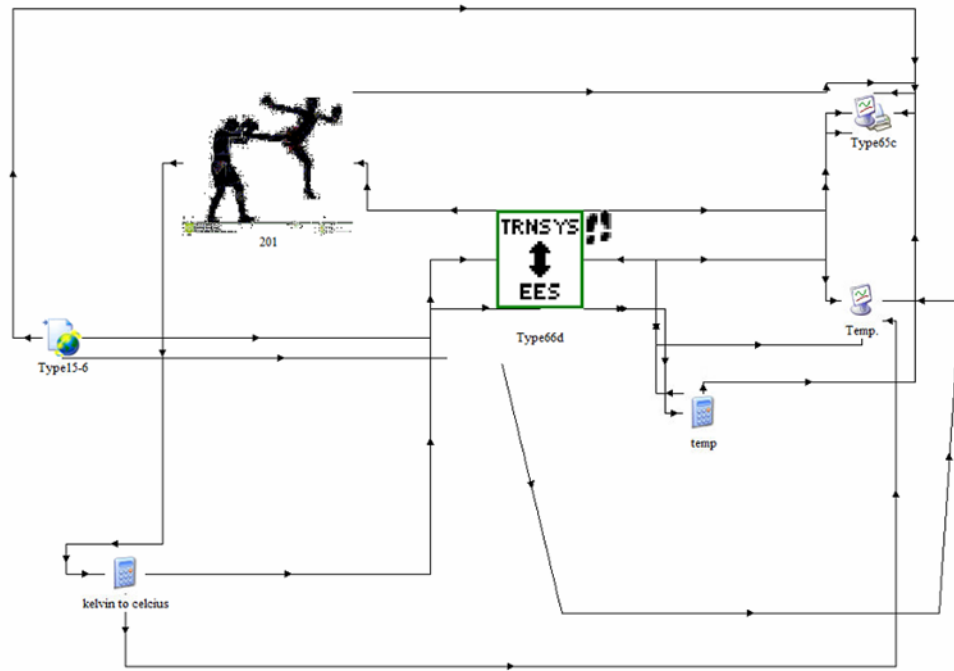
F-A 14. Trnsys Platform
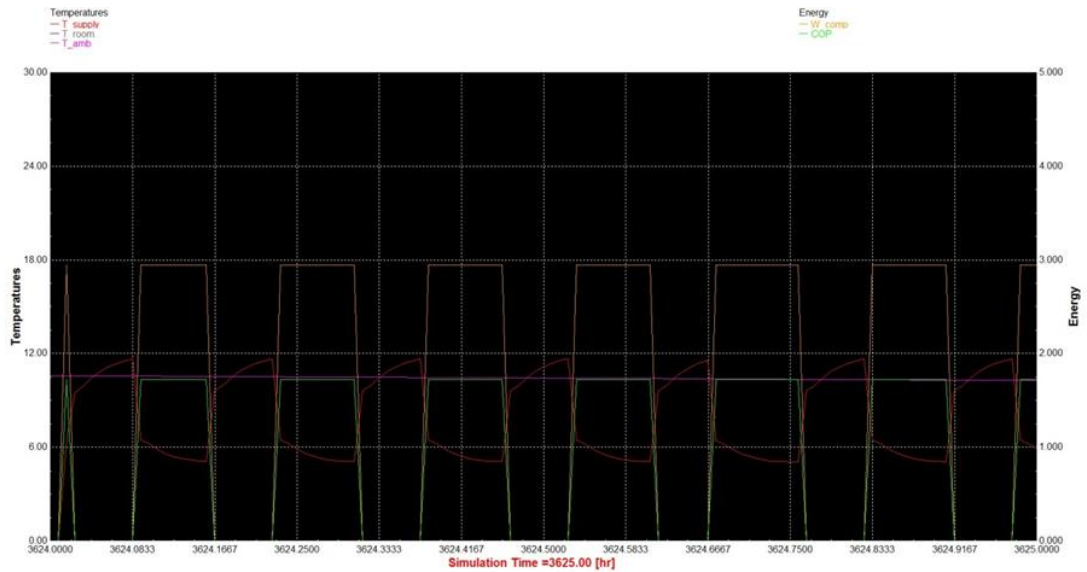
F-A 15. CFD/EES coupling results

The TRNSYS component programming was implemented as follow:

```fortran
SUBROUTINE TYPE101 (TIME,XIN,OUT,T,DTDT,PAR,INFO,ICNTRL,*)
!***********************************************************************
**************************
! Object: Call FLUENT
! Simulation Studio Model: Call FLUENT
!
! Author: parpas demetris
! Date:       2014
!
! Revision history:
! 2006-05-25: DAA - In order to compile this type with IVF, the function
SLEEP is found in the
!                    portability library DFPORT.
!
! (Comments and routine interface generated by TRNSYS Studio)
!***********************************************************************
**************************
!

!    TRNSYS acess functions (allow to acess TIME etc.)
    USE TrnsysConstants
    USE TrnsysFunctions
    USE DFPORT, ONLY: SLEEP


!------------------------------------------------------------------
--------------------------------------------------
!    REQUIRED BY THE MULTI-DLL VERSION OF TRNSYS
     !DEC$ATTRIBUTES DLLEXPORT :: TYPE201
!------------------------------------------------------------------
---------------------------------------------
!------------------------------------------------------------------
--------------------------------------------------
!    TRNSYS DECLARATIONS
    IMPLICIT NONE                 !REQUIRES THE USER TO DEFINE ALL VARIABLES
BEFORE USING THEM
```

```fortran
      DOUBLE PRECISION XIN    !THE ARRAY FROM WHICH THE INPUTS TO THIS
TYPE WILL BE RETRIEVED
      DOUBLE PRECISION OUT    !THE ARRAY WHICH WILL BE USED TO STORE THE
OUTPUTS FROM THIS TYPE
      DOUBLE PRECISION TIME   !THE CURRENT SIMULATION TIME - YOU MAY USE
THIS VARIABLE BUT DO NOT SET IT!
      DOUBLE PRECISION PAR    !THE ARRAY FROM WHICH THE PARAMETERS FOR
THIS TYPE WILL BE RETRIEVED
      DOUBLE PRECISION STORED !THE STORAGE ARRAY FOR HOLDING VARIABLES
FROM TIMESTEP TO TIMESTEP
      DOUBLE PRECISION T              !AN ARRAY CONTAINING THE RESULTS
FROM THE DIFFERENTIAL EQUATION SOLVER
      DOUBLE PRECISION DTDT   !AN ARRAY CONTAINING THE DERIVATIVES TO
BE PASSED TO THE DIFF.EQ. SOLVER
      INTEGER*4 INFO(15)              !THE INFO ARRAY STORES AND PASSES
VALUABLE INFORMATION TO AND FROM THIS TYPE
      INTEGER*4 NP,NI,NOUT,ND !VARIABLES  FOR  THE  MAXIMUM  NUMBER  OF
PARAMETERS,INPUTS,OUTPUTS AND DERIVATIVES
      INTEGER*4 NPAR,NIN,NDER !VARIABLES  FOR  THE  CORRECT  NUMBER  OF
PARAMETERS,INPUTS,OUTPUTS AND DERIVATIVES
      INTEGER*4 IUNIT,ITYPE   !THE UNIT NUMBER AND TYPE NUMBER FOR THIS
COMPONENT
      INTEGER*4 ICNTRL        !AN ARRAY FOR HOLDING VALUES OF CONTROL
FUNCTIONS WITH THE NEW SOLVER
      INTEGER*4 NSTORED       !THE  NUMBER  OF  VARIABLES  THAT  WILL  BE
PASSED INTO AND OUT OF STORAGE
      CHARACTER*3 OCHECK              !AN  ARRAY  TO  BE  FILLED  WITH  THE
CORRECT VARIABLE TYPES FOR THE OUTPUTS
      CHARACTER*3 YCHECK              !AN  ARRAY  TO  BE  FILLED  WITH  THE
CORRECT VARIABLE TYPES FOR THE INPUTS
      !-----------------------------------------------------------------
------------------------------------------------------

      !-----------------------------------------------------------------
------------------------------------------------------
      !    USER DECLARATIONS - SET THE MAXIMUM NUMBER OF PARAMETERS (NP),
INPUTS (NI),
      !   OUTPUTS (NOUT), AND DERIVATIVES (ND) THAT MAY BE SUPPLIED FOR THIS
TYPE
      PARAMETER (NP=4,NI=20,NOUT=20,ND=0,NSTORED=20)
      !-----------------------------------------------------------------
------------------------------------------------------

      !-----------------------------------------------------------------
------------------------------------------------------
      !   REQUIRED TRNSYS DIMENSIONS
      DIMENSION XIN(NI),OUT(NOUT),PAR(NP),YCHECK(NI),OCHECK(NOUT), &
            STORED(NSTORED),T(ND),DTDT(ND)
      INTEGER NITEMS,NO
      !-----------------------------------------------------------------
------------------------------------------------------
      !-----------------------------------------------------------------
------------------------------------------------------
      !   ADD DECLARATIONS AND DEFINITIONS FOR THE USER-VARIABLES HERE

      INTEGER         ios, i_sleep, i
      LOGICAL         fileFound
      LOGICAL(4)      bWait                !wait/no wait for new process to
end
      LOGICAL         O_FLAG
      LOGICAL         scriptFound
```

```fortran
    INTEGER*4        prochand,thrdhand
    CHARACTER        CMDLINE*200          !Command line to call FLUENT
    CHARACTER        (len=maxPathLength)                          ::
scriptFileName,resultsFileName,textLine
    CHARACTER        (len=maxPathLength)                          ::
pathFluent,optionsFluent,pathFluentScrip
    CHARACTER (len=maxPathLength)    :: MSGFluent(2)

    INTEGER mode                 ! Mode
    INTEGER callingMode          ! Calling mode
    INTEGER luScript       ! Logical unit number for script file at each
time step
    INTEGER luResults       ! Logical unit number of intermediate file
that returns the results from FLUENT
    INTEGER nResultsFluent ! Number of outputs read from FLUENT
    INTEGER nModifyBC        ! Number of variables to modify boundary
conditions
    DOUBLE PRECISION resultsFluent !Array with results from fluent
    DOUBLE PRECISION modifyBC       !Array with information to update
boundary conditions
    DIMENSION resultsFluent(NOUT)
    DIMENSION modifyBC(NOUT)

    INTEGER          cf    ! Control function

    DATA scriptFound /.true./
    DATA MSGFluent(1) /'Error opening script file.'/
    DATA MSGFluent(2) /'Error opening results file.'/

!-----------------------------------------------------------------------
-------------------------------------------------------
!   SET THE VERSION INFORMATION FOR TRNSYS
    IF(INFO(7).EQ.-2) THEN
        INFO(12)=16
        RETURN 1
    ENDIF
!-----------------------------------------------------------------------
-------------------------------------------------------

!-----------------------------------------------------------------------
-------------------------------------------------------
!   DO ALL THE VERY LAST CALL OF THE SIMULATION MANIPULATIONS HERE
    IF (INFO(8).EQ.-1) THEN
        IUNIT=INFO(1)
        ITYPE=INFO(2)
        RETURN 1
    ENDIF
!-----------------------------------------------------------------------
-------------------------------------------------------

!-----------------------------------------------------------------------
-------------------------------------------------------
!   DO ALL THE VERY FIRST CALL OF THE SIMULATION MANIPULATIONS HERE
    IF (INFO(7).EQ.-1) THEN

!    SET SOME INFO ARRAY VARIABLES TO TELL THE TRNSYS ENGINE HOW THIS
TYPE IS TO WORK
        NO       = JFIX(PAR(3)+0.1)    !Number of outputs
        INFO(6)  = NO
        callingMode = JFIX(PAR(4)+0.1) !Calling mode
```

```fortran
        IF (callingMode == 1) INFO(9) = 1  !Dynamic coupling - Iterative
calling
        IF (callingMode == 2) INFO(9) = 2   !Static coupling  - Call
after all components have converged
        INFO(10) = 0     !STORAGE FOR VERSION 16 HAS BEEN CHANGED

!     SET THE REQUIRED NUMBER OF INPUTS, PARAMETERS AND DERIVATIVES THAT
THE USER SHOULD SUPPLY IN THE INPUT FILE
!     IN SOME CASES, THE NUMBER OF VARIABLES MAY DEPEND ON THE VALUE OF
PARAMETERS TO THIS MODEL....
        NIN       = JFIX(PAR(2)+0.1) + 1
        NPAR     = NP
          NDER     = ND

!      CALL THE TYPE CHECK SUBROUTINE TO COMPARE WHAT THIS COMPONENT
REQUIRES TO WHAT IS SUPPLIED IN
!      THE TRNSYS INPUT FILE
          CALL TYPECK(1,INFO,NIN,NPAR,NDER)

!      CALL RCHECK(INFO,YCHECK,OCHECK)

!      SET THE NUMBER OF STORAGE SPOTS NEEDED FOR THIS COMPONENT
        NITEMS   = 2 + NO
          CALL setStorageSize(NITEMS,INFO)

!      RETURN TO THE CALLING PROGRAM
        RETURN 1
      ENDIF
!--------------------------------------------------------------------
----------------------------------------------------


!--------------------------------------------------------------------
----------------------------------------------------
!   DO ALL OF THE INITIAL TIMESTEP MANIPULATIONS HERE - THERE ARE NO
ITERATIONS AT THE INTIAL TIME
     IF        (TIME       <        (getSimulationStartTime()       +
getSimulationTimeStep()/2.D0)) THEN

!      SET THE UNIT NUMBER FOR FUTURE CALLS
        IUNIT  = INFO(1)
        ITYPE  = INFO(2)
!--------------------------------------------------------------------
----------------------------------------------------
!      READ IN THE VALUES OF THE PARAMETERS IN SEQUENTIAL ORDER
        mode        = JFIX(PAR(1)+0.1)     ! Mode - for future upgrades
        NIN         = JFIX(PAR(2)+0.1) + 1 ! Number of total inputs to the
component
        NO          = JFIX(PAR(3)+0.1)       ! Number of outputs
          callingMode = JFIX(PAR(3)+0.1)     ! Calling  mode  -  1  for
Dynamic, 2 for Static

!      CHECK THE PARAMETERS FOR PROBLEMS AND RETURN FROM THE SUBROUTINE
IF AN ERROR IS FOUND
        IF ((MODE < 1) .OR. MODE >1 ) CALL TYPECK(-4,INFO,0,1,0)
          IF ( NIN <0 )                              CALL         TYPECK(-
4,INFO,0,2,0)
          IF ( NO  < 0)                              CALL         TYPECK(-
4,INFO,0,3,0)
          IF   ((callingMode<1).OR.(callingMode>2))    CALL    TYPECK(-
4,INFO,0,4,0)
```

```fortran
!   --CALL FLUENT FOR THE FIRST TIME-----------------------------------
---------------------------
!     In this first call, Fluent may initialize the flow and create the
output file needed
!     for the solution of the other components.
!      Fluent opens, solves the text script, creates a text file and
closes.

      !Open script file and write the information for the updated
boundary conditions
      scriptFileName = TRIM(getLabel(IUNIT,3))

      ! if relative path (no colon in second position or backslash in
first position), add path to script file
      IF((.NOT.(index(scriptFileName,":")==2))              .and.
(.NOT.(index(scriptFileName,"\")==1)) ) THEN
        scriptFileName   =   trim(getTrnsysInputFileDir())   //   '\'//
trim(scriptFileName)
      ENDIF

      luScript = getNextAvailableLogicalUnit()
      OPEN (luScript, FILE = scriptFileName, STATUS ='UNKNOWN')
       CLOSE(luScript,STATUS='DELETE')
      OPEN (luScript, FILE = scriptFileName, STATUS ='NEW')

       !Find results
      resultsFileName = TRIM(getLabel(IUNIT,4))
      ! if relative path (no colon in second position or backslash in
first position), delete path from results file
      IF((index(resultsFileName,":")==2)                    .OR.
(index(resultsFileName,"\")==1)) THEN
        resultsFileName                                              =
TRIM(resultsFileName(index(resultsFileName,'\',back=.true.)+1:maxPathL
ength))
      ENDIF




!   ----------------------------------------------------------------
---------------------------------
!   User defined 1.  INITIALIZATION OF FLUENT SIMULATION--------------
---------------------------------
!   ----------------------------------------------------------------
---------------------------------
!   Modify them according to the number of boundary condition data that
needs to be updated
      !Update boundary conditions
      nModifyBC = 1                        !Size  of  array  that  sends
information to the subroutine UPDATEBOUNDARY,
       modifyBC(1) = XIN(2)

      nResultsFluent = 1            !Size   of   array   that   returns
information from the subroutine
                               !READ_FLUENT_RESULTS.
!   ----------------------------------------------------------------
---------------------------------
!   ----------------------------------------------------------------
---------------------------------

      !Update boundary conditions
```

```fortran
      CALL                                        UPDATEBOUNDARY
(luScript,nModifyBC,modifyBC,scriptFileName,resultsFileName)
      CLOSE (luScript,STATUS='KEEP')

      !Call fluent
      pathFluent   = getLabel(IUNIT,1)
        optionsFluent = getLabel(IUNIT,2)
      CMDLINE    =   TRIM(pathFluent)  //"  "//TRIM(optionsFluent)//"
"//TRIM(scriptFileName)
        bwait  = .TRUE.
        CALL CALLPROGRAM(CMDLINE,bwait,prochand,thrdhand)

      !Read the results from FLUENT
      fileFound = .FALSE.
      luResults = getNextAvailableLogicalUnit()

        i_sleep = 1
        ios = 1
        do i_sleep=1,10
        CALL SLEEP(95)
          OPEN (luResults, FILE= resultsFileName, STATUS = 'OLD', IOSTAT
= ios)
        IF (ios == 0) then
              EXIT
          ENDIF
      enddo

      IF (ios == 0) then
          OPEN (luResults, FILE= resultsFileName, STATUS = 'OLD')
          CALL                                    READ_FLUENT_RESULTS
(luResults,nResultsFluent,resultsFluent)
        CLOSE (luResults,STATUS='DELETE')
        ELSE
          CALL MESSAGES(-1,MSGFluent(2),'fatal',IUNIT,ITYPE)
          RETURN 1
        ENDIF


!   ----------------------------------------------------------------
--------------------------------
!   User defined 2. UPDATE THE OUTPUTS FOR THE COUPLING WITH THE OTHER
COMPONENTS-----------------------
!   ----------------------------------------------------------------
--------------------------------
!    PERFORM ANY REQUIRED CALCULATIONS TO SET THE INITIAL VALUES OF THE
OUTPUTS HERE
      !Modify these values according to the outputs from Fluent
      OUT(1) = resultsFluent(1)
      OUT(2) = resultsFluent(2)
      OUT(3) = resultsFluent(3)
      OUT(4) = resultsFluent(4)
!   ----------------------------------------------------------------
--------------------------------
!   ----------------------------------------------------------------
--------------------------------

!      PERFORM ANY REQUIRED CALCULATIONS TO SET THE INITIAL STORAGE
VARIABLES HERE
      NITEMS = 2 + NO
        STORED(1)= luScript
        STORED(2)= luResults
```

```fortran
      DO i = 1,NO
        STORED(2 + i) = OUT(i)
        ENDDO
!    PUT THE STORED ARRAY IN THE GLOBAL STORED ARRAY
      CALL setStorageVars(STORED,NITEMS,INFO)

!    RETURN TO THE CALLING PROGRAM
      RETURN 1

    ENDIF
!----------------------------------------------------------------------
--------------------------------------------------


!----------------------------------------------------------------------
--------------------------------------------------
!    *** ITS AN ITERATIVE CALL TO THIS COMPONENT ***
!----------------------------------------------------------------------
--------------------------------------------------

!    RE-READ THE PARAMETERS IF ANOTHER UNIT OF THIS TYPE HAS BEEN CALLED
SINCE THE LAST
!    TIME THEY WERE READ IN
      IF(INFO(1).NE.IUNIT) THEN
        !reset the unit number
          IUNIT = INFO(1)
          ITYPE = INFO(2)
        !REREAD THE PARAMETERS
        MODE  = JFIX(PAR(1)+0.1)       ! Mode
        NIN   = JFIX(PAR(2)+0.1) + 1
        NO    = JFIX(PAR(3)+0.1)
      ENDIF

      !REREAD THE STORAGE VALUES
      NITEMS  = 2 + NO
        CALL getStorageVars(STORED,NITEMS,INFO)
      luScript  = STORED(1)
        luResults = STORED(2)

!    READ THE INPUTS
      cf        = JFIX(XIN(1) +0.1)

!    ------------------------------------------------------------------
----------------------------------
!    User defined 3. UPDATE THE INPUTS FOR THE COUPLING WITH THE OTHER
COMPONENTS----------------------
!    ------------------------------------------------------------------
----------------------------------
!    Modify this according to the special application
      !Update boundary conditions
      nModifyBC = 1
        modifyBC(1) = XIN(2)
      nResultsFluent = 1
!    ------------------------------------------------------------------
----------------------------------
!    ------------------------------------------------------------------
----------------------------------

      IF (cf >0.5) THEN
!    Update boundary conditions and run simulations
```

```fortran
        !Open script file and write the information for the updated
boundary conditions
        scriptFileName = TRIM(getLabel(IUNIT,3))

        ! if relative path (no colon in second position or backslash in
first position), add path to script file
        IF((.NOT.(index(scriptFileName,":")==2))              .and.
(.NOT.(index(scriptFileName,"\")==1)) ) THEN
           scriptFileName  =  trim(getTrnsysInputFileDir())  // '\'//
trim(scriptFileName)
        ENDIF

!       Write boundary condition to modify
        OPEN (luScript, FILE = scriptFileName, STATUS ='UNKNOWN')
          CLOSE(luScript,STATUS='DELETE')
        OPEN (luScript, FILE = scriptFileName, STATUS ='NEW')

        CALL                                              UPDATEBOUNDARY
(luScript,nModifyBC,modifyBC,scriptFileName,resultsFileName)
        CLOSE (luScript,STATUS='KEEP')

        !Call fluent
        pathFluent    = getLabel(IUNIT,1)
          optionsFluent = getLabel(IUNIT,2)
        CMDLINE    = TRIM(pathFluent)  //"  "//TRIM(optionsFluent)//"
"//TRIM(scriptFileName)
          bwait   = .TRUE.
          CALL CALLPROGRAM(CMDLINE,bwait,prochand,thrdhand)

        !Read the results from FLUENT
        fileFound = .FALSE.

          i_sleep = 1
          ios = 1
          DO i_sleep=1,10
          CALL SLEEP(95)
            OPEN (luResults, FILE= resultsFileName, STATUS = 'OLD',
IOSTAT = ios)
          IF (ios == 0) THEN
               EXIT
             ENDIF
        ENDDO

        IF (ios == 0) then
              OPEN (luResults, FILE= resultsFileName, STATUS = 'OLD')
              CALL                                    READ_FLUENT_RESULTS
(luResults,nResultsFluent,resultsFluent)
           CLOSE (luResults,STATUS='DELETE')
           ELSE
             CALL MESSAGES(-1,MSGFluent(2),'fatal',IUNIT,ITYPE)
             RETURN 1
           ENDIF

! -----------------------------------------------------------------
----------------------------------
!   User defined 4. SET THE OUTPUTS FROM THIS MODEL IN SEQUENTIAL ORDER
AND GET OUT---------------------
! -----------------------------------------------------------------
----------------------------------
        OUT(1) = resultsFluent(1)
        OUT(2) = resultsFluent(2)
```

```fortran
        OUT(3) = resultsFluent(3)
        OUT(4) = resultsFluent(4)
!     -----------------------------------------------------------------
----------------------------------
!     -----------------------------------------------------------------
----------------------------------

!     PUT THE STORED ARRAY IN THE GLOBAL STORED ARRAY
        DO i = 1,NO
           STORED(2 + i) = OUT(i)
           ENDDO
        CALL setStorageVars(STORED,NITEMS,INFO)

        ELSE
!     Do not do anything if controlfunction is zero
!     Keep the values of the outpus from the previous timestep
        DO i = 1,NO
           OUT(i) = STORED(2+i)
           ENDDO
        ENDIF

        RETURN 1

CONTAINS


!     -----------------------------------------------------------------
----------------------------------
!     User defined 5. MODIFY  THE  SUBROUTINES  UPDATEBOUNDARY  AND
READ_FLUENT_RESULTS------------------------
!     -----------------------------------------------------------------
----------------------------------
   SUBROUTINE
UPDATEBOUNDARY(luScript,nModifyBC,modifyBC,scriptFileName,resultsFileN
ame)
!     This  subroutine  writes  the  new  information  for  the  boundary
conditions in FLUENT

        USE TrnsysConstants

     IMPLICIT NONE
        INTEGER, INTENT(IN)          :: luScript
        INTEGER, INTENT(IN)          :: nModifyBC
        DOUBLE PRECISION, INTENT(IN) :: modifyBC

        DIMENSION modifyBC(nModifyBC)


        DOUBLE PRECISION v_boundary

     CHARACTER (len=12) vStr
     CHARACTER (len=maxPathLength)      :: scriptFileName,resultsFileName

     !Modify according to specific application
        v_boundary = modifyBC(1)

        WRITE (vStr,'(F5.2)') v_boundary
        vStr = TRIM(ADJUSTL(vStr))

     WRITE (luScript,'(A4)')  "f/rc"          !File / read case
        WRITE (luScript,'(A15)') "chamber.cas"
```

```
    WRITE (luScript,'(A4)')   "f/rd"              !File / read  data
      WRITE (luScript,'(A23)') "chamber.dat"
      WRITE (luScript,'(A42)') "define/boundary-conditions/mass-flow-
inlet"        !Define/Boundary Conditions/mass flow inlet
      WRITE (luScript,'(A4)')  "sock"              !zone id/name
      WRITE (luScript,'(A3)')  "yes"               !Reference        Frame:
Absolute [yes]
      WRITE (luScript,'(A3)')  "yes"               !Mass              Flow
Specification Method: Mass Flow Rate [yes]
      WRITE (luScript,'(A)')   ""             !Use  Profile  for  Mass  Flow
Rate? [no]
      WRITE (luScript,'(A)')   ""             !Mass    Flow    Rate    (kg/s)
[0.9592000000000001]
      WRITE (luScript,'(A)')   ""             !Use    Profile    for    Total
Temperature? [no]
      WRITE (luScript,'(A4)')  vStr    !"new temperature from trnsys
      WRITE (luScript,'(A)')   ""             !Use      Profile      for
Supersonic/Initial Gauge Pressure? [no]
      WRITE (luScript,'(A)')   ""             !Supersonic/Initial    Gauge
Pressure (pascal) [0]
      WRITE (luScript,'(A2)')  "no"              !Direction
Specification Method: Direction Vector [no] no
      WRITE (luScript,'(A3)')  "yes"             !Direction
Specification Method: Normal to Boundary
      WRITE (luScript,'(A)')   ""             !Turbulent     Specification
Method: K and Omega [no]
      WRITE (luScript,'(A)')   ""            !Turbulent Specification Method:
Intensity and Length Scale[no]
      WRITE (luScript,'(A)')   ""            !Turbulent Specification Method:
Intensity and Viscosity Ratio [yes]
      WRITE (luScript,'(A)')   ""         !Turbulent Intensity (%) [5]
      WRITE (luScript,'(A)')   ""         !Turbulent Viscosity Ratio [10]
      WRITE (luScript,'(A13)') "solve/iterate"        !Solve/iterate
       WRITE (luScript,'(A3)')  "1"                 !number of iterations
      WRITE (luScript,'(A5)')  "f/wcd"    !File/Write case-data"
      WRITE (luScript,'(A11)') "chamber.cas"
    WRITE (luScript,'(A3)')  "yes"           !Overwrite?
    WRITE (luScript,'(A7)')  "plo/plo"  !Plot/plot
    WRITE (luScript,'(A3)')  "yes"           !Plot node values?
    WRITE   (luScript,'(A20)')   resultsFileName   !Filename   !WRITE
(luScript,'(A3)')WRITE (luScript,'(A3)') "yes"        !       "yes"
Overwrite?
      WRITE (luScript,'(A3)')  "yes"             !Order points
      WRITE (luScript,'(A2)')  "no"              !Y   Axis    direction
vector? [no]
      WRITE (luScript,'(A2)')  "no"              !Y  Axis  curve  length?
[no]
      WRITE (luScript,'(A11)') "temperature"        !Cell function
    WRITE (luScript,'(A3)')  "yes"         !y axis direction vector
    WRITE (luScript,'(A1)')  "0"           !ix [1]
    WRITE (luScript,'(A1)')  "0"           !iy [0]
    WRITE (luScript,'(A1)')  "0"           !iz [0] 0
    WRITE (luScript,'(A6)')  "sensor"          !surface    id/name(1)
[()]
    WRITE (luScript,'(A5)')  "tknee"           !surface    id/name(1)
[()]
    WRITE (luScript,'(A5)')  "thead"           !surface    id/name(1)
[()]
    WRITE (luScript,'(A8)')  "tceiling"          !surface    id/name(1)
[()]
    WRITE (luScript,'(A)')   ""                 !Surface 2
```

```fortran
        WRITE (luScript,'(A4)') "exit"


    END SUBROUTINE UPDATEBOUNDARY

!---------------------------------------------------------------------
---------------

    SUBROUTINE READ_FLUENT_RESULTS (luResults,Nresults,results)

        USE TrnsysConstants

     IMPLICIT NONE
     INTEGER, INTENT(in)              :: luResults, Nresults
        DOUBLE PRECISION, INTENT(out) :: results

    DIMENSION results(Nresults)

    CHARACTER (len=maxPathLength)     :: textLine

        READ (luResults,'(A)') textLine !(title "temperature")
        READ  (luResults,'(A)')  textLine     !(labels  "temperature"
"Position")
        READ (luResults,'(A)') textLine !
        READ (luResults,'(A)') textLine  !((xy/key/label "sensor")
      READ (luResults,'(A1, F10.0)') textLine, results(1) !0
    277.985
        READ (luResults,'(A)') textLine    !
        READ (luResults,'(A)') textLine    !
        READ (luResults,'(A)') textLine  !((xy/key/label "tknee")
        READ (luResults,'(A1, F10.0)') textLine, results(2) !knee
temperature
        READ (luResults,'(A)') textLine    !
        READ (luResults,'(A)') textLine    !
        READ (luResults,'(A)') textLine  !((xy/key/label "thead")
        READ (luResults,'(A1, F10.0)') textLine, results(3) !head
temperature
        READ (luResults,'(A)') textLine    !
        READ (luResults,'(A)') textLine    !
        READ (luResults,'(A)') textLine  !((xy/key/label "tceiling")
        READ (luResults,'(A1, F10.0)') textLine, results(4) !ceiling
temperature

    END SUBROUTINE READ_FLUENT_RESULTS


END SUBROUTINE TYPE101
```